CROUZON SYNDROME:

A Clinical and Three Dimensional Radiographic Analysis of Craniofacial Morphology and Surgery

Timothy William Proudman M.B., B.S.

A thesis submitted for the degree of Master of Surgery

Australian Cranio-Facial Unit
Women's and Children's Hospital, Adelaide
and Royal Adelaide Hospital,
and
Department of Surgery,
Faculty of Medicine
The University of Adelaide
1995

TABLE OF CONTENTS

DECLARATION

I declare that this thesis contains no material that has been accepted for the award of any other degree or diploma in any University or other tertiary institution and that, to the best of my knowledge and belief, the thesis contains no material previously published or written by another person, except where due reference is made in the text.

I consent to this copy of my thesis being made available for photocopying and loan if accepted for the award of the degree.

Timothy William Proudman

ACKNOWLEDGMENTS

This project has been supported by The University of Adelaide, Post-Graduate Research Scholarship, The Australian Cranio-Facial Unit (ACFU), Women's and Children's Hospital Adelaide and Royal Adelaide Hospital, and the Department of Plastic and Reconstructive Surgery, Royal Adelaide Hospital.

I acknowledge the contribution of the members of The Australian Cranio-Facial Unit (D. J. David AC, Head of Unit) in examining and treating all the patients reported in this thesis. Extensive clinical records, clinical photographs and radiographs collected by members of the ACFU have made this project possible.

I am grateful to the following University Departments and individuals who allowed their dried skeletal collections to be examined, photographed and recorded on CT tapes:

The Department of Anatomy (Professor J. Priedkalns, Head of Department), The University of Adelaide Medical School, Frome Road, Adelaide, South Australia. Mr Jim Johnson assisted with obtaining the material.

The Department of Anatomy (Professor B. Gannon, Head of Department), Flinders University, Bedford Park, South Australia. Mr Carlos Kordjin assisted with obtaining the material.

The Department of Restorative Dentistry (Emeritus Professor T. Brown, Head of Department), The Adelaide Dental School, The Adelaide Dental Hospital, The University of Adelaide, Frome Road, Adelaide, South Australia. Professor Grant Townsend assisted with obtaining the material.

The Department of Anatomy (Professor J. Stone, Head of Department), The University of Sydney, New South Wales, Australia. Dr Greg Doran assisted with obtaining the material.

The Department of Anatomy (Professor G. Campbell, Head of Department), The University of Queensland, St Lucia, Brisbane, Queensland, Australia. Dr Wally Wood assisted with obtaining the material.

The Department of Dentistry (Professor G Seymour, Head of Department), The University of Queensland, St Lucia, Queensland, Australia. Dr Kon Romaniuk assisted with obtaining the material.

The Department of Archaeology and Paleoanthropology (Professor G. Connah, Head of Department), University of New England, Armidale, New South Wales, Australia. Dr Peter Brown assisted with obtaining the material.

Professor Donald Simpson, Department of Neurosurgery, Women's and Children's Hospital, North Adelaide, South Australia (private collection).

Dr Amanda Abbott, Senior Research Scientist, Australian Cranio-Facial Unit, Women's and Children's Hospital, North Adelaide, South Australia (private collection).

I would like to thank the Department of Radiology (Dr L. Morris, Head of Department) of the Women's and Children's Hospital for their tremendously valuable assistance in performing CT scans of the dried skeletal material. In particular, the efforts of Mr Graham Truman (Chief Radiographer), assisted by Mr Nick Zabanias, Mr Chris James, and Ms Amanda Sierp (Radiographers) are acknowledged.

The Department of Radiology (Dr P. Sherbourne, Head of Department) at Royal Prince Alfred Hospital, Camperdown, New South Wales, Australia performed CT scans of the dried skeletal material from the University of Sydney and kindly forwarded the tapes to our department. This was only possible due to the direct efforts of the Chief Radiographers, Ms Sheila Ryan and Ms Kay Cook. They were assisted by Mr Kim Mann, Mr Frank Carbon and Mr Stanley Haviland (Radiographers).

Dr Ian Holten (Research Fellow) obtained and coordinated the transfer of some of the skeletal material and CT data tapes from around the country. Dr David Netherway (Principal Research Scientist, Australian Cranio-Facial Unit) assisted with this and also provided enormous

technical assistance in the handling and transfer of the CT tape data to hard and optical disk. When computing difficulties arose, Dr Netherway acted as an invaluable trouble shooter.

I would like to thank the following for their help and support in the preparation of this manuscript:

Guidance has been gratefully received from Professor Tasman Brown and Dr John Abbott (Director and Deputy Director, Research Unit, Australian Cranio-Facial Unit respectively). Mr Mark Moore (Consultant Surgeon, Australian Cranio-Facial Unit) has provided added stimulus to many aspects of the project. Dr Bruce Clark (Neuro-radiologist, Department of Radiology, Women's and Children's Hospital, Adelaide) assisted in the examination of the central nervous system CT scans.

Discussion with Cranio-Facial Unit members has been invaluable in the investigation of Crouzon syndrome. Specific thanks in this area go to Mr James Trott (Deputy Director), Mr Ahmad Hanieh, Professor Donald Simpson (Neurosurgery), Mr John Tomich (ENT Surgery), Ms Alison Bagnall (Speech Pathology), and Mrs Jeanette Barritt (Social Work).

Mrs Bernadette Jury, Mrs Claire Pumpa and Ms Susanna Pecorari provided secretarial support for this project. Assistance with photographs of the skulls and patients was provided by Mr Chris Sprod and Mr Mark Stevens and illustrations by Ms Jan Nicol and Mr Greg Helbers.

Special thanks go to Mrs Louise Netherway for her excellent research support, and expert assistance with compilation and editing of the manuscript.

Invaluable support was also provided by Rodney and Jean Wicks and William and Esme Proudman during the preparation of this manuscript.

Penultimately, I thank the kind and generous support and guidance of my supervisors, Dr Amanda Abbott, Dr David Netherway and Mr David David. I was privileged to work in the department with these people. I believe I have benefited greatly from their wisdom and scientific approach and I hope this work will repay, in part, the trust they have shown in me.

My final thanks are to my wife Susanna for her tremendous practical help, advice and support, without whose help this project would not have been possible. My greatest love go to my wife, Susanna, and daughter, Rebecca.

SUMMARY

The clinical and radiographic appearance of Crouzon syndrome has been analysed for a population of 59 patients. The range of cranio-facial manifestations (and non cranio-facial features) and the natural history of the deformity provide an insight into the pathological processes occurring in Crouzon syndrome. The medical and surgical management of patients with this deformity is discussed.

The cranio-facial morphology of Crouzon syndrome has been analysed using cranio-facial osseous landmark co-ordinate data in three dimensions. The landmark co-ordinate data were determined from computer tomography records of 8 patients with Crouzon syndrome (in 4 different age groups). In addition, osseous landmark co-ordinate data were determined from computer tomography records of age-matched normal dried skulls. These data provided an experimental standard of normal cranio-facial morphology and were used for comparison with the data collected from the patients with Crouzon syndrome to generate a mathematical description of the morphology of this syndrome. The accuracy of landmark co-ordinate identification was assessed. Measurements of the size and shape of individual cranio-facial bones were made to demonstrate the morphology of each bone (anatomical units) including the sutures and synchondroses.

A statistical comparison of individual cranio-facial bones of each Crouzon patient with the age-matched experimental standards revealed areas of significant variation from normal. As with the clinical data, variability between patients and between age groups was revealed. Specific patterns of morphology for the individual bones in Crouzon syndrome were determined. The detailed analysis of the severity and extent of the deformities provided insight into understanding of the pathological forces which contribute to the malformation and provided substantial morphological information upon which strategies for surgical intervention can be based.

The nature of the surgical intervention in each of 5 patients was analysed from osseous landmark co-ordinate data derived from the bony elements before and after surgical modification (surgical units), although only short term follow up was available for analysis. A comparison of the dimensions of the pre-operative surgical unit with those of the experimental standard surgical unit further demonstrated the pathological morphology of this condition. The distance of surgical shift of each bony component was measured by comparison of the pre-operative surgical unit with the post-operative surgical unit. This enabled analysis of the methods undertaken and the effectiveness of surgical manoeuvres on patient morphology. Comparison of the post-operative surgical unit with the experimental standard demonstrated the extent of the variation from the experimental standard remaining after surgery. While surgery dealt with the functional considerations, the morphological analysis demonstrated that only the facade of the pathology was manipulated in the patients examined.

The present investigation demonstrates the clinical and radiographic features, in detail, of the craniofacial morphology of Crouzon syndrome. Quantification from three dimensional computed tomography reconstructions provides detailed information on the pathological morphology for each individual with Crouzon syndrome and is able to demonstrate some of the changes occurring immediately after surgical manipulation. This analysis, utilising a recently developed method, re-examines these issues and provides the framework for future developments in this field.

CHAPTER 1

INTRODUCTION

1.1 Background to the Present Investigation

Crouzon syndrome is an autosomal dominant inherited condition with complete penetrance and variable expressivity. Sporadic cases are also common. Recent genetic research has identified an abnormality, located on the long arm of chromosome ten, at the site of the gene that encodes for fibroblast growth factor receptor 2 (Preston et al., 1994; Reardon et al., 1994; Li et al., 1994). Crouzon syndrome is expressed as a complex disorder primarily of bone development. While involvement of the craniofacial skeleton is most profound (and diagnostic), other regions of the body may also be involved (for example, cervical spine and elbows). Examination of the craniofacial skeleton reveals fusion of the calvarial sutures, shallow orbits producing proptosis, and maxillary hypoplasia leading to a Class III malocclusion, all with variable severity related to the variable expression of the gene and the age of the patient (Figure 1.1). The bony distortion also produces structural and functional effects on adjacent structures. The development of the brain, the eyes, the ears, normal speech, the upper airway, the occlusion and the soft tissue envelope may all be disturbed to varying degrees. Variation within the disorder is a common feature and adds to the difficulty in assessment and management.

In 1912 in Paris, Crouzon produced a clear and detailed description of the calvarial, orbital and maxillary deformity in a 29 year old woman and her 3 year old son. The mother had a broad frontal bone with a prominence at the apex of the skull and ridging in the parietal region. Exophthalmos, a divergent squint, marked prognathism, lower lip protrusion and a parrot's beak nose were also noted. The son had similar features, including a high arched palate. Two cousins had a mild deformity and Crouzon believed a "forme fruste" existed. He suggested a teratological basis to the condition and emphasised the familial nature by naming the condition 'hereditary craniofacial dysostosis'.

Two years later, Chatelin published his thesis on Crouzon's cases. He described the radiographic deformity of the thin vault walls with increased digital markings. He found an increased facial angle and a reduction in the height of the maxilla, which accounted for the facial deformity.

The first case where the condition was neither inherited or familial, was reported by Comby in 1926.

One of the earliest theories of the patho-physiology of craniofacial dysostosis described the condition as a 3 stage process (Crouzon and Regnault, 1933). The first stage consisted of calvarial synostosis and maxillary hypoplasia. The second stage comprised compensatory dilatations of the skull, either as wide fontanelles or with increased digital marking on the endocranium. The third stage, which may or may not occur, was typified by compression of the brain, which they believed produced the headaches, mental retardation, anosmia. exophthalmos and lastly, blindness.

The first large study of 219 patients with craniosynostoses included 15 with Crouzon syndrome (Bertelsen, 1958). Details of the cranial and orbital deformity were highlighted, such as the depression of the cribriform plate of the ethmoid bone with lateral displacement of the ethmoid air cells into the orbit, contributing to the proptosis and hypertelorism.

Surgical treatment of craniosynostosis was advocated for the prevention of mental retardation and blindness. Initial difficulties in the late 19th century were overcome with the advent of safe neurosurgery in the early 20th century and in 1927, Faber and Towne performed a prophylactic linear craniectomy on a baby with premature synostosis. This surgery was also performed on children with Crouzon syndrome. In 1948, Ingraham et al. used alloplastic materials to wrap around the edges of the linear craniectomies, in order to prevent regrowth and recurrent synostosis. This method has now been widely discarded. Safety and surgical results improved as the procedures became standardised.

While the functional benefits of the neurosurgical procedures were readily appreciated, attempts at aesthetic correction of the maxillary deformity of the Crouzon face only occurred in the 1950's. Facial maxillary reconstruction was pioneered by Gillies, based on his experience in

Figure 1.1 Variation in clinical presentation of three patients with Crouzon syndrome at different ages. (a) Infant. (b) Five years. (c) Adult.

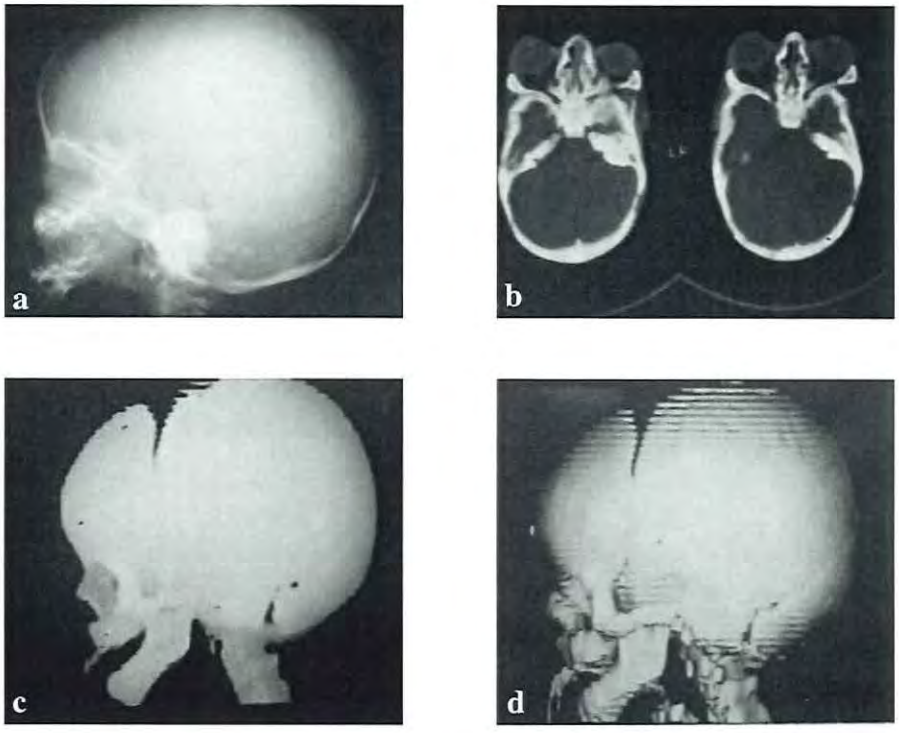

Figure 1.2 Imaging methods of an infant with Crouzon syndrome. (a) Lateral radiograph. (b) Axial CT scan. (c) 3D CT reconstruction. (d) 3D CT enhanced reconstruction.

the First and Second World Wars. Together with Harrison, he performed a Le Fort osteotomy for maxillary correction of Crouzon syndrome in 1951, offering dramatic improvement in facial aesthetics for the first time. From 1958 into the 1970's, Tessier pioneered the concept of craniofacial surgery, initially treating the facial deformities of Crouzon and Apert syndromes. By combining the expertise and experience of the neurosurgeon and the plastic surgeon, anterior facial advancement could be undertaken with safety. This generated the development of multidisciplinary craniofacial units, a concept that has now been well-promoted (Munro, 1975; David, 1977) and adopted world-wide.

The understanding of cranio-facial growth and development has increased at embryological, structural and histo-biochemical levels (Enlow, 1968; Bjork, 1966; Laitinen, 1956). The development of a composite theory of cranio-facial growth involving the primary growth centres interacting with local environmental factors was postulated by Van Limborgh (1970). This combined the intrinsic theories of suture fusion of Virchow (1851), Sicher (1952) and Scott (1956) with the dural attachment concepts of Moss (1954, 1957, 1958, 1959). This composite theory provides a reasonable explanation for the complex variable morphology seen both within a normal population, between races and within the syndromal craniosynostosis patients (David et al., 1982).

The development of concepts of normal growth provide the comparison on which the theories of pathological deformity are based and provide a rationale for the management for these conditions (David et al., 1982). Craniosynostosis has been broadly divided into primary and secondary, with the primary craniosynostosis being divided into the syndromal and non-syndromal types (David et al., 1982). Cohen (1975, 1979, 1986) produced a comprehensive study of all the syndromes associated with craniosynostosis. This aimed to clarify syndrome diagnosis in an attempt to improve patient care and genetic counselling.

A detailed examination and review of the clinical disorder of Crouzon syndrome, with documentation of the radiographic abnormalities by cephalometric analysis, was produced by Kreiborg in 1981. His thesis is the benchmark for these aspects of Crouzon syndrome. He assessed both the morphology and growth. The main quantitative findings included flattening of the parietal skull regions, a short and narrow cranial base, short shallow orbits, a short

maxilla which is inclined backwards and retrognathic in relation to the anterior cranial base, a constriction of the naso-pharyngeal airway and an extended head position in relation to the cervical column.

Kreiborg's monograph recognised the need for further investigation into craniofacial anomalies and in particular Crouzon syndrome, when introducing his thesis.

> "The purpose of the present investigation was to describe, and where possible to quantify, the clinical and radiographic aspects of Crouzon syndrome in a relatively large sample with the main emphasis on morphology and growth.
>
> Such information is very scarce in the literature and further knowledge is becoming increasingly needed in view of the dramatic advances in the field of craniofacial surgery which have evolved during the last 10 - 15 years. Furthermore, information derived from such studies may add insight into general developmental mechanisms related to craniofacial morphogenesis."
>
> Kreiborg, 1981

Examination of a dried skull from an individual with Crouzon syndrome provided information on the cranial base pathology (Kreiborg and Bjork, 1982). The majority of descriptions of the craniofacial morphology of Crouzon syndrome have been qualitative. Quantitative data has been produced using surface measurements or two dimensional (2D) radiographs (Kolar et al., 1988; Kreiborg, 1981).

Significant advances in radiographic imaging have occurred since the 1960's. Computed tomography (CT), (Hounsfield, 1973), now with three dimensional (3D) reconstructions (Herman and Lui, 1977), produces images which provide greater detail of the craniofacial structures. These methods are now widely available. Conventional radiography produces a 2D image by overlapping the points from 3D structures. These overlapping points interfere with the visualisation of many areas, particularly in the craniofacial region. CT scans produce high resolution tomograms, visualising the area of interest without the interference of any other structures. 3D reconstruction from tomographic data produces an image of the craniofacial

skeleton which is an accurate spatial representation of the patient and is, therefore, easier to interpret (Abbott, 1988) (Figure 1.2).

Quantifying the 3D CT data provides a detailed and accurate description of the bony morphology. The data may be analysed in several ways. The advantage of reproducing 2D cephalometric measurements from the 3D CT data is the ready availability of normal data for comparison but this approach does not utilise the 3D advantage. Volumetric measurements have produced useful information on pre- and post-operative volumes of the cranial vault and orbits, providing a quantitative assessment of the effects of surgical intervention (Bite et al., 1985; Posnick et al., 1992). Limited regional investigation of the cranio-orbito-zygomatic complex has also been undertaken using 2D CT slices (Carr et al., 1992). In 1988, Abbott developed techniques of landmark identification and measurement of the craniofacial skeleton from the 3D CT reconstruction images.

After further modifications of the methods for 3D CT landmark identification and analysis (Abbott et al., 1990a; Abbott et al., 1990b), this anatomical approach has been adopted by the ACFU. By analysing each bone and measuring its dimensions as an individual anatomic unit, information about the complex integrated structure of the craniofacial skeleton becomes available. In particular, it is possible to measure the dimensions of the interfaces between the cranial bones, that is, the sutures and synchondroses. The development of appropriate 3D experimental standards from age-matched controls using the same method, provides the opportunity to compare the structural configuration of the craniofacial skeleton of the patient with that of the standard and comment, in some detail, on the morphological differences.

These events, combined, with the awareness for the need for continued investigation in this field, led to the investigations reported in this thesis.

1.2 The Objectives of the Project

The objectives of the project were:

(i) to contribute to the current understanding of the variation and severity of the clinical manifestations of a population of patients with Crouzon syndrome and the related medical, social and surgical management problems.

(ii) to develop a quantitative description of Crouzon syndrome, based on the determination of the position of anatomical landmarks in 3D, derived from CT scan data;

(iii) to develop an experimental standard devised from an unaffected population, to enable statistical comparison between the data from patients with Crouzon syndrome with the data from an age-matched normal population. This analysis may define a common pattern or patterns of pathology in these individuals;

(iv) to compare the pre- and post-operative positions of craniofacial elements to determine the short term effects of surgery (No long term follow up data was available to allow for analysis of degree and rate of relapse or the long term results); and

(v) to use this analysis to demonstrate the detailed information generated by three dimensional computed tomography measurements on the pathology of Crouzon syndrome enabling a new assessment of the underlying pathological processes of Crouzon syndrome that may help in improving the strategies required to deal with the complex management issues.

1.3 The Significance of the Project

The significance of this project is fourfold.

Firstly, the population data collected in this study represent a large addition to the body of information of the natural history of Crouzon syndrome, reporting both the pathology and treatment of this condition.

The application of a method for measurement in three dimensions for describing craniofacial morphology has been applied and evaluated, showing it to be reproducible and accurate.

The measurement data collected (in 3D) for Crouzon syndrome describes in detail a large number of anatomical structures in the craniofacial region and highlights the complex and variable nature of the bony pathology of this condition. This analysis allows a new assessment of the patho-physiology of the craniofacial morphology of Crouzon syndrome. It also has the power to analyse, in detail, the particular deformity of an individual, potentially allowing the surgical correction to be tailored to the individual, rather than the reverse.

Finally, the short term effects of surgical intervention are scrutinised by the pre- and post-operative 3D measurements, and this comparison challenges us to strive to improve the strategies for surgical correction of the deformities in this syndrome.

In summary, the understanding of this condition has been increased by both the qualitative description of the clinical data and the quantitative CT analysis. This has implications for how the diagnosis is made, for the long term management of the condition and for the timing of and type of surgical treatment.

CHAPTER 2

THE CLINICAL AND RADIOGRAPHIC FEATURES OF A POPULATION WITH CROUZON SYNDROME

2.1 Introduction

The Australian Cranio-Facial Unit (ACFU) (formerly South Australian Cranio-Facial Unit) was formed in 1975 at the Women's and Children's Hospital (formerly Adelaide Children's Hospital) in conjunction with the Royal Adelaide Hospital. The aim was to assess and treat patients with congenital and acquired cranio-facial deformities. The ACFU now provides a well-established and comprehensive service to Australia and South East Asia. The evaluation and documentation of a large population of patients with craniofacial disorders, over a long period of time, provide the source for the clinical and radiographic data which are analysed here.

This chapter presents the detailed clinical and radiographic data of the population of 59 patients with Crouzon syndrome seen at the ACFU between 1975 and 1992. The natural history of this condition is demonstrated and complements the data generated in the only other published large population study of Crouzon syndrome reported by Kreiborg in 1981. In addition, the effects of surgical intervention on this natural history are reported. Cephalometric analysis and growth studies were not performed, however the findings reported by Kreiborg are reviewed where relevant. The ACFU patient data and accompanying literature review provide the background for the quantitative analysis of Crouzon syndrome described in the following chapters.

2.2 The Population

A total of 59 patients with Crouzon syndrome from the ACFU in Adelaide, South Australia were available for study. The patients attended between 1975 and 1992. A total of 19 patients was personally examined by the author in 1988 and 1991.

On initial investigation, a larger number of patients (n = 74) was identified. Fifteen of these

patients were not included in the study. Seven of the 15 were seen by team members of the ACFU in overseas clinics or recorded by correspondence only and hence, inadequate information was available for assessment. Eight patients had their diagnosis amended after careful analysis, with the Medical Genetics Department, of the clinical notes, radiographs and photographs. The amended diagnoses included Pfeiffer syndrome (1 case), Saethre-Chotzen syndrome (5 cases), maxillary hypoplasia (1 case), and familial bicoronal synostosis (1 case).

In the population studied, a wide range of presentations was seen, due to the nature of referrals from local, interstate and international sources - from neonates to adults who had had no treatment or multiple procedures at other centres. The data analysis was therefore of a markedly heterogeneous group.

2.3 Method of Data Collection

The clinical and radiographic data from 1975 to 1992 were reviewed for this thesis. Regular review of patients by all members of the multidisciplinary craniofacial team (including radiology) and the completion of standardised examination and treatment protocols since 1975 produced a vast bank of data available for study. The common difficulties of retrospective patient record review were minimised by this standardised approach. Unfortunately, not all clinical and radiographic aspects for all 59 patients had been recorded. Table 2.1 details the number of patient records available for each component assessed.

2.4 Results and Discussion

2.4.1 Demography

Sex Distribution

Of the 59 patients with complete records, there were 33 females (56%) and 26 males (44%). The sex distribution in Kreiborg's sample was found to be 46% females and 54% males. Crouzon syndrome has an approximately equal sex distribution consistent with its autosomal dominant inheritance pattern.

Age at Presentation

The age at presentation is shown in Table 2.2.

Table 2.1 Number of patient records available for the analysis of each parameter

Demographic Data		59
Genetic Data		57
Cranial Morphology		53
Central Nervous System	(clinical)	59
	(CT scan)	40
Ophthalmology		52
Otorhinolaryngology		46
Speech and Occlusion		52
Non-craniofacial		
Cervical Spine	(radiographic)	42
Upper Limb	(clinical)	55
	(radiographic)	12
Psychosocial		59
Surgical Management		59
Deaths		59

Table 2.2 Age of 59 patients with Crouzon syndrome at presentation to the ACFU

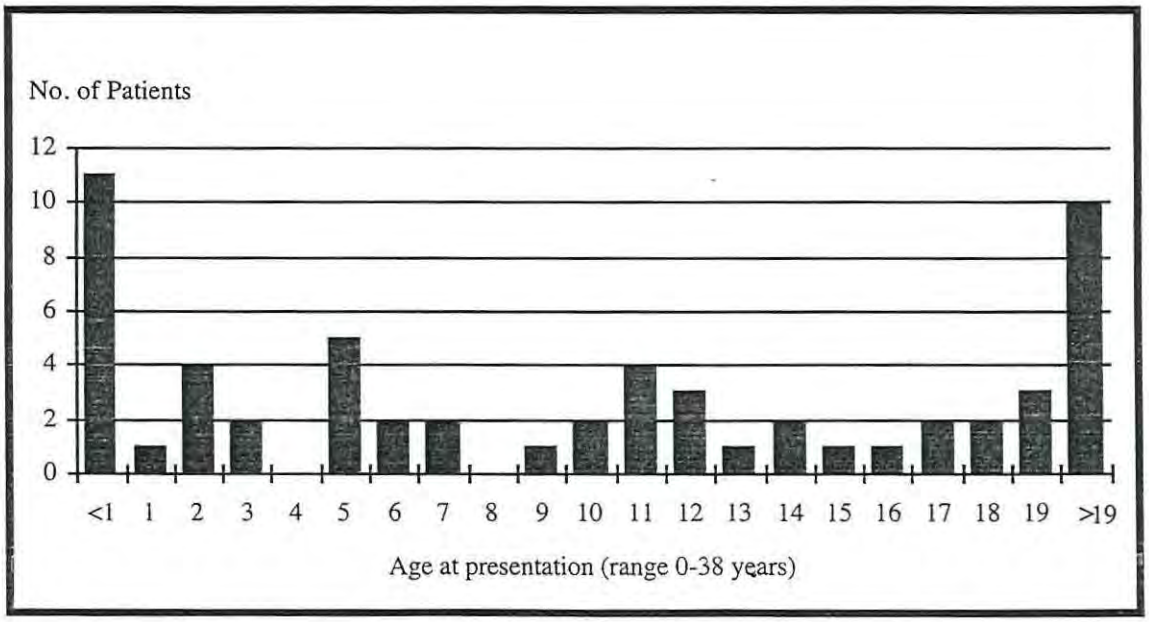

The age at presentation is important as the condition varies with time and this determines the type of treatment. Eighteen patients were seen under 3 years of age, when rapid brain enlargement and development still greatly influences the shape of the skull. Eleven patients presented before 1 year of age with 10 of these in the first 3 months of life. At this age, surgical release of sutures may optimise the correction of the calvarial deformity. Ten children were seen between the ages of 3 years and 10 years. In this period, treatment is predominantly expectant (David et al., 1982). Thirteen patients were aged from 10 and 15 years, when orbitostenosis and faciostenosis are most evident and growth is nearing completion, allowing definitive functional and cosmetic surgical correction to be undertaken. Eighteen adults (16 years and over) were also seen. The surgical treatment of all patients is more fully described in 2.4.10 (Surgical Management).

Country of Origin

Thirty nine patients were from Australia, and 20 were resident in other countries (Table 2.3).

Table 2.3 Country of origin of 59 patients with Crouzon syndrome presenting to the ACFU

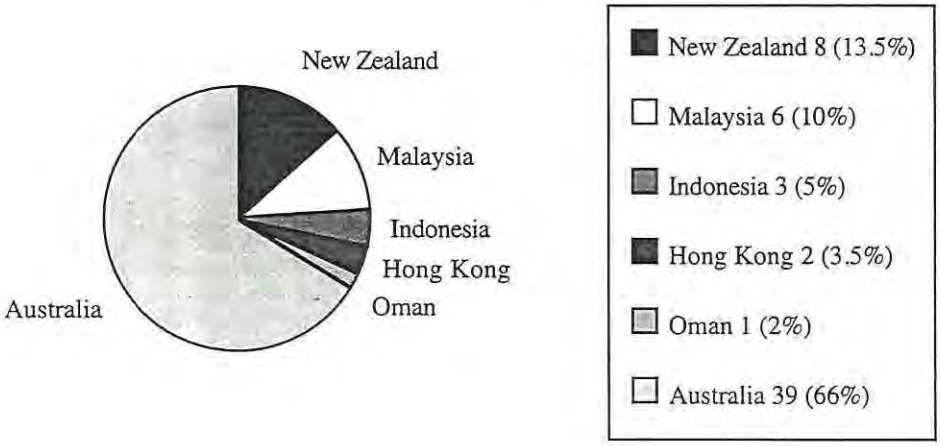

Trends in the type of referrals reflect the changing patterns of surgical practice. The majority of referrals have come from within Australia. Sixteen of the 39 Australian patients have come from within the State of South Australia. The patients from Australia and New Zealand were of European Caucasian background. Of those from Malaysia, Indonesia, Hong Kong and Oman, 5 were of Chinese origin and 7 were native South East Asians. The ACFU provides assistance

to Asian countries neighbouring Australia, where craniofacial expertise is not available and referrals from this source have grown.

Birth Rate

Crouzon syndrome accounts for between 3 and 7% of all the craniosynostosis patients (Bertelsen, 1958; Hunter and Rudd, 1977). Cohen (1986) initially reported a frequency of approximately 1 in 25,000 of the general population. Martinez-Frias et al. (1991) reported the birth prevalence of 15.5 per million (equivalent to 1 per 64,500 live births), and this was comparable with the prevalence found by Cohen and Kreiborg (1992) using the indirect method (16.5 per million).

Since 1975, 7 children have been born with Crouzon syndrome in South Australia. This reflects an approximate prevalence of 1 per 41,400 live births (based on a mean of 19,319 live births per year from 1979 to 1989 inclusive, S.A. Health Commission.). This is equivalent to a birth prevalence of 24.2 per million. In all studies, it is possible that infants born with mild forms have not been recognised in the community and hence have not been referred to craniofacial or other medical centres, thereby underestimating the birth prevalence. On the other hand, if no children with Crouzon syndrome are born in South Australia in the next few years, the birth prevalence may be over-estimated. This is supported by other data (Martinez-Frias et al., 1991; Cohen and Kreiborg, 1992).

Previous Surgery

Of the 59 patients who presented, 23 had undergone 1 or more surgical procedures prior to attending the ACFU (Table 2.4). The most common operations were craniectomies and/or shunt insertions in infants or children. Five corrective craniofacial procedures had been performed at other centres and the tracheostomies listed were related to these procedures. Three patients had previously had mandibular surgery; 2 had mandibular setbacks in an attempt to improve the facial profile and a third was a child who had a bilateral condylectomy to reduce the degree of relative mandibular prognathism that had been predicted to occur with growth. Eye surgery was limited and several cosmetic procedures had been performed. Further discussion of surgery is found in 2.4.10 (Surgical Management).

Table 2.4 Previous surgical procedures (often multiple) in the population of 59 patients with Crouzon syndrome presenting to the ACFU

None		36
Neurosurgery		
	Craniectomies	17
	Shunt	3
Craniofacial surgery		
	Fronto-orbital advance	2
	Mandibular surgery	3
	Fronto-facial advance	1
	Tracheostomy	2
	Le Fort III osteotomy	1
	Repair Dural Tear	1
	Le Fort I osteotomy	1
Ophthalmological surgery		
	Tarsorrhaphy	3
	Squint correction	2
Aesthetic surgery		
	Bone Graft	1
	Dermo-fat graft	1

Conclusion

When reviewing the data obtained from these patients, it should be borne in mind that the ACFU has been presented with a diverse population of patients; from many countries, at various ages and often following surgical intervention. Drawing conclusions from these patients is compounded by a deforming condition which itself varies between individuals and that changes with the growth of the individual.

2.4.2 Medical Genetics

Crouzon's original description (1912) was the first to describe the hereditary nature of this condition. Numerous family studies have since been reported, and demonstrate an autosomal

dominant inheritance, with complete penetrance and variable expressivity (Flippen, 1950; Bertelsen, 1958; Shiller, 1959; Cohen, 1975; Kreiborg and Jensen, 1977; Kreiborg, 1981). Sporadic cases are presumed to be new mutations. Recent genetic research has identified an abnormality, located on the long arm of chromosome ten in patients with Crouzon syndrome, at the site of the gene that encodes for fibroblast growth factor receptor 2 (Preston et al., 1994; Reardon et al., 1994; Li et al., 1994). At the ACFU, a reliable family history was recorded in 57 of the 59 individuals studied. Fourteen of these 57 patients had a positive family history consistent with autosomal dominant inheritance, representing 24.6% of the sample (Table 2.5).

Table 2.5 Genetic data recorded from the population of 57 patients with Crouzon syndrome

	Familial	Sporadic
No. of Patients	14	43
Percentage of Total	24.6 %	75.4 %

Variable expressivity was seen in the family members. The remaining 43 patients (75.4%) represent new mutations, a figure which is high relative to those quoted in other studies by Atkinson (1937) of 38% and Kreiborg (1981) of 56%. The reason for the high level in this population is not clear. Atkinson reviewed the first reported cases in the literature and commented on their pattern of inheritance. It is probable that the early reports he reviewed were biased towards the familial cases, which were more easily recognised and consistent with the initial familial reports of Crouzon (1912). Kreiborg's sample represented an older population than that seen at the ACFU. As a result, there were more adults of child bearing age in his sample and hence offspring with the syndrome.

Jones et al. (1975) and Kreiborg (1981) have found that increased paternal age at the time of conception is statistically significant in producing new mutations in Crouzon syndrome. Of the 28 Australian-born patients with no family history, the paternal age was recorded in 23 and the maternal age in 22. The median paternal age was 35 years (range 22-56) and the mean maternal age was 30 years (range 21-39). The median paternal age in Australia ranged from 29.1 in 1960, increased to 31.1 years in 1989 with a median of 30.0 years (Australian Bureau of

Statistics). This is lower than in the Crouzon population. The median maternal age was recorded from 1980 to 1989, ranging from 26.13 to 27.93 with a median of 26.97.

Of the 17 patients older than the age of 16 studied in this series, 3 had offspring with Crouzon syndrome. A woman and her son were already under the care of staff members of the Adelaide Children's Hospital (now Women's and Children's Hospital) when the South Australian Cranio-Facial Unit (now ACFU) was formed in 1975. A 31 year old man moved to Adelaide from New Zealand, where he had undergone maxillary surgery. At the time of his presentation, his wife was pregnant. Genetic counselling indicated the 50% risk to their unborn child. Their daughter was born with the condition. Older sibs in these 2 families were not affected. The third patient, seen as an adult, was counselled regarding the 50% risk of having an affected child. She decided to have a child and her daughter had typical features of Crouzon syndrome of a less severe nature than her mother.

While the method for genetic screening for Crouzon syndrome has not been developed, prenatal diagnosis in parents with a family history may be aided by ultrasound examination. Prenatal diagnosis of Crouzon syndrome was suggested by routine ultrasound investigation at 22 weeks gestation in a twin pregnancy at the ACFU. Repeat ultrasound examination at 35 weeks confirmed the diagnosis of craniostenosis and proptosis (Figure 2.1). The father had mild features of craniostenosis. Subsequent delivery of twins with Crouzon syndrome occurred at 36 weeks (Figure 2.2). Details of the clinical features of the twins were published (David et al., 1991) and are described later in the relevant sections. Despite 36 patients having received formal genetic counselling, which included discussion with ACFU staff, many patients subsequently reported inadequate knowledge of the genetic implications of their condition. Several cases required further counselling.

2.4.3 Cranial Morphology

Variable cranial shape has been widely reported in Crouzon syndrome and the population at the ACFU was examined to determine the degree of variation. Head shape was assessed by cranial width and length measured on presentation. The cranial index (C.I.) was calculated (C.I. = width/length). Head circumference measurements and radiographic examination of suture patency and evidence of a copper-beaten appearance were also studied.

Figure 2.1

Ultrasound of a 35 week old fetus showing brachycephaly and proptosis consistent with Crouzon syndrome.

Figure 2.2 Twin infants with Crouzon syndrome.

The C.I. ranged from 62.7 - 105.4 with a mean of 83.2 (Table 2.6). The majority of the patients (66%) had a brachycephalic head shape (C.I. > 80). Eleven patients had oxycephaly in association with the brachycephalic skull shape and 5 cases of triphyllocephaly were seen in this sample of Crouzon syndrome, all with the C.I. > 85 (range 88.6 - 105.4).

Ten patients (19%) had a C.I. < 75 (dolichocephalic) and 3 cases had marked scaphocephaly where the C.I. was less than 70. No cases of trigonocephaly were seen. Patients with significant plagiocephaly were not included in the diagnosis of Crouzon syndrome.

Variation of the cranial shape was noted by Crouzon in his early studies of the condition. Bertelsen (1958) found the C.I. ranged from 71.7 - 97.5 (mean 79.3) in the 10 patients he examined and remarked that such a range of variation had not been observed in any form of simple cranial synostosis. Bertelsen also noted a familial tendency to have similar head shapes. Kreiborg, on the other hand, found great variation in the head shape of his group, along with variation in maxillary deformity and in the degree of exophthalmos. Only 3 families were examined in the ACFU series, making the data inconclusive. A father and daughter were both scaphocephalic with indices of 67.3 and 62.7 respectively, a mother and daughter had indices of 86.1 and 73.1, with twin brothers having indices of 104.4 and 105.4.

Table 2.6 The cranial index measured in 53 patients with Crouzon syndrome at the ACFU

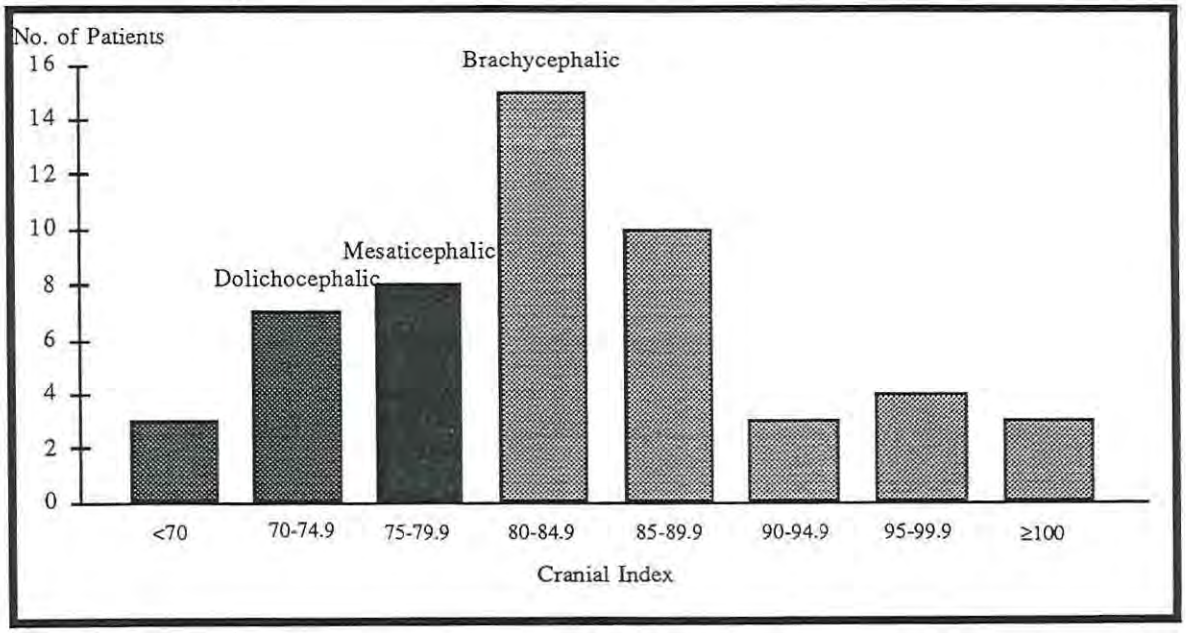

Head circumference measurements were spread between the 2nd to 98th percentiles of the normal population (22 below the mean for the normal and 21 above). Four patients were above the 98th percentile and 2 were below the 2nd percentile. Kreiborg's population (1981), on the other hand, had a statistically significant smaller head circumference than their normal population, with 80% of patients measurements below the mean.

In Crouzon syndrome, radiographic evidence of calvarial suture patency does not imply that sutural growth is normal; however, absence of a cranial suture before the age of 30, excluding the metopic suture, is indicative of a pathological condition. Computerised tomography has improved the ease of detection of patent sutures, particularly in the 2D axial cuts through the calvaria. The radiographs in this series revealed 1 or multiple sets of fused sutures in 92% of patients. Of these patients, the distribution of sites of suture fusion is recorded in Table 2.7. The most common site of fusion was at the coronal sutures. All patients over the age of 15 had all sutures fused. Five infants did not have radiographic evidence of suture synostosis, despite showing signs of craniostenosis. Partial suture fusion, low coronal suture fusion, or incomplete suture calcification may account for this finding.

Table 2.7 Calvarial suture fusion determined by radiographs in 59 patients with Crouzon syndrome at the ACFU

Normal appearance	5	9%
Coronal suture absent	6	10%
Coronal + Sagittal sutures absent	3	5%
Coronal + Sagittal + Lambdoid sutures absent	42	71%
Sagittal + Lambdoid sutures absent	3	5%

Increased digital markings are often seen in the craniosynostosis patient (Bertelsen, 1958). While the radiographs of 74% of patients in this series exhibited this feature (Figure 2.3), Kreiborg found that more than 90% of his patients had this radiographic finding. This has been related to a "chronic" degree of raised intracranial pressure with increased endocranial bone resorption. It may also be present in acute raised intracranial pressure. Following craniotomy and alleviation of the raised pressure, the copper-beaten appearance usually reduces in severity. The markings also decrease with time, presumed to be due to a cessation of brain growth and continued calvarial bone growth (Kreiborg, 1981).

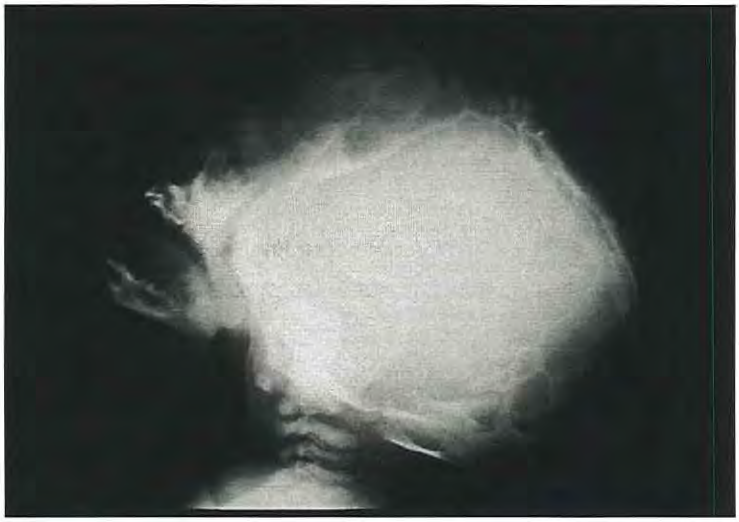

Figure 2.3 Lateral radiograph of an infant with Crouzon syndrome showing a copper–beaten appearance.

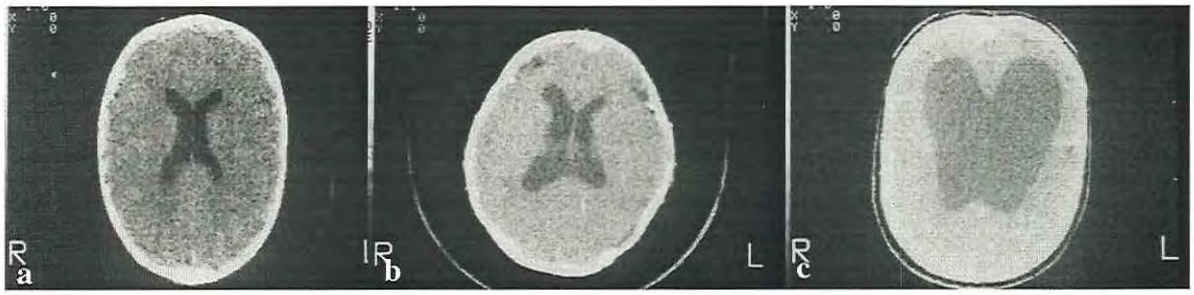

Figure 2.4 Ventricular patterns found on CT scan in patients with Crouzon syndrome. (a) Mild enlargement. (b) Moderate enlargement. (c) Severe enlargement/hydrocephalus.

Figure 2.5 CT scan of a patient with Crouzon syndrome showing schizencephaly.

2.4.4 Central Nervous System

For centuries, an abnormal appearance has been assumed to imply a reduced intelligence due to both folklore and ignorance. Despite the potential for bony distortion interfering with neurological function, the majority of individuals with Crouzon syndrome have normal intelligence. The most common intracranial problem is raised intracranial pressure which is found in a number of cases and may cause headaches and papilloedema. This may lead to loss of eyesight and decreased intellectual performance in some, but not all, untreated patients.

The central nervous system is intimately related to the developing cranial bones. Indeed, it was the disturbance in cerebral and visual function by the craniostenosis which prompted the development of surgical intervention. Headaches, deterioration in mental and visual function along with radiographic evidence of craniostenosis are regarded as primary indications for surgery.

Clinical Findings

Neurological problems included epilepsy in 3 patients. Headaches were reported in 8 patients, which were consistent with raised intracranial pressure in 5 children and related to sinusitis, post-operatively, in 2 adults. No cause for intermittent headache was found in the final patient despite investigation, and the problem resolved spontaneously with time. Many patients (n = 25) underwent neuro-psychological testing and decreased intelligence (intelligence quotient < 70) was found in only 3. Many infants exhibited some degree of developmental delay related to poor feeding, obligatory mouth breathing and recovery from surgery. Future assessment of mental function in this group will be of interest.

Central Nervous System Imaging

In the past, autopsy examination, air ventriculography and angiography provided the best information about the morphology of the central nervous system (CNS). Improvements in non-invasive imaging (CT and Magnetic Resonance (MR)) have allowed the structure and form of the central nervous system to be examined in greater detail (Proudman et al., 1995).

Thirty eight CT head examinations were available for review. Some had been performed during CT examination of the craniofacial skeleton and the CT slices were taken parallel to the Frankfort horizontal. One CT scan did not extend to the cranial vertex giving an incomplete view of the ventricles. Brain scans were performed at 1 cm thick slices at 1 cm intervals and the films were reviewed with an experienced neuro-radiologist. The radiographs were examined for ventricular size. An increase in ventricular size was graded subjectively into three groups; mild ventriculomegaly, moderate ventriculomegaly and severe ventriculomegaly. Asymmetry of the ventricles, change in ventricular size following surgery and any other white and grey matter (non-ventricular) findings were also reported. One patient had an MR scan performed.

Ventricular Findings

Radiographic review demonstrated that 6 of the brain scans were within normal limits. A further four patients had been shunted prior to their initial examination at the ACFU and also had ventricular size and shape within normal limits. The most striking finding on the remaining CT scans was the lateral ventricular pattern (Table 2.8, Figure 2.4). Twenty five cases had some degree of ventricular enlargement. This ranged in severity from mild non-progressive ventriculomegaly in 18 patients to ventriculomegaly of a moderate degree in 4 and to a severe degree (hydrocephalus) in 3 (Figure 2.4). Asymmetry of lateral ventricular dilatation was evident in 7 cases and, in 9 patients, prominence was seen of the anterior (1), posterior (1), or temporal horns (7). The third ventricle was enlarged in 16 cases whereas the fourth ventricle was abnormal in only 1 instance. Thirteen patients had both enlarged third ventricles and ventriculomegaly. A degree of cerebral aqueduct stenosis or a structural brain abnormality may be responsible for this. The extracerebral fluid space was prominent on 7 of the CT scans. Whilst it was uniformly enlarged in 5 cases it was restricted to the cisterna magna in one case and in the anterior temporal region in another.

Non-ventricular Findings

Non-ventricular deformities were not seen as frequently as ventricular abnormalities (Table 2.9). Schizencephaly in the left temporal region was seen in 1 case (Figure 2.5). A wide arachnoid space adjacent to the pineal gland in another patient suggested the appearance of a possible arachnoid cyst or a dermoid. The septum pellucidum was not visualised in some slices

of the scans of 2 patients (although the scans were of good quality), suggesting absence of this structure. Decreased cerebral mass was found in 1 patient.

Follow up CT scans were available in 11 patients, including 4 of the infants who underwent shunt insertion. In 1 patient, hydrocephalus with raised intracranial pressure was evident at the time of presentation, the initial procedure being a shunt decompression. In other cases, hydrocephalus without raised intracranial pressure had been managed expectantly.

Table 2.8 Ventricular abnormalities seen on CT scan in 35 patients with Crouzon syndrome at the ACFU

- Lateral Ventricular abnormality		
	Ventriculomegaly	
	Mild	18
	Moderate	4
	Severe/Hydrocephalus	3
	Lateral Ventricle Asymmetry	
	Left	6
	Right	1
	Prominent Ventricular Horns	
	Anterior	1
	Posterior	1
	Temporal	7
Enlarged Third Ventricle		16
Enlarged Fourth Ventricle		1

Table 2.9 Non-ventricular abnormality seen on CT scan in 35 patients with Crouzon syndrome at the ACFU

Schizencephaly	1
Wide arachnoid space adjacent pineal	1
Partial absence septum pellucidum	2
Decreased cerebral mass	1

Fronto-orbital advance and posterior craniectomy had been performed in some cases, allowing the dilated ventricles to assist the brain drive promoting calvarial growth (Hanieh et al., 1989). Following surgery, the patients were monitored by repeated clinical examination, cranial ultrasound or CT scan. Four infants required shunt insertion after surgery following progressive hydrocephalus.

On the other hand, 7 patients (aged 2-28 years) had no change in their ventricular pattern on repeat CT scan (3 months to 4 years later). Six of these had decompressive surgery, such as fronto-orbital or fronto-facial advancement and 1 had no surgery at all. This finding suggests that the calvarial craniostenosis does not necessarily play a role in the development of the ventricular pattern. Ventricular shape is, therefore, most likely related to a primary brain deformity. The cranial base which is not operated on, may locally influence the development.

Clearly, some patients will develop progressive hydrocephalus, and some will not; there do not appear to be any predictive factors seen on CT.

Magnetic resonance imaging was performed in 1 patient, aged 11 years, with failing eyesight due to raised intracranial pressure. This demonstrated the optic nerve sheaths distended by subarachnoid fluid, consistent with the clinical picture. The ventricles were not grossly enlarged but showed mild ventriculomegaly with asymmetry. The corpus callosum and gyri appeared normal. The sella turcica appeared to be slightly larger than normal and there was evidence that the pituitary was compressed by either the third ventricle or the suprasellar cistern extending into the fossa. Following bilateral decompressive craniotomies, repeat MR imaging showed improvement in the optic nerve distension; however the pituitary fossa findings persisted. This method of investigation provides valuable information on the CNS structure.

Discussion

Early reports of brain pathology in Crouzon syndrome are autopsy case reports or larger studies which examine all the craniosynostoses together (Eshbaugh, 1948; Gross, 1959). Findings include hypoplasia of the corpus callosum, micro-gyri and features suggesting a change in proportions of the brain, that is, decreased volume in the middle and anterior cranial fossae, stretch of the diencephalon and firm flattened gyri (Eshbaugh, 1948; Gross, 1959). They

supported the concept that distortion of the cranial bones by the synostosis is responsible for the distortion of the brain.

Since these reports, patient management has improved, particularly in the areas of radiological investigation and surgical techniques. Attention has been directed to the relationship between mental retardation, hydrocephalus, raised intracranial pressure and craniostenotic deformity. The information which has emerged is worthy of review.

Carmel et al. (1981) reported the CT scans of 24 patients with simple craniostenosis and found distortion of the ventricular system associated with sagittal, unicoronal and lambdoid synostosis. Following surgical release, many of the distortions tended to correct themselves, suggesting the abnormalities were due to increased local pressure on the brain at the fusion site.

Renier et al. (1982) measured the intracranial pressure (ICP) in 92 patients with craniosynostosis (including 4 with Crouzon syndrome) and found it to be elevated in one third, normal in one third and borderline increased in one third. Following surgery, the ICP measurements reverted to normal. A statistically significant relationship between raised ICP and decreased mental level was identified and they recommended that ICP measurement may be useful in determining the optimal timing of surgical intervention.

Many studies have reported hydrocephalus in association with Crouzon syndrome (Fishman et al., 1971; Hunter and Rudd, 1977; Marsh and Vannier, 1985; Noetzel et al., 1985; Hanieh et al., 1989). Noetzel et al. (1985) prospectively performed CT scans on 50 patients with craniosynostosis including 12 with Crouzon syndrome. Six of the Crouzon CT scans were normal, 2 showed hydrocephalus and the remaining 4 demonstrated non-progressive ventriculomegaly - a moderate ventricular dilatation that did not progress over time and was not associated with raised intracranial pressure. Little, if any, change was seen following craniofacial surgery. In Crouzon and other craniosynostosis conditions, they found that the dilatation was almost always asymmetric, with usually a normal appearance of the temporal horns. They postulated that the ventriculomegaly was a distinct entity from hydrocephalus, but that it also resulted from abnormal development of the central nervous system and not from the local effects of the fused sutures.

Golabi et al. (1987) reported 3 cases of Crouzon syndrome with hydrocephalus in a series of 250 patients with craniosynostosis. This series reviews the features of the central nervous system in Crouzon syndrome, as well as in other related synostosis conditions, without differentiating between them.

A comprehensive review of the CNS findings in Apert syndrome was reported by Cohen and Kreiborg (1990). While the abnormalities in Apert syndrome involve an apparently similar craniostenotic process, the CNS abnormalities reported differ from those seen in our series of Crouzon syndrome patients. Cohen and Kreiborg combine their findings with all those described in the literature and do not give an indication of the frequency of each abnormality. It is also not clear in their paper whether radiographic or autopsy examination of the CNS was carried out on all the patients in their group. Presumably insufficient data accounts for the lack of frequency information. However, in examining their own 114 Apert patients, non-progressive ventriculomegaly was found in 2 patients and progressive hydrocephalus in none, although others have reported this finding. Agenesis of the corpus callosum was identified in 5 cases, but this has been reported infrequently in the literature in Crouzon syndrome (Kreiborg, 1981) and was not seen in our patients. Absent or defective septum pellucidum (which may be a marker for congenital anomalies) was seen in 3 of the Apert group and 2 of our Crouzon group.

Many other abnormalities such as megalencephaly, gyral abnormalities, hippocampal abnormalities, encephalocele, apparent malformation of mid-line thalamic structures, hypoplasia of cerebral white matter and heterotopic grey matter were reported in Cohen and Kreiborg's group. Magnetic resonance imaging provides greater detail of the cerebral matter and is therefore more sensitive to abnormalities in this region. Cohen and Kreiborg recommend that this investigation be performed on all patients.

The different trends in the CNS abnormalities of Crouzon and Apert syndromes which are emerging suggest that a primary developmental brain disorder is responsible. A more severe degree of brain matter abnormality in Apert syndrome with a greater incidence of mental retardation is contrasted with the predominantly non-progressive ventricular deformity of

Crouzon syndrome, with a low proportion of mentally retarded individuals. MR imaging of Crouzon and Apert patients need to be undertaken to elucidate this further.

2.4.5 Ophthalmology

Exorbitism is the ophthalmological hallmark of Crouzon syndrome; however, many other deformities may also be seen. In 1958, Bertelsen examined the craniosynostosis with an emphasis on the ophthalmological problems and reported a high frequency of visual impairment. Due to a lack of bony support and protection of the globe, strabismus, exposure keratitis and conjunctivitis may be found.

Fifty ACFU case records with specialist ophthalmologist reports were available for review and the results are presented in Table 2.10.

Exorbitism due to hypoplasia of the bony orbit, was found to a varying degree in all patients. Other ocular abnormalities may accompany this (Figures 2.6 and 2.7). Hypertelorism was found in 78% of patients using medial and lateral canthal and interpupillary measurements (defined as measurements over the 97th percentile). Decreased acuity was found in 24% of ACFU patients. Strabismus was seen in 34%, with keratitis in 14% and optic atrophy in 12%. Kreiborg reported strabismus in 75% of his patients. Half of his cases had exposure conjunctivitis or keratitis, and half had poor vision in 1 or both eyes. Optic atrophy has been recorded by many authors with debate as to its aetiology. Possible mechanisms include raised intracranial pressure (Bertelsen, 1958) or constriction of the optic canals (Wood-Smith et al., 1976). Two patients reported globe dislocation just prior to attending the ACFU for treatment. Tarsorrhaphy was performed as a prophylactic procedure in several cases. Ptosis, either unilateral or bilateral, occurred in 14%. This abnormality is more commonly associated with Saethre-Chotzen syndrome where it is seen in over 75% of patients (Pantke et al., 1975). Orbital dystopia was found to a minor degree in 5 patients (10%), however the other clinical and genetic factors strongly favoured the diagnosis of Crouzon over Saethre-Chotzen syndrome. Nystagmus and coloboma of the iris, reported in other series (Ellis, 1937; Walker and Wybar, 1975; Kreiborg, 1981), were also seen in a few cases (Figure 2.6).

Table 2.10 Ophthalmological abnormalities found in 50 patients with Crouzon syndrome at the ACFU

Orbital			
	Exorbitism		50
	Hypertelorism		39
	Dystopia		5
Ocular			
	Decreased Acuity		12
	Strabismus	divergent	16
		convergent	1
	Optic atrophy		6
	Papilloedema		6
	Nystagmus		2
	Exposure keratitis		7
	Globe dislocation		2
	Coloboma		2
Extra-ocular			
	Oculomotor palsy		1
	Ptosis	bilateral	5
		unilateral	2

In general, fewer abnormal ophthalmological findings were seen in the ACFU group of patients, compared with Kreiborg's group. It is unclear why there is this difference; however, the older mean age of Kreiborg's group of patients may have been a factor in some of the abnormalities. Thirty seven of the 61 patients were over 16 years of age compared with 16 of the 59 in the ACFU group. The oldest patient in Kreiborg's group was 78 years of age, with 2 being recruited from the State Institute for the Blind, Copenhagen. It is also unclear what forms of treatment had been provided to the group of patients. At the ACFU, surgical interventions which provide bony protection to the eyes, fastidious care and early management of eye abnormalities may help prevent loss of vision, the long term sequela of strabismus and keratitis.

2.4.6 Otorhinolaryngology

Deformity of the cranial base and the maxilla may have a profound effect on the structure and function of the ear, nose and throat. This may vary from chronic middle ear effusions to life-threatening airway difficulties.

Figure 2.6

Adult patient with Crouzon syndrome showing proptosis, hypertelorism, strabismus, ptosis and colobomata of the iris.

Figure 2.7

Axial CT scan showing severity of proptosis in a 1 month old infant with Crouzon syndrome.

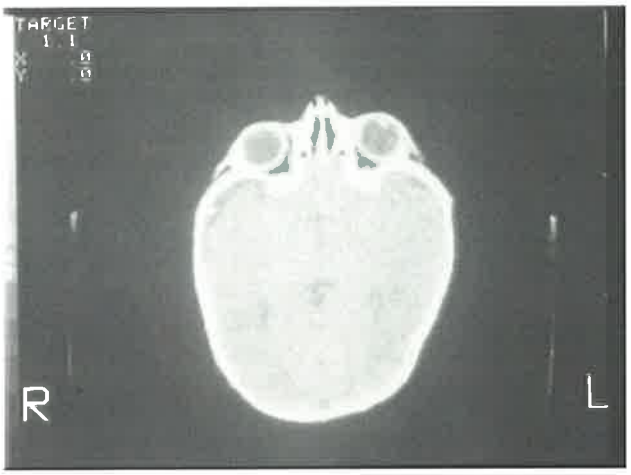

Figure 2.8

3D CT reconstruction of a 15 year old patient with Crouzon syndrome with atresia of the external auditory canal and calcification of the stylohyoid ligament.

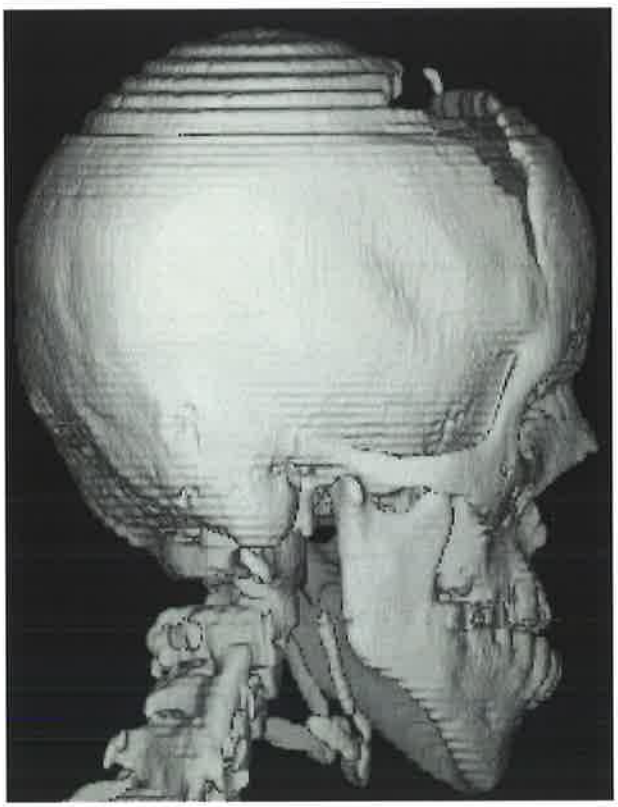

Fifty records of ear, nose and throat examinations of patients with Crouzon syndrome were available. Audiograms were available in a number of cases, as well as some CT scans of the temporal bone for middle and inner ear examination.

Otological findings

External auditory canal stenosis or atresia (Figure 2.8), ossicular chain dysfunction and middle ear effusion and infection are the primary abnormalities seen in Crouzon syndrome and may result in conductive hearing loss (Table 2.11).

Patients with abnormalities of the pinna included 2 with prominent ears and 1 with low set ears. Anthropological measurements (Farkas, 1978) have revealed minor growth variations, with low set and wide disproportionate ears in 2 thirds of Crouzon patients. Grade I microtia has also been recorded in 1 case (Corey et al., 1987).

Atresia and stenosis of the external auditory canal occurred in 20% of patients in this series. The most common bony deformity is temporal bone hypoplasia (Nager and de Reynier, 1948; Baldwin, 1968). Congenital middle ear anomalies and chronic effusions and infections may also contribute to conductive hearing deficits (30%). Kreiborg (1981) found 10% of his patients had atresia of the auditory canals and mild to moderate conductive hearing loss was present in approximately half of his cases.

Table 2.11 Otological abnormalities in 50 patients with Crouzon syndrome at the ACFU

Normal		28
Pinna abnormality		3
External canal stenosis		6
External canal atresia		4
Middle ear effusion/infection		14
Cholesteatoma		2
Mild to moderate conductive hearing loss		15
unilateral	5	
bilateral	10	
Sensi-neural hearing loss		1
Mixed hearing loss		1

An increase in the frequency of ear disease from 37% in infants to 62% in older patients has been observed (Corey et al., 1987). Based on cephalometric data, the authors of this report suggested that the alteration of the naso-pharyngeal skeletal and soft tissue dimensions results in eustachian tube dysfunction, both of which worsen with age. It is possible that early midface advancement surgery may help middle ear function in Crouzon syndrome and prevent loss of hearing, but this is yet to be proven.

Oro-pharynx and Airway

Cleft lip and palate, cleft palate alone and bifid uvulae have been seen in association with Crouzon syndrome by Peterson and Pruzansky (1974), Selle and Jacobs (1977) and Kreiborg (1981). The only palatal deformity seen in the ACFU population was 1 patient with a bifid uvula. Bilateral palatal swellings have been reported in Crouzon syndrome but are more common in Apert syndrome where they have been associated with excess acid mucopolysaccharide in the palatal mucosa (Solomon et al., 1973). In this series, the presence or absence of lateral palatal swellings were not recorded. The palate was described as being high and arched in 40 patients (70%). However, the abnormality may consist of a narrow maxillary arch with palatal swellings, giving the impression of a high midline to the palate. This is supported by Kreiborg's analysis (1981) of dental impressions which found the height of the palate to be normal, but the width of the maxillary arch reduced.

Recent interest has centred on the airway management of patients with Crouzon syndrome in whom airway problems may occur at many levels. A deviated nasal septum may result in partial nasal obstruction. Maxillary hypoplasia producing a shallow and narrow posterior nasal space filled with soft palate and tongue, may also produce nasal airway obstruction. When the structural deformity is significant or the patient has an upper respiratory tract infection, obligatory mouth breathing is seen and the patient may experience obstructive sleep apnoea, with significant oxygen desaturation. This may be particularly damaging in infants, where it may not be detected.

Cephalometric analysis in adults (Kreiborg, 1981) demonstrated that the nasopharyngeal airway is reduced due to a retrognathic maxillary position and a reduced posterior maxillary height. Constriction of the larynx and trachea have also been noted in some cases of Crouzon, Apert

and Pfeiffer syndrome (Devine et al., 1984; Mixter et al., 1990). Correcting upper airway problems will not affect this deformity. The management of airway problems remains controversial and varies with the aetiology of the obstruction (2.4.10 Surgical Management).

2.4.7 Speech and Occlusion

Speech contributes greatly to an individual's ability to communicate, function socially and be accepted by his or her peers. A review of the records of speech assessment in 33 patients was performed. Articulation disorders and hyponasality (usually of a mild to moderate degree) were the most common findings, seen in 30 and 29 of the patients, respectively (Table 2.12). Hypernasality was seen in 5 patients.

Table 2.12 Severity of speech disorder in 33 patients with Crouzon syndrome at the ACFU

	Normal	Mild	Moderate	Severe
Articulation disorder	3	17	12	1
Hyponasality	4	12	13	4
Hypernasality	28	3	2	0

Prior to midface advancement surgery, nasendoscopy was routinely performed. Post-operative assessment and speech therapy are vital in overall patient management.

All the 17 adult patients and the 14 patients aged between 8 and 16, had class III dental occlusion except 2 who had class I occlusion. A detailed clinical description of the dental development is outside the realms of this thesis. Further detail of maxillary structure is reported in Chapter 3.

2.4.8 Non-Craniofacial Features

Introduction

Abnormalities of non-craniofacial regions are minor, but recognised, features of Crouzon syndrome (Proudman et al., 1994). Recognised features include cervical spine fusion, elbow deformity, calcification of the stylohyoid ligament and acanthosis nigricans (Kreiborg, 1981;

Breitbart et al., 1989). While providing an additional dimension to the clinical picture of Crouzon syndrome, these non-obligatory scattered findings may confound the understanding of the condition and its diagnosis. Few large population studies on the non-craniofacial manifestations of Crouzon syndrome are available. This section reviews such a population and addresses some of these issues.

While cervical anomalies in Crouzon patients have been documented in the past, little comment has been made on possible relationships with calvarial severity, progression in pathology with time and growth, and the symptomatic nature of any deformity seen.

Casenotes were reviewed for reports of neck problems and any related neurological problems. 40 patients had radiographs of the cervical spine. Formal spine radiographs were available in 4 patients, with 2 having several studies. Another 36 had lateral and AP cephalometric radiographs adequate enough to be able to make limited comments on the cervical spine. The same radiographs were examined for evidence of stylohyoid ligament calcification.

Upper limb deformities have a well known association with the craniosynostosis syndromes, these often being the differentiating features in the nosologic process. The distinctive features of complex syndactyly in Apert syndrome and the broad, deviated thumbs and toes of Pfeiffer syndrome enable these patients to be distinguished. There appears to be no clearly characteristic pattern of upper limb abnormality in Crouzon syndrome.

Clinical examination of the upper limb was recorded in 55 patients. Radiographic assessment was available in some of the cases where an abnormality was recorded and also, in those patients who had undergone hand-wrist radiography to assess skeletal maturity prior to orthognathic surgery. Features which could not be analysed due to the retrospective nature of this review included dermatoglyphics, measured range of joint movements and clinical and radiographic changes with growth.

The clinical records were also examined for reports of acanthosis nigricans, other musculoskeletal abnormality, visceral and other anomalies.

The Cervical Spine

Clinical reference to neck stiffness was found in 4 patients with Crouzon syndrome, 1 of whom complained of intermittent pain. Range of movement had not been recorded. Neurological symptoms were present in 1 case. This was an 11 year old boy who presented with a left hemiparesis. The cervical spine radiographs revealed atlanto-axial subluxation and C4-C5 vertebral body fusion (Figure 2.9). The hemiparesis resolved but vertebral instability necessitated a surgical posterior arch fusion of C1-C2. The patient had no further symptoms or signs until his death at the age of 19 following a fall. Autopsy revealed evidence of acute cervical spinal cord compression.

In the ACFU series, radiographic abnormality of the cervical spine was seen in 16 of the cases (40%) (Table 2.13). The most common anomaly of the cervical spine seen in this Crouzon population was fusion of the vertebral bodies (30%), in particular fusion between C2 and C3 vertebral bodies with or without fusions of other vertebrae (Figure 2.10). In addition, 3 other patients had narrow disc spaces and slightly abnormally shaped vertebral bodies. Some abnormalities were not seen on early radiographs but appeared on later examinations indicating the progressive nature of this problem. It is therefore possible some of the infants in this series will display radiographic features of cervical fusion in the future and that the true incidence is higher. Two adult patients had scoliosis in association with the cervical spine fusion.

The reported incidence of radiographic abnormality of the cervical spine in Crouzon syndrome is between 32% and 39% (Kreiborg, 1981; Golabi et al., 1984; Hemmer et al., 1987). Fusion of the cervical spine is not a common finding in the normal population with an incidence of 0.5% (Shands and Bundens, 1956). Kreiborg (1981) reported that 14 of his 15 Crouzon patients with cervical spine abnormality had C2-C3 fusion. On the other hand, cervical spine fusion has been reported in Apert syndrome with an incidence of between 67% and 71% with a predilection for C5-C6 vertebrae (Kreiborg, 1987; Hemmer et al., 1987). The reason for the difference is not known. Hemmer et al. (1987) suggested that there may be a fundamental difference in the underlying osseous patho-physiology, which may account for the difference in the acral manifestations of these two conditions. In contrast, they found patients with Pfeiffer syndrome presented with similar craniofacial features and similar incidence and level of cervical

spine abnormality to patients with Crouzon syndrome. They were unable to distinguish between their Pfeiffer and Crouzon patients according to the cervical spine anomaly.

Table 2.13 Radiographic findings of the cervical spine in 40 patients with Crouzon syndrome at the ACFU

Normal			24
Vertebral Fusion			12
Body	C2-C3	5	
	C2-C3-C4-C5	1	
	C2-C3, C5-C6	2	
	C4-C5	2	
Post. Arch	C2-C3	1	
	C4-C5	1	
High Atlas			4
Large Odontoid			1
Atlanto-Axial Subluxation			1

Cephalometric analysis of the cervical spine of Crouzon patients by Kreiborg (1981), found the cervical column to be short compared to controls and related this to short vertebral body height and the presence of fusions. The head was also held extended on the cervical spine, which helped to maintain an adequate upper airway.

There is little in the way of symptomatic evidence of cervical spine anomalies in these patients in the literature, apart from neck stiffness but this population data highlights the importance of the cervical spine in overall patient management. Firstly, an abnormality may produce neurological symptoms with possibly fatal consequences. Secondly, manipulation of the patient's neck during endotracheal intubation or during the forced maxillary disimpaction of a Le Fort osteotomy may be potentially hazardous. Pre-operative clinical and radiographic analysis of the cervical spine may be advisable for this group.

Calcification of the Stylohyoid Ligament

Lateral cephalometric radiographs and CT scans revealed calcification of the stylohyoid ligament in 50% of patients at the ACFU (Figure 2.11). Calcification was not seen under the age of 4 years; however, radiographs of the same patients at a later stage revealed progressive

Figure 2.9 Lateral cervical spine radiographs (neutral, extension and flexion) in the patient with Crouzon syndrome with atlanto–axial subluxation.

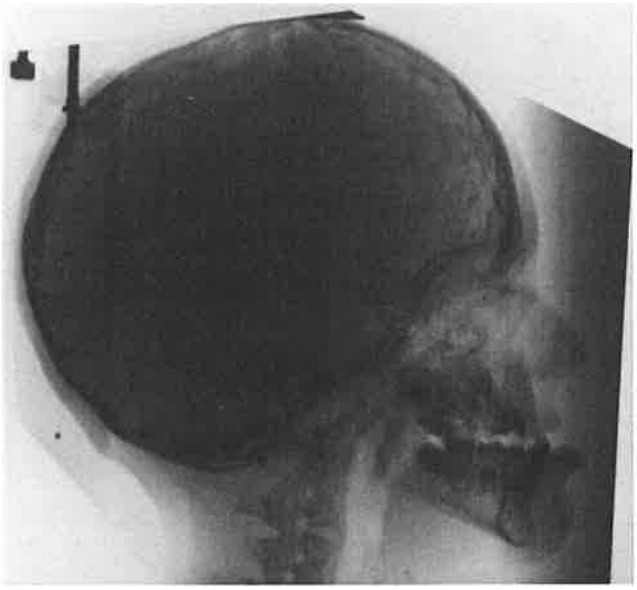

Figure 2.10 Lateral radiograph in a patient with Crouzon syndrome showing fusion of C2–3 and C4–5 vertebral bodies.

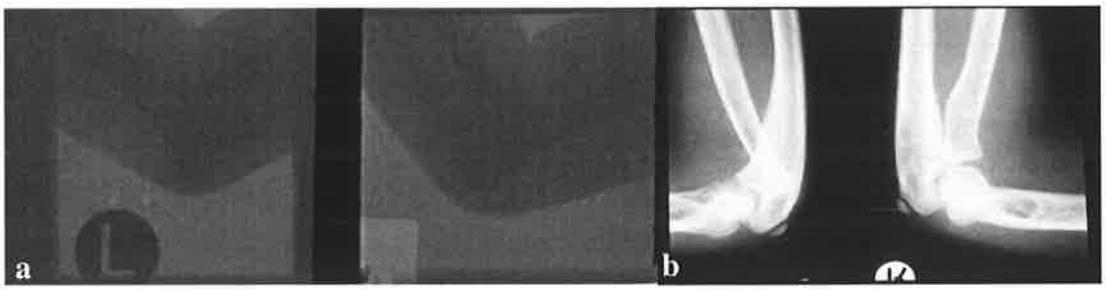

Figure 2.11 Elbow radiographs in two patients with Crouzon syndrome.
(a) Complete humero–radio–ulnar synostosis.
(b) Subluxation of the left radial head.

calcification of the ligament. The reported incidence of stylohyoid calcification is between 39% and 88%. (Kreiborg, 1981; Golabi et al., 1984). The youngest patient reported was a 3 month old child where progression of calcification was observed in longitudinal studies (Kreiborg, 1981). The high incidence of 88% (Kreiborg, 1981) may be accounted for, in part, by an older age of his population of patients. Calcification is also seen in Apert syndrome, but not in association with the simple synostoses. Ligament calcification has been reported in normal patients and may be associated with pharyngeal pain, but this was not observed in the present or any other series. There does not appear to be any other clinical problem.

Acanthosis Nigricans

Acanthosis nigricans, characterised by hyperpigmented, hyperkeratotic lesions usually found in the flexures and on the neck, may be associated with many disease processes including a variety of congenital syndromes. No patients were seen with acanthosis nigricans at the ACFU.

In the literature, there are 10 cases reported in association with Crouzon syndrome (Breitbart et al., 1989). In 8 of these, the patients were female (both Crouzon syndrome and acanthosis have equal sex distributions) and the face was predominantly affected, rather than the flexures. The early age of onset has also been noted (Koizumi et al., 1992). The possibility of an abnormal growth factor or cell receptor, causing both the craniofacial and dermatological defects, has been hypothesised (Suslak et al., 1985). Experience suggests the likelihood of prominent scarring in this group of patients and due care should be taken.

The Upper Limb

(i) The Elbow

Elbow abnormalities were recorded in 10 patients (18.2%). Limitation in elbow movement was the predominant problem (unilateral in 5 patients and bilateral in 5) and included 1 case of cubitus valgus. Radiographic examination performed in 6 of these patients showed bilateral elbow synostosis in 1 and radial head subluxation or dislocation in 5 (Figure 2.11) which were associated with hypoplasia of the radial head and capitellum. A cubitus valgus deformity was

also found with 1 of this latter group. Fixed flexion deformities of the shoulders, knees and hips were also seen in the case of elbow synostosis.

Elbow deformities including stiffness, subluxation of the radial head and ankylosis have been reported in Crouzon syndrome by several authors. The majority have been isolated case reports (Polinelli and Imoda, 1963; Baldwin, 1968; Kushner et al., 1972). Bertelsen (1958) described 2 of 15 patients with Crouzon syndrome with anterior subluxation of the radial head. Kreiborg (1981) found 10 patients with stiff elbows (16%), but did not comment on this further, and included the same 2 patients from Bertelsen's group with subluxation of the radial head.

It is clear a proportion of patients with Crouzon syndrome will have elbow abnormalities (18.2% in this group). It is difficult to assess whether this is related to the severity of craniofacial deformity due to the small number of patients. Of the 5 infants with cloverleaf calvarial deformity in the series of 59 Crouzon patients, 1 had bilateral elbow synostosis, 2 had unilateral radial head subluxation, 1 was normal and the fifth cloverleaf child did not have a limb examination recorded. Thus 3 of the 10 cases of elbow abnormality, including the most severe case with complete elbow synostosis, were in patients with a severe craniofacial deformity.

The presence or absence of elbow deformity may be due to variable expression of the syndrome with increased prevalence in the more severe forms of the syndrome. Alternatively, a separate genetic mechanism may be responsible. Extensive family data of the clinical and radiographic appearance of the elbow are not available to support either theory. This precludes significant comparison of this group of Crouzon syndrome patients with those without elbow abnormalities. The only family data in this series of patients is the twins with Crouzon syndrome who both had anterior dislocations of the radial head at the right elbow with the position on the left side being within normal limits. No other families with more than 1 affected member had elbow deformities. Long term follow up of any offspring will be of interest.

Both unilateral and bilateral deformities at the elbow have been seen. This is unlike the symmetrical and bilateral nature of the acrocephalosyndactylia. The variable incidence of elbow abnormality and its seemingly random involvement of 1 or other or both limbs indicate that this is not an obligatory manifestation in Crouzon syndrome.

(ii) The Hand

Clinical assessments of the hands revealed abnormality in 5 patients. Unilateral simple incomplete syndactyly was found in the second web space of 1 patient and third web space in another patient. Bilateral clinodactyly of the little fingers was present in 2 cases with generalised brachydactyly in another. X-ray findings confirmed the presence of brachydactyly and clinodactyly and in 1 of these revealed hypoplasia of the middle phalanx of the little finger.

Hand deformity has been rarely described in Crouzon syndrome. A case of ectrodactyly has been reported (Garcin et al., 1932). Kaler et al. (1982) evaluated 15 patients with Crouzon syndrome for abnormalities in hand bone length with metacarpo-phalangeal pattern profile analysis. The length of the proximal phalanx of the thumb and proximal and middle phalanges of the ring finger were used as the variables to derive a discriminant function for Crouzon syndrome of 88.3% compared with a control group. It is interesting to note that the proximal phalanx of the thumb is deformed in Pfeiffer syndrome. This study also examined the data of 7 patients with Pfeiffer syndrome and 8 with Carpenter syndrome and found similarities in the hand deformities in these 2 groups. The proximal phalanx of the thumb was relatively short compared with the essentially normal first metacarpal. The middle phalanges were relatively small in each syndrome pattern. They suggested a common developmental mechanism varying in extent and/or duration, which acts on the hand skeleton in each of these genetically distinct conditions.

Pattern profile measurements of the hand were not performed in the population presented here. Clinodactyly of the little finger, present in 2 cases, is a relatively common congenital hand abnormality often found in isolation, but also with a host of congenital anomalies. Brachydactyly, seen in 1 patient, cannot be adequately explained. It may represent an extreme or generalised variant of the shortened measurements described by Kaler et al. (1982). The hypoplasia of the middle phalanx of the little finger of 1 patient was consistent with these measurements.

Soft tissue syndactyly is another relatively common congenital hand anomaly. It is recorded in up to 25% of patients with Saethre-Chotzen syndrome (Pantke et al., 1975). The patients described here had unilateral syndactyly and no other frequently encountered features of that

syndrome, such as facial asymmetry, low set frontal hair line or ptosis, all seen in over 75% of Saethre-Chotzen patients (Pantke et al., 1975).

In summary, patients with Crouzon syndrome may exhibit peripheral skeletal manifestations especially at the elbow. Minor deformities of the hand may be seen in this syndrome. Other clinical features may therefore be necessary to distinguish Crouzon syndrome from other disorders associated with hand abnormalities, such as Saethre-Chotzen and Jackson-Weiss syndromes (Jackson et al., 1976).

Additional Anomalies

Other anomalies may also be seen in Crouzon syndrome patients. The severity and incidence of these do not yet suggest a nosologic difference. Anomalies, not described above, seen at the ACFU, are shown in Table 2.14. Calcaneo-cuboid coalition has been previously described in 1 case (Craig and Goldberg, 1977). Musculoskeletal anomalies would be expected to be more commonly associated with Crouzon syndrome. Visceral disorders however are rare and appear to represent unrelated anomalies.

Table 2.14 Incidental non-craniofacial abnormalities in 55 patients with Crouzon syndrome at the ACFU

None		47
Musculoskeletal		
	Pectus excavatum	1
	Femoral intorsion	1
	Bilateral calcaneovalgus	1
	Bilateral pes planus	1
Visceral		
	Cardiac	
	Mitral valve prolapse	1
	Gastrointestinal	
	Gastro-oesophageal reflux	1
	Anterior placed anus	1
	Haematological	
	Von Willebrand's disease	1

Body Height

Body height was not recorded in the ACFU population. Kreiborg (1981) reported the height of Crouzon patients to be significantly below average. The length of the radius measured from radiographs, was significantly shorter than normal in females (n=8), but not males (n=8).

Conclusion

Crouzon syndrome is not just a craniofacial deformity. It is a dysplastic condition which can affect other areas of bone and chondral growth, such as the spine and elbows. Ligaments and soft tissues may also be involved. The patho-physiology of this condition is not yet fully understood. The wide range of non-craniofacial manifestations occurs with varying frequency (Table 2.15). These features are not obligatory in terms of the clinical presentation of Crouzon syndrome. Pathological involvement may arise from the proximity of genes determining craniofacial growth with those affecting cervical spine and elbow development or by some other as yet unknown mechanism.

Table 2.15 Summary of frequency of non-craniofacial manifestations of Crouzon syndrome in the population of patients treated at the ACFU

Cervical Spine Anomaly	40 %
Stylohyoid Calcification	50 %
Acanthosis Nigricans	0 %
Elbow Abnormality	18 %
Minor Hand Deformity	10 %
Other Musculoskeletal Anomaly	7 %
Visceral Anomaly	7 %

2.4.9 Psychosocial Issues

While the main thrust of this paper has been directed at structural deformity, any description of Crouzon syndrome would be incomplete without a consideration of the psycho-social impact of this condition. The psychosocial effects can only be estimated in the population studied. All patients and families interviewed by members of the social work department, to address personal, family and other issues. Psychological testing was performed in selected older

children (Section 2.4.4 Central Nervous System). The detailed issues are considered outside the scope of this thesis. Crouzon syndrome patients share experiences with patients who have other facial disorders and have to cope with social and psycho-social penalties associated with being facially different (Cohn et al., 1985). There are also the problems of abnormal speech and hearing which may compromise social interaction. The concept of having an hereditary genetic defect must also be dealt with by the patient and family.

Patients with Crouzon syndrome suffer teasing at school and find themselves socially isolated. Their future vocation and likelihood of marriage may also be limited (Cohn et al., 1985). They may consider themselves different from the general population and be angry towards a society which emphasises facial beauty. They may try to present an overly positive attitude to their health providers and may have difficulty discussing their problems.

Surgery, by providing the possibility of improvement in facial aesthetics, produces benefits in psycho-social development and peer acceptance. Controversy exists over the role of earlier facial skeletal surgery (in childhood and adolescence) (Mühlbauer et al., 1989; McCarthy et al., 1990). Improvement in mid-facial dimensions at a young age are balanced by the need for further surgery as the deformity recurs during facial growth.

2.4.10 Surgical Management

Introduction

The previous sections describe the complex and variable deformities of Crouzon syndrome, correspondingly, its management involves a variety of medical and allied specialists. The concept of interdisciplinary cooperation for treating these conditions was developed during the mid 1950's by Paul Tessier of the Plastic Surgical Service of the Centre Medico-Chirurgical Foch in Paris. Tessier pioneered many of the currently performed craniofacial procedures. The multidisciplinary team approach, strongly advocated by Munro (1975) and David et al. (1982), to ensure that all aspects of the condition are adequately managed, aims to reduce morbidity and mortality. Management decisions are based on a series of specialist opinions concerning the patient's psycho-social development (for example, psychiatrist, psychologist and social worker), the general medical condition (for example, cardiologist, respiratory physician), the

craniofacial functional deformity (for example, ophthalmologist, neurosurgeon, radiologist) and facial aesthetic aspects (for example, plastic surgeon) to name a few areas. Many of the specialist roles overlap so all information is brought together in a forum where individual views, including those of the patient, are presented in order to decide a management strategy. The natural history of Crouzon syndrome (and other craniofacial conditions) in individual patients changes with time, implying that regular patient reassessment is needed and that the management strategy should evolve.

Surgical intervention has become almost routine in Crouzon syndrome, with resultant effects on the natural history and outcome. A review of the surgical management at the ACFU is presented here in order to clarify the rationale used in treatment and to highlight some of the problems and controversy in this area. Of the 57 patients in the series, 48 underwent surgery at the ACFU. All patients survived. The results of surgery in some patients in this study have been previously reported (David and Sheen, 1990).

Surgical Procedures

Table 2.16 lists the major procedures performed on the patients at the ACFU. Craniectomy was performed in 14 patients and depended on the sutural region involved and the age of the patient. Coronal suture involvement and lack of orbital volume was managed by fronto-orbital advancement (n=23) (Figure 2.12). One patient who underwent craniectomy elsewhere with silastic sheet insertion 5 years previously, presented with recurrent calvarial suture fusion (Figure 2.13) demonstrating the inadequacy of this technique. Five patients required ventriculo-peritoneal shunts for progressive hydrocephalus (Section 2.4.4 Central Nervous System).

The lower airway may be narrowed independently of the upper airway. Examination to identify of the level of pathology to the upper or lower airway is imperative before deciding upon a mode of therapy. Laryngomalacia, tracheomalacia or continuous cartilaginous rings are difficult to treat and conservative management is preferable, depending on the degree of oxygen desaturation in the infant. Severe problems may require surgical intervention.

A narrow upper airway may be improved by adenoidectomy and tonsillectomy. Midface deformity may contribute to airway obstruction and may be corrected by Le Fort III osteotomy

and advancement. Rigid fixation of the maxilla is difficult to achieve in the very young and splitting of the soft palate may be essential in order to maintain the airway. In the past, tracheostomy was used in infants with severe oxygen desaturation. At the ACFU, three infants required palatal surgery (5 procedures), such as uvulopalatopharyngoplasty or mid-palatal split.

A wide range of procedures was performed in adolescence and adulthood to correct the untreated calvarial, orbital and midface deformities (Table 2.16). One adult patient undergoing a fronto-facial advance, had a free rectus abdominus flap inserted behind the frontal bone flap. The aim was to obliterate the extradural deadspace and to seal the communication to the nasal cavity. This patient subsequently lost the frontal bone flap following extradural infection (Figure 2.14). Moore et al. (1991) postulated interference by the flap with the gravitational drainage of the extradural space as a probable cause.

Table 2.16 Major craniofacial procedures (multiple or combined) performed on 48 patients with Crouzon syndrome at the ACFU

Craniectomy		14
Sagittal	3	
Lateral decompression	5	
Posterior	6	
Shunt		5
Palatal surgery for airway management		5
Fronto-orbital advance		23
Fronto-facial advance		22
Le Fort III osteotomy		12
Trans-cranial	3	
Sub-cranial	9	
Le Fort I osteotomy		3
Mandibular osteotomy (excluding genioplasty)		3
Rectus abdominus free flap		1
Tracheostomy		27
Levant frame		8

Figure 2.12 Photographs of a 5 year old girl with Crouzon syndrome before and after Fronto-Orbital Advance surgery.

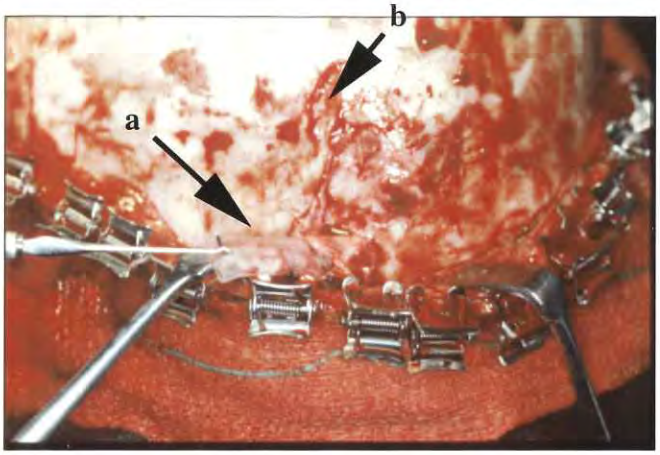

Figure 2.13 Operative finding in a 5 year old patient with Crouzon syndrome who underwent a sagittal craniectomy with silastic sheet insertion during infancy. (a) Silastic sheet. (b) Groove in bone with fusion beneath silastic.

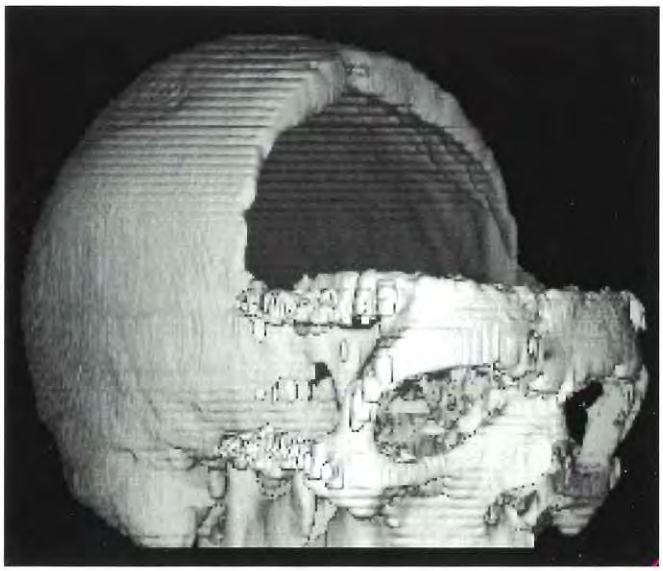

Figure 2.14 Post-operative 3D CT reconstruction of a patient with Crouzon syndrome showing complete loss of the frontal bone following Fronto-Facial Advance.

Secondary Surgery

Secondary surgery was performed predominantly on adult patients. Once the skeletal framework was in place, correction of the soft tissue deformity or any minor bony irregularity could be undertaken (Table 2.17).

Table 2.17 Secondary surgery performed on 21 patients with Crouzon syndrome at the ACFU

Onlay bone graft	11
Burring of bone graft	4
Removal of screws	4
Rhinoplasty	13
Genioplasty	7
Peri-orbital surgery	11
Pharyngoplasty	1
Set back prominent ears	1

Complications

Sixteen of the 48 patients who underwent 65 major procedures suffered one or more complications (Table 2.18). Fronto-facial advance surgery was the most common procedure followed by complication. All the infective complications followed this procedure and occurred in the older patients, a finding typical of craniofacial surgery (David and Cooter, 1987). Loss of the frontal bone followed the infection in 4 of these patients (Table 2.18, Figure 2.14). This required removal of the entire frontal bone and delayed reconstruction.

Persistent CSF leakage, requiring further surgical intervention, occurred in 4 patients of varying ages following fronto-facial advance in 3 and Le Fort III advance in 1.

One patient suffered the most devastating complication of bilateral blindness. This resulted from an extradural haematoma, which exerted traction on the optic nerves, but remained undetected due to the surgical advancement. Another patient suffered unilateral blindness due to intra-orbital optic nerve compression.

Anosmia was noted in one patient however the presence or absence of anosmia was not routinely recorded in all patients post-operatively. Transient diplopia occurred in 2 further patients. Permanent damage to 1 side of the frontal branch of the facial nerve was recorded, and velopharyngeal incompetence requiring pharyngoplasty was seen in 4 patients.

Table 2.18 Complications in 16 of the 48 patients undergoing major craniofacial procedures for Crouzon syndrome at the ACFU

Infection	
Extradural	2
Osteomyelitis	
Frontal bone	4
Zygomatic bone	1
Wound	2
Chronic sinusitis	2
CSF leakage	4
Neurological deficit	
Anosmia	1
Blindness	2
Diplopia	2
Frontal branch palsy of facial nerve	
Transient	2
Permanent	1
Palatal disturbance	
Velopharyngeal incompetence	4
Palatal breakdown	1

Discussion

Indications for Surgery

The indications for intervention in Crouzon syndrome are related to the deformity and take into consideration the theoretical basis of the patho-physiology. Understanding the principles of surgical intervention and its effect on appearance and growth, also provides some insight into the condition itself. This is not intended to be a complete discussion of the medical management and surgical techniques used in this condition. These have been widely reported elsewhere

(Tessier, 1971a, 1971b, 1986; Munro, 1975; David et al., 1982; Marchac and Renier, 1982) and are beyond the scope of this thesis.

The goals of surgery are two-fold. Firstly, to prevent and/or treat the sequelae of craniosynostosis, which interfere with function and secondly, lessen the psycho-social impact of the condition on the patient's life by improving craniofacial aesthetics. These aspects require regular monitoring and often many operations throughout the developing individual's life.

The indications for surgery are listed in Table 2.19. The timing of surgical intervention is determined by the medical and functional indications in order to optimise the result and reduce the risk of complications. In the individual patient, these factors are also balanced against the relative psychosocial indication for surgery and the patient's age. The interplay of these factors in determining the optimal time of surgery is discussed further.

Table 2.19 Indications for major craniofacial surgery

Functional
Raised intracranial pressure
Airway obstruction
Severe proptosis/Globe dislocation
Malocclusion (relative)
Psychosocial
Aesthetic correction of craniostenosis, orbitostenosis, and faciostenosis

Historical Perspective

Tessier (1986) approached surgical intervention from an anatomical regional perspective. He described 5 levels of craniofacial framework where deformity may exist. These included:

(a) the cranial vault,

(b) the supra-orbital ridges including the fronto-naso-ethmoidal complex, the upper part of the orbital cavities and the orbital roofs,

(c) the lower orbits with body of maxilla and zygomas,

(d) the upper jaw and

(e) the mandible.

Tessier used these levels to define the location the region of deformity in a given craniofacial disorder. In the case of Crouzon syndrome, he described involvement of levels (a) to (d), with sparing of the mandible, and divided the deformity into clinical groups depending on which level was most severely involved. The deformity may be 'Upper Crouzon' with predominantly calvarial deformity with proptosis, 'Lower Crouzon' with primarily maxillary hypoplasia, or the 'Typical Crouzon', a combination of both of these. In 1971, Tessier outlined the techniques of corrective surgery at the various levels.

David et al. (1982), on the other hand, described 3 epochs in the management of patients with craniosynostosis syndromes, namely:

(a) the Early Period - up to 12 months,

(b) the Intermediate Period - 1 to 9 years of age, and

(c) the Late Period - 10 years onwards.

In the Early Period, surgery attempts to release the sutural restriction and allow a more normal expansion of the head. Raised intracranial pressure should be released in this stage and the orbits protected by fronto-orbital advancement. This also results in improved upper facial aesthetics. In the Intermediate Period, treatment is essentially expectant. Problems which may arise include raised intracranial pressure, proptosis, upper airway obstruction and severe psycho-social disturbance. The Late Period is aimed at definitive correction of the established facial deformity.

Both descriptions have merit in simplifying this complex area. Tessier's classification approaches the indications for surgery according to the site deformity. David's scheme provides a guide to the timing of surgical procedures.

Strictly speaking, surgical intervention is determined by the functional and aesthetic deformity at a particular age. An outline of management which incorporates the indication and age is presented here. This method relates the deformity of the presenting patient with the age and the effect that growth will have, following surgery, thus combining Tessier's regional pathological indications for surgery with David's age-related epochs. The indications for surgery are divided into the release of craniosynostosis (early or late) and the correction of the midface deformity (early or late).

The indications for surgery in the ACFU patients are presented in Table 2.20, using this approach.

Table 2.20 Indications for Craniofacial Surgery in the ACFU Crouzon Population

Early release of craniostenosis (≤ 2 years)		**12**
Raised intracranial pressure	7	
Aesthetic and preventative without ICP raised	5	
Late release of craniostenosis (>2 years)		**8**
Raised intracranial pressure and no previous surgery	3	
Raised intracranial pressure and previous treatment	4	
Severe orbitostenosis	1	
Early correction of midface and/or calvarial deformity (≤15 years)		**17**
Definitive (no further surgery required)	5	
Not definitive (underwent further correction)	6	
Unknown (incomplete growth)	6	
Late (definitive) correction of midface and/or calvarial deformity (>15 years)		**24**

Early Release of Craniosynostosis (<2 years)

The early release of craniosynostosis is a relatively safe and beneficial procedure and all patients in this group had this surgery in the first 14 months of life. Seven had significant deformity (5 with triphyllocephaly) with signs of raised intracranial pressure. The remainder had a lesser deformity and surgery was aimed at preventing functional and aesthetic deformity. Central nervous system growth is maximal during the first 3 years of life, during which time it reaches approximately 70% of adult size (Scammon, 1930). This implies that surgery to 'release the sutures' and allow cranial vault expansion to parallel rapid brain growth during these years should have some benefit. The earlier this is performed, the greater the likely benefit; certainly this is clearly seen in patients with the simple craniosynostoses. This benefit is not so evident in the syndromal synostoses including Crouzon syndrome. Many patients present late or may have a lesser deformity which manifests itself later. Therefore, it is appropriate to expand the

time frame of the Early Period of David et al. (1982) to include the second year of life. After the first 1-2 years management of patients with Crouzon syndrome becomes expectant, and hence the third year of life is not included in the early group.

Late Release of Craniosynostosis (>2 years)

The late release of craniosynostosis is indicated when raised intracranial pressure occurs with or without previous craniectomy or fronto-orbital advance (Figure 2.12). Three patients, who had not had prior surgery, required treatment at this stage. Four patients treated as infants (2 with craniectomy alone and 2 with fronto-orbital advance) re-presented with varying degrees of raised intracranial pressure. One of these patient who underwent silastic sheet craniectomy elsewhere 5 years previously, re-presented with recurrent calvarial suture fusion and raised intracranial pressure (Figure 2.13). One child with recurrent globe dislocation underwent fronto-orbital surgery.

Early Correction of Midface (and/or Calvarial) Deformity (≤15 years)

Early correction of orbital and/or midface deformity was performed under the age of 16 years (range 8-15 years) in 17 patients. Fronto-facial advance was undertaken in 13 of this group and Le Fort III advancement in a further 4. No further surgery was required in 5 of these, however 6 required further skeletal correction. At the time of writing, the last 6 patients had not reached skeletal maturity and final assessment or had been lost to follow up, interstate or overseas. It should be noted that there is an overlap in the age of patients undergoing the late release of craniosynostosis group and the age of patients undergoing early correction of the midface. There are also more operative procedures (n=61) than patients having surgery (n=48), as patients moved from group to group with time.

The children with significant or severe deformity seen in ACFU overseas clinics during late childhood or early adolescence were brought to Australia for surgery. They had often had no previous treatment and little in the way of support in their country of origin as cultural and social behaviour often resulted in these children being treated as outcasts. It was felt appropriate to arrange surgery, as the child may not have been presented to the clinic again. This had a

secondary advantage of informing the local medical authorities of the help that is available for these children.

While it is generally accepted that craniectomy and fronto-orbital advance in an infant may optimise the drive of the growing brain to improve the cranial contour (Marchac and Renier, 1979) and midface correction in the adult will be permanent, controversy exists over the timing of surgery for the treatment of the midface deformity in childhood and adolescence (McCarthy et al., 1990). Maximal psycho-social benefit likely to be gained from surgery is during late childhood and early adolescence when the effect of deformity on the development of body image and social interactions is most profound. Balanced against this is the impact of the surgical procedure at this age, the virtually inevitable recurrence of the deformity due to mandibular growth which continues until late adolescence, and the possible interference of surgery in the future growth of the maxilla. This disturbance in maxillary growth may result in a small scarred maxilla which may limit the definitive midface surgical procedure.

Late (Definitive) Correction of Midface and/or Calvarial Deformity (>15 years)

Twenty-four patients over 15 years of age had definitive correction of the deformity (Table 2.20).

Definitive surgical correction of midface hypoplasia, usually by fronto-facial or mid-facial advancement is undertaken near or following skeletal maturity. Those with completed skeletal growth as determined by hand radiographs, will usually be over 15 years of age and will not develop recurrent deformity due to rigid bony fixation and completed mandibular growth. Midface surgery performed in younger patients with incomplete skeletal growth will have a less predictable outcome. Despite over-correction of the occlusal deformity from class III to class II, repeated major skeletal surgery is often required. Surgery is performed earlier, not to produce the definitive skeletal shift, but for pressing psycho-social and, sometimes, medical factors such as airway difficulty. These early and late groups should be differentiated.

Conservative (Non-operative) Management

No surgery was performed on 9 patients; 2 were adults and 7 children. One adult elected not to have surgery and the other was found to have von Willebrand's disease and moderate mental

retardation with long-standing partial blindness and deafness where the risks of the cosmetic procedure outweighed the benefits.

The 7 children who had no surgery presented with mild disease between the ages of 2 and 5 years and have been followed through childhood on an annual or biannual basis. This group had not required surgery due to a lack of sequelae of untreated craniosynostosis. A minimal degree of maxillary deformity had not required early midface correction. One of these patients is now 15 years old and was to have correction of late onset midface deformity. Another patient, who recently presented to the ACFU aged 5 years, had a mild degree of optic disc swelling, a moderate degree of calvarial deformity and proptosis. A sagittal synostectomy had been performed as an infant at another centre. Fronto-orbital advance and repeat sagittal craniectomy were shortly to be performed in order to prevent raised intracranial pressure and to produce aesthetic improvement of the calvarial contour. This patient is presented in detail in Chapters 3 and 4 (Patient LW).

Early Midface Surgery for Aesthetic Benefits

Evidence now suggests that maxillary growth in untreated craniosynostosis patients in childhood is minimal (Coccaro et al., 1980; Kreiborg and Aduss, 1986), and that any growth is predominantly in the vertical plane rather than horizontal (Bachmeyer et al., 1986). Surgery to the maxilla may limit the little growth there is, which is predominantly downward. McCarthy et al. (1990) reported a series of 12 patients with craniosynostosis syndromes in whom Le Fort III osteotomy was performed under the age of 7 years. The majority of patients were placed into an exaggerated class II occlusion. Longitudinal follow up revealed low morbidity, but both vertical and horizontal growth of the mobilised maxilla was reduced. The factors which may possibly prevent growth include disturbance of maxillary growth centres, the insertion of bone graft, post-operative muscular and soft tissue scarring, devascularisation of the nasomaxillary complex and failure of the procedure to release synostosed sutures within the mobilised segment (Bachmeyer et al., 1986; McCarthy et al., 1990). At this stage, Le Fort III osteotomy in childhood is justified for medical reasons. Further investigation will determine whether it should be routinely implemented for psycho-social reasons.

2.4.11 Deaths

No patient died during surgical management at the ACFU. Four patients are known to have perished at a later date. The death of 1 adult was associated with atlanto-axial subluxation and was described in detail in the preceding section on the cervical spine (2.4.8 Non-Craniofacial Features).

Three infants died from respiratory complications in their home country, some months after discharge from the ACFU. Limited information is available, but it is understood 2 suffered acute respiratory arrest and 1 had pneumonia. All infants had undergone surgical correction of a cloverleaf calvarial deformity. It is probable that intermittent airway obstruction was a chronic problem but was not appreciated at the time. A neurologically mediated respiratory arrest cannot be ruled out.

These deaths highlight the possibility of significant airway abnormality, particularly in those patients with severe craniostenosis. Thorough assessment and treatment of any upper or lower airway obstruction may minimise these fatalities.

2.5 Discussion and Suggested Management Plan for Crouzon Syndrome

The aim of this chapter has been to review the current understanding of Crouzon syndrome. Emphasis has been placed on the clinical and radiographic data and the surgical management of the patients treated at the ACFU. The clinical features are summarised in Table 2.21, along with a comparison of Kreiborg's findings from 1981. From this information and the literature, recommendations for the management of patients with Crouzon syndrome have been made below. The direction of future investigations has also been discussed (Chapter 3).

Demography

The incidence of Crouzon syndrome in South Australia is approximately 1 in every 41,400 live births. The demographic data demonstrate the trend in referral patterns. Early referral to a major craniofacial centre provides the best opportunity for dealing with the surgical, allied medical and psycho-social problems, as well as establishing a lifelong contact and support network for the patient and family.

Continued education of general practitioners regarding the availability of these services and of the population in general should be encouraged. Members of all specialities should be prepared to refer these patients to their respective colleagues at a recognised craniofacial centre, for the benefit of the holistic treatment of the patient and to enable the ongoing study of these individuals.

Medical Genetics

Crouzon syndrome is an autosomal dominant condition with variable expressivity and presumed complete penetrance. Seventy four and a half percent of the patients in this population were due to new mutations, suggesting an increase in this form of presentation, which may implicate changing social and environmental factors. Formal genetic counselling was provided for 63% of patients by the Medical Genetics Department of the Women's and Children's Hospital. In this population, many patients expressed uncertainty or denial some time following the counselling.

Family history and relevant genetic details should be recorded in all patients with Crouzon syndrome. Photographic details and examination of family members should be carefully documented. Adequate genetic counselling should be provided to all patients and reinforced in adolescents to ensure future decisions on family planning are well-informed. It should be routine for parents and/or the patient to have discussions with the medical geneticist, social worker and treating surgical staff. A letter to outline the details of discussion is currently provided by the Medical Genetics Department for all patients seen at the ACFU. Routine review of patients would be desirable when attending for definitive surgical correction aged approximately 16 years.

Cranial Morphology

There is great variation in the presentation of the calvarial deformity. This implies a broader growth disturbance affecting a variety of anatomical locations. The commonest deformity recorded is brachycephaly. Radiographic examination assists in determining which sutures are involved, but is not sufficiently sensitive in all cases. The use of the CT scan has improved the visualisation of sutures and may delineate partial fusions more easily. CT visualisation and measurement of the cranial base sutures and synchondroses is one of the aims of this project (Chapter 3).

Full head CT scans should be performed on all patients as a form of baseline investigation. Annual CT examinations would provide an extensive body of data on the growth of these patients. However, the resultant accumulated dose of radiation exposure to infants and young children and the acceptable safety level is not precisely known. At this stage, the imaging techniques should be used for medical indications only.

Central Nervous System

Although intellectual capacity is usually normal in this population, structural deformity of the brain is a common finding on CT scan. Non-progressive ventriculomegaly, found in 51% of patients, appears to be a primary brain deformity, but may be distorted secondary to the abnormal cranial base and vault. Surgical release does not correct the ventriculomegaly.

Progressive hydrocephalus with attendant neurological deficits may occur in a small proportion of patients. Abnormality of the cerebral matter is uncommon, compared with Apert syndrome.

Magnetic Resonance Imaging should be performed on all patients with Crouzon syndrome to provide structural details of the CNS not visible on CT scan. This data may clarify the extent of the involvement of the brain in this disorder.

Ophthalmology

After proptosis, ocular hypertelorism is the most common finding. Decreased acuity may occur secondary to optic atrophy, strabismus and exposure keratitis. Early surgery to provide skeletal protection and correct raised intracranial pressure may help prevent late loss of vision. The occasional findings of coloboma, nystagmus, ptosis and mild dystopia may also be seen in other craniosynostosis syndromes and care needs to be taken in accurate syndrome diagnosis.

Otorhinolaryngology

Atresia or stenosis of the external auditory meatus represents a significant structural abnormality. Hearing loss may also be due to a primary middle ear abnormality or secondary to eustachian tube dysfunction. Close surveillance is warranted to minimise the effects of middle ear disease.

Airway problems in Crouzon syndrome, particularly in infancy, may be life threatening. Lesser degrees of airway obstruction may result in non-specific problems such as behavioural disturbance, poor performance at school and irritability. Sleep studies to detect oxygen desaturation should be performed on all patients, irrespective of age. Depending on the degree and duration of desaturation, surgical treatment may offer relief, allowing normal neurological development and long term survival of severely affected infants. Location of the site of airway pathology is necessary in order to decide the mode of treatment.

Non-Craniofacial Features

Cervical Spine

Abnormalities in this area include the progressive fusion of vertebral bodies seen in 40% of ACFU patients investigated. Significant pathology needs to be identified and treated. Care should be taken during surgery to ensure neural damage does not occur. Reassessment of the cervical spine should occur periodically, to monitor any changes and improve the understanding of the natural history of this abnormality.

Cervical spine screening of all patients is recommended on presentation to the ACFU and at regular intervals of approximately 2 or 3 years thereafter. Recent cervical spine radiographs should be reviewed prior to surgery.

Upper Limb

Deformity of the elbow and hand may be overlooked in units concentrating on the craniofacial deformity. The involvement of the elbow in some patients is unexplained. A relationship with severity cannot be established from the available data. Hand abnormalities may be important in syndrome diagnosis. An assessment of all patient clinical characteristics may be more relevant than minor degrees of deformity.

Other Abnormalities

Complete clinical and radiographic documentation of all associated abnormalities will ensure appropriate treatment is performed. Accurate syndrome diagnosis and understanding of the condition will also be improved.

Psychosocial

There is little psychosocial information for populations with Crouzon syndrome in the literature. Efforts to document and standardise data collection may help provide a picture of the effects of the deformity and the effects of surgery.

Surgical Management

Surgical intervention at the extremes of growth are well established.

Midface advancement surgery in childhood is controversial. Early synostosis of the maxillary sutures is reflected in the degree of hypoplasia. Surgery may compromise potential growth of the maxilla. Psychosocial factors, however, may lead to a need for early surgery. Serial measurements of the maxilla during childhood will determine the rate of growth. When growth has ceased or is minimal, midface advancement will have little or no effect on the future development of the maxilla and aesthetic surgery as early as possible after maxillary growth ceases may have enormous psychosocial benefits. Significant complications were found most frequently in the adult population undergoing fronto-facial advance.

Deaths

Four patients in the series are known to have died (7%). The cause of death in 3 patients was related to respiratory arrest. Airway obstruction or centrally-mediated factors have been implicated. In the final patient the cervical spine deformity was a major factor. Careful assessment and follow up of patients and knowledge of these problems would hopefully minimise early mortality.

Conclusion

Crouzon syndrome has protean and complex manifestations and appropriate examination and assessment of these patients requires the involvement of multiple medical specialties. Awareness of all craniofacial and non-craniofacial manifestations will assist in the investigation, management and research of this condition.

Table 2.21 Comparison of clinical findings in Crouzon Syndrome in population studies by Kreiborg (1981) and at the ACFU (1995)

(see following page)

Table 2.21 (continued)

Origin of Study		Kreiborg (1981)	ACFU (1995)
Patients Reviewed		**61**	**59**
Incidence of Abnormalities		%	%
Genetics	Familial	44	25
	New mutation	56	75
Cranial Deformity	Brachycephalic	NR	65
	Mesocephalic	NR	17
	Dolichocephalic	NR	18
	(Triphyllocephalic)	NR	(8)
Fused Sutures	Coronal	2	12
	Coronal + Sagittal	19	5
	Coronal + Sagittal + Lambdoid	75	71
	Sagittal + Lambdoid	4	5
Neurological	Headaches	29	14
	Epilepsy	12	2
	Mental deficiency	3	5
CNS Structure	Agenesis corpus callosum	2	0
	Schizencephaly	NR	2
	Ventriculomegaly - mild	NR	51
	- moderate	NR	11
	- severe	NR	9
Ophthalmological	Proptosis	100	100
	Hypertelorism	NR	78
	Dystopia	NR	10
	Strabismus	77	34
	Decreased acuity	46	24
	Optic atrophy	22	12
	Papilloedema	NR	12
	Exposure keratitis	12	14
	Nystagmus	12	4
	Coloboma of iris	2	4
	Ptosis	NR	14

NR = not recorded

Table 2.21 (continued)

Origin of Study		Kreiborg (1981)	ACFU (1995)
Patients Reviewed		**61**	**59**
Incidence of Abnormalities		%	%
ENT	Pinna abnormality	NR	6
	Hearing loss	55	34
	External canal stenosis	NR	12
	External canal atresia	13	8
	Middle ear disease	NR	28
	Cholesteatoma	NR	4
	Cleft palate	3	0
	Cleft lip	2	0
	Bifid uvula	9	2
	Lateral palate swellings	50	NR
Airway	Obligatory mouth breathing	32	38
	Oxygen desaturation	NR	8
Occlusion	Class I	NR	4
	Class III	72	96
	Mesial molar occlusion	70	NR
	Anterior open bite	60	NR
	Cross bite	84	NR
Speech	Articulation disorder	NR	90
	Hyponasality	NR	88
	Hypernasality	NR	10
Non-CF Features	Cervical spine anomalies	30	40
	Stylohyoid lig. calcification	88	50
	Elbow stiffness	16	18
	Radius dislocation	3	8
	Ankylosis	0	2

NR = not recorded

CHAPTER 3

THE THREE DIMENSIONAL QUANTITATIVE ANALYSIS OF THE CRANIOFACIAL MORPHOLOGY OF CROUZON SYNDROME

3.1 Introduction

Significant advances have been made in the investigation and understanding of the pathology of Crouzon syndrome in the field of genetic mapping. Recent work has identified the site of the gene responsible for Crouzon syndrome (Preston et al., 1994; Reardon et al., 1994; Li et al., 1994) and other craniosynostosis syndromes (Jabs et al., 1993) on the long arm of chromosome 10. Mutations in this gene, which encodes for fibroblast growth factor receptor 2, are found in patients with Crouzon syndrome. Patients with Jackson-Weiss syndrome also have a gene mutation identified on the same chromosome (Li et al., 1994). Future developments should identify the genes responsible for other craniosynostosis syndromes and determine their relationship with each other. This information may help unravel the specific biological abnormalities in Crouzon syndrome. Genetic mapping is outside the scope of this thesis and not considered further.

On a practical level, however, management of these patients still continues to improve. The management of patients with Crouzon syndrome is directed towards preventing the medical complications and providing an acceptable aesthetic result as demanded by our society.

The clinical features and natural history of Crouzon syndrome are a direct result of the structural deformities and their effects on function. The nature and extent of the deformities are highly variable. Visualisation of the structural pathology greatly assists in the assessment and management of patients. Recent interest has therefore focussed on advances in imaging techniques.

The analysis of craniofacial deformity previously relied on cephalometry (Broadbent, 1931) and anthropometry (Boyd, 1980). The development of Computed Tomography (CT) (Hounsfield, 1973) and 3D CT reconstructions (Herman and Lui, 1977) allowed examination of the

craniofacial skeleton in great detail. These radiographic techniques provide extensive qualitative information on the pathological features of Crouzon syndrome and other craniofacial disorders (Hemmy et al., 1983; Marsh and Vannier, 1983; David et al., 1990). In addition, the images provide a spatial comparison before and after surgical intervention.

Quantification of CT data followed the qualitative analysis. Aided by advances in computer imaging software, such as Analyze[1] and Persona[2], and geometric techniques (Bookstein, 1991), several approaches have been taken (Vannier et al., 1984; Cutting et al., 1985; Cutting et al., 1986; Marsh et al., 1986; Salyer et al., 1986). In 1988, Abbott developed techniques of landmark definition and analysis of the craniofacial skeleton from the 3D CT reconstruction images. After further work on the techniques for measurement from 3D CT reconstructions (Abbott et al., 1990a; Abbott et al., 1990b), this method of investigation has been adopted by the ACFU.

In this project these techniques have been applied to 3D CT data of patients with Crouzon syndrome. In addition analysis of 3D CT data from age matched control skulls was performed.

The aim of this three-dimensional metric analysis of the craniofacial skeleton was to accurately identify the sites of the pathological processes in Crouzon syndrome. A statistical comparison of patients with and without Crouzon syndrome may provide evidence to support or contradict currently held patho-physiological concepts. Quantitative data from 3D CT provide additional meaning to the existing qualitative spatial interpretation of the problems that need to be overcome and may assist in the measured planning of surgical procedures.

[1] Analyze: A Comprehensive Operator-Interactive Software Package for Multidimensional Medical Image Display and Analysis. The Mayo Foundation of Rochester, Minnesota, USA.

[2] Persona: 3D Medical Imaging and Analysis. The Institute of Cranio-Facial Studies. North Adelaide, South Australia.

3.2 Materials

3.2.1 Patient Selection

Of the 59 patients with Crouzon syndrome seen at the ACFU between 1975 and 1991, 24 patients had CT scans. Unfortunately, the majority of these scans were incomplete studies of the craniofacial skeleton with the region of interest being dictated by surgical considerations (for example, peri-orbital structures or excluding the mandible). Only 8 patients had complete CT scans. These CT scans were performed according to a standardised protocol (Section 3.3.1 CT Scan Protocols).

Six of these patients had not undergone any previous surgery and thus represented the natural expression of Crouzon syndrome. Prior to attending the ACFU one patient (LW) aged 5 years and 9 months, had undergone a sagittal craniectomy in the first year of life and another patient (HC) aged 15, had undergone a fronto-orbital advance at 10 years of age.

While linear craniectomy may alter the craniofacial morphology, this effect appears to be limited in patients with craniosynostosis syndromes (Kreiborg, 1981). As will be described in the text, Patient LW had the typical clinical features of Crouzon syndrome with recurrent fusion of the sagittal suture and raised intracranial pressure. It would seem that this surgery had only a temporary effect on morphology.

The second patient had a forward shift of the fronto-orbital bar and the frontal bone. This manoeuvre was performed some 5 years prior to his presentation to the ACFU and exact details of the surgery performed were not available. At presentation his deformity had recurred. While the fronto-orbital region of the patient does not represent the complete unoperated "pure" deformity, the cranial base and maxilla had not been operated on. In view of this and the limited amount of complete 3D CT data available, these 2 patients were included in the study.

The 8 patients were allocated to categories according to age (Table 3.1). The categories were determined by the age groups of the dried skulls available for statistical comparison (Section 3.2.2 Experimental Standard). While the majority of patients had a close age match, Patient RN in the first category of 6 months was not closely matched. Subdividing this category to

accommodate the rapid growth changes, was not possible due to the lack of age-matched controls. The weight given to results for this patient is therefore less than for the other patients.

Seven of the patients underwent surgery and post-operative CT reconstructions were available for analysis in 6 of these. The patient photographs, plain radiographs and 3D CT reconstructions are shown in Figures 3.1 - 3.8. The post-operative images are also seen in the figures and are analysed in Chapter Four. Threshold settings for optimal CT reconstruction are also shown (Table 3.1) and are discussed further in Section 3.3.2 (3D CT Scan Reconstruction and Interpretation).

Table 3.1 Details of 8 patients with Crouzon syndrome undergoing analysis of 3D CT reconstructions

Age Category	Name	Sex	Age at initial CT scan	Type of Surgery and Age	Age at Post op CT scan	Threshold (Hounsfield units)
6 months	RN	M	1 month	Fronto-orbital advance (4 months)	10 months	126
6 months	SH	F	5 months	Fronto-orbital advance (7 months)	8 months	126
2 years	JS	F	21 months	Fronto-orbital advance (22 months)	22 months	126
2 years	IP	M	21 months	Fronto-orbital advance (22 months)	22 months	126
6 years	LW	M	5.5 years	Extended Fronto-orbital advance (5.75 years)	6 years	151
6 years	AY	M	5.75 years	nil	—	126
Adult	HC	M	15 years	Fronto-facial advance (15 years)	15 years	176
Adult	TS	M	27 years	Fronto-facial advance (27 years)	incomplete CT	176

3.2.2 Experimental Standard

3.2.2.1 Introduction

In utilising 3D coordinate data of anatomic landmark position no standard 3D data representing the normal population was available for comparison. Cephalometric standard data (Riolo et al.,

1974)` were found to be inadequate. For example, some cephalometric measurements represented distances cast by overlying shadows which were not seen on the 3D CT images. Additionally, there was insufficient detail in the cephalometric data to cover all the distances and angles which could be reliably identified with this method (Section 3.3.8 Measurements). Population cephalometric data were not available for children under the age of 6 years and 4 of the 8 patients examined fell into this category. Selected measurements from CT scans in normal patients have been made in limited regions of the craniofacial skeleton (Waitzman et al., 1992a; Waitzman et al., 1992b). These were measured from axial CT slice data alone and were inadequate to act as standards due to the desire for greater detail in this investigation. In addition, the measurements were available in the literature well after the establishment of the existing project in 1991.

Comparative full head CT scans of the normal population were needed in sufficient numbers to develop an experimental standard for statistical use. Several options were considered in producing suitable normal population material for comparison. Firstly, CT scans of children with normal craniofacial morphology were considered. However, subjecting normal children to ionising radiation is not acceptable. Ethical difficulty was also encountered when attempting to develop a normal standard by performing CT scans of recently deceased children. Skeletal material from dried Caucasian skulls (of the type found in anatomy departments) posed no major ethical considerations nor radiation hazard (Figure 3.9). These were readily available, easily transported for CT examination and therefore were used for this project.

3.2.2.2 Dried Skull Specimens

Dried skulls were collected from around Australia with assistance from and in collaboration with Dr I. Holten (Research Fellow, ACFU). A full list of Anatomy and Dental departments, and private individuals, contributing to this project are listed in the Acknowledgments. The skulls were of Caucasian origin and ranged in age from perinatal to adult (Figure 3.9). The skulls were labelled, examined clinically, photographed, and underwent cephalometric radiographs (Figure 3.10). From examination and radiographs, the skulls were aged according to the dental development (Moorrees et al., 1963a; Moorrees et al., 1963b) with the assistance of Professor T. Brown (Director of Research, Australian Cranio-Facial Unit).

This avenue of investigation was limited by the uncertain origin, sex and precise age of the skulls. Additionally, the dried skulls had an element of shrinkage (Bergland, 1963) and of variable trauma to the bony prominences associated with time but generally the results were of excellent quality.

CT scans of the skulls were performed according to the same protocol used in the Crouzon population, in both the CT scanner at the Department of Radiology, Women's and Children's Hospital, Adelaide (Figure 3.11) and the Department of Radiology at Royal Prince Alfred Hospital, Camperdown, Sydney. A total of 72 skulls of varying ages underwent this procedure. Twenty four skulls were selected representing 6 skulls in each of the corresponding 4 age groups (Table 3.2). These skulls were measured and used as the experimental standard for the age group.

Table 3.2 Details of the 24 dried skulls used to generate the experimental standard

Age Category	Designation, Age and Threshold (Hounsfield units)					
6 months	A1 4 - 6 mths -724	B3 2 mths -824	B4 2 mths -824	B6 8 - 12 mths -724	S2 8 - 12 mths -724	Simp1 6 mths -624
2 years	A2 18 mths -674	B11 24 mths -724	B7 18 mths -724	B8 20 mths -674	B9 24 mths -624	S3 24 mths -624
6 years	A4 6 yrs -624	B15 6 yrs -624	B16 6 yrs -624	B18 5 - 6 yrs -624	S7 6 yrs -624	S8 6 - 7 yrs -624
Adult	Abb1 Adult -624	D6 Adult -624	D7 Adult -624	D8 Adult -624	S18 Adult -624	Simp3 Adult -624

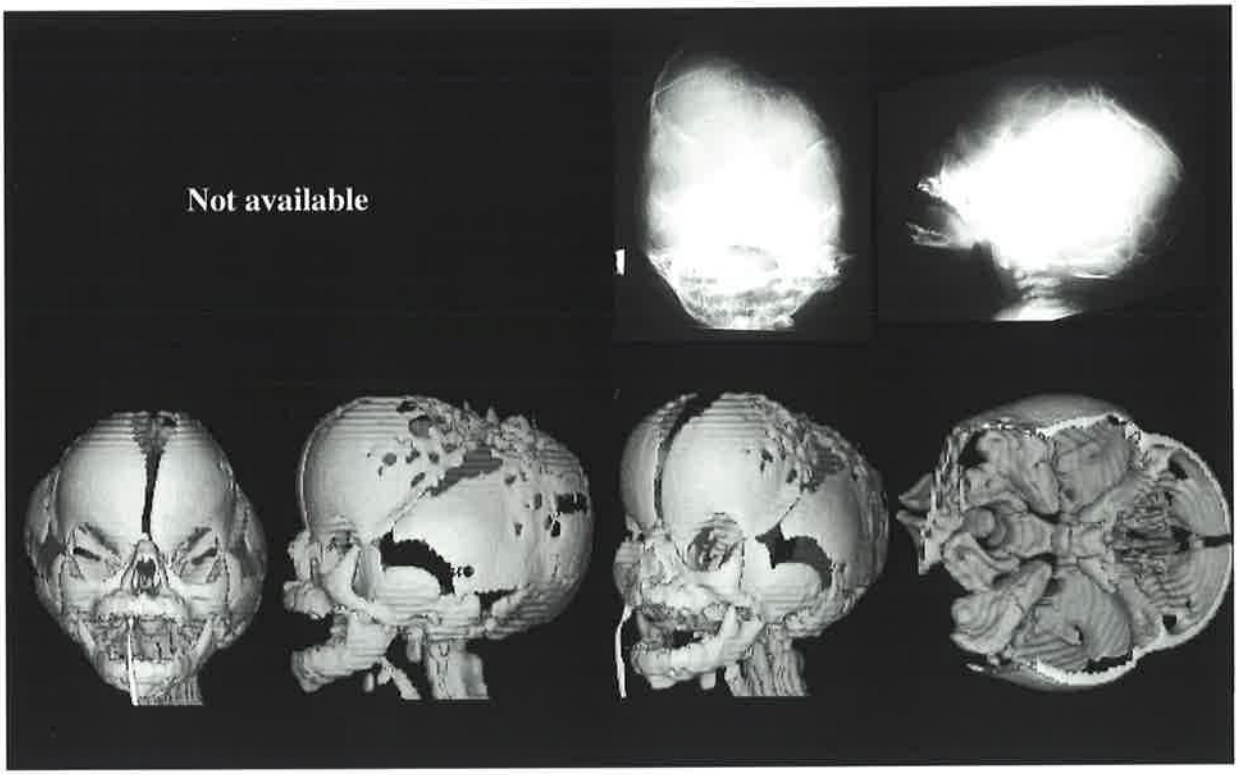

Pre-operative images (1 month of age).

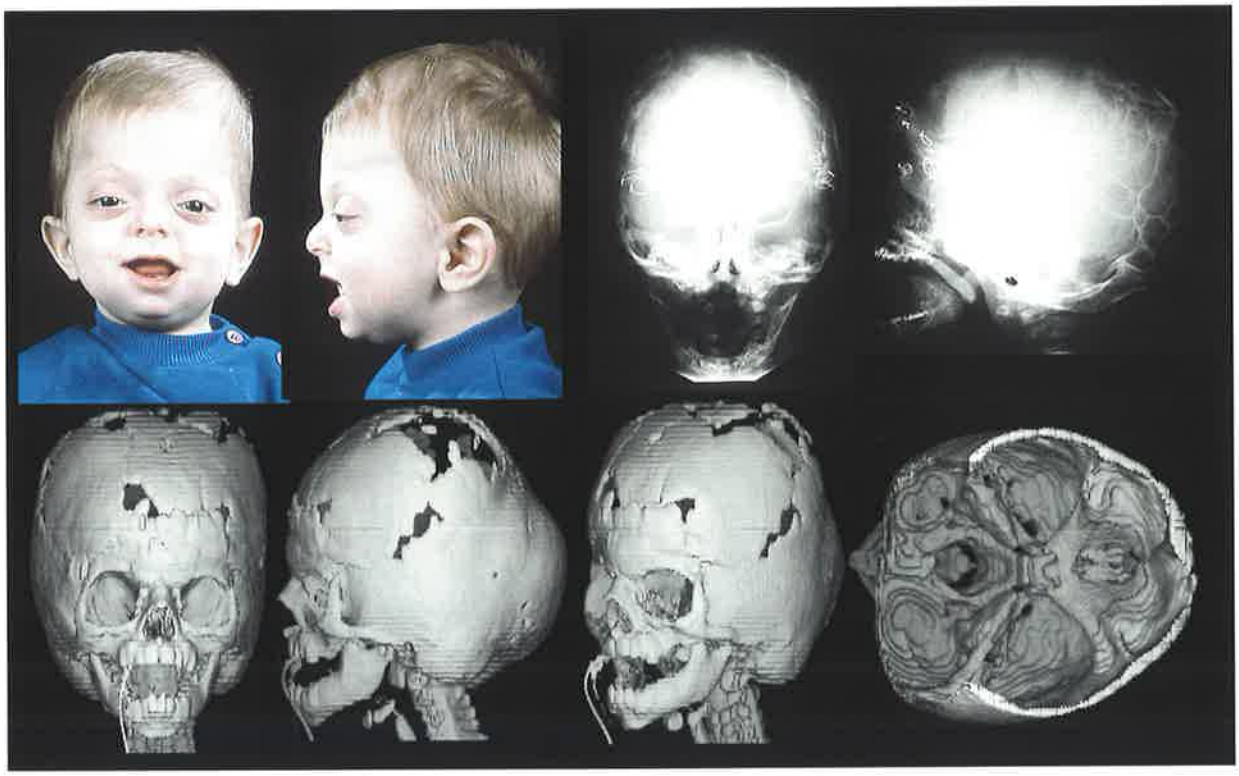

Post-operative images (10 months of age).

Figure 3.1 Pre-operative and post-operative photographs, radiographs and 3D CT reconstructions of Patient RN.

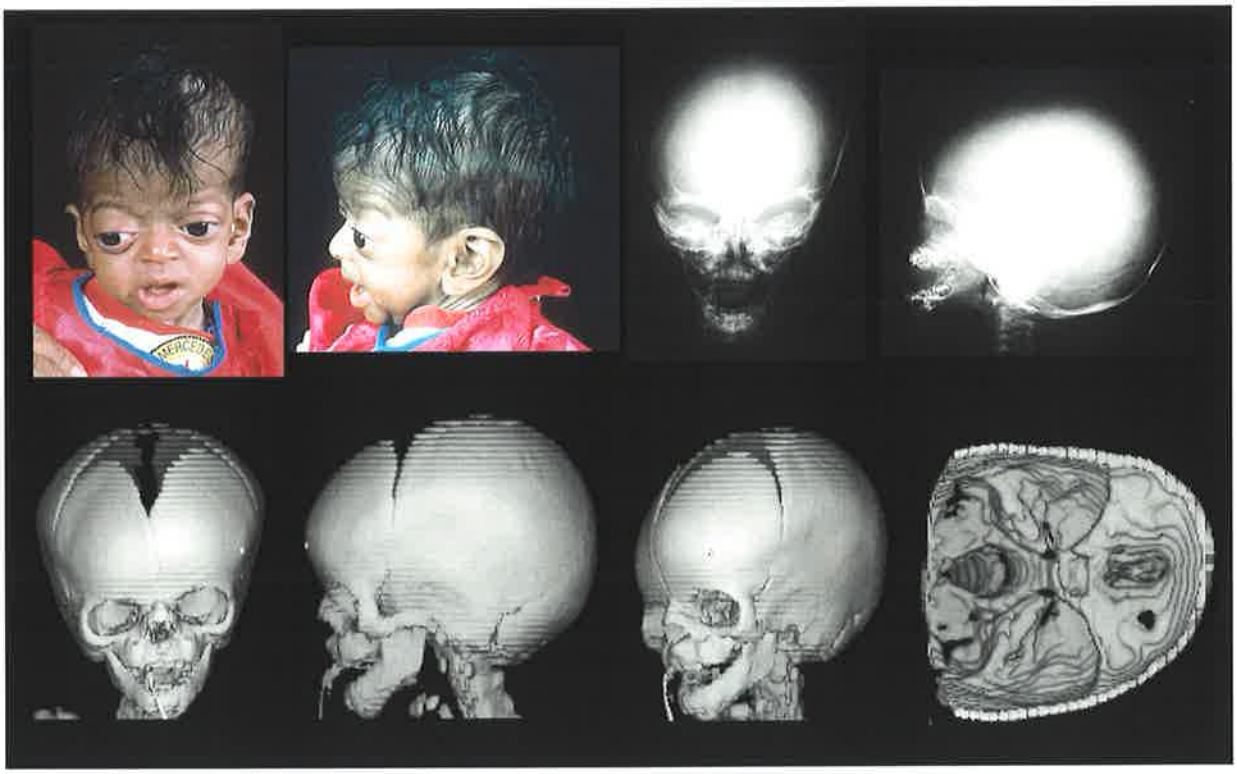

Pre-operative images (5 months of age).

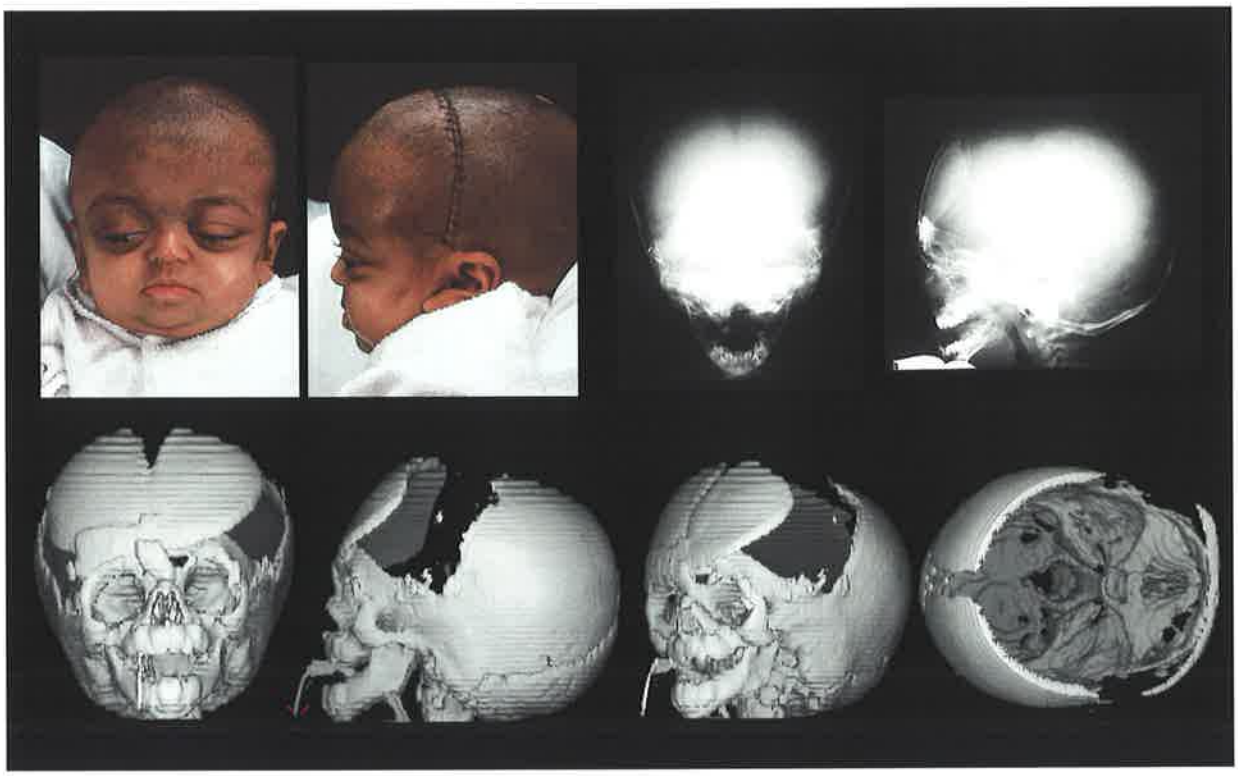

Post-operative images (8 months of age).

Figure 3.2 Pre-operative and post-operative photographs, radiographs and 3D CT reconstructions of Patient SH.

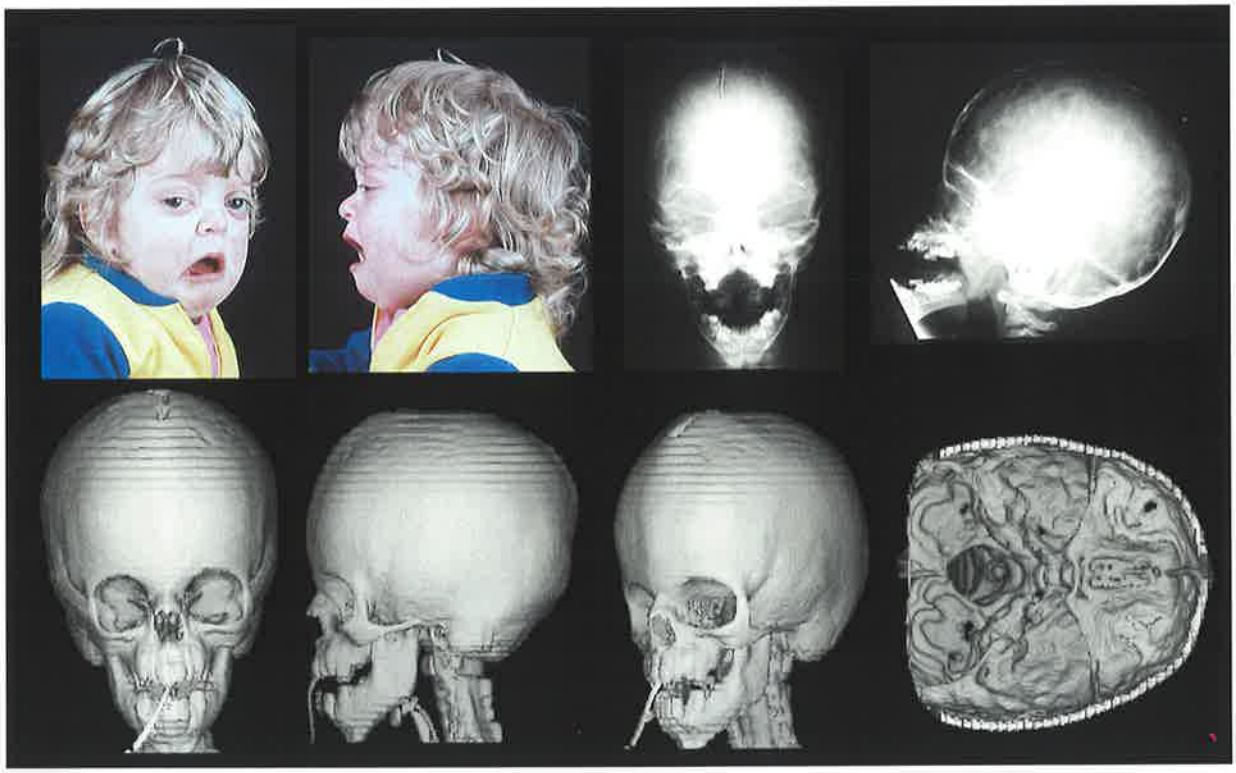

Pre-operative images (21 months of age).

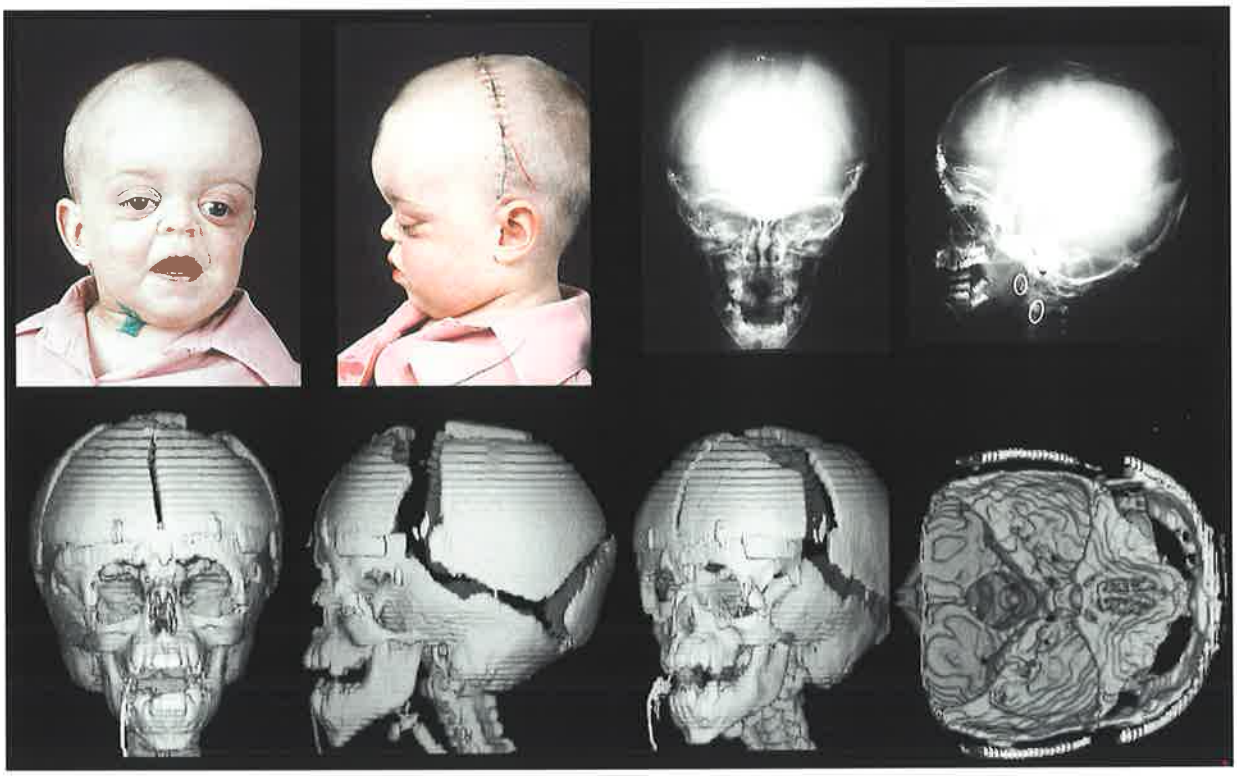

Post-operative images (22 months of age).

Figure 3.3 Pre-operative and post-operative photographs, radiographs and 3D CT reconstructions of Patient JS.

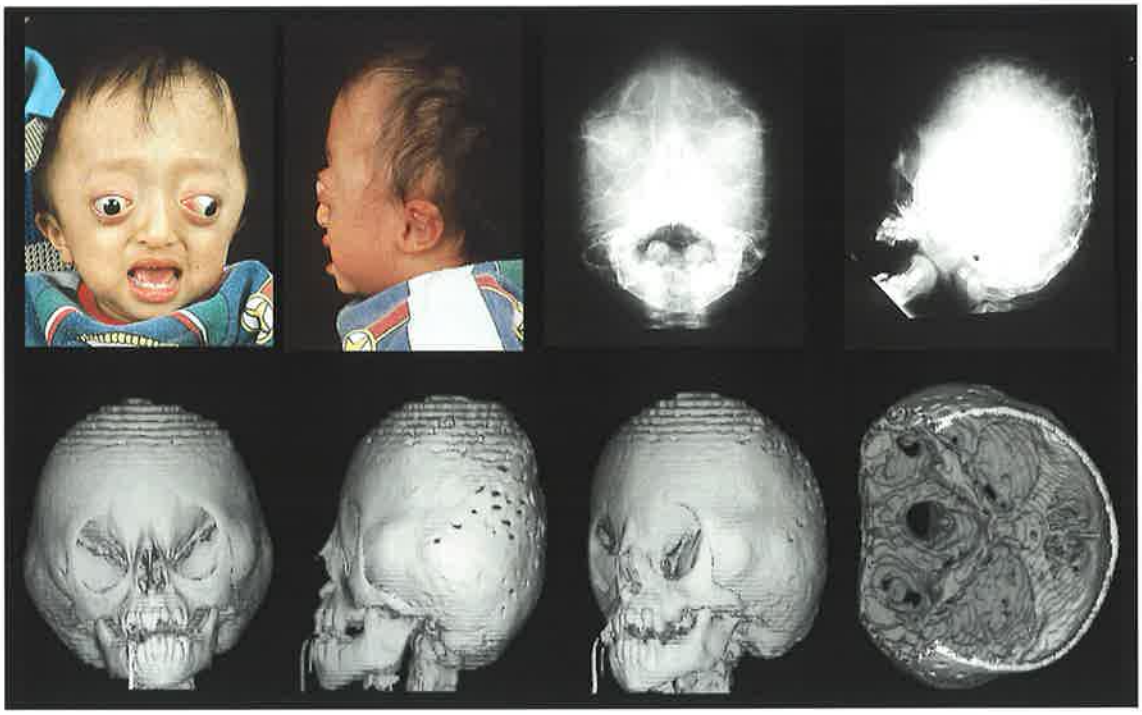

Pre-operative images (21 months of age).

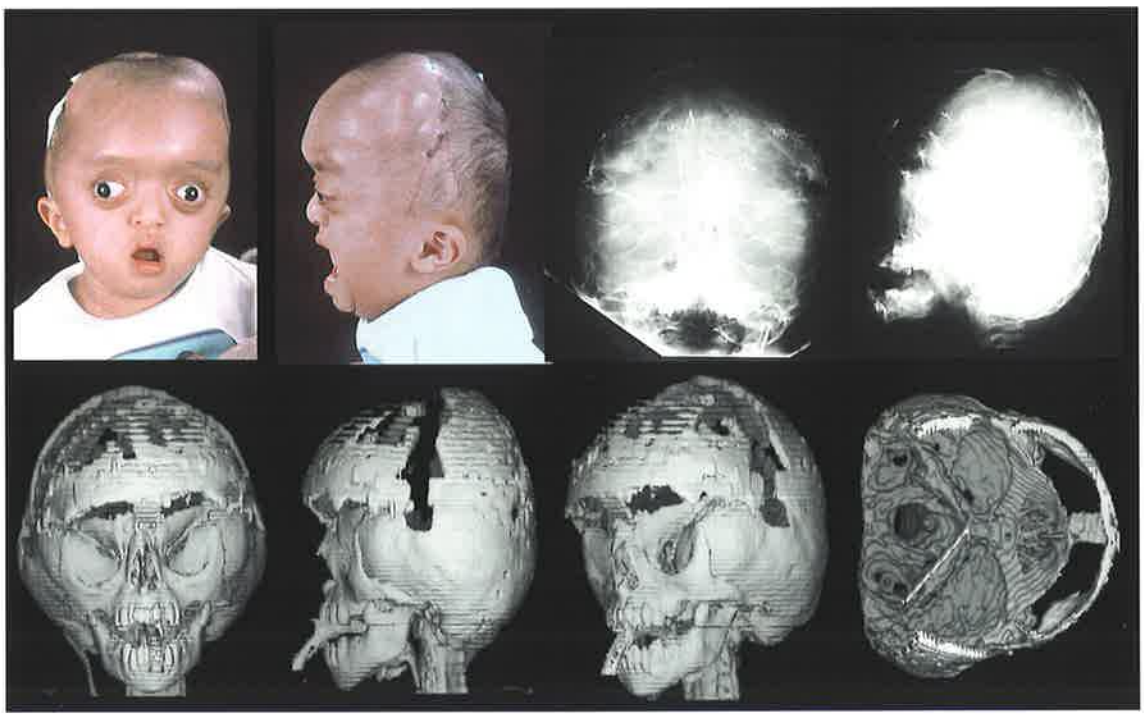

Post-operative images (22 months of age).

Figure 3.4 Pre-operative and post-operative photographs, radiographs and 3D CT reconstructions of Patient IP.

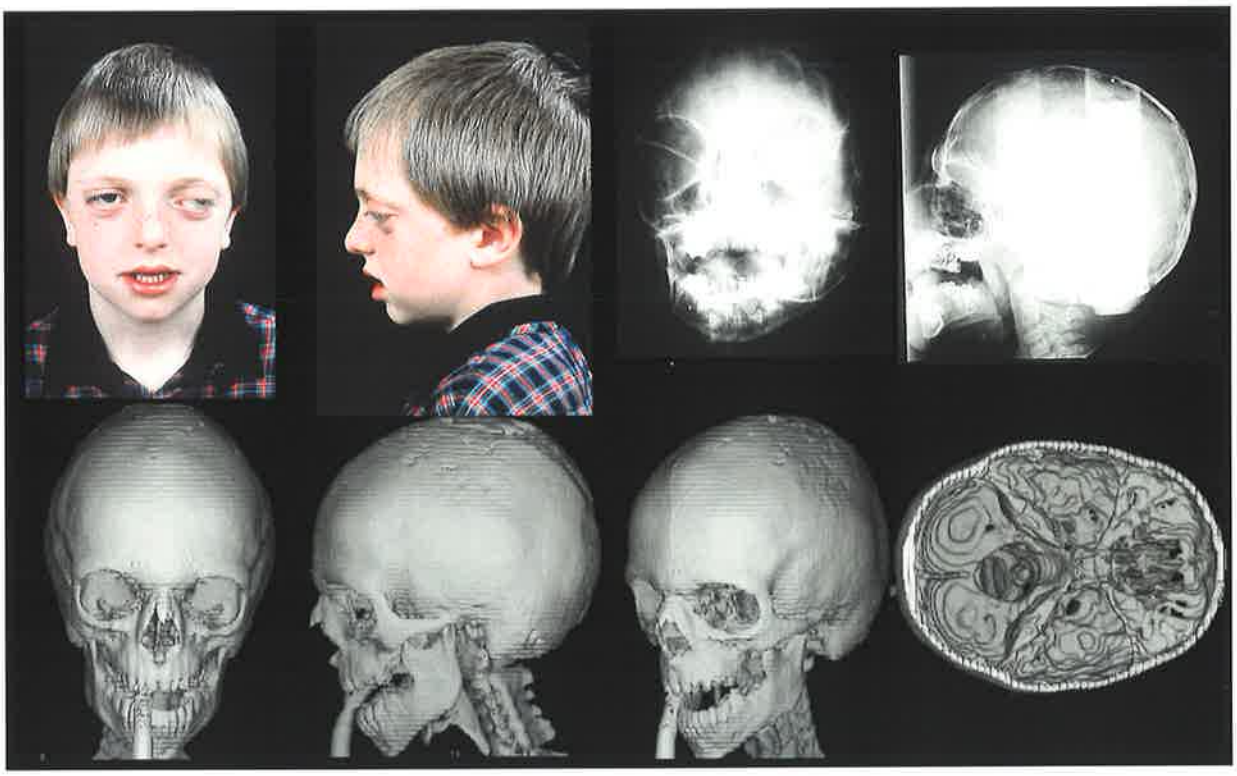

Pre-operative images (5.5years of age).

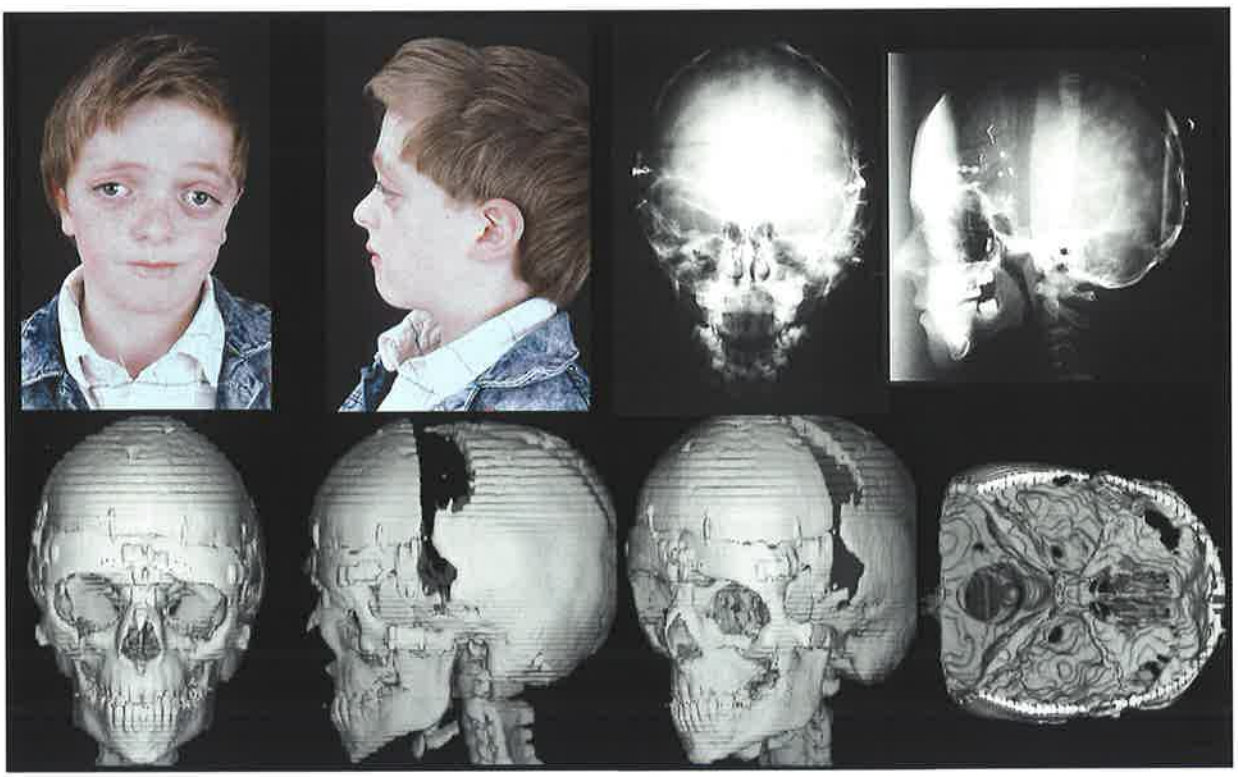

Post-operative images (6 years of age).

Figure 3.5 Pre-operative and post-operative photographs, radiographs and 3D CT reconstructions of Patient LW.

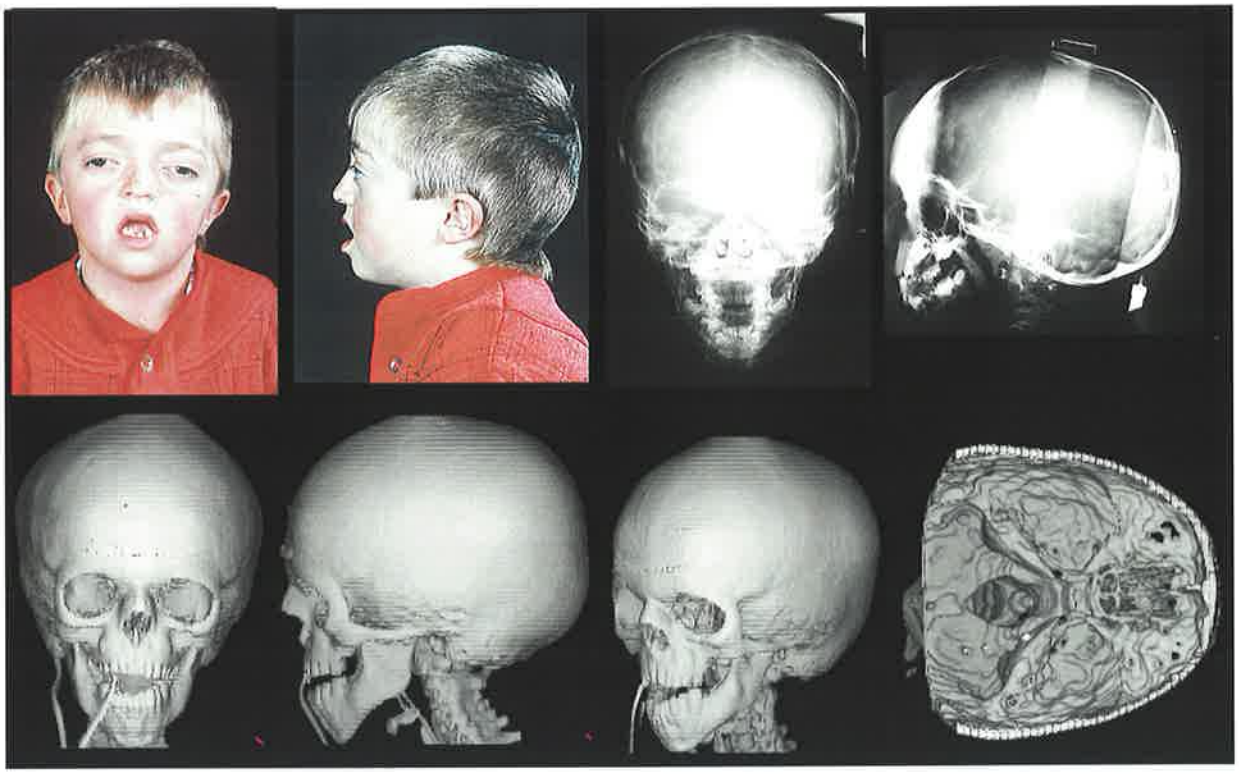

Pre-operative images (5.75 years of age).

No surgery performed.

Post-operative images.

Figure 3.6 Pre-operative photographs, radiographs and 3D CT reconstructions of Patient AY.

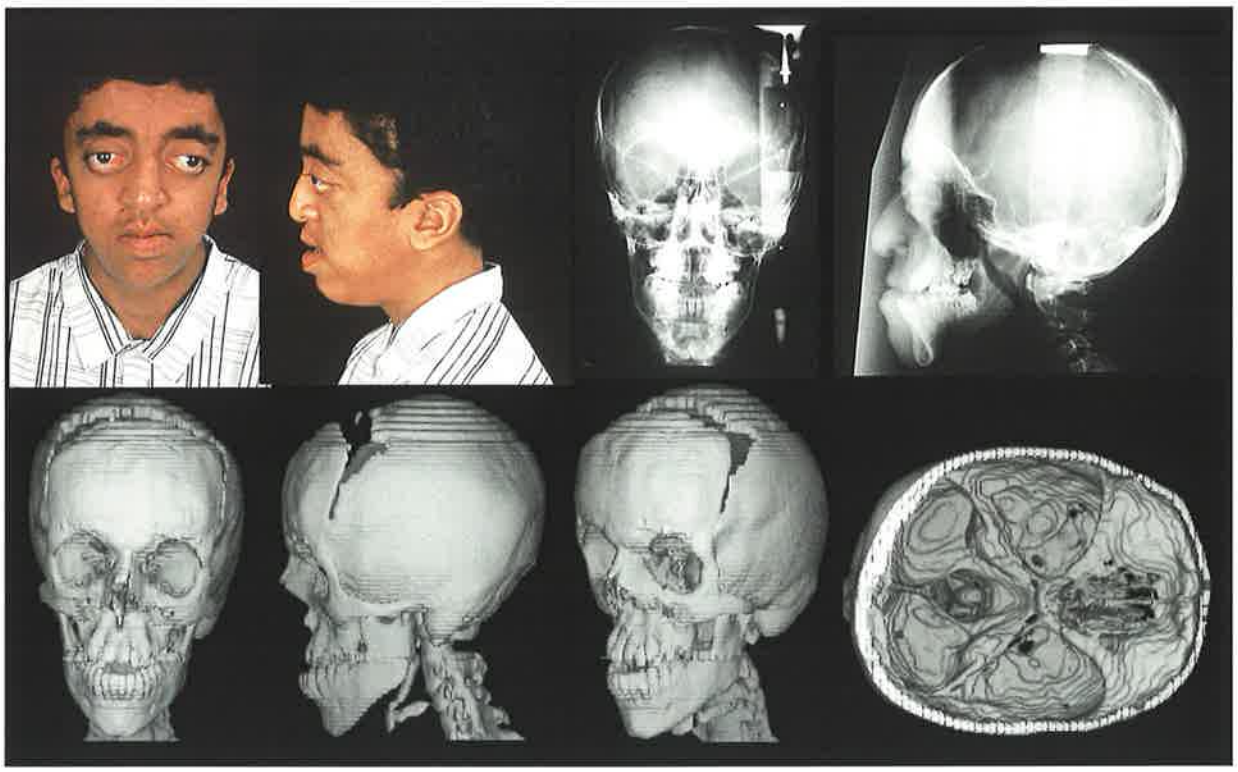

Pre-operative images (15 years of age).

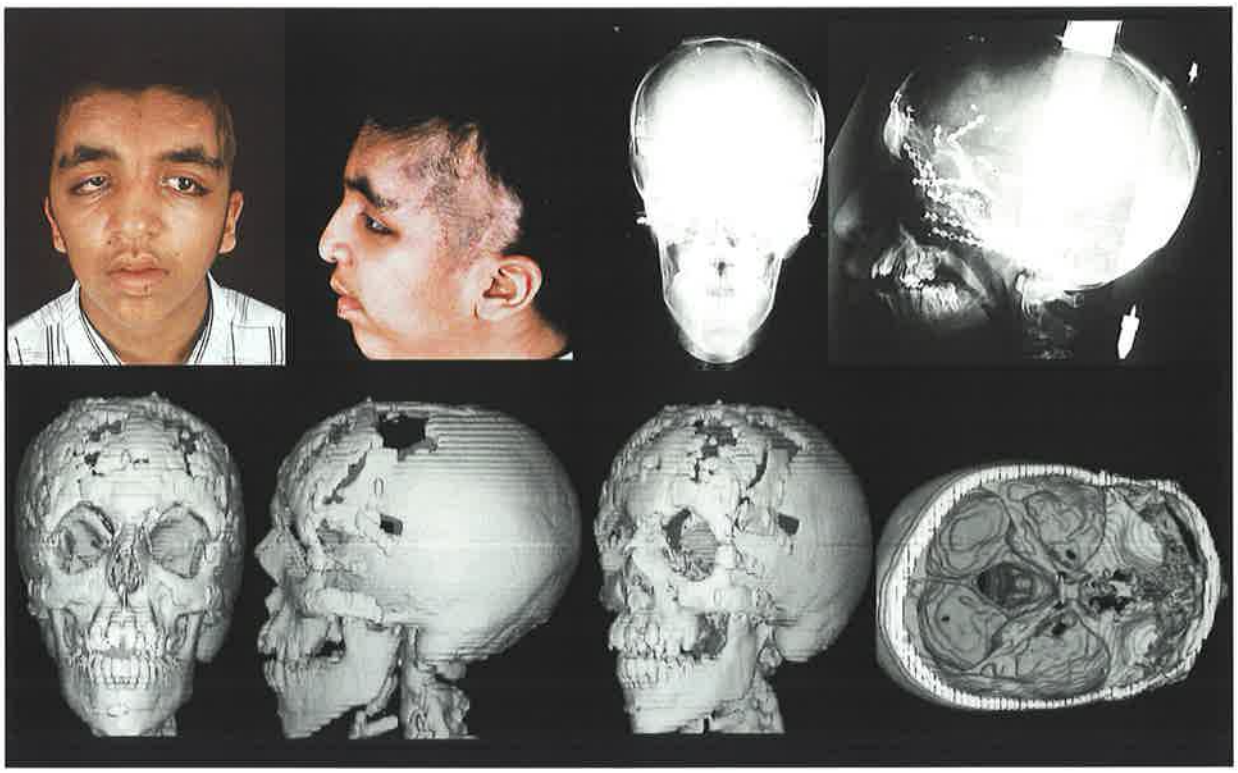

Post-operative images (15 years of age).

Figure 3.7 Pre-operative and post-operative photographs, radiographs and 3D CT reconstructions of Patient HC.

Pre-operative images (27 years of age).

Inadequate post-operative CT scan.

Data not analysed.

Post-operative images.

Figure 3.8 Pre-operative photographs, radiographs and 3D CT reconstructions of Patient TS.

Figure 3.9 Series of dried skulls ranging from birth to 18 years of age.

Figure 3.10 Cephalometric radiographs of dried skull specimens to assist with determination of the age of the material.

Figure 3.11 Computed tomography scan performed at the Women's and Children's Hospital with the assistance of Mr G Truman (Chief Radiographer) on General Electric Scanner Series 8800.

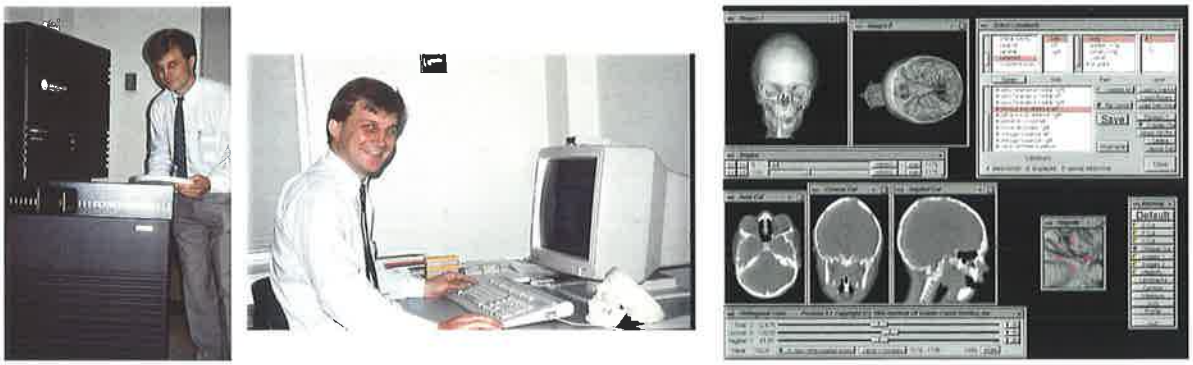

Figure 3.12 Transfer of CT data via half inch computer tape to a Silicon Graphics workstation and generation of images using Persona software.

Figure 3.13 Examples of photographs and 3D CT reconstructions of Dried Skulls in the four age groups.

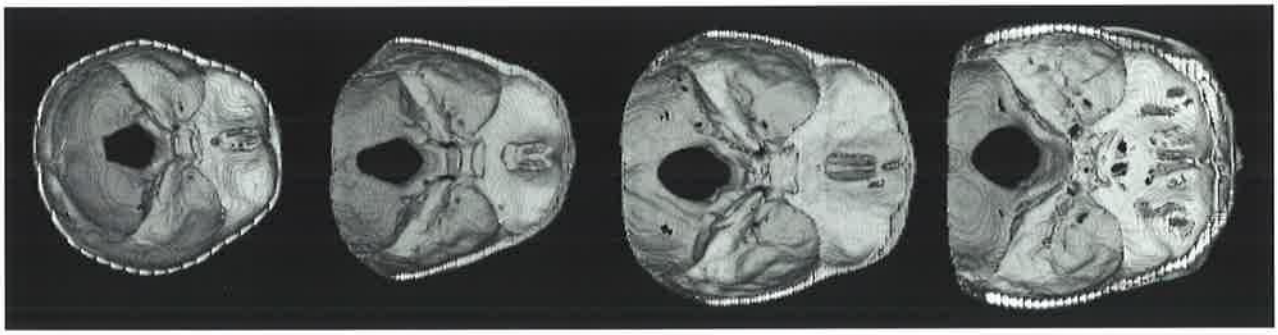

Figure 3.14 3D CT reconstructions of the cranial base for the skulls shown in Figure 3.13.

3.3 Method

3.3.1 CT Scan Protocols

CT scans of the patients with Crouzon syndrome were performed using a General Electric (GE) CT/T 8800 Scanner[3] at the Department of Radiology, Women's and Children's Hospital, Adelaide (Figure 3.11). The majority of CT scans of the dried skulls were performed on the same scanner, while those obtained from Sydney were scanned with the General Electric CT/T 9800 Scanner[3] at the Department of Radiology, Royal Prince Alfred Hospital, Sydney. All the scans were performed according to a standard protocol with 5 on 5 mm slices through the calvarial structures and 5 on 3 mm slices through the orbits to the symphysis mentis. A clean air CT slice above the vertex and below the symphysis was also performed to ensure no data were lost. A film copy of the 3D CT reconstructions were produced by the same departments. This allowed immediate clinical use and provided the basis for deciding optimal scans for closer examination. The CT data were stored onto half inch computer tape and the selected patient and dried skull data were transferred to Silicon Graphics[4] Workstation Iris Power Series 4D220/GTX (64Mb RAM, 2Gb hard disk) and Silicon Graphics[4] Workstation Elan R4000 (96 Mb RAM, 1 Gb hard disk) for analysis in the ACFU (Figures 3.12 - 3.14).

3.3.2 3D CT Scan Reconstruction and Interpretation

Three-dimensional CT scan derived data, while producing an accurate representation of the craniofacial skeleton, is limited by the resolution of the data acquisition (slice thickness). Variable factors affecting the reproduction of CT images have been well described (McCullough, 1977; Fullerton and White, 1979; Koehler et al., 1979; Baxter and Sorenson, 1981; Christiansen et al., 1986; David et al., 1990). The skulls were rendered several times at different thresholds to produce the best reproduction.

In those patients with marked endocranial resorption, high thresholds may produce errors of exclusion in thin bones, such as, the ethmoid bone, the calvaria and the middle cranial fossa. In

[3] General Electric Company, Medical Systems Group, Wisconsin, USA

[4] Silicon Graphics Corporation, Mountain View, California, USA

addition, errors of inclusion may occur at the edges of the bones at the calvarial and cranial base sutures and synchondroses and at the cranial base and facial foraminae. Difficulty with a particular threshold selection for 3D CT reconstructions was overcome by interactive reference to the axial slices of the original data. The thresholds selected for the 3D CT reconstructions are listed in Table 3.1.

3.3.3 Analysis of the Craniofacial Skeleton

Following transfer of the CT data on half inch computer tape to the Silicon Graphics Workstation, the software program "Persona" was used to determine the anatomic landmark positions (Figure 3.12). The steps taken in the 3D landmark identification and analysis are described in Sections 3.3.5 to 3.3.9.

3.3.4 Definition of Anatomical Units

The craniofacial skeleton is a complex integrated structure. The craniofacial bones are comprised of embryological subunits (ossification centres) which fuse to produce the individual bone. The bones then combine with each other to form anatomical regions such as the orbit, nasal cavity or maxillary complex. The craniofacial bones have been used as the basis for the anatomical units described this study.

Using the detailed 3D CT reconstruction, it was possible to visualise key anatomical landmarks on the perimeters of each of the craniofacial bones. The lacrimal, palatine and inferior conchal bones were difficult to separate from their neighbouring bones and thus were included with the adjacent bone forming an anatomical unit. The cranial base sutures and craniofacial dimensions and angles were also measured to determine what patterns, if any, existed in the Crouzon population.

The anatomical units examined were:

(i) The Mandible

(ii) The Maxilla and Nasal Bones (including palatine and inferior concha)

(iii) The Frontal Bone

(iv) The Zygomatic Bone

(v) The Vomer

(vi) The Ethmoid (including lacrimal)

(vii) The Sphenoid

(viii) The Temporal Bone

(ix) The Parietal Bone

(x) The Occipital Bone

(xi) Cranial Base Sutures

(xii) Craniofacial Dimensions and Angles

Diagrams of the bony components are shown in the Figures 3.15 - 3.26, with the definition of the key bony landmarks (and the measurements made) listed in the legends for these figures.

The key landmarks enabled true dimensions of the bones to be identified and recorded as coordinates in 3 dimensions. From these, measurements of distances and angles were calculated. The landmarks selected by Abbott (1988) were initially used and were modified during the investigation to more accurately represent the "anatomical units". These now provide the landmarks found in "Persona" (Section 3.3.5 "Persona" 3D Medical Imaging and Analysis Software). This program was used to locate in 3D, 225 landmarks on the craniofacial skeleton of each patient and 214 on each dried skull.

3.3.5 "Persona" 3D Medical Imaging and Analysis Software

"Persona" software provided simultaneous visualisation of the CT craniofacial data in both 2D and 3D. Two-dimensional cuts through the 3D data volume were presented in 2D axial (Z axis), coronal (Y axis), and sagittal (X axis) windows. Thus, while the CT data was acquired as axial images any landmark could be identified in all 3 planes (Figure 3.12). Precise location of landmarks was primarily performed using these images. Landmarks were recorded by the program as a coordinate in 3D following selection of the defined site.

Three-dimensional reconstructions of the skull with rotations about the Z axis in 6° steps were also available. A second 3D reconstruction with the top axial slices omitted and rotation in the X axis enabled visualisation of the internal cranial base. These images were enlarged two-fold to improve the ease of location of landmarks but were not used for the precise voxel selection. These facilities were assisted by the use of a magnification window which increased the image

region by a factor of 2. Three-dimensional stereoscopic images could also be viewed directly on the monitor with stereo glasses. The stereoscopic images needed no enlargement. These images enabled confirmation of the landmark location.

3.3.6 Method of Landmark Identification

Generally, where the point could be readily seen on the 3D reconstruction, initial identification was made using 2 or more views to locate the surface point by the process of triangulation. The 2D slices were then utilised to locate the appropriate pixel. Slices could be stepped through in the 3 planes to find the best possible position. The point chosen was then checked on the 3D images. Occasionally, points could not be readily seen on the 3D images (for example, vomerine points, jugular foramen points and some external cranial base points where the cervical vertebrae obscured the view) and the 2D slices were used alone.

3.3.7 Landmark Accuracy

Calculation of the error of the method was performed by the process of double determination (Brown and Abbott, 1989; Abbott et al., 1990b). The 8 Crouzon syndrome patients and 10 dried skulls (Simp1, S2, B7, B3, B5, S6, S7, S8, S18, Simp3) selected from the experimental standard group had the landmarks determined on 2 separate occasions, approximately 1 month apart. The landmarks of each determination were then compared by the process of least squares and repeated median and the differences recorded.

The calculation revealed variation in the double determinations between landmarks on both the dried and Crouzon skulls. The landmark accuracy for all points is shown in Appendix 1. The median relocation error for the Crouzon patients was 1.0 mm (range 0.4 - 5.3 mm) producing a pooled relocation error of 1.3 mm (225 landmarks). The dried skulls recorded a median relocation error of 0.9 mm (range 0.3 - 2.8 mm) producing a pooled relocation error of 1.2 mm (214 landmarks).

Many of the landmarks available on "Persona" and used in the calculation of the error of the method were not used in the measurement analysis. In particular, those landmarks that were not readily identified or not considered to be an essential part of the anatomical unit were excluded.

3.3.8 Measurements

3.3.8.1 Introduction

A host of methods of measurement of anthropological and radiological specimens are available for the assessment of size and shape. They include the following: distance and angle measurements, least squares matching (Sneath, 1967), repeated median fitting (Siegel, 1982), homologous distances and log measurements (Healy and Tanner, 1981), and biorthogonal grid/strain analysis of finite elements (Bookstein, 1987; Abbott et al., 1990a).

In this study, distance and angle measurements made up the majority of the analysis. This method gives basic information about the dimensions of the objects under investigation. As this is a relatively new method of investigation, it was appropriate to verify its accuracy and analyse the basic data. The measurements of distances and angles were based on the outlines of the cranial bones and thus provided new information, not only about their individual dimensions but also the adjoining surfaces - the sutures and synchondroses. The method of calculation of distances and angles is recorded in the footnote[5].

The number of landmarks and hence measurements may be considered to be overinclusive, but was considered necessary as this method was applied for the first time to this data. In some patients, some landmarks were not able to be recorded and hence several measurements were not possible (Section 3.4 Results).

---

[5] **Methods of Measurement of Distances and Angles.**

As all landmarks were recorded as 3D coordinate data the measurement of distances and angles was possible. Calculations were made by determining the distance d_{ij}, between 2 landmarks whose positions are specified by the vectors $\mathbf{x}_i = (x_i, y_i, z_i)$ and $\mathbf{x}_j = (x_j, y_j, z_j)$. The distance, d_{ij}, is the magnitude of the vector difference between the points: $d_{ij} = |\mathbf{x}_i - \mathbf{x}_j|$; that is $d_{ij} = \sqrt{[(x_i - x_j)^2 + (y_i - y_j)^2 + (z_i - z_j)^2]}$

The angle, q, between 2 vectors defined by 3 landmarks $\mathbf{x}_i, \mathbf{x}_j, \mathbf{x}_k$ is calculated from the dot product of difference vectors (that is, the vectors $(\mathbf{x}_i - \mathbf{x}_j)$ and $(\mathbf{x}_k - \mathbf{x}_j)$):

$$\cos(q) = \frac{(\mathbf{x}_i-\mathbf{x}_j)\ |\mathbf{x}_k-\mathbf{x}_j|}{|\mathbf{x}_i-\mathbf{x}_j|\ |\mathbf{x}_k-\mathbf{x}_j|}$$

Similarly the angle, q, between two vectors, specified by the landmarks $\mathbf{x}_i$, $\mathbf{x}_j$, $\mathbf{x}_k$, and $\mathbf{x}_l$, (that is, the vectors $(\mathbf{x}_j - \mathbf{x}_i)$ and $(\mathbf{x}_l - \mathbf{x}_k)$) is given by

$$\cos(q) = \frac{(\mathbf{x}_j-\mathbf{x}_i)\ (\mathbf{x}_l-\mathbf{x}_k)}{|\mathbf{x}_j-\mathbf{x}_i|\ |\mathbf{x}_l-\mathbf{x}_k|}$$

3.3.8.2 Measurement of Distances, Dimensions and Angles

All dimensions of the craniofacial bones were measured, particularly the interfaces between the individual cranial bones, that is, the sutures and synchondroses. The principal approach was the measurement of known anatomic units (that is, craniofacial bones) rather than of craniofacial regions (that is, orbits and nasal cavity).

The measurements for each anatomical unit were divided into 3 groups:

(i) Distances - representing the measurement between adjacent landmarks which specifically form the outline of the cranial bone or anatomical unit.

(ii) Dimensions - representing measurement between landmarks which do not follow the outline of the cranial bone but represent overall bony size (maximum width, length etc.)

(iii) Angles - representing the shape of the anatomical unit. Interpretation was made difficult by the 3D nature of the study. Angles were measured by 2 methods. The angle between 3 points was measured or between the projected bisection of 2 lines (4 points).

The distances, dimensions and angles are represented diagrammatically in Figures 3.15 - 3.26 and defined in the legend for the figures.

Due to the complex nature of the examination of the craniofacial bones, the more complex anatomical units were subdivided for ease of recording and interpretation. This was particularly necessary for the ethmoid, sphenoid and temporal bones. The method of subdivision is shown in the representation of the anatomical units in Figures 3.15 - 3.26.

3.3.9 Statistical Analysis

3.3.9.1 Creation of an Experimental Standard

Experimental standards were created which corresponded to each of the 4 age groups (that is, 6 months, 2 years, 6 years and adult). The experimental standard was derived from the average of the measurements taken from the landmarks selected on the 6 skulls in each age of the 4 age

groups. The mean and standard deviations for the measurements of the age-matched normal skulls were determined and are listed in Appendix 2. The statistical data were used for the comparison with the corresponding measurements of the anatomical units in each of the 8 patients with Crouzon syndrome.

3.3.9.2 Comparison of the Experimental Standard and Crouzon Population

Following the creation of the experimental standard for the measurements, a statistical comparison was then undertaken for each of the patients in the Crouzon population. Z scores were calculated from the measurements from the individual Crouzon syndrome patients compared with the patient data for each measurement. The statistically significant results at the 5% level ($Z < 1.96$ and $Z > 1.96$) were identified and reported as being increased or decreased in distance, dimension or angle compared with the experimental standard population.

Due to the limitations of the study, such as the small number of controls in each age group (n = 6) and the often small distances measured, the results may more closely represent trends rather than truly significant findings and are interpreted in the light of this. Log measurements and strain analysis were not undertaken in this study.

Limitations of the data available for study include the size of the sample of individuals with Crouzon syndrome (n=6), the spread of the age of the patients (6 months, 2 years, 6 years and adult hood) and the ethnicity of the Caucasian population with Crouzon syndrome. As it was not possible to select large numbers of individuals with Crouzon syndrome for the study, the population studied represented the population that had adequate data available and it therefore seems reasonable to use this data.

Inherent in the presentation of Crouzon syndrome is variation in severity of the condition. A large number of variables were selected for measurement, representing the outlines of the cranial bones and their related sizes and shapes. While there are many measurements in a small heterogenous sample the detailed measurement analysis allows examination of where the severity of the condition is expressed in an individual patient.

This study is not intended to provide all the answers to the morphological pathology of Crouzon. However, using the recently described powerful tool of measurement of 3D CT data,

new clues may be found to the morphology by comparison of the anatomical units of patients and enables comments to made on the possible mechanisms of these differences.

Figures 3.15(a)-(f) **Diagrammatic representations of the Mandible showing the key Landmarks identified and the Distances, Dimensions and Angles measured**

Landmark Definitions

cdl/cdr	**condylion laterale left/right:** The most lateral point on the condylar head.
cbl/cbr	**coronoid base left/right:** The minimum distance from gonion to the inferior limit of the anterior border of the coronoid process (usually located near or at the junction of the ramus with the body of the mandible).
ctl/ctr	**coronoid tip left/right:** The most superior point on the coronoid process.
em1il/em1ir	**ectomolare 1st inferius left/right:** The most lateral point on the alveolar ridge, opposite the centre of the mandibular first molar.
gn	**gnathion:** The most inferior point on the mandibular symphysis in the mid-sagittal plane (sometimes referred to as menton).
gol/gor	**gonion left/right:** A point on the angle of the mandible located by the bisection of the angle formed by the mandibular line and the ramus line.
id	**infradentale:** The most antero-superior point on the mandibular alveolar margin in the mid-sagittal plane.
mnl/mnr	**mandibular notch left/right:** The most inferior point on the mandibular notch (sigmoid notch).

Figures 3.15(a)-(f) (Mandible continued):

Legend for Figures 3.15(a) and 3.15(b)

Distance Definitions

Left		Right	
id-em1il	L anterior superior body	**id-em1ir**	R anterior superior body
em1il-cbl	L posterior superior body	**em1ir-cbr**	R posterior superior body
id-cbl	L total superior body	**id-cbr**	R total superior body
cbl-ctl	L anterior ramus	**cbr-ctr**	R anterior ramus
ctl-mnl	L anterior mandibular notch	**ctr-mnr**	R anterior mandibular notch
mnl-cdl	L posterior mandibular notch	**mnr-cdr**	R posterior mandibular notch
cdl-gol	L posterior ramus	**cdr-gor**	R posterior ramus
gol-gn	L inferior body	**gor-gn**	R inferior body

Figure 3.15(a): Mandible
(anterior aspect)
Landmarks and Distances

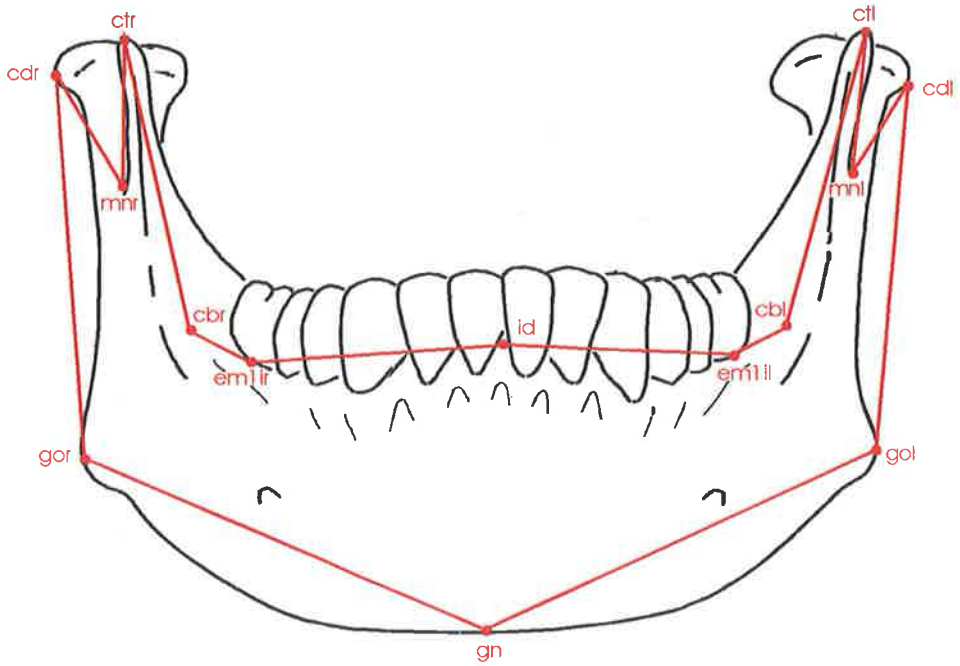

Figure 3.15(b): Mandible
(left lateral aspect)
Landmarks and Distances

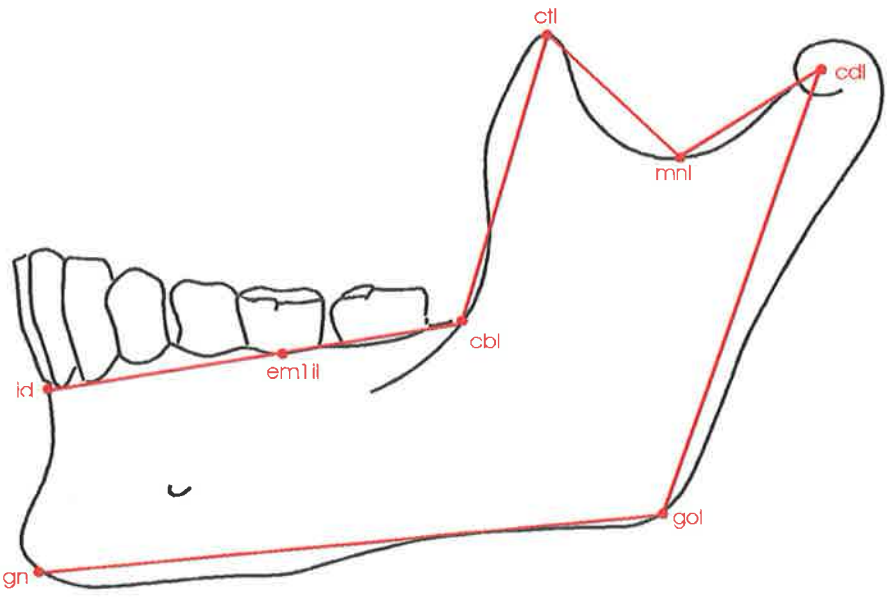

Figures 3.15(a)-(f) (Mandible continued):

Legend for Figures 3.15(c) and 3.15(d)

Dimension	Definitions
gol-gor	Intergonial dimension
cdl-cdr	Intercondylar dimension
cbl-cbr	Intercoronoid base dimension
em1il-em1ir	Intermolar dimension
cdl-ctl	L Superior ramus width
gol-cbl	L inferior ramus width
cdr-ctr	R Superior ramus width
gor-cbr	R inferior ramus width
gn-id	Anterior symphyseal height
gn-cdr	R total mandibular length

Figure 3.15(c): Mandible
(anterior aspect)
Dimensions

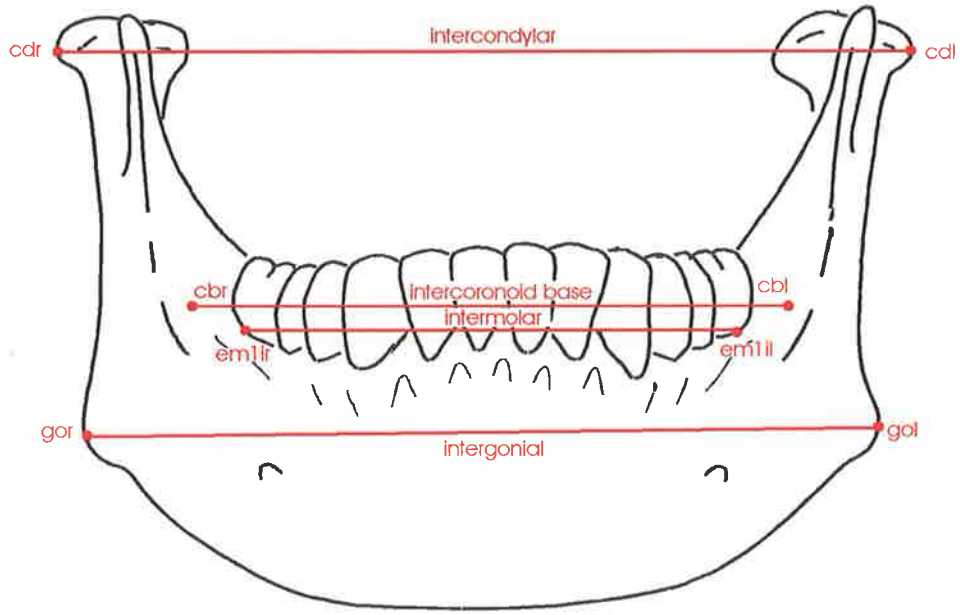

Figure 3.15(d): Mandible
(left lateral aspect)
Dimensions

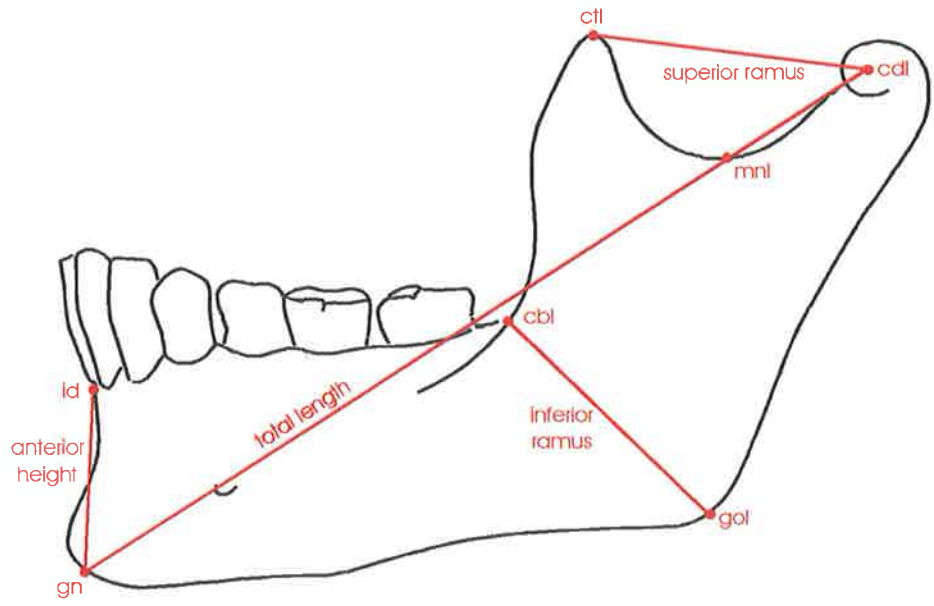

Figures 3.15(a)-(f) (Mandible continued):

Legend for Figures 3.15(e) and 3.15(f)

Angle Definitions

cdl-mnl-ctl	L mandibular notch angle
cdr-mnr-ctr	R mandibular notch angle
cdl-gol-gn	L gonial angle
cdr-gor-gn	R gonial angle
ctl-cbl-id	L coronoid base angle
ctr-cbr-id	R coronoid base angle
ctl-cbl-em1il	L coronoid-dental base angle
ctr-cbr-em1ir	R coronoid-dental base angle
gol-gn-id	L symphyseal angle
gor-gn-id	R symphyseal angle
gol-gn-gor	Anterior mandibular angle

Figure 3.15(e): Mandible
(left lateral aspect)
Angles

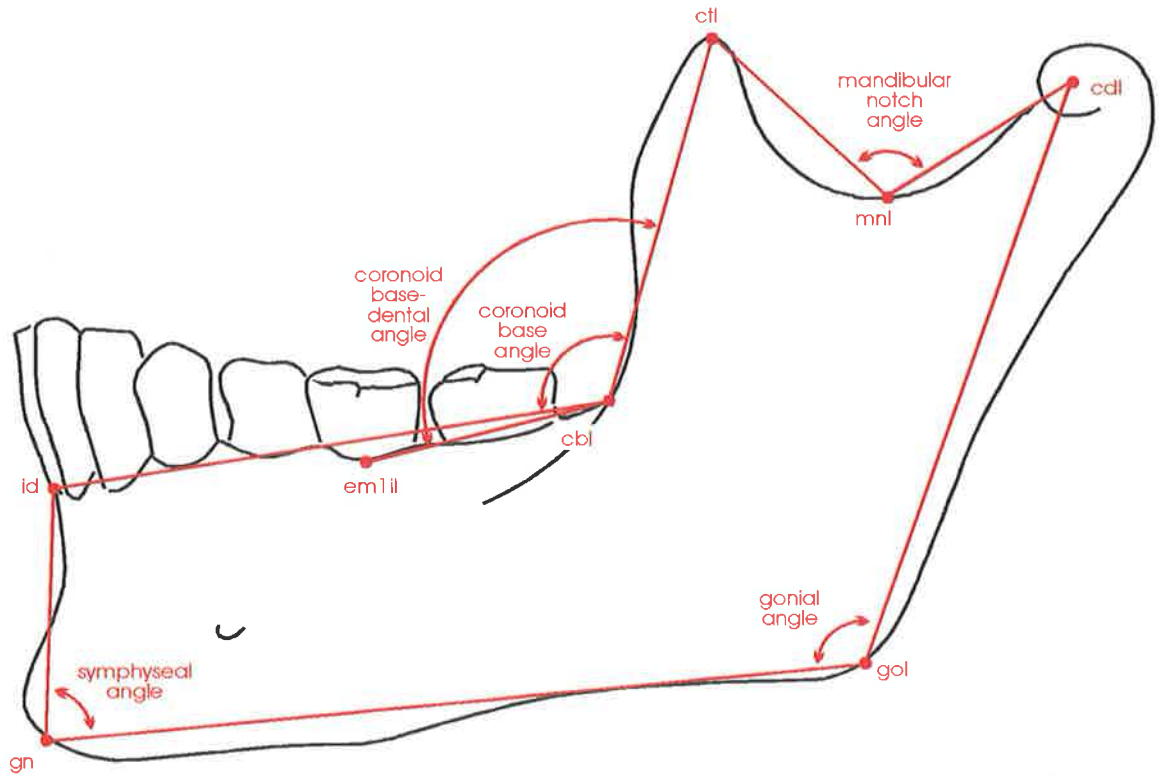

Figure 3.15(f): Mandible
(anterior aspect)
Angles

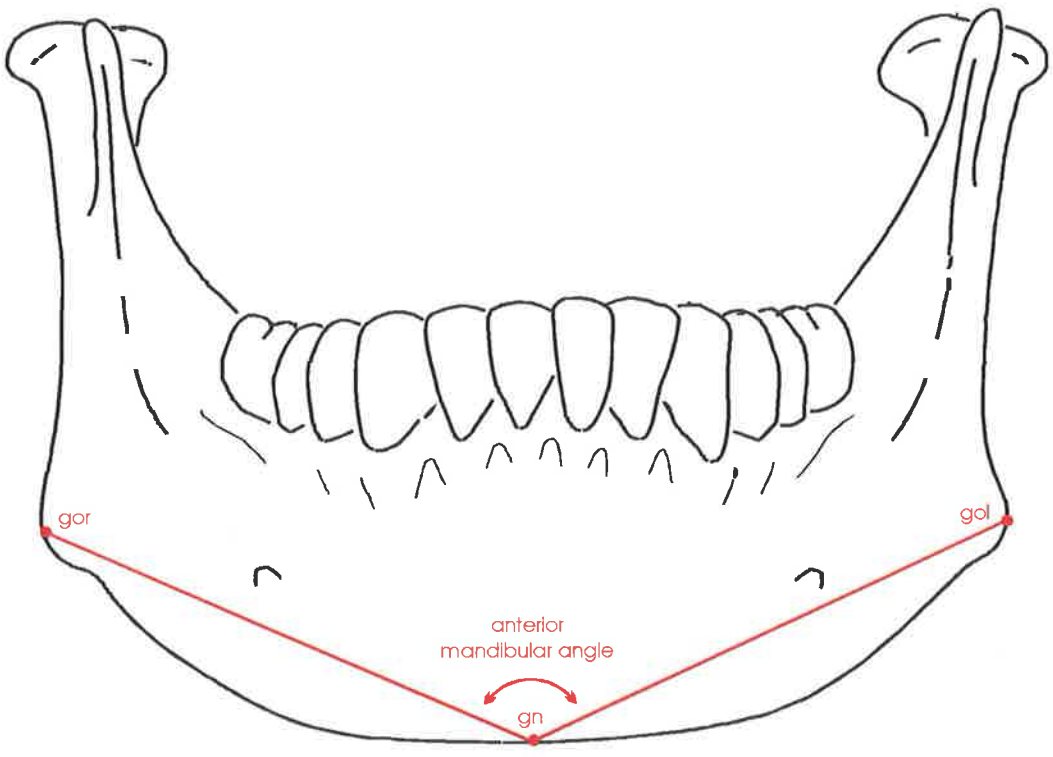

Figures 3.16(a)-(h) **Diagrammatic representations of the Maxilla and Nasal Bones showing the key Landmarks identified and the Distances, Dimensions and Angles measured**

Landmark Definitions

all/alr	**alare left/right:** The most lateral point on the anterior nasal aperture.
ans	**anterior nasal spine:** The apex of the anterior nasal spine. (Also known as spinal point (sp) or acanthion (ac)).
ecsl/ecsr	**ecto-canine superius left/right:** The most anterior point on the alveolar ridge, opposite the centre of the maxillary canine.
em1sl/em1sr	**ectomolare 1st superius left/right:** The most lateral point on the alveolar ridge, opposite the centre of the maxillary first molar.
gpfl/gpfr	**greater palatine foramen left/right:** The centre of the greater palatine foramen.
inml/inmr	**inferior naso-maxillare left/right:** The most inferior point on the naso-maxillary suture.
iobfl/iobfr	**inferior orbital fissure left/right:** The most anterior point on the margin of the inferior orbital fissure.
msl/msr	**maxillare superius left/right:** The most postero-superior point on the maxilla determined from CT slice images. (located in sagittal view as the most superior point on the maxillary surface, at the junction of orbital and infra-temporal surfaces.)
mxtl/mxtr	**maxillary tuberosity left/right:** The most postero-inferior point in the midline of the maxillary tuberosity.
morl/morr	**medial orbitale left/right:** The most medial point on the orbital margin in the region of the fronto-lacrimal suture. (Located near the craniometric point Dacryon).
na	**nasale:** The tip of the nasal bone.
n	**nasion:** The most anterior point of the frontonasal suture. (If suture not clearly identified then the deepest point on the nasal notch can be substituted in the midline.)
nlil/nlir	**naso-lacrimal inferius left/right:** The most antero-inferior point on the margin of the naso-lacrimal groove as it exits the orbit (usually this point is located at the small spicule of bone covering the lateral wall of the naso-lacrimal groove and the inferior orbital rim).
orl/orr	**orbitale left/right:** The most inferior point on the infra-orbital margin.
pns	**posterior nasal spine:** The apex of the posterior nasal spine.
pr	**prosthion:** The most antero-inferior point on the maxillary alveolar margin in the mid-sagittal plane.
snml/snmr	**superior naso-maxillare left/right:** The most superior point on the naso-maxillary suture.
zmil/zmir	**zygomaxillare inferius left/right:** The lowest point on the external suture between zygomatic and maxillary bones.(in the region of the craniometric landmark, zygomaxillare).

Figures 3.16(a)-(h) (Maxilla and Nasal Bones continued):

Legend for Figures 3.16(a) and 3.16(b)

Maxillary Distance Definitions

Left		Right	
	Orbital Region		
snml-morl	L fronto-maxillary suture	**snmr-morr**	R fronto-maxillary suture
nlil-morl	L frontal process orbital rim	**nlir-morr**	R frontal process orbital rim
msl-nlil	L medial orbital floor	**msr-nlir**	R medial orbital floor
msl-iobfl	L posterior lateral orbital floor	**msr-iobfr**	R posterior lateral orbital floor
orl-iobfl	L anterior lateral orbital floor	**orr-iobfr**	R anterior lateral orbital floor
orl-nlil	L maxillary infra-orbital rim	**orr-nlir**	R maxillary infra-orbital rim
	Anterior Wall		
zmil-orl	L anterior zygo-maxillary suture	**zmir-orr**	R anterior zygo-maxillary suture
zmil-em1sl	L lateral maxillary wall	**zmir-em1sr**	R lateral maxillary wall
em1sl-pr	L anterior alveolar margin	**em1sr-pr**	R anterior alveolar margin
ans-all	L lower pyriform margin	**ans-alr**	R lower pyriform margin
all-inml	L upper pyriform margin	**alr-inmr**	R upper pyriform margin
inml-snml	L naso-maxillary suture	**inmr-snmr**	L naso-maxillary suture
	pr-ans	Anterior alveolar height	
	Lateral Wall		
em1sl-mxtl	L posterior alveolar margin	**em1sr-mxtr**	R posterior alveolar margin
mxtl-msl	L posterior maxillary wall	**mxtr-msr**	R posterior maxillary wall
msl-iobfl	L posterior lateral orbital floor	**msr-iobfr**	R posterior lateral orbital floor
iobfl-zmil	L post. zygo-maxillary suture	**iobfr-zmir**	R post. zygo-maxillary suture

Nasal Bone Distance Definitions

Central

na-n	Nasal length

Left		Right	
na-inml	L inferior nasal width	**na-inmr**	R inferior nasal width
inml-snml	L naso-maxillary suture	**inmr-snmr**	R naso-maxillary suture
n-snml	L fronto-nasal suture	**n-snmr**	R fronto-nasal suture

Figure 3.16(a): Maxilla and Nasal Bones
(anterior aspect)
Landmarks and Distances

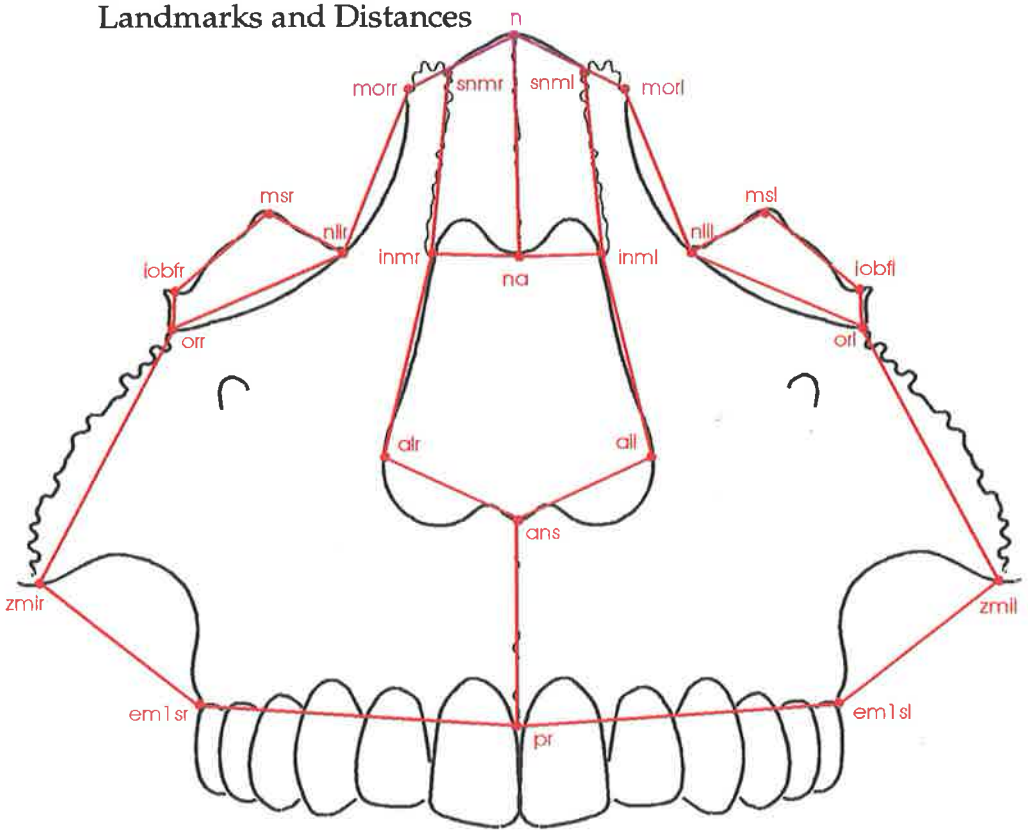

Figure 3.16(b): Maxilla and Nasal Bones
(left lateral aspect)
Landmarks and Distances

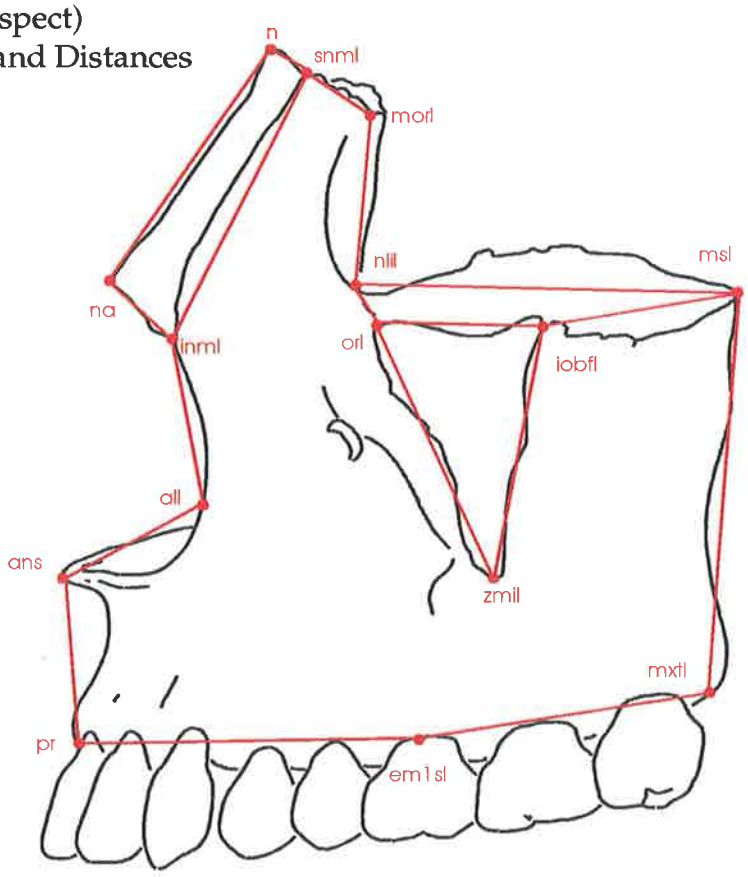

Figures 3.16(a)-(h) (Maxilla and Nasal Bones continued):

Legend for Figure 3.16(c)

Maxillary Distance Definitions

Palate

Left		Right	
em1sl-gpfl	L posterior palatal height	**em1sr-gpfr**	R posterior palatal height
gpfl-pns	L posterior palatal width	**gpfr-pns**	R posterior palatal width
		pns-ans	superior palatal length

Figure 3.16(c): Maxilla and Nasal Bones
(inferior palatal aspect)
Landmarks and Distances

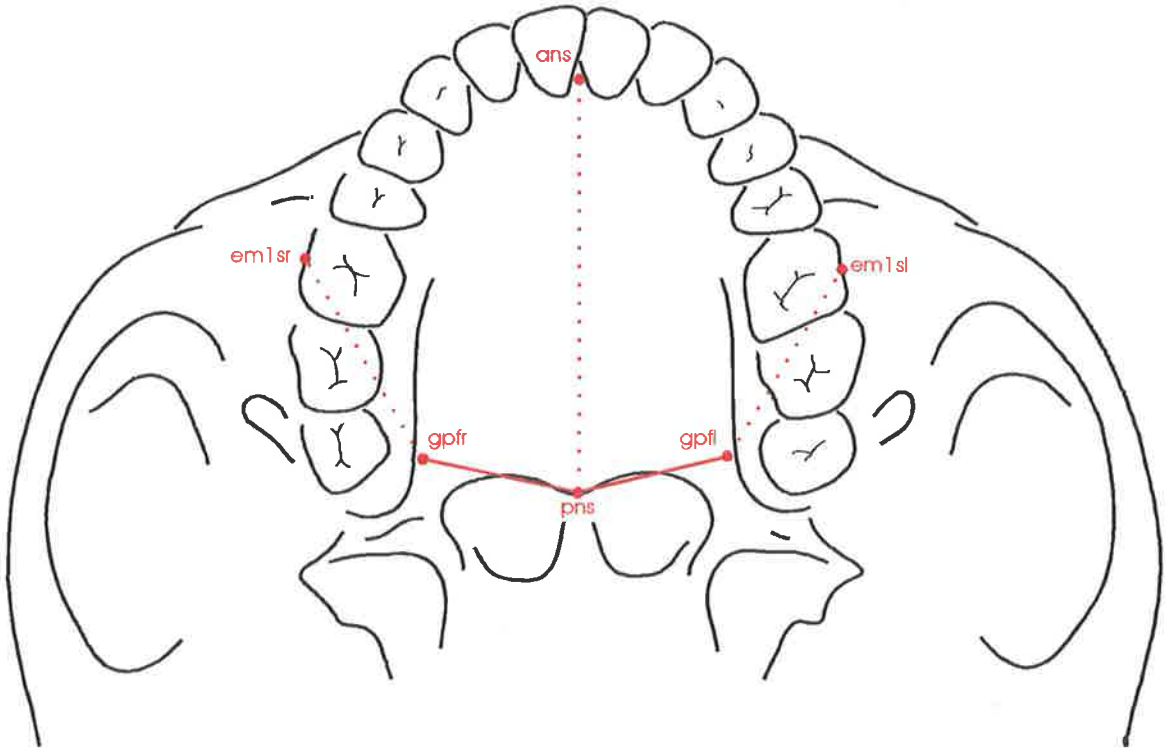

Figures 3.16(a)-(h) (Maxilla and Nasal Bones continued):

Legend for Figures 3.16(d) and 3.16(e)

Maxillary Dimension Definitions

n-pr	Anterior midline height
morl-em1sl	L lateral height
morr-em1sr	R lateral height
gpfl-msl	L posterior height
gpfr-msr	R posterior height
msl-inml	L superior length
msr-inmr	R superior length
gpfl-gpfr	Posterior palatal width
ecsl-ecsr	Anterior inter-canine width
zmil-zmir	Maximum maxillary width
orl-orr	Superior (inter-orbital rim) width
na-ans	Nasal aperture height
all-alr	Nasal aperture width

Nasal Bone Dimensions

inml-inmr	Inferior width
snml-snmr	Superior width

Figure 3.16(d): Maxilla and Nasal Bones
(left lateral aspect)
Dimensions

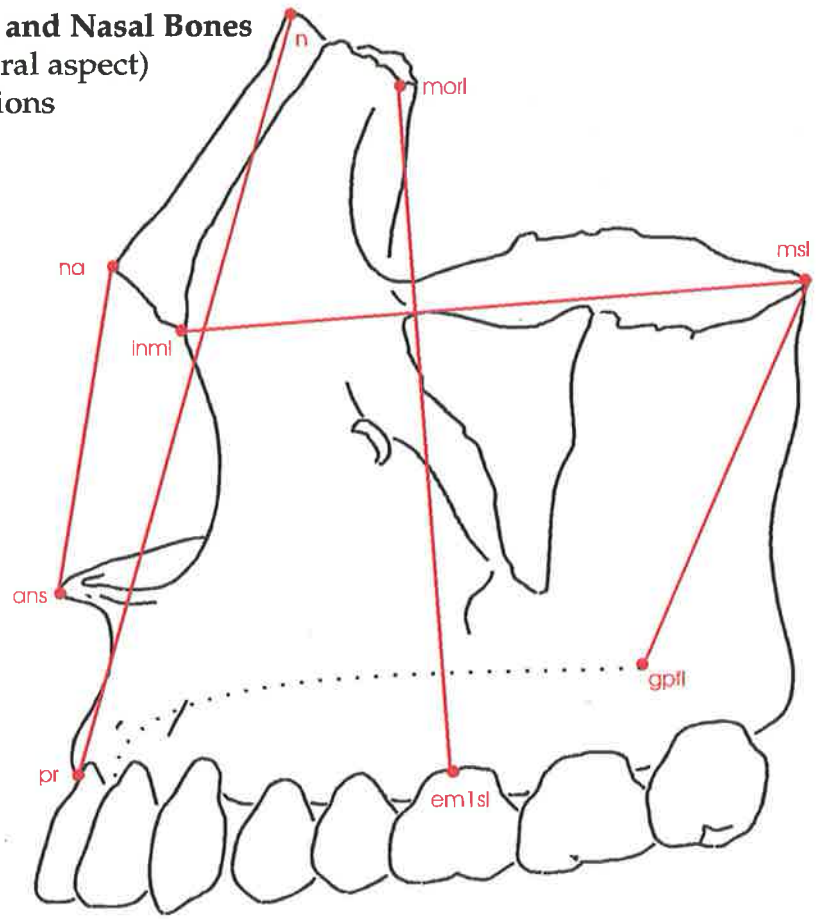

Figure 3.16(e): Maxilla and Nasal Bones
(anterior aspect)
Dimensions

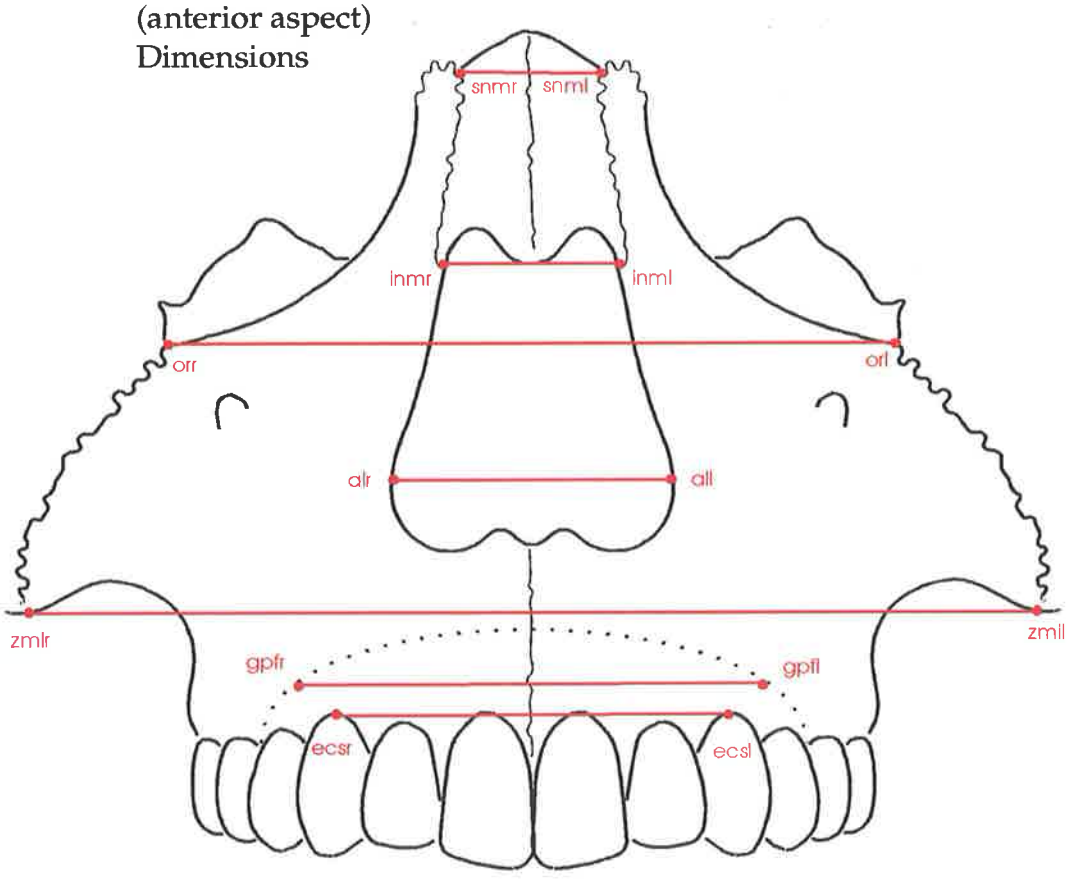

Figures 3.16(a)-(h) (Maxilla and Nasal Bones continued):

Legend for Figures 3.16(f) and 3.16(g)

Maxillary Angle Definitions

nlil-msl-iobfl	L orbital floor angle
nlir-msr-iobfr	R orbital floor angle
msl-gpfl-em1sl	L posterior inferior angle
msr-gpfr-em1sr	R posterior inferior angle
iobfl-msl/msr-iobfr	Superior maxillary splay
snml-msl/em1sl-pr	L superior/occlusal angle
snmr-msr/em1sr-pr	R superior/occlusal angle
ans-pns/em1sl-pr	L palatal/occlusal angle
ans-pns/em1sr-pr	R palatal/occlusal angle

Nasal Bone Angle Definitions

s-n-na	Nasal/anterior cranial base angle
snml-n-snmr	Superior nasal bone angle
inml-na-inmr	Inferior nasal bone angle
inml-snml/snmr-inmr	Splay of nasal bones

Figure 3.16(f): Maxilla and Nasal Bones (anterior aspect) Angles

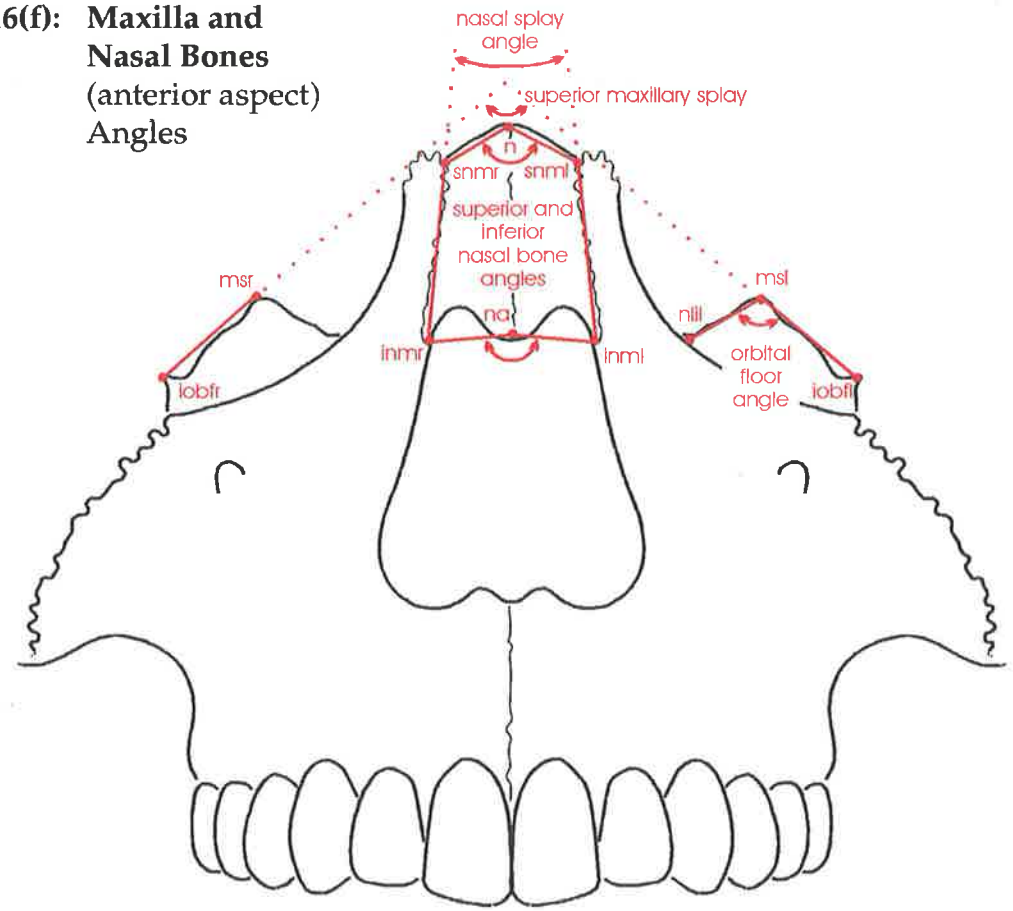

Figure 3.16(g): Maxilla and Nasal Bones (left lateral aspect) Angles

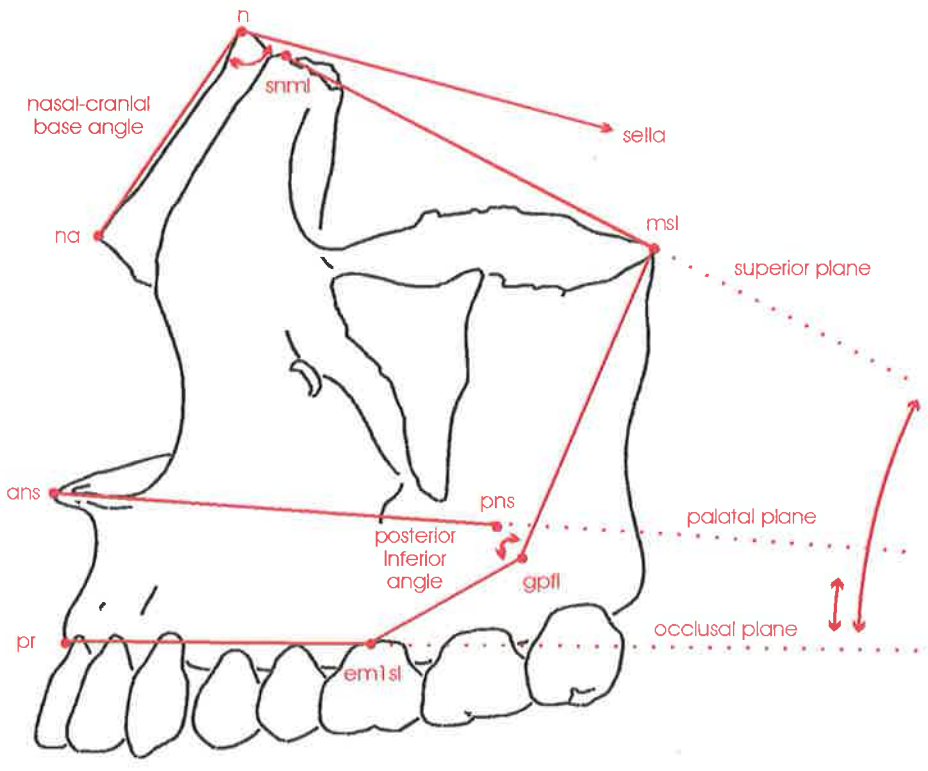

Figures 3.16(a)-(h) (Maxilla and Nasal Bones continued):

Legend for Figure 3.16(h)

Palatal Angle Definitions

gpfl-ans-gpfr	Anterior palatal angle
gpfl-pr-gpfr	Maxillary arch angle

Figure 3.16(h): Maxilla and Nasal Bones
(inferior palatal aspect)
Angles

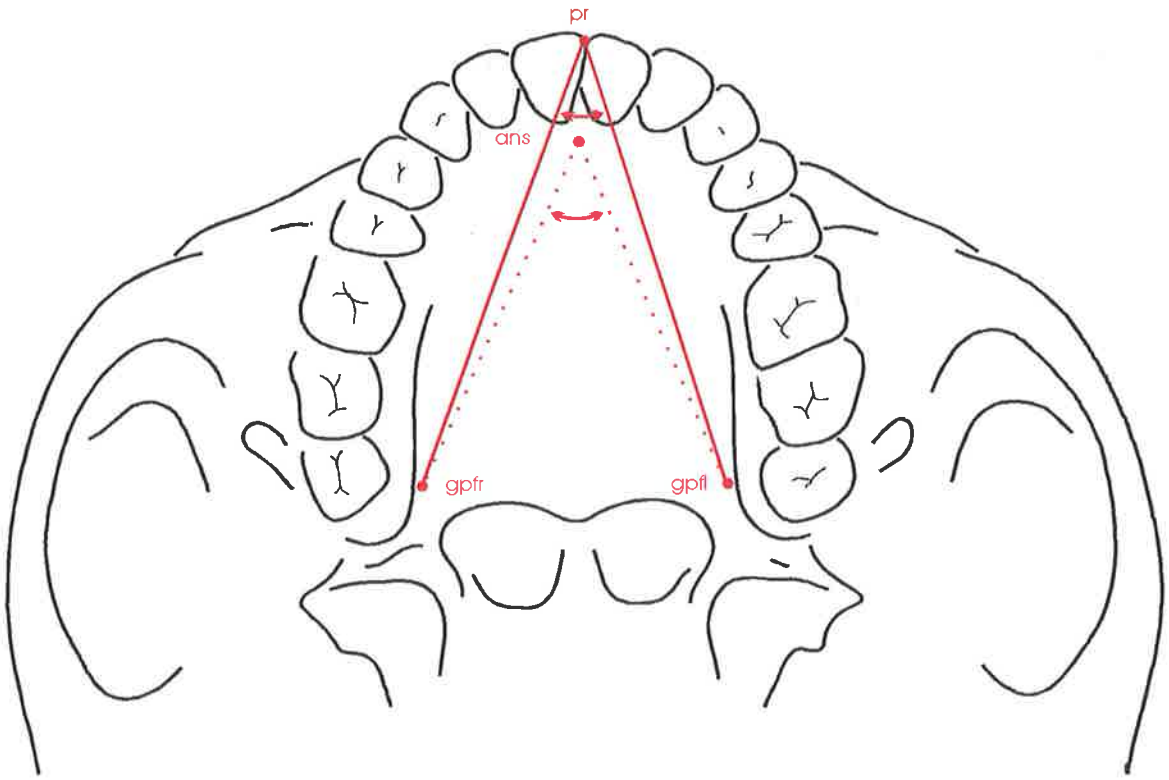

Figures 3.17(a)-(c) **Diagrammatic representations of the Frontal Bone showing the key Landmarks identified and the Distances and Dimensions measured**

Landmark Definitions

br	**bregma:** The intersection of the sagittal and the coronal sutures on the surface of the cranial vault.
g	**glabella:** The most prominent point in the mid-sagittal plane between the eyebrow ridges.
cpal/cpar	**cribriform plate anterius left/right:** The most antero-lateral point on the cribriform plate.
cppl/cppr	**cribriform plate posterius left/right:** The most postero-lateral point on the cribriform plate.
fc	**foramen caecum:** The centre of the foramen caecum.
morl/morr	**medial orbitale left/right:** The most medial point on the orbital margin in the region of the fronto-lacrimal suture.
n	**nasion:** The most anterior point of the frontonasal suture. (If suture not clearly identified then the deepest point on the nasal notch can be substituted in the midline.)
spcl/spcr	**sphenion c left/right:** The junction of the coronal suture and the sphenoid bone.
spal/spar	**sphenoidale anterior left/right:** The most anterior point on the posterior margin of the lesser wing of sphenoid at the junction with the frontal bone (see sphenoid).
snml/snmr	**superior naso-maxillare left/right:** The most superior point on the naso-maxillary suture.
sorl/sorr	**superior orbitale left/right:** The most superior point on the supra-orbital margin.
sobfl/sobfr	**superior orbital fissure left/right:** The most lateral point on the margin of the superior orbital fissure.
slorl/slorr	**supero-lateral orbitale left/right:** The intersection of the fronto-zygomatic suture with the lateral orbital rim (almost the intersection of the curve of the supra-orbital rim with the lateral orbital rim.
zfl/zfr	**zygo-frontale left/right:** The point located at the posterior extremity of the fronto-zygomatic suture. (see zygomatic bone)
zfsl/zfsr	**zygo-frontale sphenoidale left/right:** The point located at the intersection of the frontal, zygomatic and sphenoid bones. (see sphenoid and zygomatic bone)

Figures 3.17(a)-(c) (Frontal Bone continued):

Legend for Figures 3.17(a), 3.17(b) and 3.17(c)

Distance Definitions

Left	Supra-orbital Region	Right
n-snml	L fronto-nasal suture	**n-snmr**	R fronto-nasal suture
snml-morl	L fronto-maxillary suture	**snmr-morr**	R fronto-maxillary suture
morl-sorl	L superior medial orbital rim	**morr-sorr**	R superior medial orbital rim
sorl-slorl	L superior lateral orbital rim	**sorr-slorr**	R superior lateral orbital rim
slorl-zfl	L fronto-zygo suture (anterior)	**slorr-zfr**	R fronto-zygo suture (anterior)
zfl-zfsl	L fronto-zygo suture (lateral)	**zfr-zfsr**	R fronto-zygo suture (lateral)
zfsl-slorl	L fronto-zygo suture (medial)	**zfsr-slorr**	R fronto-zygo suture (medial)

Ethmoid Attachment

n-fc Nasal root projection

fc-cpal	L fronto-ethmoid attachment (ant)	**fc-cpar**	R fronto-ethmoid attachment (ant)
cpal-cppl	L fronto-ethmoid attachment (crib)	**cpar-cppr**	R fronto-ethmoid attachment (crib)
cppl-ofaml	L fronto-ethmoid attachment (post)	**cppr-ofamr**	R fronto-ethmoid attachment (post)
morl-ofaml	L fronto-ethmoid attachment (orbital)	**morr-ofamr**	R fronto-ethmoid attachment (orbital)

Sphenoid Attachment

ofaml-sobfl	L superior orbital fissure	**ofamr-sobfr**	R superior orbital fissure
sobfl-zfsl	L fronto sphenoid suture (orbital)	**sobfr-zfsr**	R fronto sphenoid suture (orbital)
spal-cppl	L lesser wing length	**spar-cppr**	R lesser wing length

Dimension Definitions

g-n	Glabellar height
s-g	Glabellar prominence
sorl-spal	L anterior cranial fossa depth
sorr-spar	R anterior cranial fossa depth
sorl-sorr	Anterior superior orbital width
slorl-slorr	Anterior supero-lateral orbital width
spal-spar	Posterior width

Figure 3.17(a): Frontal Bone
(anterior aspect)
Landmarks and Distances

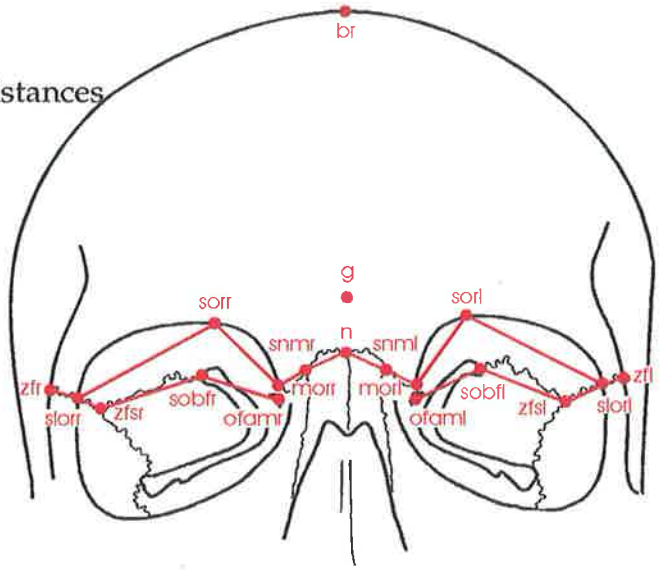

Figure 3.17(b): Frontal Bone
(superior aspect)
Landmarks, Distances
and Dimensions

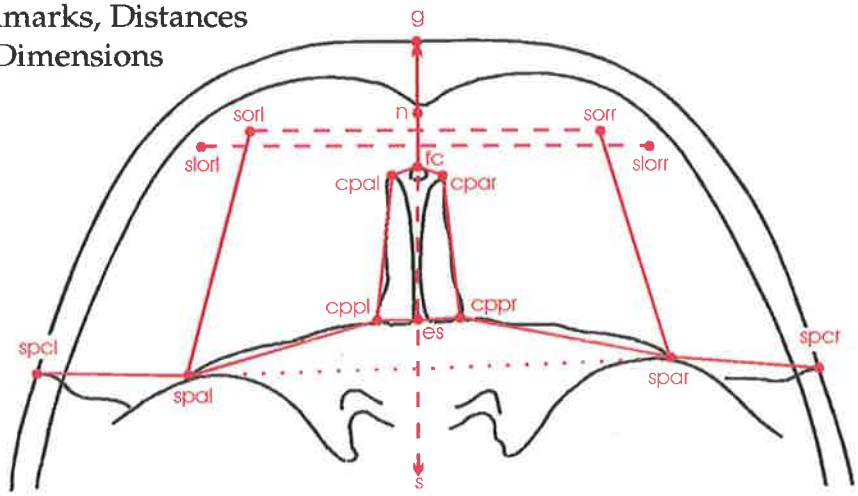

Figure 3.17(c): Frontal Bone
(left lateral aspect)
Landmarks and Distances

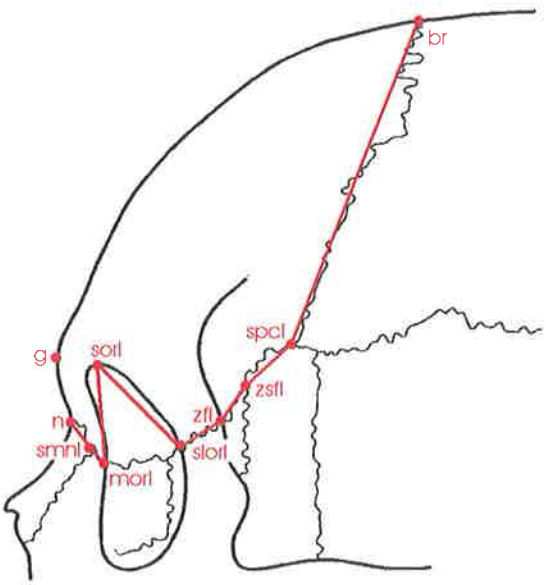

Figures 3.18(a)-(c) **Diagrammatic representations of the Zygomatic Bone showing the key Landmarks identified and the Distances and Dimensions measured**

Landmark Definitions

gwll/gwlr **greater wing laterale left/right:** A point located at the junction of the inferior orbital fissure with the suture between the greater wing of the sphenoid and the zygomatic bone. The point can be visualised from within the orbital cavity and at the base of the temporal fossa. The landmark is found at the inferior notch of the spheno-zygomatic suture.

iobfl/iobfr **inferior orbital fissure left/right:** The most anterior point on the margin of the inferior orbital fissure.

ilorl/ilorr **infero-lateral orbitale left/right:** The point is determined approximately mid-way between the sutures limiting the zygomatic bone or, alternatively, at the intersection of the anterior projection of the maxillary border of the inferior orbital fissure with the lateral orbital rim.

lorl/lorr **lateral orbitale left/right:** The most lateral point on the orbital rim.

orl/orr **orbitale left/right:** The most inferior point on the infra-orbital margin.

parl/parr **pre-articulare left/right:** The most superior point on the lower border of the zygomatic arch located anterior to point articular eminence.

slorl/slorr **supero-lateral orbitale left/right:** The intersection of the fronto-zygomatic suture with the lateral orbital rim (almost the intersection of the curve of the supra-orbital rim with the lateral orbital rim.

zfl/zfr **zygo-frontale left/right:** The point located at the posterior extremity of the fronto-zygomatic suture.

zfsl/zfsr **zygo-frontale sphenoidale left/right:** The point located at the intersection of the frontal, zygomatic and sphenoid bones.

zmil/zmir **zygomaxillare inferius left/right:** The lowest point on the external suture between zygomatic and maxillary bones.(in the region of the craniometric landmark, zygomaxillare).

ztl/ztr **zygo-temporale left/right:** The mid-point of the bony concavity formed between the frontal and temporal processes of the zygomatic bone.

Figure 3.18(a)-(c) (Zygomatic Bone continued):

Legend for Figures 3.18(a), 3.18(b) and 3.18(c)

Distance Definitions

Left		Right	
orl-iobfl	L zygo-maxillary suture (orbital)	**orr-iobfr**	R zygo-maxillary suture (orbital)
iobfl-gwll	L inferior orb fissure (ant height)	**iobfr-gwlr**	R inferior orb fissure (ant height)
zfsl-gwll	L spheno-zygomatic suture	**zfsr-gwlr**	R spheno-zygomatic suture
zfsl-slorl	L fronto-zygo suture (medial)	**zfsr-slorr**	R fronto-zygo suture (medial)
slorl-zfl	L fronto-zygo suture (anterior)	**slorr-zfr**	R fronto-zygo suture (anterior)
zfl-zfsl	L fronto-zygo suture (lateral)	**zfr-zfsr**	R fronto-zygo suture (lateral)
orl-ilorl	L infero-lateral orbital rim	**orr-ilorr**	R infero-lateral orbital rim
ilorl-lorl	L infero-lateral orbital rim	**ilorr-lorr**	R infero-lateral orbital rim
lorl-slorl	L lateral orbital rim	**lorr-slorr**	R lateral orbital rim
zfl-ztl	L lateral frontal process	**zfr-ztr**	R lateral frontal process
ztl-parl	L zygomatico-temporal suture	**ztr-parr**	R zygomatico-temporal suture
parl-zmil	L inferior arch	**parr-zmir**	R inferior arch
zmil-orl	L zygo-maxillary suture	**zmir-orr**	R zygo-maxillary suture

Dimension Definitions

Left		Right	
slorl-zmil	L zygomatic height	**slorr-zmir**	R zygomatic height
parl-orl	L zygomatic length	**parr-orr**	R zygomatic length
gwll-ilorl	L zygomatic lateral depth	**gwlr-ilorr**	R zygomatic lateral depth

Figure 3.18(a): Zygomatic Bone
(anterior aspect)
Landmarks and Distances

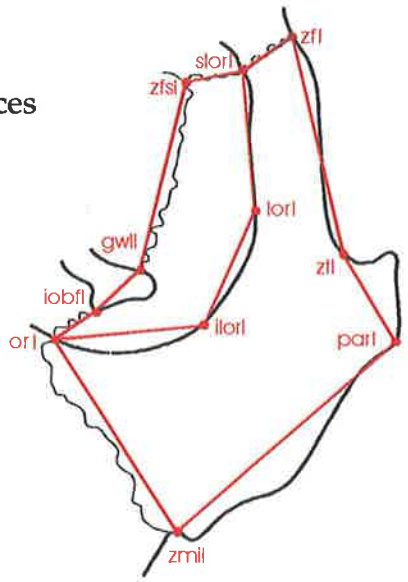

Figure 3.18(b): Zygomatic Bone
(lateral aspect)
Landmarks and Distances

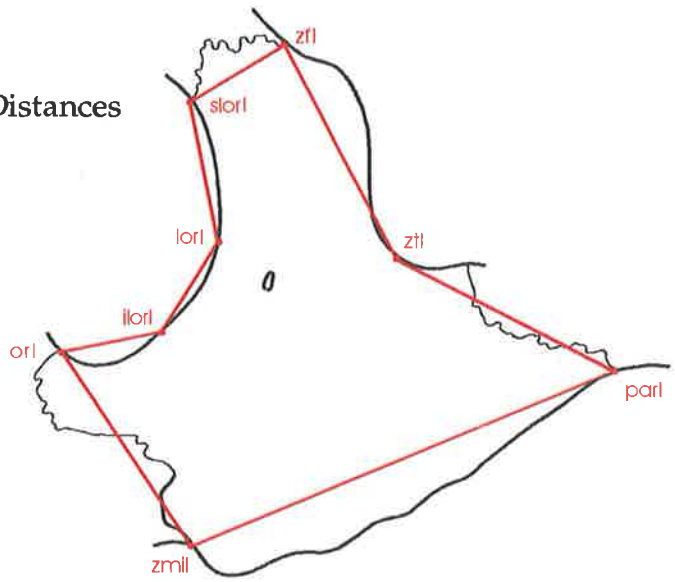

Figure 3.18(c): Zygomatic Bone
(anterior aspect)
Dimensions

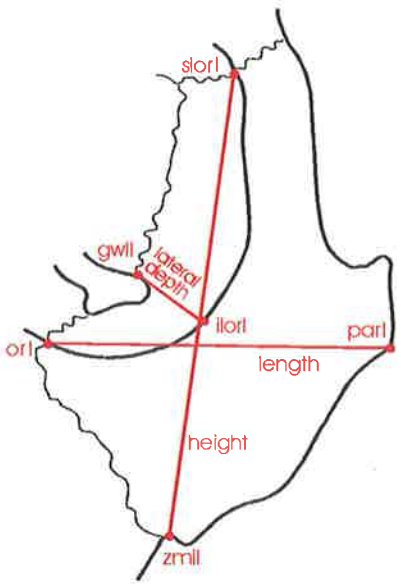

Figures 3.19 **Diagrammatic representation of the Vomer showing the key Landmarks identified and the Distances, Dimension and Angle measured**

Landmark Definitions

ans	**anterior nasal spine:** The apex of the anterior nasal spine. (Also known as spinal point (sp) or acanthion (ac)).
h	**hormion:** The most posterior and medial point on the junction of the vomer and sphenoid bones.
pns	**posterior nasal spine:** The apex of the posterior nasal spine.
vei	**vomo-ethmoid inferius:** The most inferior point on the vomer ethmoid suture.
ves	**vomo-ethmoid superius:** The most superior point on the vomer ethmoid suture.

Figure 3.19 (Vomer continued):

Legend for Figure 3.19

Distance	Definitions
ans-pns	Palatal length
pns-h	Posterior choanal height
h-ves	Spheno-vomerine junction
ves-vei	Ethmoid-vomerine junction
vei-ans	Septal attachment

Dimension	Definition
h-ans	Vomerine length

Angle	Definition
s-n/h-ans	Vomerine angle

Figure 3.19: Vomer
(mid-sagittal plane)
Landmarks, Distances, Dimensions and Angles

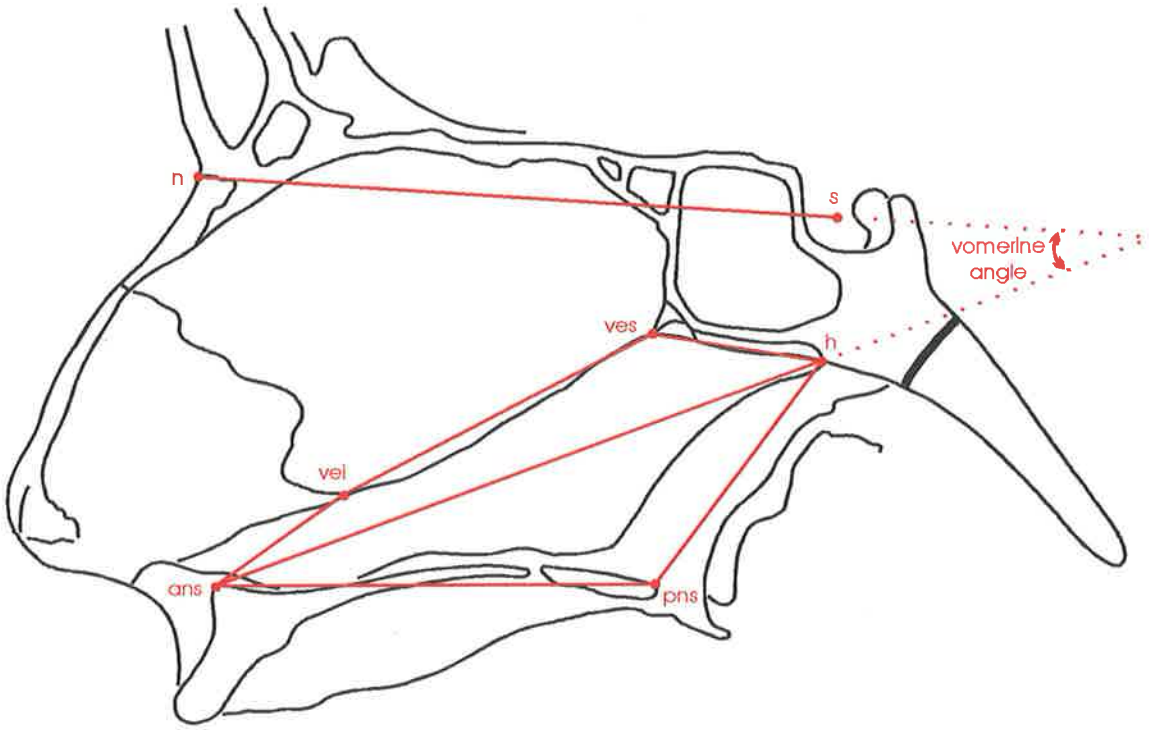

Figures 3.20(a)-(h) **Diagrammatic representation of the Ethmoid Bone showing the key Landmarks identified and the Distances, Dimensions and Angles measured**

Landmark Definitions

cpal/cpar	**cribriform plate anterius left/right:** The most antero-lateral point on the cribriform plate.
cppl/cppr	**cribriform plate posterius left/right:** The most postero-lateral point on the cribriform plate.
cg	**crista galli:** The tip of the crista galli.
es	**ethmoid spine:** The tip of the ethmoid spine.
fc	**foramen caecum:** The centre of the foramen caecum.
msl/msr	**maxillare superius left/right:** The most postero-superior point on the maxilla determined from CT slice images. (located in sagittal view as the most superior point on the maxillary surface, at the junction of orbital and infra-temporal surfaces.)
morl/morr	**medial orbitale left/right:** The most medial point on the orbital margin in the region of the fronto-lacrimal suture.
nlil/nlir	**naso-lacrimal inferius left/right:** The most antero-inferior point on the margin of the naso-lacrimal groove as it exits the orbit (usually this point is located at the small spicule of bone covering the lateral wall of the naso-lacrimal groove and the inferior orbital rim).
ofaml/ofamr	**optic foramen anterior medial left/right:** The medial margin of the anterior opening of the optic canal.
vei	**vomo-ethmoid inferius:** The most inferior point on the vomer ethmoid suture.
ves	**vomo-ethmoid superius:** The most superior point on the vomer ethmoid suture, at the junction with the sphenoid body.

Figure 3.20(a)-(h) (Ethmoid Bone continued):

Legend for Figures 3.20(a), 3.20(b) and 3.20(c)

Lateral Ethmoid Plate

Distance Definitions

Medial Orbital Wall

Left		Right	
nlil-morl	L anterior border lateral plate	**nlir-morr**	R anterior border lateral plate
morl-ofaml	L frontal ethmoid attachment (orbital)	**morr-ofamr**	R frontal ethmoid attachment (orbital)
ofaml-msl	L posterior border lateral plate	**ofamr-msr**	R posterior border lateral plate
msl-nlil	L inferior border lateral plate	**msr-nlir**	R inferior border lateral plate

Frontal Ethmoid Attachment

Left		Right	
morl-cpal	L frontal ethmoid attachment (ant)	**morr-cpar**	R frontal ethmoid attachment (ant)
cppl-ofaml	L frontal ethmoid attachment (post)	**cppr-ofamr**	R frontal ethmoid attachment (post)

Dimension Definitions

msl-msr	Posterior inferior width
nlil-nlir	Anterior inferior width
morl-morr	Anterior superior width
ofaml-ofamr	Posterior superior width

Angle Definitions

nlil-morl/morr-nlir	Anterior lateral projection of lateral plate
msl-ofaml/ofamr-msr	Posterior lateral projection of lateral plate

Figure 3.20(a): Ethmoid - Lateral Plate
(left lateral aspect)
Landmarks and Distances

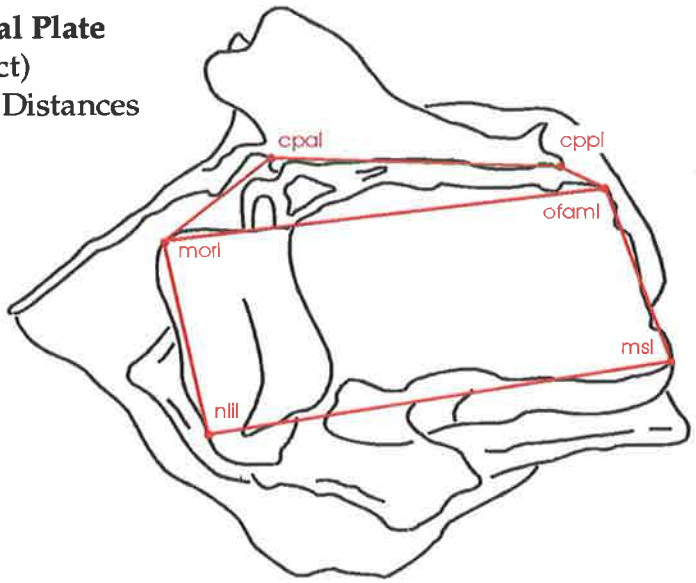

Figure 3.20(b): Ethmoid - Lateral Plate
(superior aspect)
Dimensions

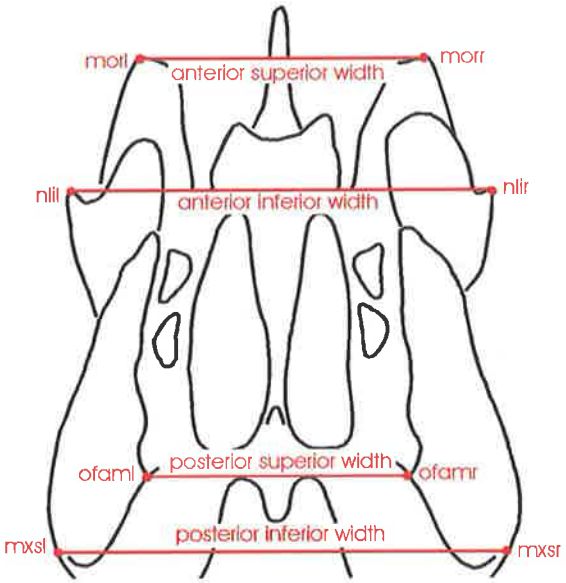

Figure 3.20(c): Ethmoid - Lateral Plate
(superior aspect)
Angles - (splay of lateral plates)

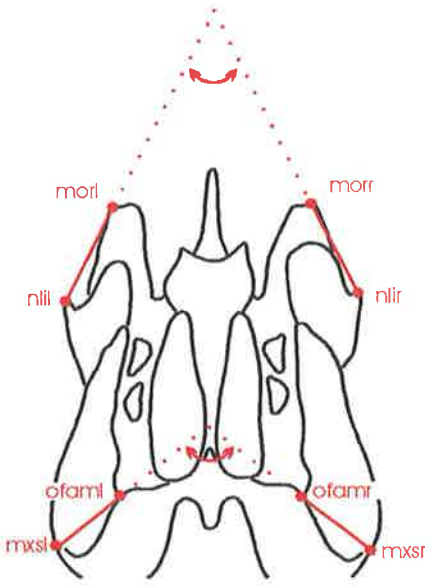

Figure 3.20(a)-(h) (Ethmoid Bone continued):

Legend for Figures 3.20(d), 3.20(e) and 3.20(f)

Ethmoid Cribriform Plate

Distance Definitions

Left		Right	
fc-cpal	L anterior cribriform plate	**fc-cpar**	R anterior cribriform plate
cpal-cppl	L lateral cribriform plate	**cpar-cppr**	R lateral cribriform plate
es-cppl	L posterior cribriform plate	**es-cppr**	R posterior cribriform plate

Angle Definitions

s-n/cpal-cppl	L angle lateral cribriform plate cf SN
s-n/cpar-cppr	R angle lateral cribriform plate cf SN
n-s/es-fc	Medial angle of plate cf SN

Figure 3.20(d): **Ethmoid**
- Cribriform Plate and Lateral Plate
(superior aspect)
Landmarks and Distances

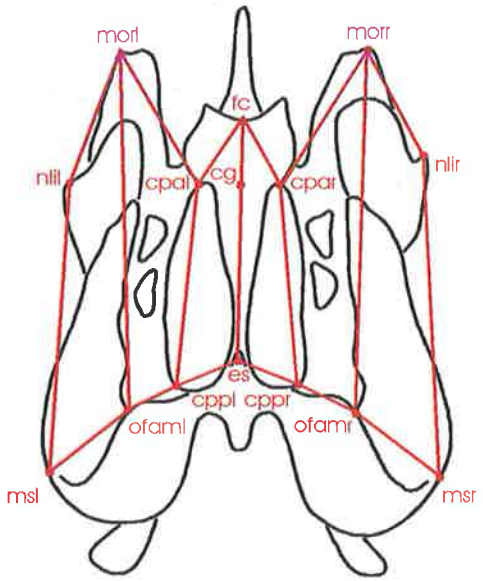

Figure 3.20(e): **Ethmoid**
- Cribriform Plate
(superior aspect)
Angles

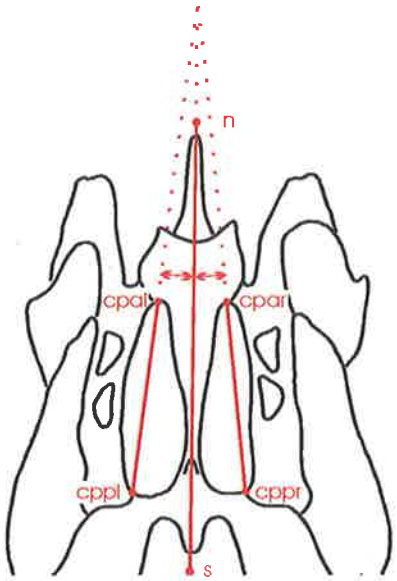

Figure 3.20(f): **Ethmoid**
- Cribriform Plate
(left lateral aspect)
Angles

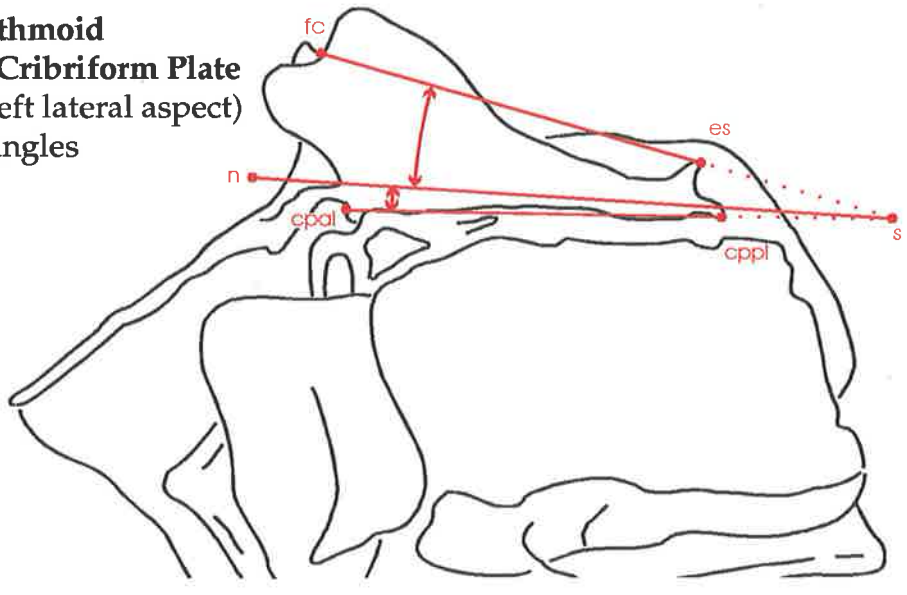

Figure 3.20(a)-(h) (Ethmoid Bone continued):

Legend for Figures 3.20(g) and 3.20(h)

Medial Ethmoid Plate

Distance	Definitions
fc-cg	Anterior height crista galli
cg-es	Posterior height crista galli
es-ves	Spheno-ethmoid medial plate junction
ves-vei	Ethmoid-vomerine junction
vei-n	Septal attachment
n-fc	Nasal projection

Dimension	Definitions
vei-cg	Maximum medial plate height
n-es	Maximum medial plate length

Figure 3.20(g): Ethmoid - Medial Plate
(mid-sagittal plane)
Landmarks and Distances

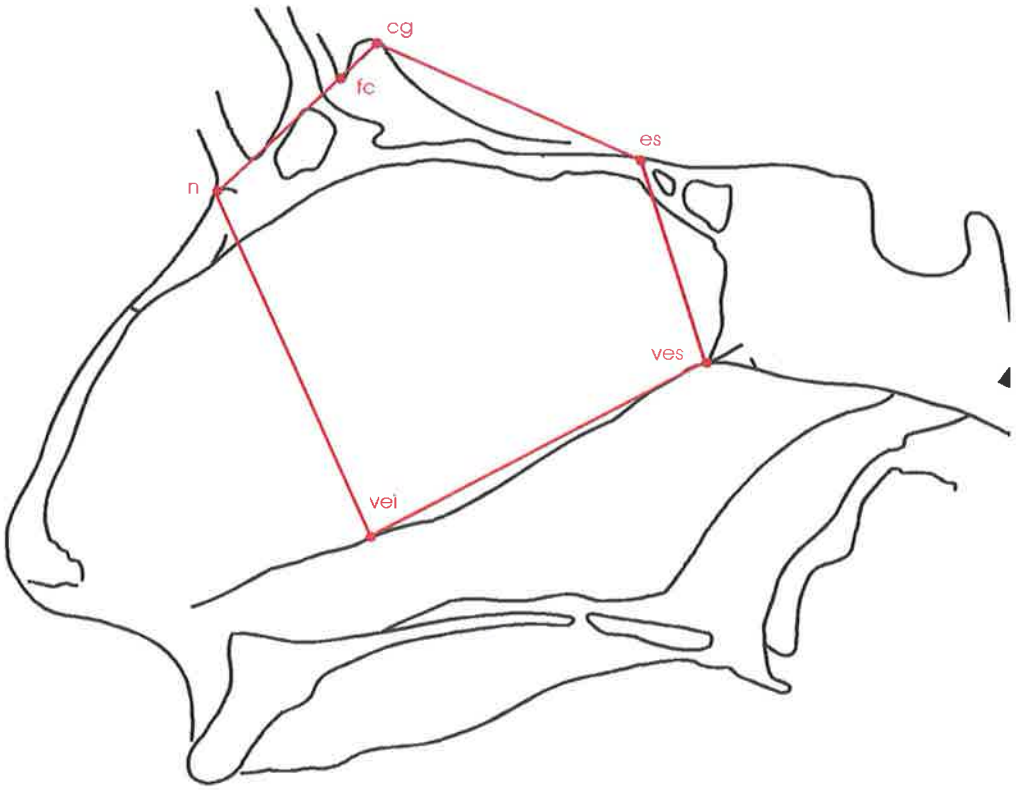

Figure 3.20(h): Ethmoid - Medial Plate
(mid-sagittal plane)
Dimensions

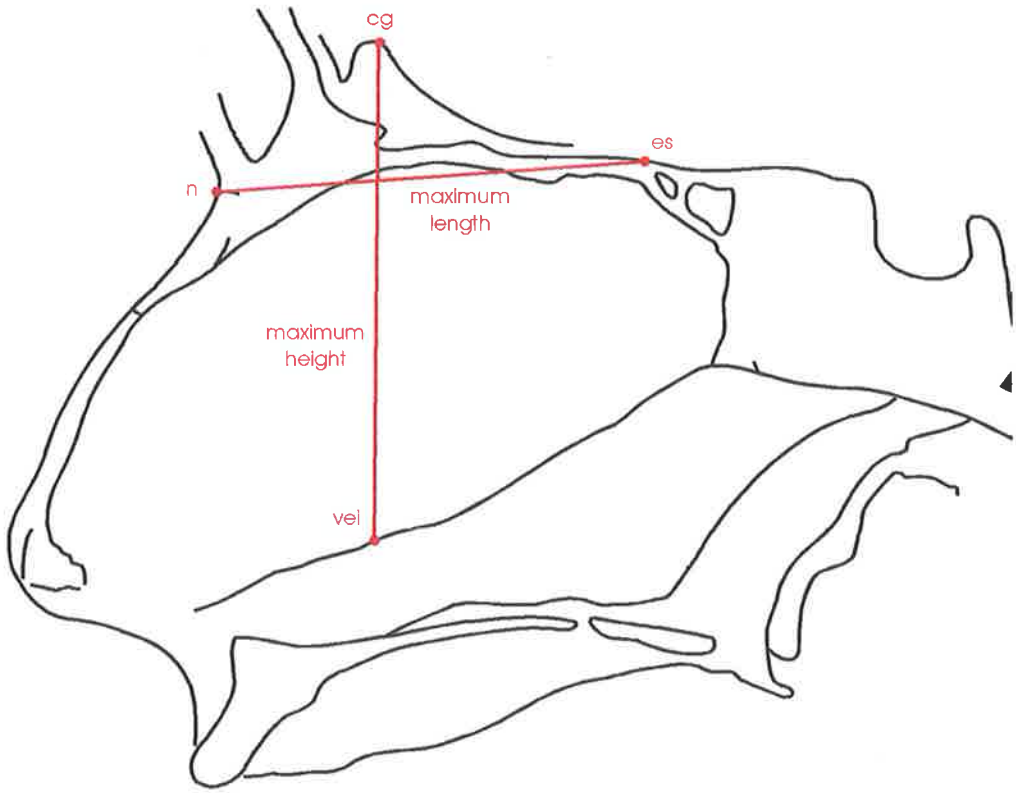

Figures 3.21(a)-(j) **Diagrammatic representation of the Sphenoid Bone showing the key Landmarks identified and the Distances, Dimensions and Angles measured**

Landmark Definitions

acl/acr **anterior clinoid left/right:** The most posterior point on the anterior clinoid of the lesser wing of the sphenoid bone. In the cases of bridging between the anterior and posterior clinoid the point is determined at the anterior prominence mid-way along the bridge.

cppl/cppr **cribriform plate posterius left/right:** The most postero-lateral point on the cribriform plate. (see ethmoid)

es **ethmoid spine:** The tip of the ethmoid spine. (see ethmoid)

foil/foir **foramen in ovale left/right:** The mid point of the internal opening of the foramen ovale.

fisl/fisr **foramen in spinosum left/right:** The mid point of the internal opening of the foramen spinosum. On occasion this point was not always visible, and a point adjacent to the postero-lateral margin of the foramen ovale was utilised for the internal point.

fool/foor **foramen out ovale left/right:** The mid point of the external opening of the foramen ovale, at the level of the skull base.

fosl/fosr **foramen out spinosum left/right:** The mid point of the external opening of the foramen spinosum, at the level of the skull base. If not seen, the notch between the petrous temporal bone and the greater wing of the sphenoid were used externally.

gwll/gwlr **greater wing laterale left/right:** A point located at the junction of the inferior orbital fissure with the suture between the greater wing of the sphenoid and the zygomatic bone. The point can be visualised from within the orbital cavity and at the base of the temporal fossa. The landmark is found at the inferior notch of the spheno-zygomatic suture (see zygomatic bone).

gwml/gwmr **greater wing mediale left/right:** The most inferior point of the superior orbital fissure, where the greater wing of the sphenoid joins the body of the sphenoid, (just above the floor of the foramen rotundum).

hnl/hnr **hamular notch left/right:** The deepest point of the hamular notch located centrally between the maxillary tuberosity and the pterygoid process of the sphenoid.

hpl/hpr **hamular process left/right:** The tip of the hamular process of the medial pterygoid plates of the sphenoid.

h **hormion:** The most posterior and medial point on the junction of the vomer and sphenoid bones. (see vomer)

msl/msr **maxillare superius left/right:** The most postero-superior point on the maxilla determined from CT slice images. (located in sagittal view as the most superior point on the maxillary surface, at the junction of orbital and infra-temporal surfaces.) (see maxilla)

Figures 3.21(a)-(j) (Sphenoid Bone continued):

Landmark Definitions (continued):

ofaml/ofamr **optic foramen a medial left/right:** The medial margin of the anterior opening of the optic canal.

ofpml/ofpmr **optic foramen p medial left/right:** The medial margin of the posterior opening of the optic canal.

petal/petar **petrous anterius left/right:** The most anterior point on the crest of the petrous temporal bone at the margin of the foramen lacerum and the base of the posterior clinoid (see temporal bone).

pcl/pcr **posterior clinoid left/right:** The most superior and lateral point on the posterior clinoid.

ptll/ptlr **pterygo-lateralis left/right:** The most lateral point on the lateral pterygoid plate located at the posterior/inferior angle.

ptsl/ptsr **pterygo-superius left/right:** The postero-superior extremity of the medial pterygoid plate, where it approximates the apex of the petrous temporal bone. (see temporal bone)

s **sella:** The centre of the sella turcica.

spal/spar **sphenoidale anterior left/right:** The most anterior point on the posterior margin of the lesser wing of sphenoid (see frontal bone).

spcl/spcr **sphenion c left/right:** The junction of the coronal suture and the sphenoid bone (see frontal bone).

sptl/sptr **sphenion t left/right:** The intersection of the temporal, parietal and sphenoid bones (see temporal and parietal bones).

sobfl/sobfr **superior orbital fissure left/right:** The most lateral point on the margin of the superior orbital fissure.

zfl/zfr **zygo-frontale left/right:** The point located at the posterior extremity of the fronto-zygomatic suture (see zygomatic bone).

zfsl/zfsr **zygo-frontale sphenoidale left/right:** The point located at the intersection of the frontal, zygomatic and sphenoid bones (see zygomatic and frontal bones).

ves **vomo-ethmoid superius:** The most superior point on the vomer ethmoid suture, at the junction with the sphenoid body.

Figure 3.21(a)-(j) (Sphenoid Bone continued):

Legend for Figures 3.21(a) and 3.21(b)

Sphenoid Lesser Wing

Distance Definitions

Left		Right	
ofaml-acl	L medial wing	**ofamr-acr**	R medial wing
acl-spal	L lateral wing (posterior)	**acr-spar**	R lateral wing (posterior)
spal-es	L lateral wing (anterior)	**spar-es**	R lateral wing (anterior)

Dimension and Angle Definitions

1	**spal-spar**	Maximum lesser wing width
2	**spal-es-spar**	Lesser wing superior angle
3	**n-s/acl-spal**	L lateral projection (anterior angle)
	n-s/acr-spar	R lateral projection (anterior angle)

Figure 3.21(a): Sphenoid - Lesser Wing
(posterior aspect)
Landmarks and Distances

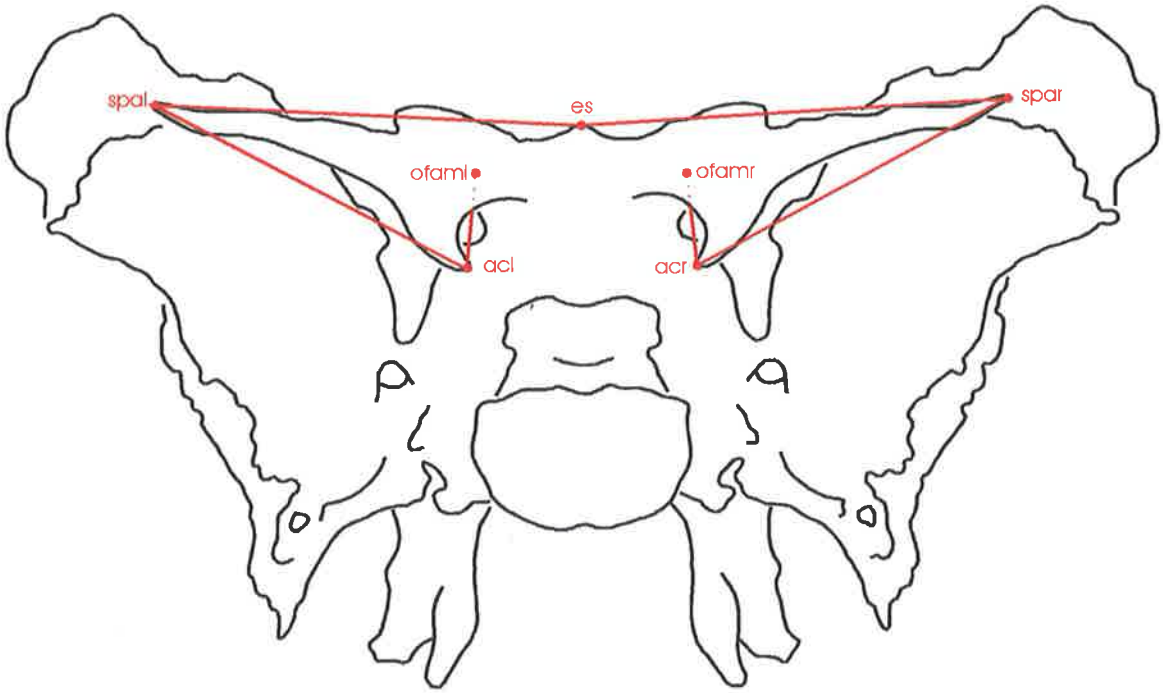

Figure 3.21(b): Sphenoid - Lesser Wing
(posterior aspect)
Dimensions and Angles

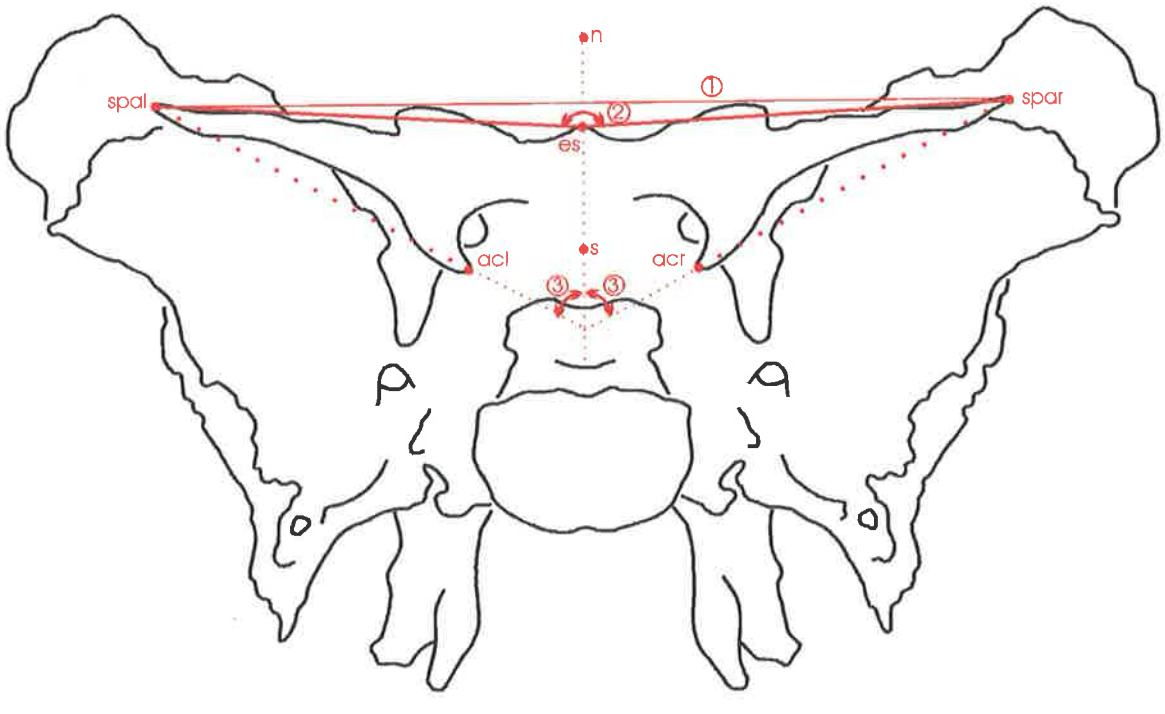

Figure 3.21(a)-(j) (Sphenoid Bone continued):

Legend for Figures 3.21(c) and 3.21(d)

Sphenoid Pterygoid Plate

Distance Definitions

Left		Right	
ptsl-hpl	L medial pterygoid plate	**ptsr-hpr**	R medial pterygoid plate
hpl-hnl	L medial hamular notch	**hpr-hnr**	R medial hamular notch
hnl-ptll	L lateral hamular notch	**hnr-ptlr**	R lateral hamular notch
ptll-fool	L lateral pterygoid plate	**ptlr-foor**	R lateral pterygoid plate

Angle Definitions

Left		Right	
n-s/ptsl-hpl	L pterygoid axis	**n-s/ptsr-hpr**	R pterygoid axis

Figure 3.21(c): Sphenoid - Pterygoid Plate
(posterior aspect)
Landmarks and Distances

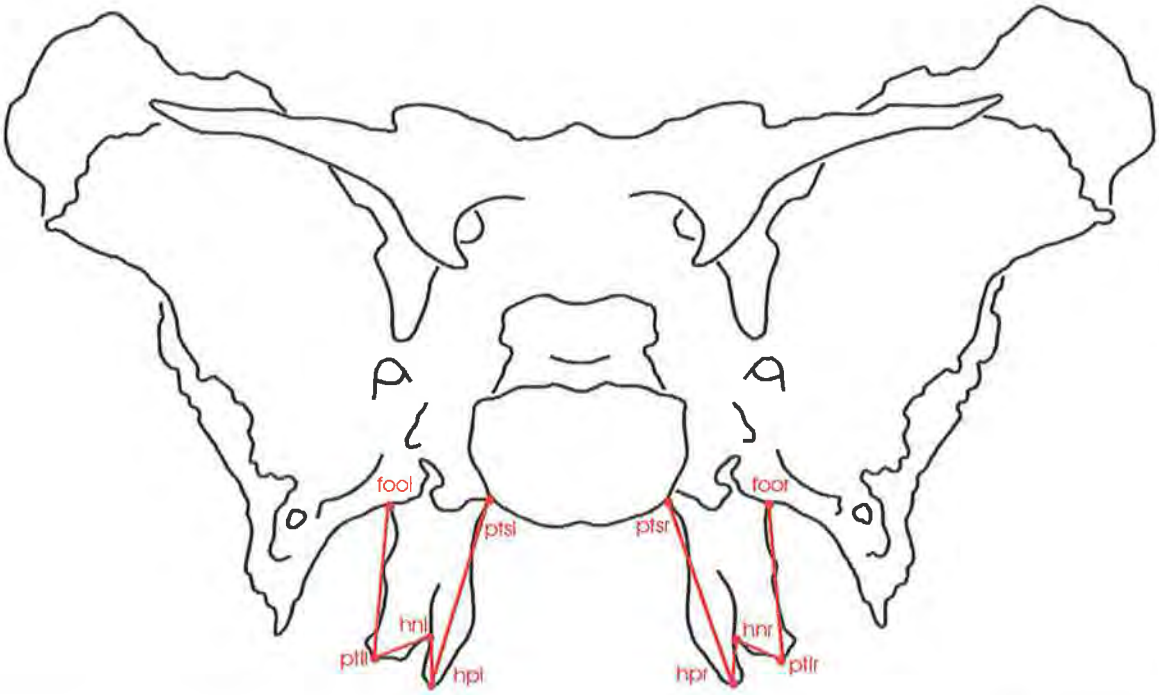

Figure 3.21(d): Sphenoid - Pterygoid Plate
(sagittal aspect)
Angle

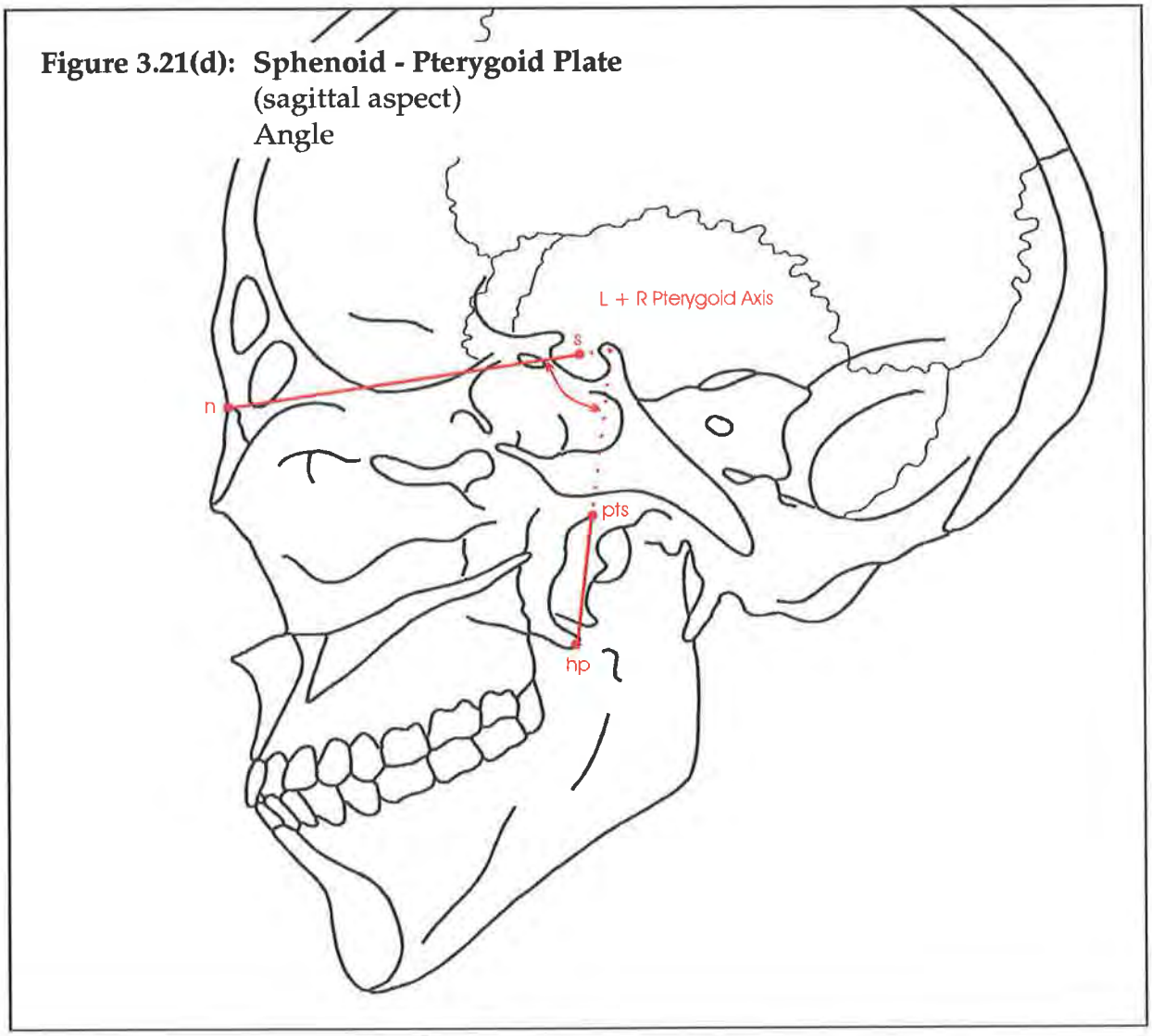

Figure 3.21(a)-(j) (Sphenoid Bone continued):

Legend for Figures 3.21(e) and 3.21(f)

Sphenoid Greater Wing

Distance Definitions - Greater Wing (Lateral)

Left		Right	
fosl-gwll	L anterior middle cranial fossa	**fosr-gwlr**	R anterior middle cranial fossa
zfsl-gwll	L spheno-zygomatic suture	**zfsr-gwlr**	R spheno-zygomatic suture

Distance Definitions - Greater Wing (Orbital)

Left		Right	
gwll-gwml	L inferior lateral orbital length	**gwlr-gwmr**	R inferior lateral orbital length
gwml-sobfl	L superior orbital fissure height	**gwmr-sobfr**	R superior orbital fissure height
sobfl-zfsl	L spheno-frontal suture (orbital)	**sobfr-zfsr**	R spheno-frontal suture (orbital)

Distance Definitions - Greater Wing (Posterior)

Left		Right	
fosl-ptsl	L spheno-petrous temporal suture (inf)	**fosr-ptsr**	R spheno-petrous temporal suture (inf)
fosl-petal	L posterior middle cranial fossa	**fosr-petar**	R posterior middle cranial fossa

Figure 3.21(e): Sphenoid - Greater Wing
(posterior aspect)
Landmarks and Distances

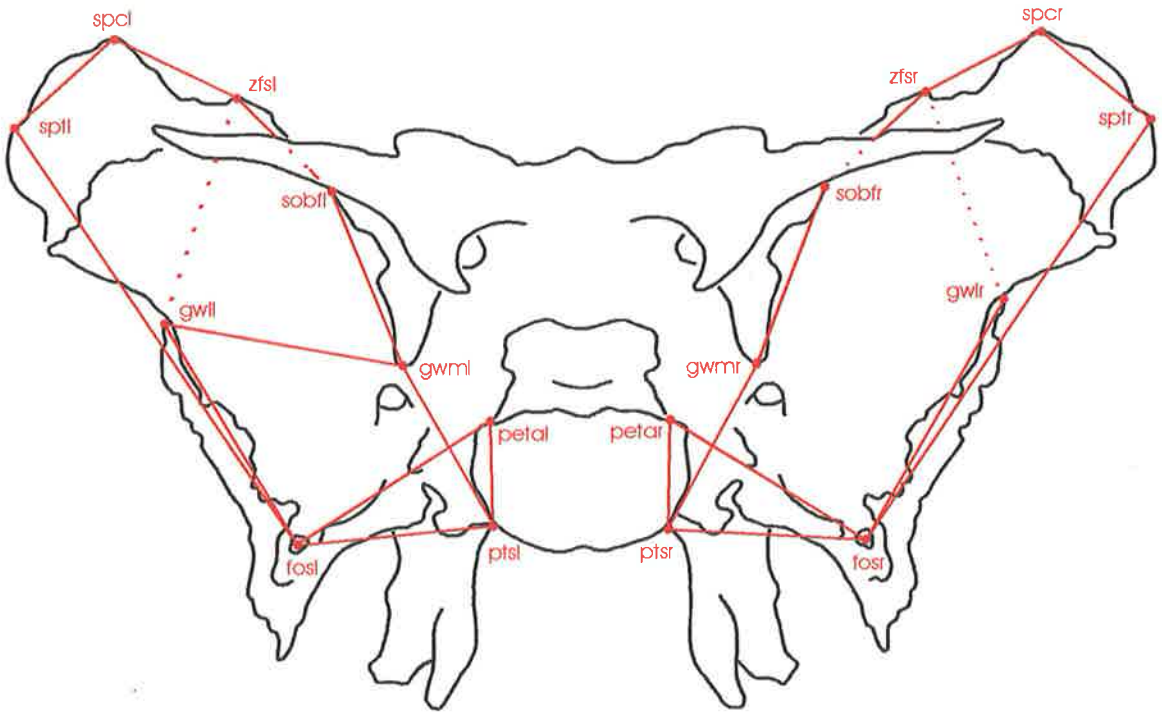

Figure 3.21(f): Sphenoid - Greater Wing
(anterior aspect)
Landmarks and Distances

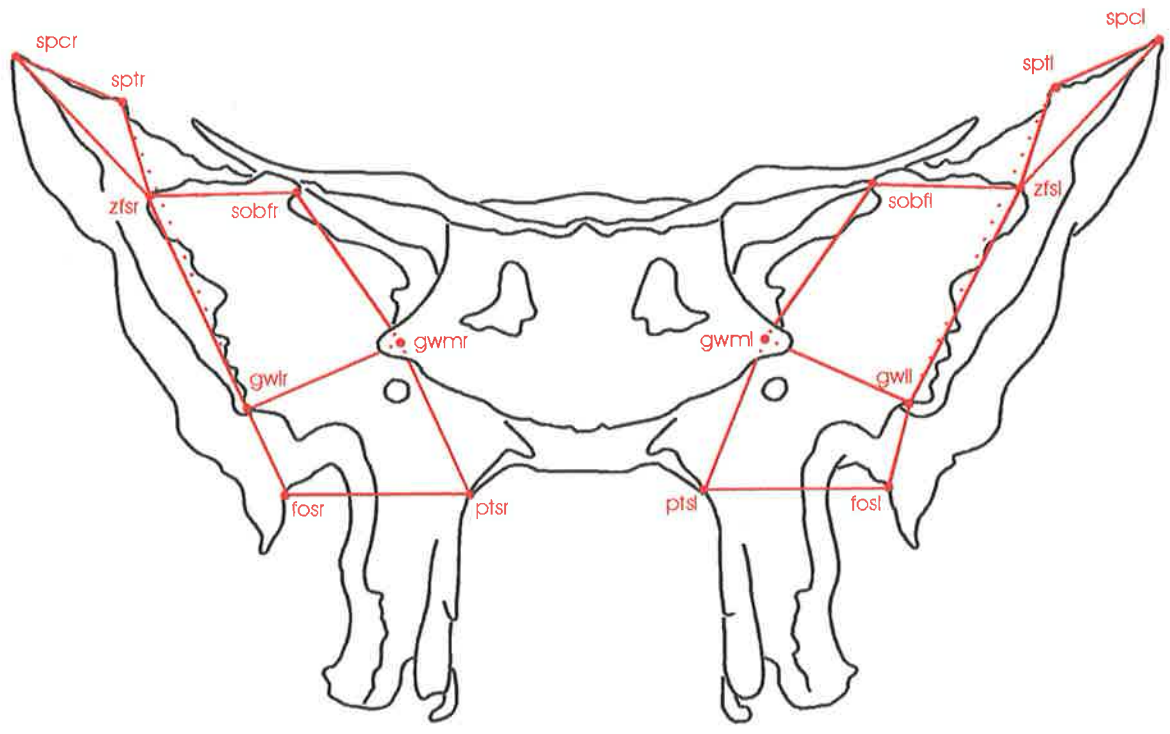

Figure 3.21(a)-(j) (Sphenoid Bone continued):

Legend for Figure 3.21(g)

Sphenoid Greater Wing

Dimension Definitions

	fosl-fosr	Posterior sphenoid width

Angle Definitions

1	**zfsl-gwml-ptsl**	L angle of greater wing splay
	zfsr-gwmr-ptsr	R angle of greater wing splay
2	**zfsl-gwml/gwmr-zfsr**	Total angle of protrusion
3	**gwll-gwml/gwmr-gwlr**	Inferior greater wing protrusion
4	**fosl-petal/petar-fosr**	Posterior angle of greater wing

Figure 3.21(g): Sphenoid - Greater Wing
(posterior aspect)
Dimensions and Angles

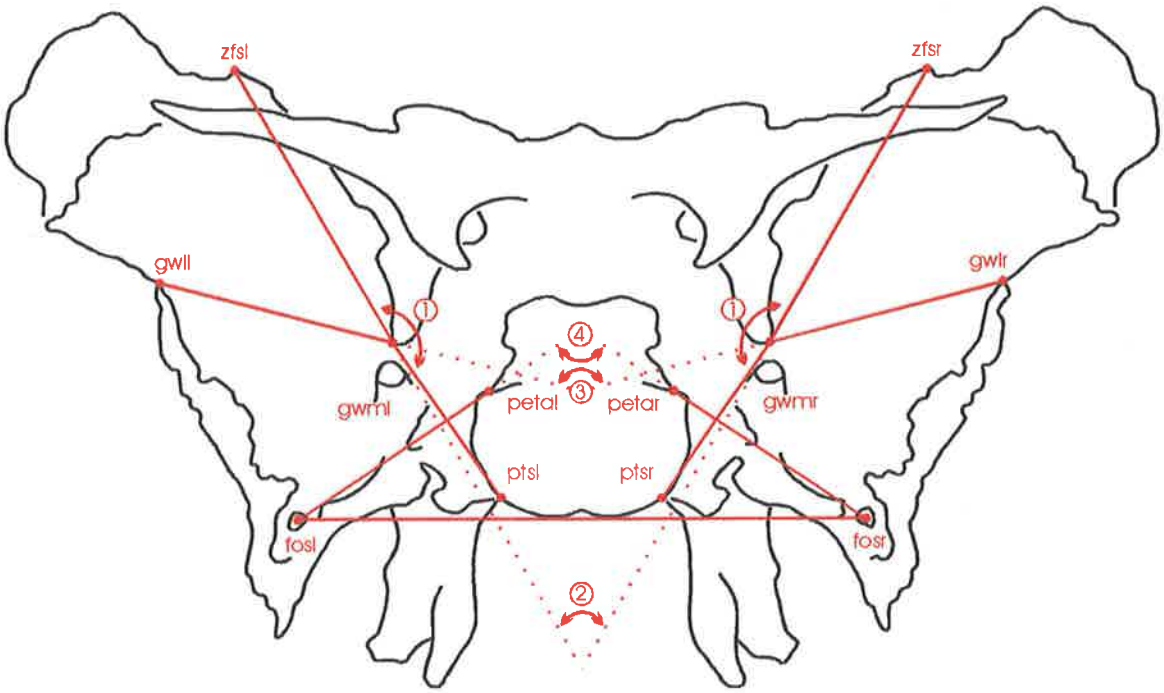

Figure 3.21(a)-(j) (Sphenoid Bone continued):

Legend for Figure 3.21(h)

Sphenoid Body

Distance Definitions

Lateral/Posterior Body

Left		Right	
gwml-ptsl	L anterior inferior length	**gwmr-ptsr**	R anterior inferior length
ptsl-petal	L spheno-occipital synchondrosis (lat)	**ptsr-petar**	R spheno-occipital synchondrosis (lat)
petal-pcl	L posterior clinoid height	**petar-pcr**	R posterior clinoid height
	pcl-pcr	Posterior clinoid width	

Anterior Body

Left		Right	
es-cppl	L spheno-ethmoid suture	**es-cppr**	R spheno-ethmoid suture
cppl-ofaml	L anterior lateral distance	**cppr-ofamr**	R anterior lateral distance
ofaml-gwml	L anterior superior length	**ofamr-gwmr**	R anterior superior length

Sella

Left		Right	
cppl-ofpml	L lateral anterior body	**cppr-ofpmr**	R lateral anterior body
ofpml-petal	L lateral sella length	**ofpmr-petar**	R lateral sella length

Base/Floor of Body

Left		Right	
h-ptsl	L posterior width	**h-ptsr**	R posterior width
	es-ves	Spheno-ethmoid medial plate junction	
	h-ves	Spheno-vomerine junction	

Figure 3.21(h): Sphenoid - Body
(posterior aspect)
Landmarks and Distances

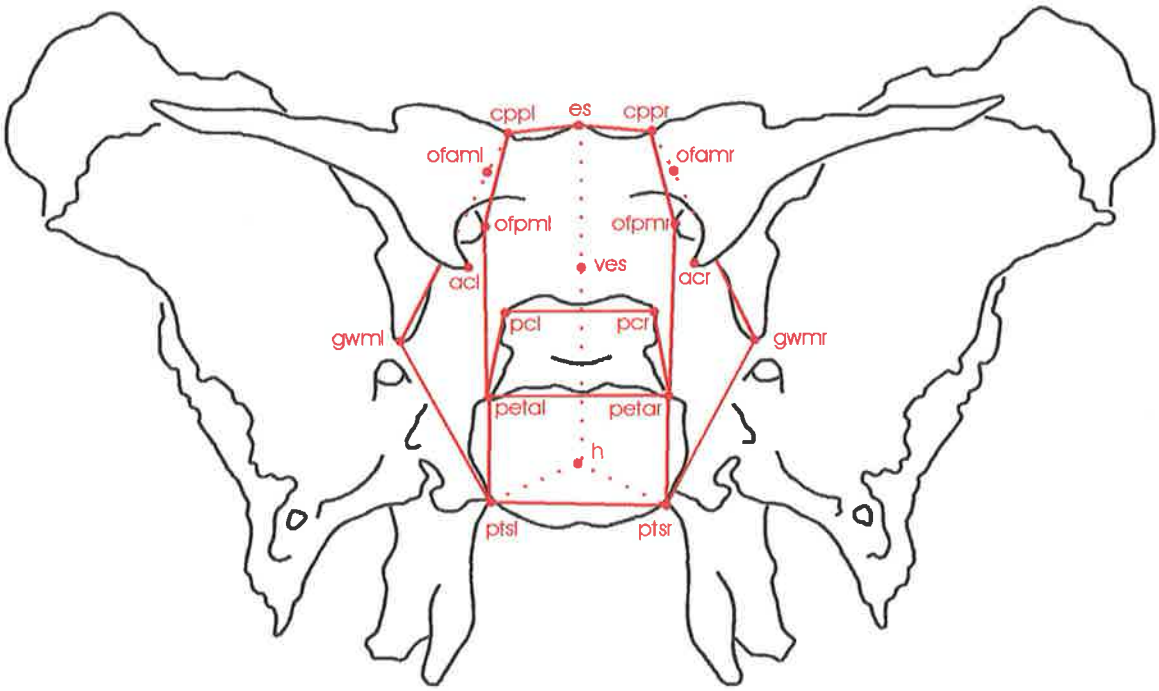

Figure 3.21(a)-(j) (Sphenoid Bone continued):

Legend for Figures 3.21(i) and 3.21(j)

Sphenoid Body

Dimension Definitions

gwml-gwmr	Anterior inferior body width
ptsl-ptsr	Spheno-occipital synchondrosis (inferior)
ofaml-ofamr	Anterior superior body width
petal-petar	Spheno-occipital synchondrosis (superior)
pcl-ptsl	L posterior body height
pcr-ptsr	R posterior body height
acl-gwml	L anterior body height
acr-gwmr	L anterior body height

Angle Definitions

1	**s-n/gwml-ptsl**	L lower body angle
	s-n/gwmr-ptsr	R lower body angle
2	**s-n/ofpml-petal**	L upper body angle
	s-n/ofpmr-petar	R upper body angle
	es-ves-h	Body floor angle

Figure 3.21(i): **Sphenoid - Body**
(posterior aspect)
Dimensions and Angles

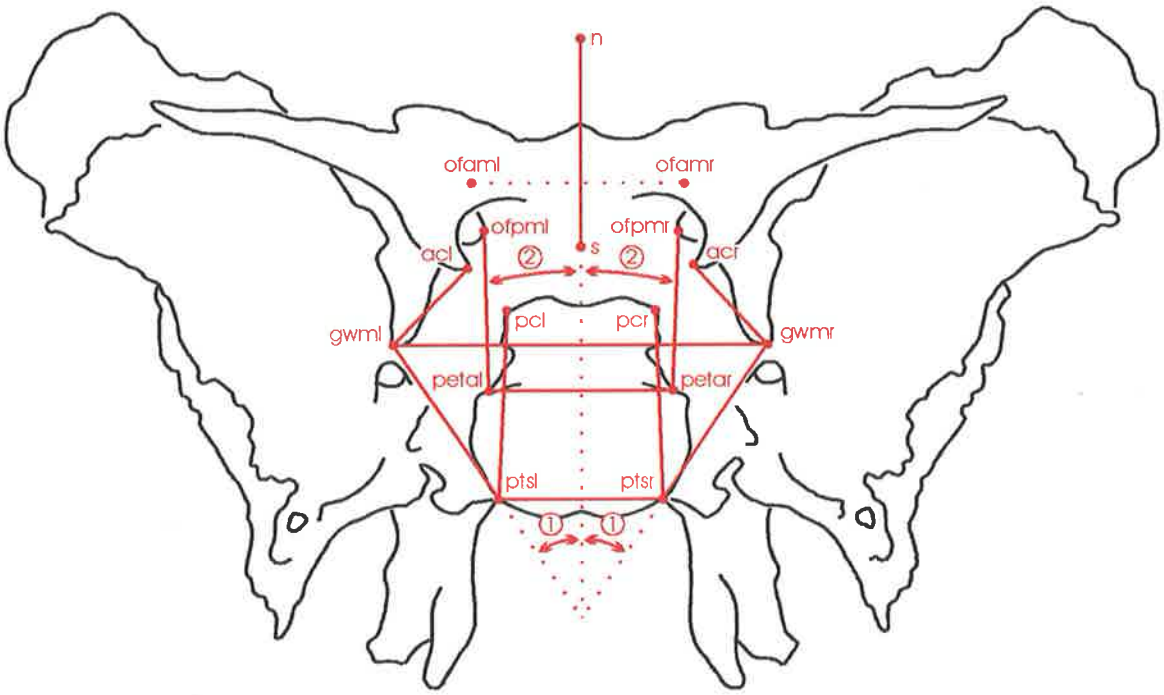

Figure 3.21(j): **Sphenoid - Body**
(mid-sagittal plane)
Landmarks, Distances and Angles

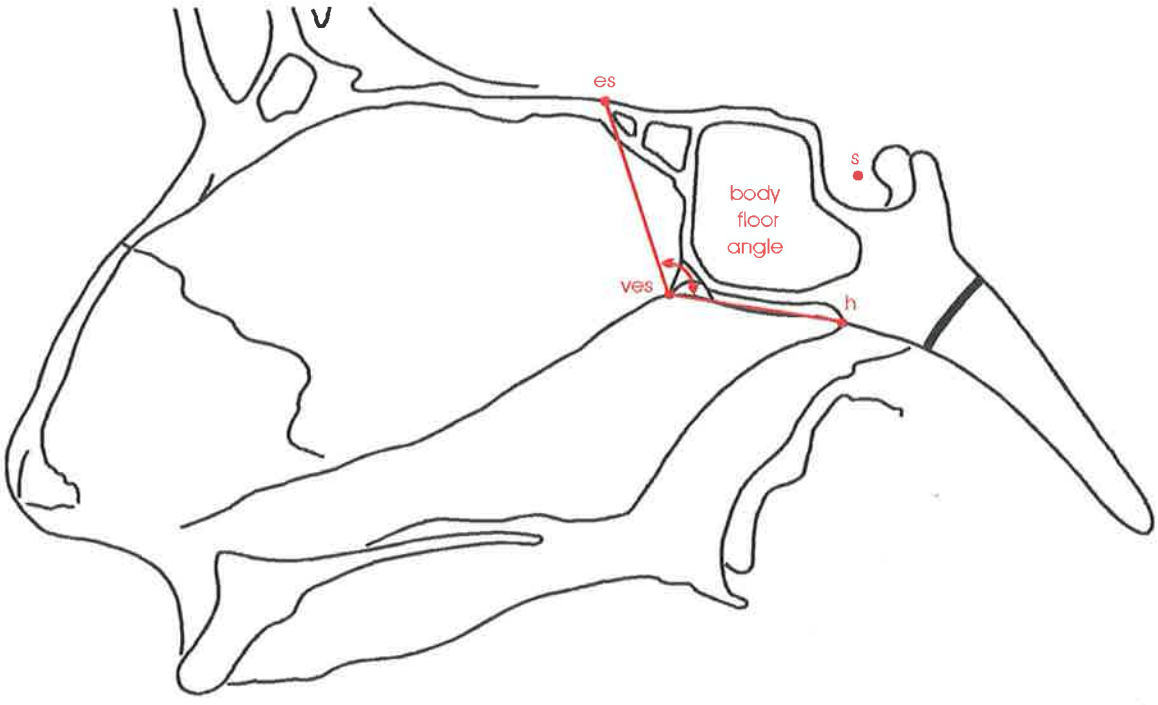

Figures 3.22(a)-(e) **Diagrammatic representations of the Temporal Bone showing the key Landmarks identified and the Distances, Dimensions and Angles measured**

Landmark Definitions

ael/aer	**articular eminence left/right:** The most infero-lateral point on the articular eminence of the temporal bone.
afl/afr	**articular fossa left/right:** The most supero-lateral point on the articular fossa of the temporal bone.
asl/asr	**asterion left/right:** The intersection between temporal, parietal and occipital sutures on the surface of the cranial vault. (see parietal and occipital)
asil/asir	**asterion inner left/right:** The intersection between temporal, parietal and occipital sutures on the inner surface of the cranial vault. (see parietal and occipital)
aul/aur	**auriculare left/right:** The most superior point on the root of the zygomatic arch nearest to craniometric point porion.
eamal/eamar	**external auditory meatus anterius left/right:** The most anterior point on the margin of the external auditory meatus.
eamil/eamir	**external auditory meatus inferius left/right:** The most inferior point on the margin of the external auditory meatus.
eampl/eampr	**external auditory meatus posterius left/right:** The most posterior point on the margin of the external auditory meatus.
pol/por	**external auditory meatus superius (ie porion) left/right:** The most superior point on the margin of the external auditory meatus.
fosl/fosr	**foramen out spinosum left/right:** The mid point of the external opening of the foramen spinosum, determined at the level of the skull base. (see sphenoid)
iaml/iamr	**internal auditory meatus left/right:** The centre of the internal auditory meatus.
jfll/jflr	**jugular foramen lateralis left/right:** The most lateral point on the jugular foramen at/near the temporal occipital suture. (see occipital)
jfml/jfmr	**jugular foramen medial left/right:** The most antero-medial point on the jugular foramen at/near the temporal occipital suture. (see occipital)
mal/mar	**mastoidale left/right:** The most inferior point on the mastoid process.
petal/petar	**petrous anterius left/right:** The most anterior point on the crest of the petrous temporal bone at the margin of the foramen lacerum and the base of the posterior clinoid.

Figures 3.22(a)-(e) (Temporal Bone continued):

Landmark Definitions (continued):

petpl/petpr **petrous posterius left/right:** The most posterior point on the crest of the petrous temporal bone at its junction with the lateral wall of the posterior cranial fossa (occipital bone).

parl/parr **pre-articulare left/right:** The most superior point on the lower border of the zygomatic arch located anterior to point articular eminence. (see zygomatic bone)

ptsl/ptsr **pterygo-superius left/right:** The postero-superior extremity of the medial pterygoid plate, where it approximates the apex of the petrous temporal bone. (see sphenoid)

sptl/sptr **sphenion t left/right:** The intersection of the temporal, parietal and sphenoid bones. (see parietal and sphenoid)

smfl/smfr **stylomastoid foramen left/right:** The centre of the external opening of the stylomastoid foramen.

ztl/ztr **zygo-temporale left/right:** The mid-point of the bony concavity formed between the frontal and temporal processes of the zygomatic bone. (see zygomatic bone)

Figures 3.22(a)-(e) (Temporal Bone continued):

Legend for Figures 3.22(a), 3.22(b) and 3.22(c)

Squamous Temporal Bone

Distance Definitions

Left		Right	
fosl-sptl	L lateral spheno-temporal suture	**fosr-sptr**	R lateral spheno-temporal suture
sptl-asl	L temporo-parietal suture	**sptr-asr**	R temporo-parietal suture
asl-mal	L occipital mastoid height	**asr-mar**	R occipital mastoid height
mal-smfl	L medial mastoid prominence	**mar-smfr**	R medial mastoid prominence

External Auditory Meatus

Distance Definitions

mal-eamil	L lateral mastoid prominence	**mar-eamir**	R lateral mastoid prominence
eamil-eampl	L inferior-posterior EAM rim	**eamir-eampr**	R inferior-posterior EAM rim
eampl-pol	L posterior-superior EAM rim	**eampr-por**	R posterior-superior EAM rim
pol-eamal	L superior-anterior EAM rim	**por-eamar**	R superior-anterior EAM rim
eamal-eamil	L anterior-inferior EAM rim	**eamar-eamir**	R anterior-inferior EAM rim

Zygomatic Process (Zygoma)

Distance Definitions

eamal-afl	L EAM-articular fossa length	**eamar-afr**	R EAM-articular fossa length
afl-ael	L articular fossa height	**afr-aer**	R articular fossa height
ael-parl	L inferior arch length	**aer-parr**	R inferior arch length
ztl-parl	L zygomatico-temporal suture	**ztr-parr**	R zygomatico-temporal suture
ztl-aul	L superior arch length	**ztr-aur**	R superior arch length

Petrous Temporal Bone

Distance Definitions

fisl-petal	L spheno-petrous temporal suture (sup)	**fisr-petar**	R spheno-petrous temporal suture (sup)
petal-jfpl	L post-med temporo-occipital suture	**petar-jfpr**	R post-med temporo-occipital suture
jfpl-asil	L lat temporo-occipital suture	**jfpr-asir**	R lat temporo-occipital suture
asil-petal	L petrous superior margin	**asir-petar**	R petrous superior margin
mal-jfll	L occipital mastoid suture (inf)	**mar-jflr**	R occipital mastoid suture (inf)
jfll-jfml	L jugular foramen width	**jflr-jfmr**	R jugular foramen width
jfml-ptsl	L med temporo-occipital suture (inf)	**jfmr-ptsr**	R med temporo-occipital suture (inf)
fosl-ptsl	L spheno-petrous temporal suture (inf)	**fosr-ptsr**	R spheno-petrous temporal suture (inf)

Figure 3.22(a): **Temporal Bone - Squamous, External Auditory Meatus and Zygoma** (left lateral aspect) Landmarks and Distances

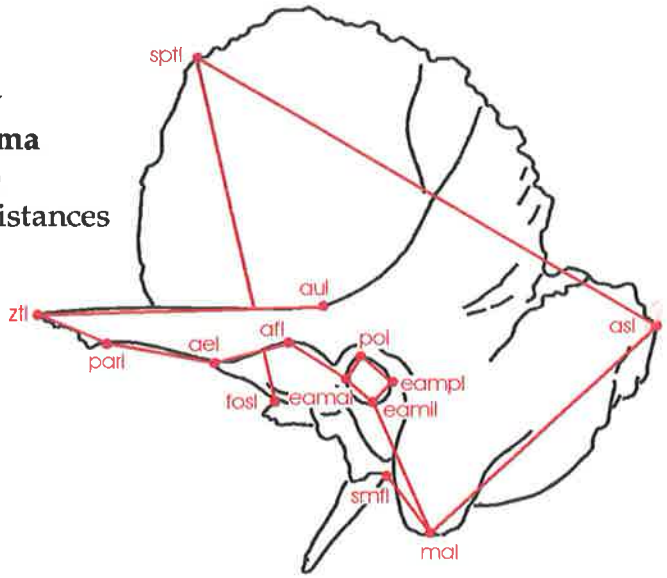

Figure 3.22(b): **Temporal Bone - Petrous** (left superior aspect) Landmarks and Distances

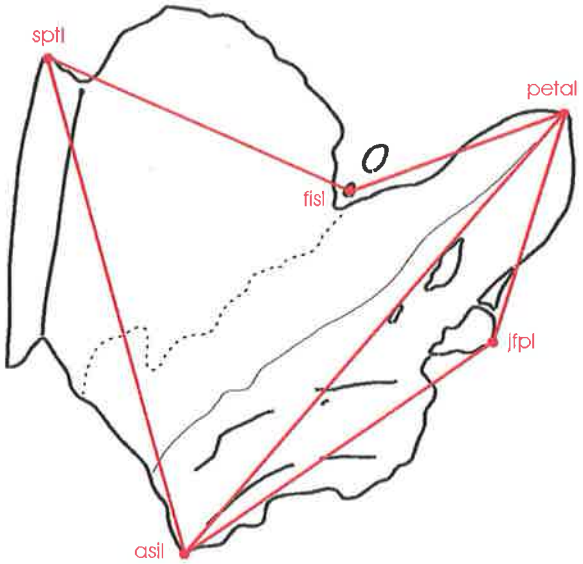

Figure 3.22(c): **Temporal Bone** (left inferior aspect) Landmarks and Distances

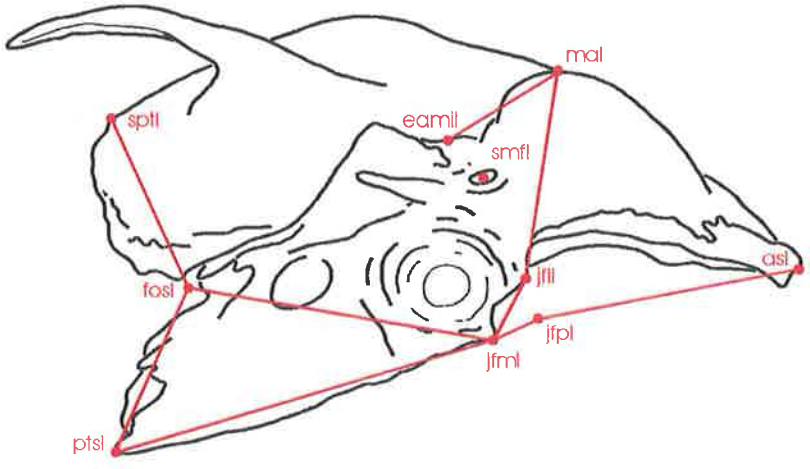

Figures 3.22(a)-(e) (Temporal Bone continued):

Legend for Figures 3.22(d) and 3.22(e)

Dimension	Definitions
petal-petpl	L petrous ridge length
petar-petpr	R petrous ridge length
iamr-iaml	Inter-internal auditory meatus dimension
pol-por	Inter-external auditory meatus dimension
jfpr-jfpl	Inter-posterior jugular foramen dimension
mal-mar	Inter-mastoid dimension

Angle	Definitions	
1	**pol-iaml/iamr-por**	Auditory canal angle
2	**petpl-petal/petar-petpr**	Petrous ridge angle
	petal-aul-ztl	L zygoma projection angle
	petar-aur-ztr	R zygoma projection angle

Figure 3.22(d): Temporal Bone
(superior aspect)
Dimensions and Angles

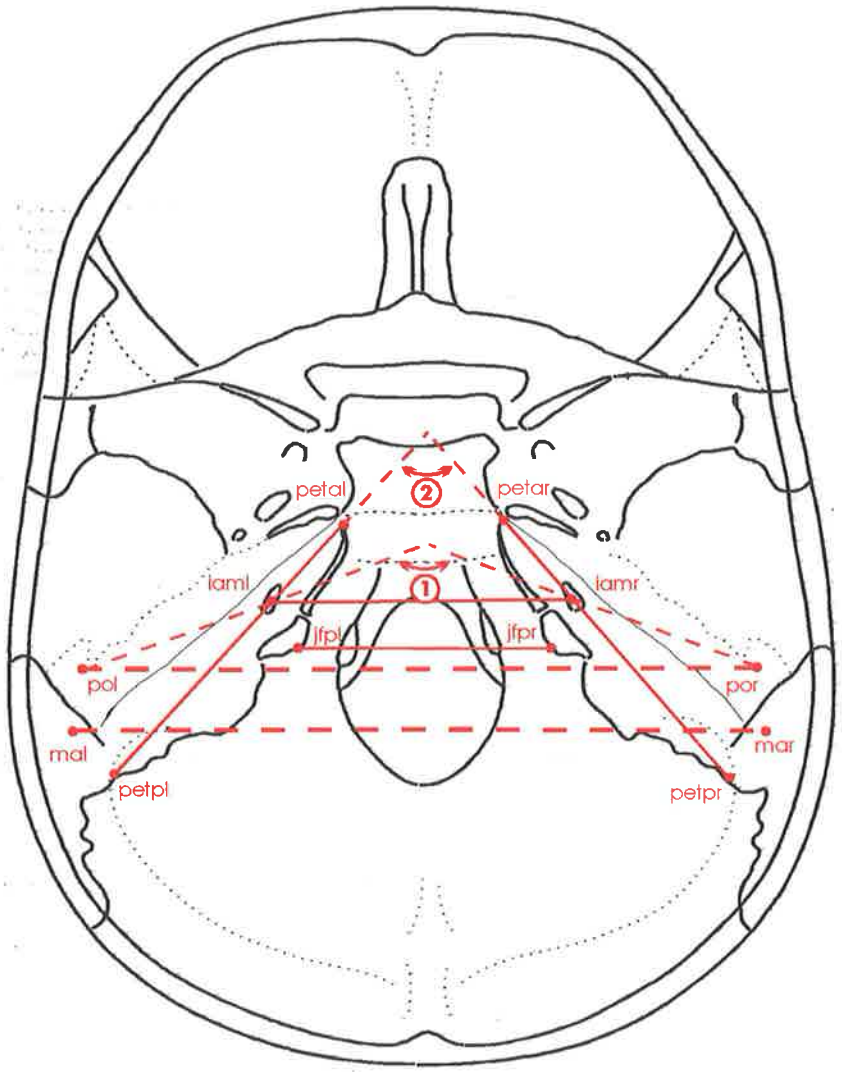

Figure 3.22(e): Temporal Bone
(left inferior aspect)
Angle

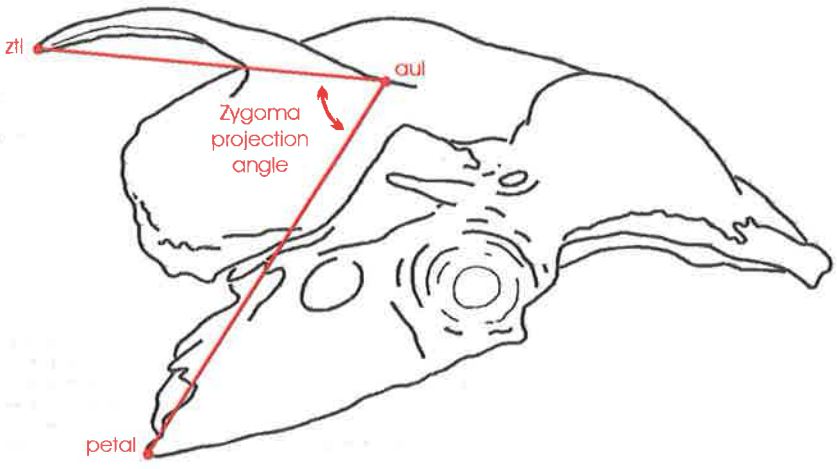

Figures 3.23 **Diagrammatic representations of the Parietal Bone showing the key Landmarks identified and the Distances and Dimensions measured**

Landmark Definitions

asl/asr	**asterion left/right:** The intersection between temporal, parietal and occipital sutures on the surface of the cranial vault (see occipital bone).
br	**bregma:** The intersection of the sagittal and the coronal sutures on the surface of the cranial vault (see frontal bone).
l	**lambda:** The intersection between the lambdoid and sagittal sutures on the surface of the cranial vault (see occipital bone).
spcl/spcr	**sphenion c left/right:** The junction of the coronal suture and the sphenoid bone (see sphenoid).
sptl/sptr	**sphenion t left/right:** The intersection of the temporal, parietal and sphenoid bones (see sphenoid).

Figures 3.23 (Parietal Bone continued):

Legend for Figure 3.23

Distance Definitions

		l-br	Sagittal suture
	Left		**Right**
br-spcl	L parietal frontal (coronal) suture	**br-spcr**	R parietal frontal (coronal) suture
spcl-sptl	L spheno-parietal suture	**spcr-sptr**	R spheno-parietal suture
sptl-asl	L temporo-parietal suture	**sptr-asr**	R temporo-parietal suture
asl-l	L occipito-parietal (lambdoid) suture	**asr-l**	R occipito-parietal (lambdoid) suture

Figure 3.23: Parietal Bone
(left lateral aspect)
Landmarks and Distances

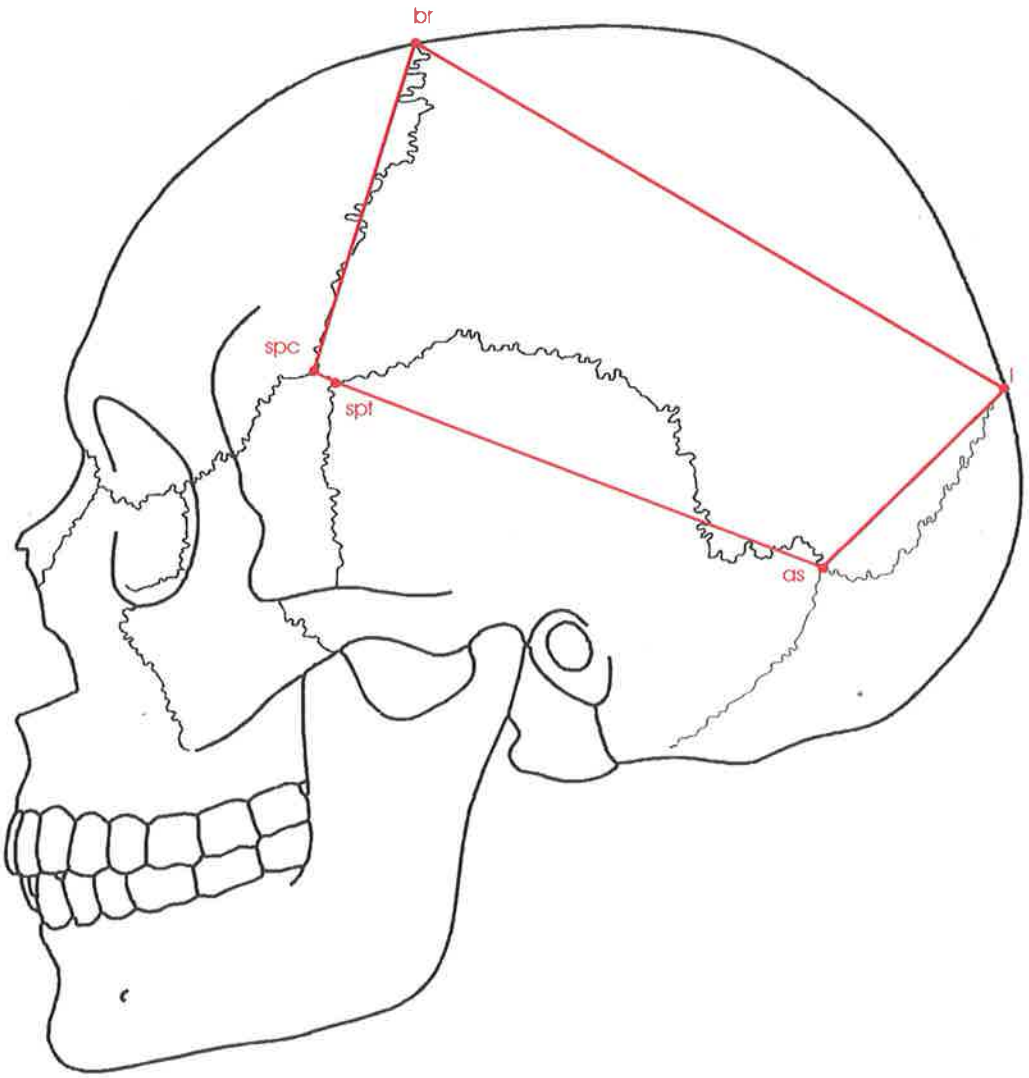

Figures 3.24(a)-(b) **Diagrammatic representations of the Occipital Bone showing the key Landmarks identified and the Distances and Dimensions measured**

Landmark Definitions

asl/asr	**asterion left/right:** The intersection between temporal, parietal and occipital sutures on the surface of the cranial vault.
ba	**basion:** The mid-sagittal point on the anterior margin of the foramen magnum (determined as the point of maximum convexity on the clivus of the skull at the anterior margin of the foramen magnum).
fmll/fmlr	**foramen magnum lateralis left/right:** The most lateral point on the margin of the foramen magnum.
iop	**internal occipital protuberance:** The most prominent point on the internal occipital crest (located at the antero-inferior attachment of falx cerebri to the occipital).
jfll/jflr	**jugular foramen lateralis left/right:** The most lateral point on the jugular foramen at/near the temporal occipital suture.
jfml/jfmr	**jugular foramen medial left/right:** The most antero-medial point on the jugular foramen at/near the temporal occipital suture.
jfpl/jfpr	**jugular foramen posterius left/right:** The most posterior point on the jugular foramen.
l	**lambda:** The intersection between the lambdoid and sagittal sutures on the surface of the cranial vault.
o	**opisthion:** The mid-sagittal point on the posterior margin of the foramen magnum.
petpl/petpr	**petrous posterius left/right:** The most posterior point on the crest of the petrous temporal bone at its junction with the lateral wall of the posterior cranial fossa (occipital bone).
ptsl/ptsr	**pterygo-superius left/right:** The postero-superior extremity of the medial pterygoid plate, where it approximates the apex of the petrous temporal bone. (see maxilla)

Figures 3.24(a)-(b) (Occipital Bone continued):

Legend for Figures 3.24(a) and 3.24(b)

Distance Definitions

Lambdoid and Cranial Base

Left		Right	
l-asl	L occipito-parietal (lambdoid) suture	**l-asr**	R occipito-parietal (lambdoid) suture
asl-jfll	L lateral temporo-occipital suture (sup)	**asr-jflr**	R lateral temporo-occipital suture (sup)
jfll-jfpl	L lateral jugular foramen	**jflr-jfpr**	R lateral jugular foramen
jfpl-jfml	L medial jugular foramen	**jfpr-jfmr**	R medial jugular foramen
jfml-ptsl	L med. temporo-occipital suture (inf)	**jfmr-ptsr**	R med. temporo-occipital suture (inf)
		ptsr-ptsl	Inferior spheno-occipital synchondrosis

Foramen Magnum

Left		Right	
ba-fmll	L anterior foramen magnum	**ba-fmlr**	R anterior foramen magnum
fmll-o	L posterior foramen magnum	**fmlr-o**	R posterior foramen magnum

Dimension Definitions

Foramen Magnum

ba-o	Foramen magnum length
fmll-fmlr	Foramen magnum width

Posterior Cranial Fossa

o-iop	Posterior cranial fossa depth
iop-l	Posterior occipital height
petpl-iop	L posterior fossa length
petpr-iop	L posterior fossa length

Figure 3.24(a): **Occipital Bone** (superior aspect) Landmarks and Distances

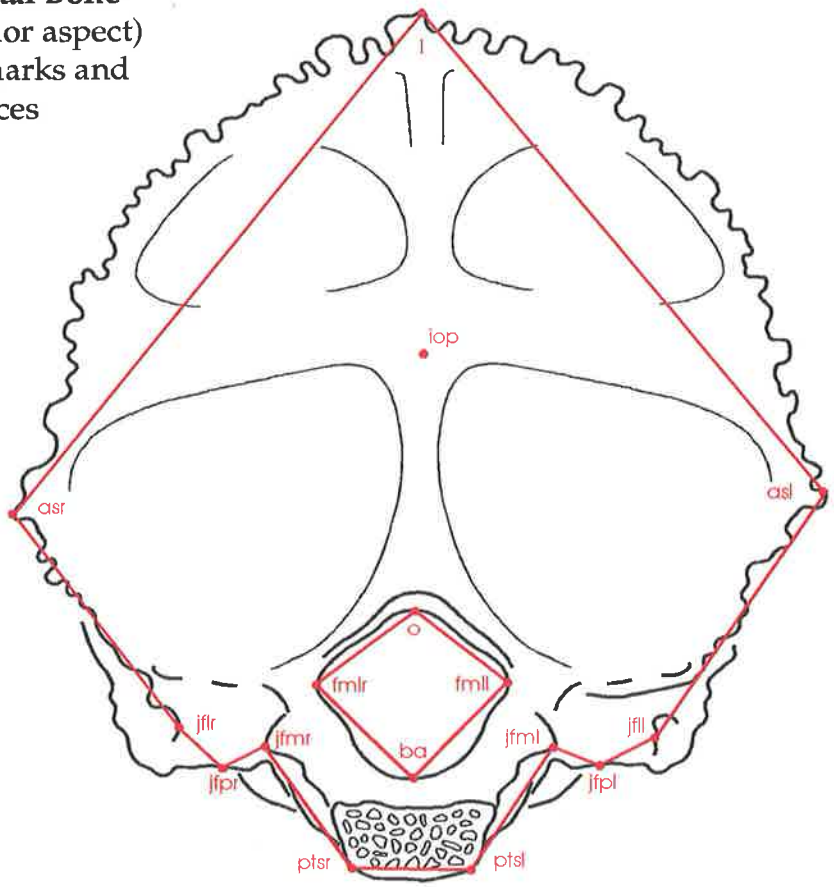

Figure 3.24(b): **Occipital Bone** (superior aspect) Dimensions

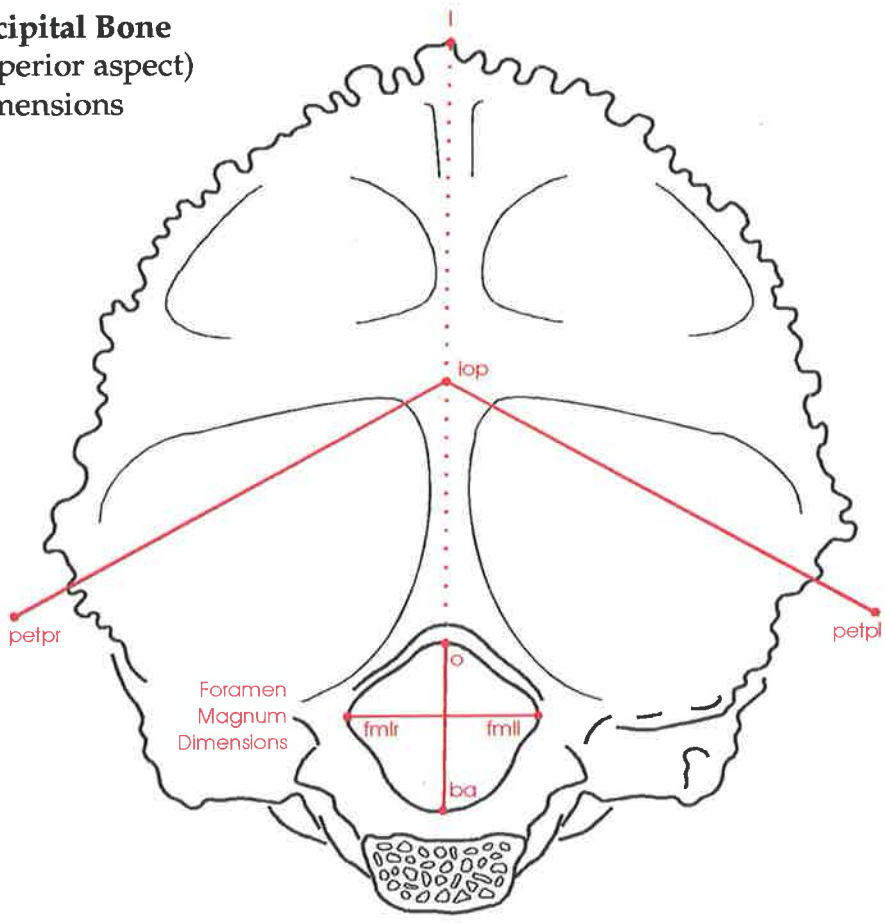

Figures 3.25 **Diagrammatic representations of the Cranial Base Sutures showing the key Landmarks identified and the Distances measured**

Cranial Base Suture Definitions

Anterior Cranial Fossa

1 **Spheno-ethmoid synchondrosis:** Distance from the posterior lateral corner of the cribriform plate (cppl/r) to the ethmoid spine (es).

2 **Spheno-frontal suture (anterior fossa):** Distance from the posterior lateral corner of the cribriform plate (cppl/r) to the most anterior convexity of the lesser wing of the sphenoid (spal/r).

3 **Spheno frontal suture (orbital):** Distance from the tip of the lesser wing of the sphenoid (spal/r) to the junction of the sphenoid, frontal and zygomatic sutures in the lateral wall of the orbit (zfsl/r).

4 **Spheno-zygomatic suture:** Distance from the junction of the sphenoid, frontal and zygomatic sutures in the lateral wall of the orbit (zfsl/r) to the inferior convexity of the lateral orbital wall (inferior limit of suture) (gwl).

Middle Cranial Fossa

5 **Spheno-squamous temporal suture:** Distance from the inferior convexity of the lateral orbital wall (inferior limit of suture) (gwl).to the centre of the foramen spinosum (fosl/r).

6 **Spheno-petrous temporal suture (superior):** Distance from the foramen spinosum (fisl/r) to the superior and medial apex of the petrous temporal bone at the junction with the sphenoid bone (petal/r).

7 **Spheno-petrous temporal suture (inferior):** Distance from the foramen spinosum (fosl/r) to the inferior and medial apex of the petrous temporal bone at the junction with the sphenoid bone (ptsl/r).

Posterior Cranial Fossa

8 **Medial Temporo-occipital suture (superior):** From the medial apex of the petrous temporal bone at the junction with the sphenoid bone to the medial edge of the jugular foramen.

9 **Medial Temporo-occipital suture (inferior):** From the most superior, posterior point of the medial pterygoid plates at the base of the skull to the junction with the sphenoid bone to the medial edge of the jugular foramen.

10 **Occipital Mastoid suture (superior):** From the lateral edge of the jugular foramen to the lateral junction of the petrous ridge with the squamous and mastoid temporal bones.

11 **Spheno-occipital synchondrosis (superior):** The distance between the medial apices of the petrous temporal bones

12 **Spheno-occipital synchondrosis (inferior):** The distance between the most superior, posterior points of the each of the medial pterygoid plates at the base of the skull

13 **Spheno-occipital synchondrosis (lateral):** The distance between the medial apex of the petrous temporal bone (petal/r) to the superior, posterior point on the medial pterygoid plate at the base of the skull (ptsl/r).

Figures 3.25 (Cranial Base Sutures continued):

Legend for Figure 3.25

Cranial Base Suture Definitions

Anterior Cranial Fossa

	Left		Right
1 **es-cppl**	L spheno-ethmoid synchondrosis	**es-cppr**	R spheno-ethmoid synchondrosis
2 **cppl-spal**	L spheno-frontal suture (ant fossa)	**cppr-spar**	R spheno-frontal suture (ant fossa)
3 **spal-zfsl**	L spheno-frontal suture (orbital)	**spar-zfsr**	R spheno-frontal suture (orbital)
4 **zfsl-gwll**	L spheno-zygomatic suture	**zfsr-gwlr**	R spheno-zygomatic suture

Middle Cranial Fossa

	Left		Right
5 **gwll-fisl**	L spheno-squamous temporal suture	**gwlr-fisr**	R spheno-squamous temporal suture
6 **fisl-petal**	L spheno-petrous temporal suture (sup)	**fisr-petar**	R spheno-petrous temporal suture (sup)
7 **fosl-ptsl**	L spheno-petrous temporal suture (inf)	**fosr-ptsr**	R spheno-petrous temporal suture (inf)

Posterior Cranial Fossa

	Left		Right
8 **petal-jfml**	L med. temporo-occipital suture (sup)	**petar-jfmr**	R med. temporo-occipital suture (sup)
9 **jfml-ptsl**	L med. temporo-occipital suture (inf)	**jfmr-ptsr**	R med. temporo-occipital suture (inf)
10 **jfll-petpl**	L occipital mastoid suture (sup)	**jflr-petpr**	R occipital mastoid suture (sup)

11	**petal-petar**	Spheno-occipital synchondrosis (sup)
12	**ptsl-ptsr**	Spheno-occipital synchondrosis (inf)

13 **ptsl-petal**	L spheno-occipital synchondrosis (lat)	**ptsr-petar**	R spheno-occipital synchondrosis (lat)

Figure 3.25: Cranial Base Sutures
(superior aspect)
Landmarks and Distances

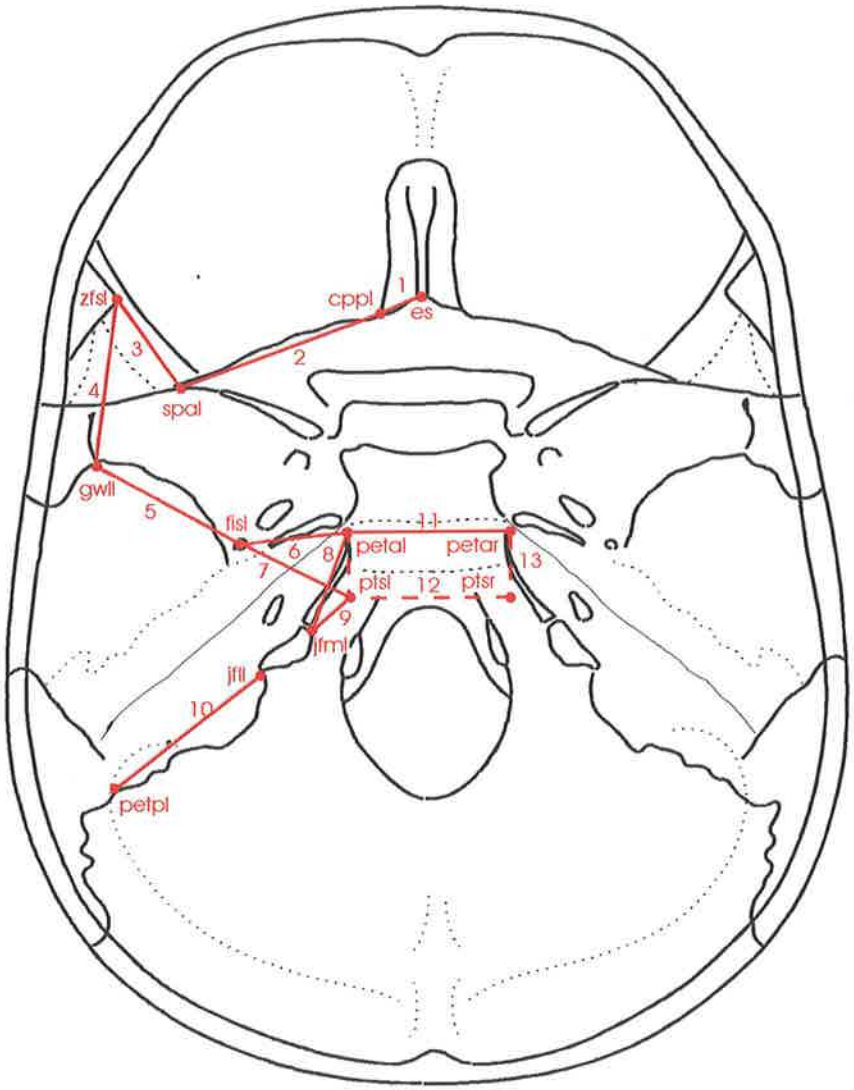

Figures 3.26(a)-(c) **Diagrammatic representations of the Craniofacial Dimensions and Angles showing the key Landmarks identified and the measurements**

Landmark Definitions

ba	**basion:** The mid-sagittal point on the anterior margin of the foramen magnum (determined as the point of maximum convexity on the clivus of the skull at the anterior margin of the foramen magnum).
n	**nasion:** The most anterior point of the frontonasal suture. (If suture not clearly identified then the deepest point on the nasal notch can be substituted in the midline.)
s s	**subspinale:** The most posterior point on the anterior contour of the maxillary alveolar process in the mid-sagittal plane. (Also known as Down's Point A).
gol/gor	**gonion left/right:** A point on the angle of the mandible located by the bisection of the angle formed by the mandibular line and the ramus line.
s	**sella:** The centre of the sella turcica.
s m	**supramentale:** The most posterior point on the anterior contour of the mandibular alveolar process in the mid-sagittal plane. (Also known as Down's Point B).

Figures 3.26(a)-(c) (Craniofacial Dimensions and Angles continued):

Legend for Figures 3.26(a), 3.26(b) and 3.26(c)

Facial Height Definitions

n-gn	Anterior facial height
s-gol	L posterior facial height
s-gor	R posterior facial height

Facial Angle Definitions

s-n-ss	SNA angle (sella-nasion-point A)
s-n-sm	SNB angle (sella-nasion-point B)

Cranial Base Angle Definition

ba-s-n	Cranial base angle

Cranial Base Dimension Definitions

ba-n	Cranial base length
ba-s	Clivus length (posterior cranial base)
s-n	Anterior cranial base length

Figure 3.26(a): **Craniofacial Dimensions and Angles**
(sagittal aspect)
Facial Heights

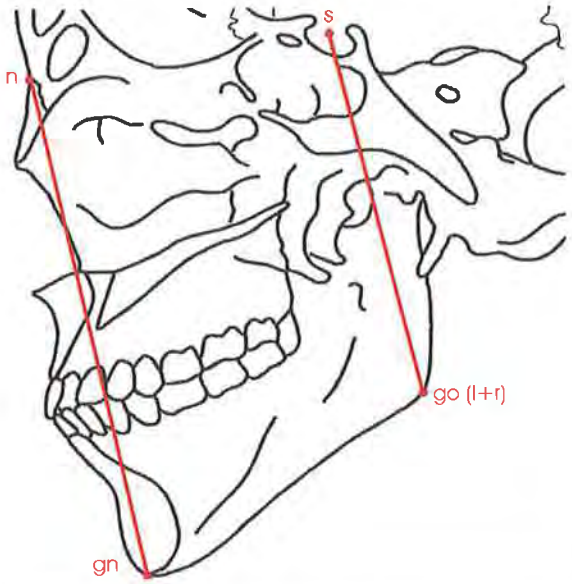

Figure 3.26(b): **Craniofacial Dimensions and Angles**
(mid-sagittal plane)
Facial Angles

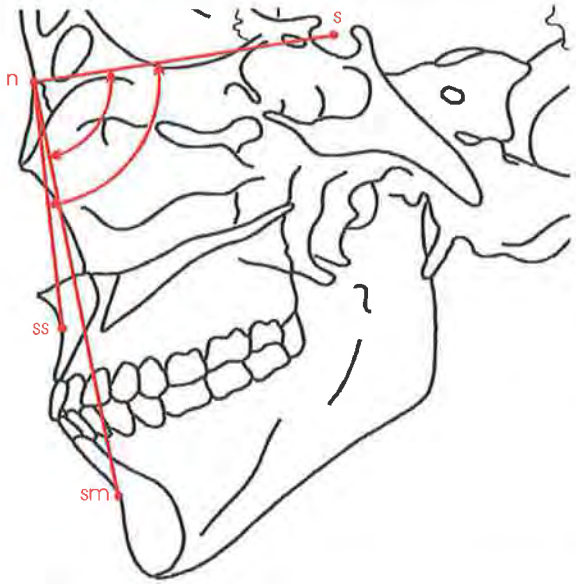

Figure 3.26(c): **Craniofacial Dimensions and Angles**
(mid-sagittal plane)
Cranial Base Dimensions and Angles

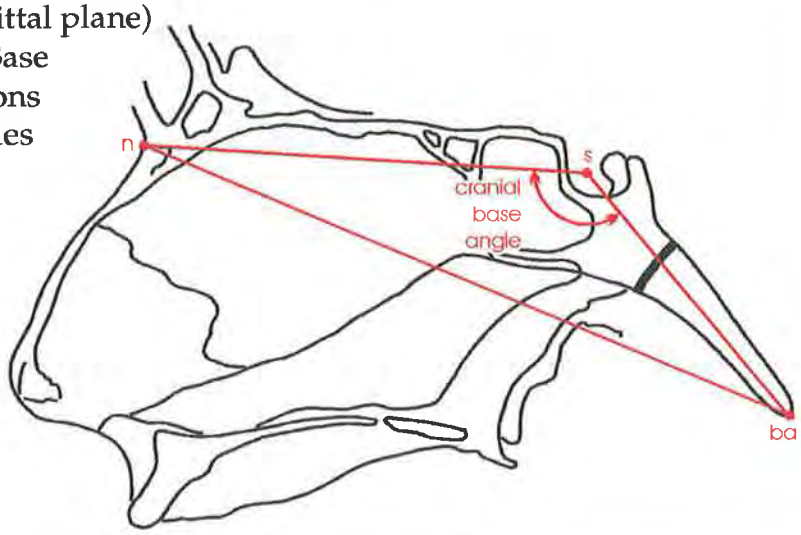

3.4 Qualitative and Quantitative Analysis of Patients with Crouzon syndrome

A summary of the clinical and qualitative radiographic findings for the patients with Crouzon syndrome is presented. Features of the 3D CT reconstructions which make landmark identification difficult are reported. The measurements derived from the 3D CT reconstruction of each patient with Crouzon syndrome are statistically compared with the data from the relevant age-matched experimental standards. These results are presented as Z score pattern profiles for each anatomical unit (Figures 3.27 - 3.38). The significantly increased and decreased Z scores ($1.96 < Z > 1.96$) are described in the accompanying text. Z scores not significantly different from the experimental standard but with an absolute value near 1.96, are reported where appropriate, as indicating a trend for the measurement to be large or small. Z scores not significantly different from the experimental standard are reported where relevant. The complete set of data (including the mean and standard deviation of the experimental standard and the patient measurement and Z score) is listed in table form in Appendix 2. The findings for the anatomical units for each patient are discussed with respect to sites of and possible mechanisms of pathogenesis. The significant findings for each patient, categorised by anatomical unit, are summarised and correlated in Table 3.3 at the end of Section 3.4. The grouped findings for each anatomical unit are also presented in the final section of this chapter (Section 3.5), where the patterns of abnormality in this group of patients are discussed.

3.4.1 Clinical and Radiographic Findings for Patient RN

Clinical Features

This patient presented at the age of 1 month, having had no previous surgery (Figure 3.1). The child's mother had a mild form of Crouzon syndrome. The clinical features of Patient RN were slightly atypical with brachycephaly and an anterior cranial ring constriction appearance (Figure 3.1). The mental state was appropriate for age with no evidence of hydrocephalus. Proptosis, a retruded nose with a parrot beak tip and a hypoplastic maxilla were present. The palate appeared to be high and arched. The upper airway was of an adequate size with no evidence of respiratory difficulty. An incomplete simple syndactyly of the hand second web space was present.

Lateral, Antero-Posterior and Basal Radiographs

The only pre-operative radiographs available were lateral and basal views. The basal view was unhelpful. The lateral radiograph was more informative as it showed the skull shape. There was a copper-beaten appearance of the calvaria in the occipital and coronal regions. Prominence of the frontal bone was evident. No calvarial sutures were present radiographically. The cranial base appeared to be more obtuse with the body of the sphenoid facing anteriorly rather than inferiorly, however this may be a feature of the patient's age rather than of any pathology. The spheno-ethmoid synchondrosis was not visualised, however the spheno-occipital synchondrosis was patent radiographically (and remained so at 5 years of age, at the time of this assessment). The maxilla was grossly hypoplastic with poor visualisation of the nasopharynx. The oropharynx and the hypopharynx were patent.

3D CT Reconstruction

Calvarial bones: The 3D CT reconstruction showed a large number of apparent defects in the calvarial bones. This was due to errors of exclusion coupled with immaturity of ossification in this 1 month old child. Defects in the temporal, parietal and occipital regions may be related to calvarial thinning due to endocranial resorption in this area. These defects corresponded to the copper-beaten appearance seen on the lateral and basal radiographs. The coronal and sagittal sutures were fused. The metopic suture was patent. The resultant head shape was atypical with anterior and bi-temporal bulging. This picture reflects the severe constriction of growth in the region of the coronal and sagittal sutures. The temporo-parietal and spheno-parietal sutures were widely patent allowing decompression of the intracranial contents.

Cranial base: Incomplete ossification of the ethmoid bone at the time of the CT scan produced a bony defect in this region. In particular, the crista galli and the foramen caecum were not visible as they ossify in the first year of life. The spheno-ethmoid synchondrosis was not clearly seen. The lesser wing of the sphenoid appeared shortened and swept up where it attached to the frontal bone. This area was thickened and broad as it ran up to the coronal suture. In the middle cranial fossa, the greater wing of the sphenoid was protruding under the frontal bone into the orbit. The anterior clinoid processes were prominent. The sella was unremarkable. The cranial base angle appeared to be within normal limits, but was more closely assessed with the

measurement analysis. The sphenoid-temporal sutures in the region of the foramen lacerum and foramen ovale in the middle cranial fossa were widely patent (as expected with this degree of immaturity). The spheno-occipital synchondrosis was present as a faint line, not a wide open gap, a finding which contrasted with the lateral radiograph. The basilar-condylar occipital synchondroses were patent on the 3D CT reconstruction. The apices of the petrous temporal bones were some distance from the sphenoid body.

Orbital Region: The long axis of the orbital aperture ran in the supero-lateral direction, producing a harlequin mask-type deformity. In this deformity, the orbits appear to be swept upwards and laterally as seen in a harlequin mask. Hypertelorism was also present. The lateral orbital walls were lengthened in the cranial direction. The fronto-zygomatic and spheno-frontal sutures of the orbit were widely patent. The medial orbital walls were difficult to visualise, due to the incomplete ossification of the ethmoid bone. The optic canal could not be seen on the 3D CT reconstructions, due to its position and was more readily seen with the 2D slice data.

Maxilla: The maxilla was comprised primarily of alveolar bone with dental buds. It was in close proximity to the cranial base.

3.4.2 Features of the CT Scan and 3D Reconstruction of Patient RN that made Landmark Identification difficult

The infra-orbital, mental and stylomastoid foramina could not be visualised. No teeth were present at this age. Ectomolare points were estimated on the most prominent molar point of the alveolus.

The crista galli, foramen caecum and bregma were not identifiable. The spheno-occipital synchondrosis was measured from the apex of the petrous temporal bones in all patients. These landmarks were readily and reliably identified in the skulls of patients of all ages and this was considered to be a more uniform method of analysis. This method becomes less accurate in the neonatal period when the synchondrosis is not precisely adjacent to the apex of the petrous temporal bones.

The separations of the frontal bone from the frontal process of the zygomatic bone and the greater wing of the sphenoid bone due to immaturity provided some difficulty in landmark

identification as the definition of the landmarks in this area was based on the junctions of these bones. As this area was of particular interest in this study, the most appropriate point on the edge of the bones adjacent the sutures was selected. The peri-orbital sutures and cranial base landmarks were identified from the regional bony contours and junctions defined in the landmarks (Figures 3.15-3.26).

3.4.3 Results and Discussion of the Quantitative Analysis of Patient RN compared with the 6 Month Experimental Standard

Figures 3.27(a)-(r)

3.4.3.1 The Mandible of Patient RN

Distances (Figure 3.27(a)): All distances between the adjacent landmarks representing the outline of the bone were not significantly different from the experimental standard.

Dimensions and Angles (Figure 3.27(b)): The dimensions were all similar to those of the experimental standard. The angles on the other hand showed greater deviation from the experimental standard. The gonial angles (cdl-gor-gn, cdr-gor-gn) were significantly larger bilaterally. The left sided coronoid base angle (ctl-cbl-id) and coronoid base-dental angles (ctl-cbl-em1il) were more acute.

Discussion: The distances, dimensions and angles of the mandible in this patient were similar except for an increase in the gonial angles and reduced coronoid base angles on the left. The mandible in Crouzon syndrome is relatively spared from deformity. Most changes become more marked with time as a result of secondary forces. Despite this abnormalities are seen in this patient at this stage.

Figure 3.27(a) Z Scores of the Distances of the Mandible for Patient RN compared with the 6 Month Experimental Standard.

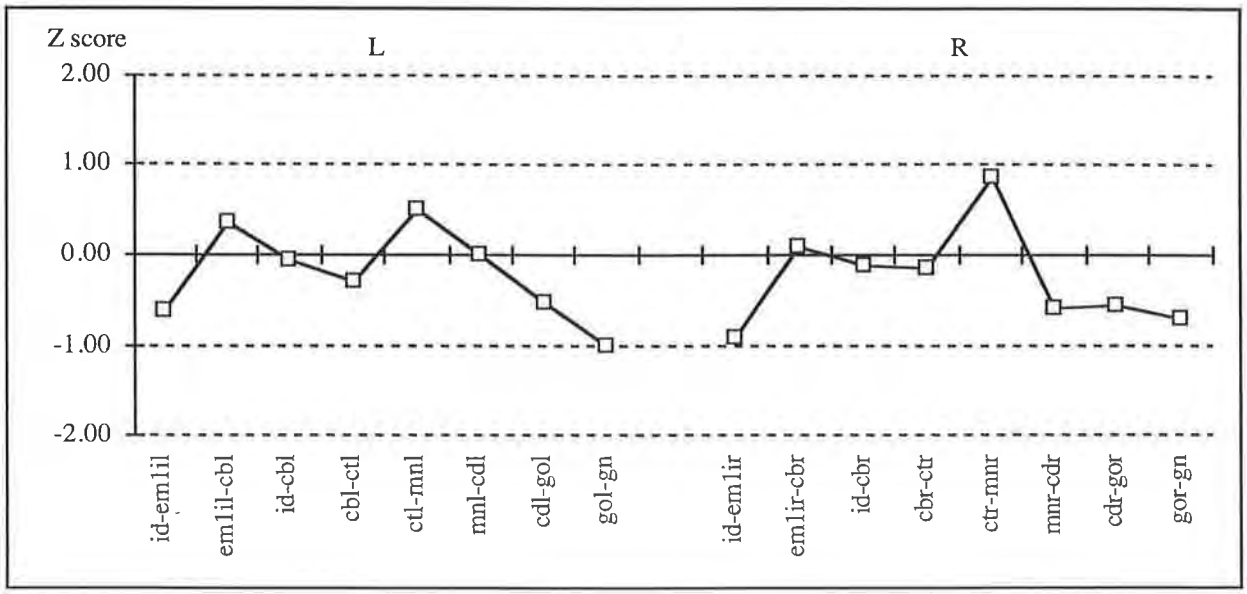

Figure 3.27(b) Z Scores of the Dimensions and Angles of the Mandible for Patient RN compared with the 6 Month Experimental Standard

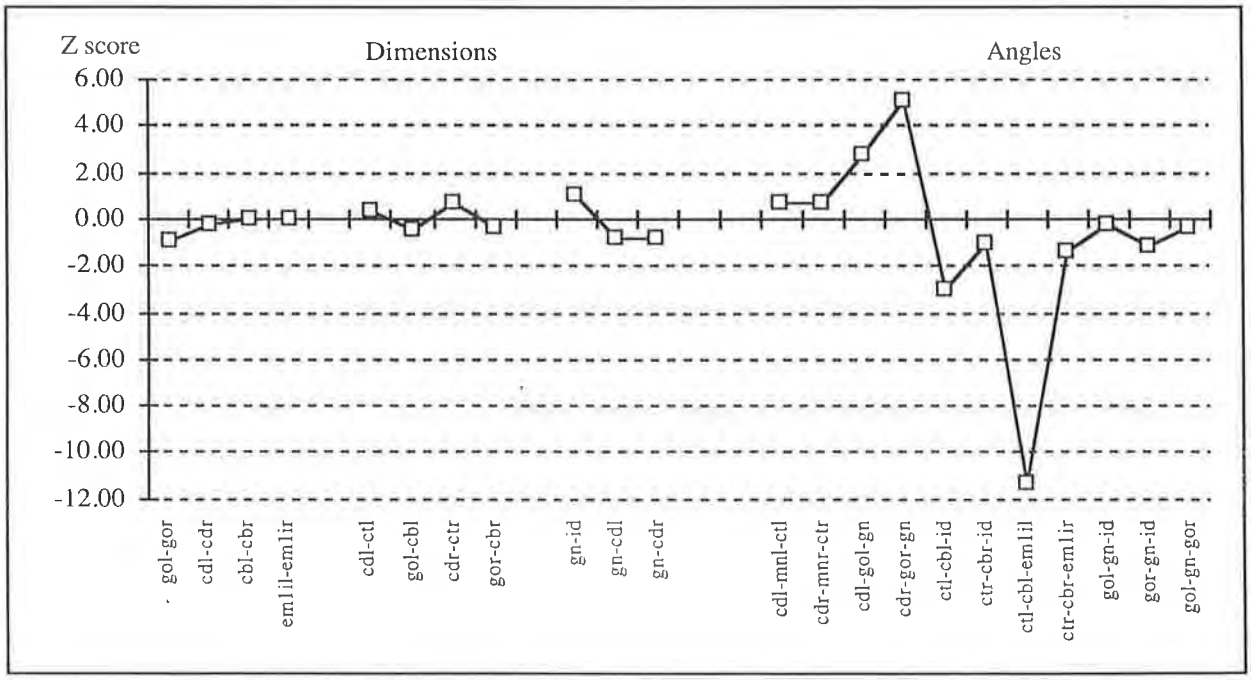

3.4.3.2 The Maxilla of Patient RN

Distances (Figure 3.27(c)): The majority of distances were within the limits of the experimental standard. The distance of the medial orbital wall from the maxillare superius point to the nasolacrimal duct was reduced significantly on the right (msr-nlir) with a tendency to be reduced on the left (msl-nlil). The distance from the inferior orbital fissure to the zygomaxillare inferius (iobfl-zmil, iobfr-zmir) was increased bilaterally. This line makes up the lateral wall of the maxilla and represents one of the articulations of this bone with the zygomatic bone.

Dimensions and Angles (Figure 3.27(d)): The dimensions of the maxilla measured were not significantly different from the experimental standard. The angles of the roof of the maxilla, also comprising the floor of the orbit (nlil-msl-iobfl, nlir-msr-iobfr), were more obtuse bilaterally than the control. The angle representing the posterior wall of the maxilla (msl-gpfl-em1sl, msr-gpfr-em1sr) was significantly more acute on the right and tended to be more acute on the left. The maxillary arch angle (from greater palatine foramen to prosthion to greater palatine foramen on the other side (gpfl-pr-gpfr)) was increased.

Discussion: The deformity of the maxilla is typically manifest at a later age than the calvarial abnormality in Crouzon syndrome. The findings in this patient suggest significant differences in size and shape of the maxilla may occur at an early age. Increased sutural distances between the maxilla and the zygomatic bone are of particular interest as early suture fusion will have a more profound impact on maxillary growth.

Figure 3.27(c) Z Scores of the Distances of the Maxilla for Patient RN compared with the 6 Month Experimental Standard

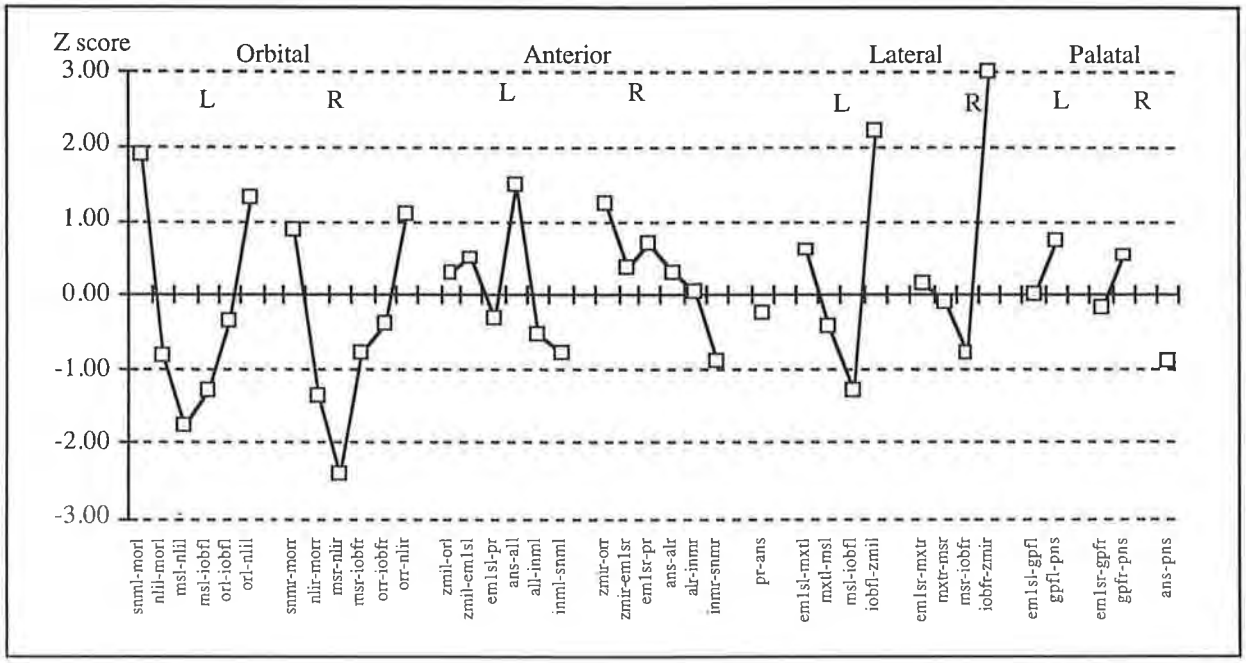

Figure 3.27(d) Z Scores of the Dimensions and Angles of the Maxilla for Patient RN compared with the 6 Month Experimental Standard

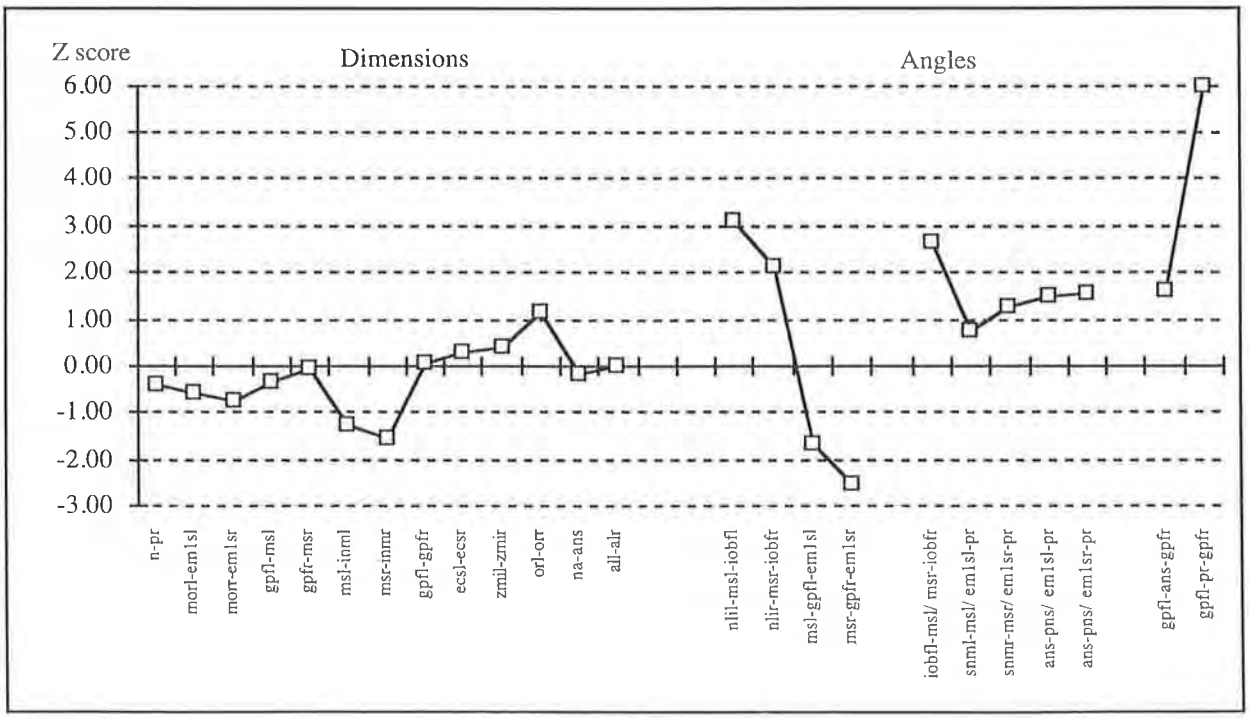

3.4.3.3 The Nasal Bones of Patient RN

Distances, Dimensions and Angles (Figure 3.27(e)): The left naso-frontal suture (n-snml) was increased in length (see also frontal bone). The remaining dimensions and the angles were not significantly different from the experimental standard.

Discussion: The nasal bones in this patient were minimally different from the experimental standard.

Figure 3.27(e) Z Scores of the Measurements of the Nasal Bones for Patient RN compared with the 6 Month Experimental Standard

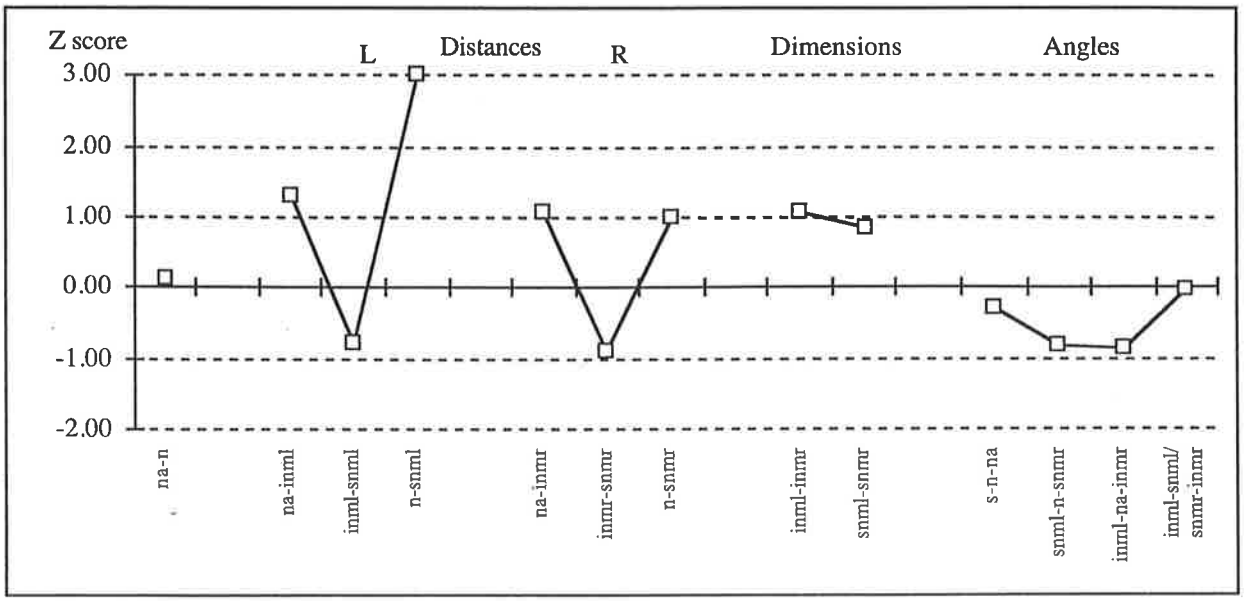

3.4.3.4 The Frontal Bone of Patient RN

Distances (Figure 3.27(f)):

Supra-orbital Region: The left fronto-nasal suture (n-snml) was lengthened (see also nasal bone) and the fronto-zygomatic suture (zfsl-slorl, zfsr-slorr) showed a tendency to be reduced compared with the experimental standard (see also zygomatic bone). The right superior-medial orbital rim (morr-sorr) was asymmetrically increased in distance from the left.

Ethmoid Attachment: The frontal ethmoid attachment was lengthened at the level of the cribriform plate (cpal-cppl, cpar-cppr), while the posterior distance to the optic foramen (cppl-ofaml, cppr-ofamr) was reduced (see also ethmoid bone).

Sphenoid Attachment: The length of the junction with lesser wing of the sphenoid (spal-cppl, spar-cppr) was reduced. Other orbital measurements are found in the description of the zygomatic and sphenoid bones and the cranial base sutures which follows. A summary of these later findings revealed the lateral distances from the lesser wing to the squamous spheno-frontal sutures (spal-spcl, spar-spcr) were lengthened and the lateral squamous suture (zfsl-spcl, zfsr-spcr) was reduced in length. The parietal attachment (spc-br) and sphenoid attachments (zfs-spc and spc-spa) were not recordable due to the fusion of sutures and hence poor visibility of landmarks in this region.

Dimensions (Figure 3.27(f)): The distance between the supra-orbital points (sorl-sorr) was increased. The distance between the lesser wing tips (spal-spar) was reduced. The depth of the anterior cranial fossa, as measured from the lesser wing tip to the supra-orbital point (sorl-spal, sorr-spar), was not significantly different from the experimental standard. This measurement does not reflect the angle of the fossa.

Discussion: The frontal bone of Patient RN exhibited a varied pattern of deformity. There were minor abnormalities in the sutural distances between the frontal bone and the nasal and zygomatic bones. Asymmetry of the supra-orbital margin was seen. Lengthening of the fronto-ethmoid attachment was contrasted with the reduction in length of the attachment to the lesser wing of the sphenoid bone. Lateral to the lesser wing the distances were increased and this may imply a sutural problem in this region in continuity with coronal suture pathology. The dimensions of the frontal bone included an increased width anteriorly and reduced width

posteriorly. The depth of the fossa was within the experimental standard range however, this distance was measured from the wide anterior and narrow posterior landmarks which may influence the dimension measured. The assessment of the frontal bone was incomplete due to difficulties in measuring the lateral part of the bone. Complete suture fusion at this site made landmark identification impossible, and landmarks were not recorded. In other areas, wide suture separation made the identification of a single landmark to represent the junction of the bones impossible. Where this occurred the most appropriate landmark on the adjacent bone was selected.

Figure 3.27(f) Z Scores of the Distances and Dimensions of the Frontal Bone for Patient RN compared with the 6 Month Experimental Standard

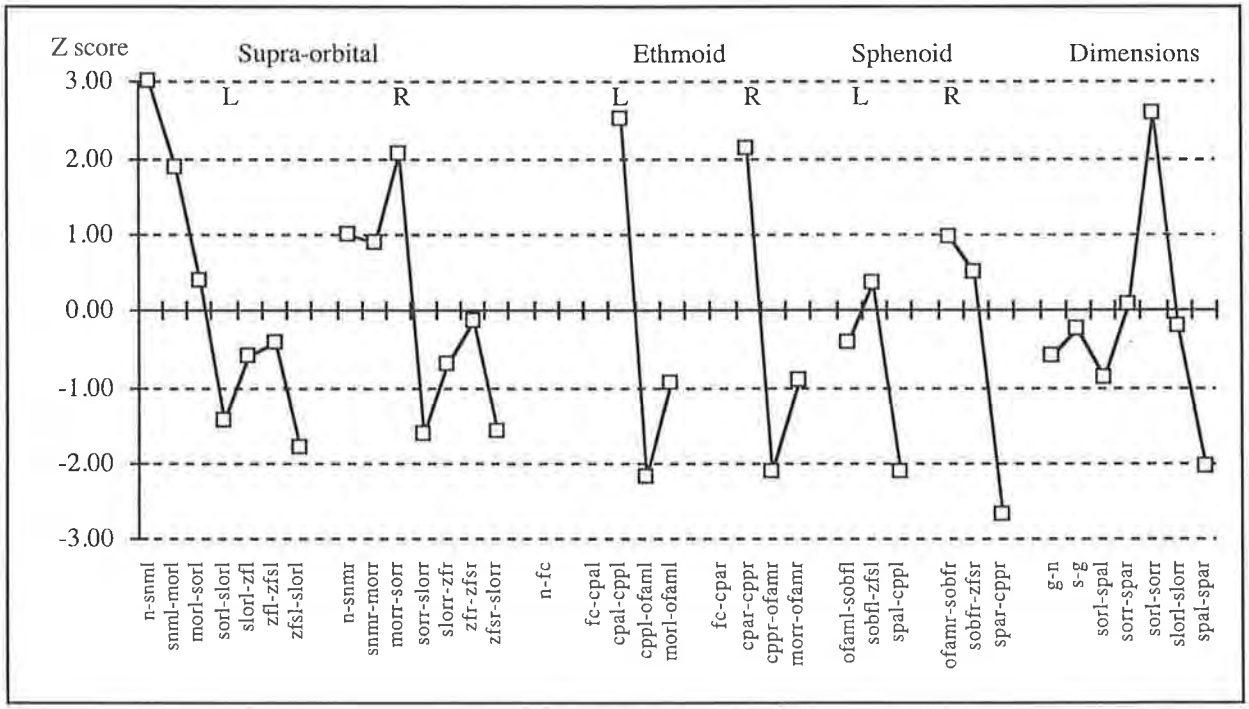

3.4.3.5 The Zygomatic Bone of Patient RN

Distances (Figure 3.27(g)): The majority of measurements were not significantly different from the experimental standard. The spheno-zygomatic suture (zfsl-gwll, zfsr-gwlr) was significantly increased bilaterally (see also sphenoid bone). On the left side, this was accompanied by an increase in the height of the lateral part of the frontal process of the zygomatic bone (zfl-ztl). The distance from the inferior orbital fissure to the greater wing was decreased on the left side (iobfl-gwll).

Dimensions (Figure 3.27(g)): The dimensions were not significantly different from the experimental standard.

Discussion: The increased length of the spheno-zygomatic suture may have been due to fusion of the suture. When the suture is fused, bone growth can only occur in the direction perpendicular to that of the normal suture. In the case of fusion of the spheno-zygomatic suture the dimensions of the zygomatic bone should reflect the growth changes with reduced anterior-posterior measurements and increased vertical height. In Patient RN the bone height tended to be increased however, the AP dimensions were not significantly different from the experimental standard. This suture fusion may have only a minimal observable influence at this early stage of development.

3.4.3.6 The Vomerine Bone of Patient RN

Distances, Dimensions and Angles (Figure 3.27(h)): All distances, dimensions and angles were not significantly different from the experimental standard.

Discussion: The vomer was not significantly abnormal in this patient at this age.

Figure 3.27(g) Z Scores of the Distances and Dimensions of the Zygomatic Bone for Patient RN compared with the 6 Month Experimental Standard

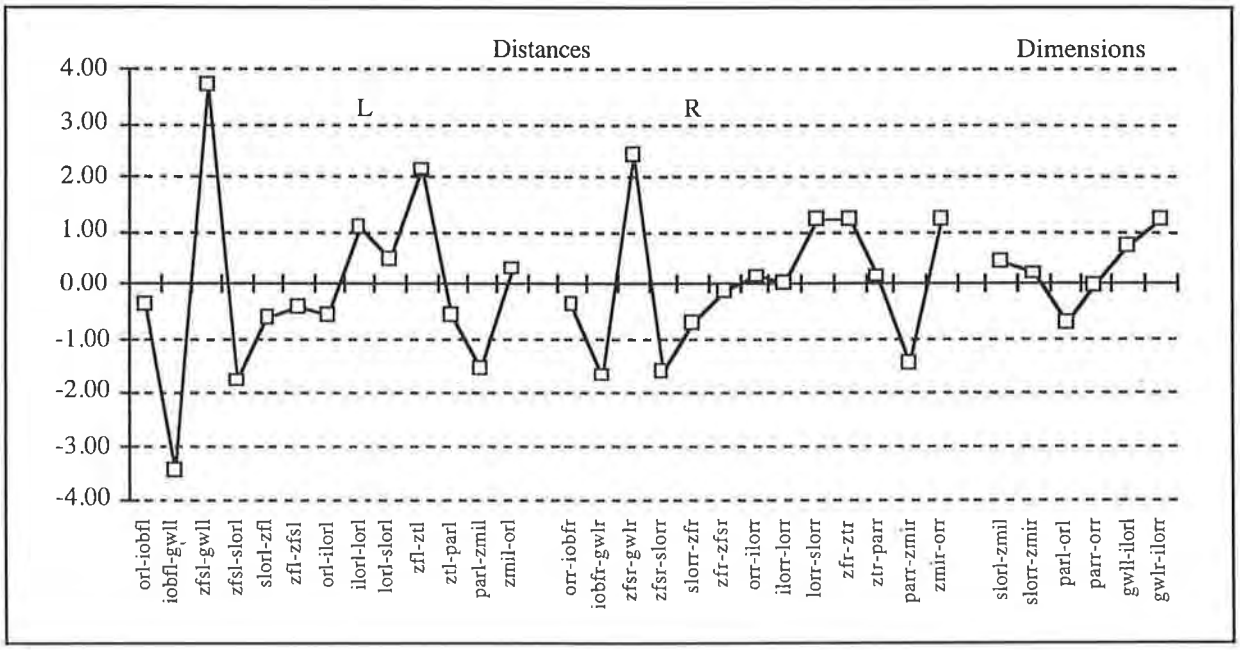

Figure 3.27(h) Z Scores of the Distances, Dimension and Angle of the Vomer for Patient RN compared with the 6 Month Experimental Standard

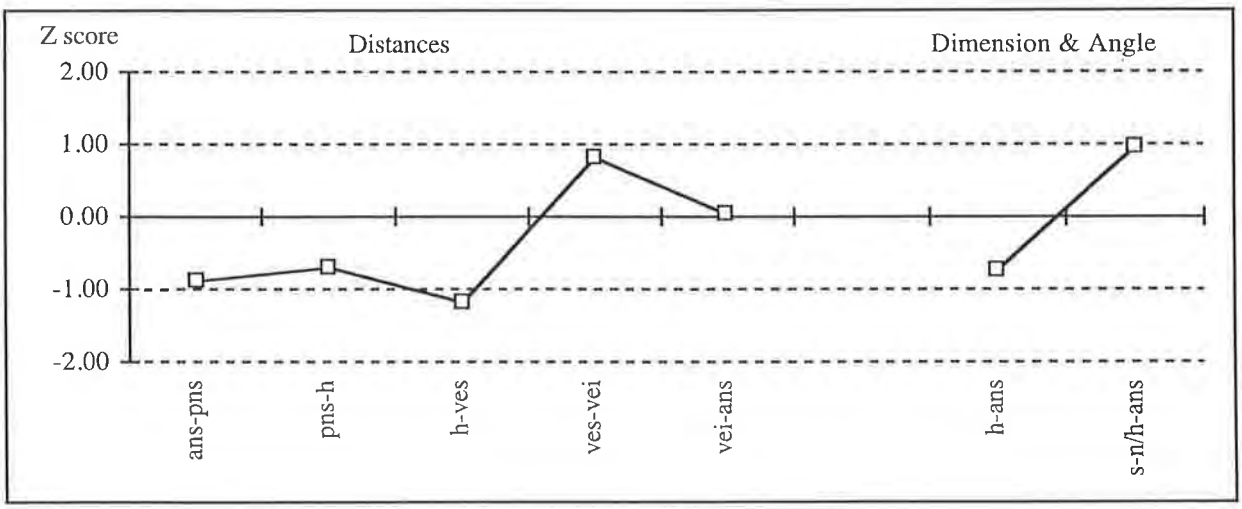

3.4.3.7 The Ethmoid Bone of Patient RN

Lateral Ethmoid Plate (Figure 3.27(i)):

Distances: The right inferior border of the lateral ethmoid plate (msr-nlir) was significantly reduced in length (see maxilla). The remainder of the lateral ethmoid plate distances, forming the medial orbital wall, were not significantly different from the experimental standard. The junction of the lateral plate with the cribriform plate, that is, its articulation with the frontal bone, showed reduced distances posteriorly (cppl-ofaml, cppr-ofamr) and a tendency for increased distances anteriorly (morl-cpal, morr-cpar) (for lateral cribriform plate distances (cpal-cppl, cpar-cppr), see cribriform plate).

Dimensions and Angles: The inter-orbital distance (morl-morr) was significantly increased. The splay of the lateral plates was not significantly different from the experimental standard.

Cribriform Plate (Figure 3.27(j)):

Distances: The lateral length of the cribriform plate (distances (cpal-cppl, cpar-cppr) was significantly increased bilaterally.

Angles: The cribriform plate angle (n-s/es-fc) was not depressed or widened.

Medial Ethmoid Plate (Figure 3.27(j)):

Distances: The medial plate was within the experimental standard range.

Dimensions: All dimensions were not significantly different from the experimental standard.

Discussion: The lateral plate was short inferiorly, while the cribriform plate was increased in length. Anteriorly, the inter-orbital distance was increased and this appeared to be a function of the increased thickness or width of the anterior fronto-ethmoid articulation (morl-cpal, morr-cpar), rather than of the cribriform plate itself. Posteriorly, this articulation was narrower producing a slight wedge shape to the ethmoid bone.

Figure 3.27(i) Z Scores of the Measurements of the Lateral Ethmoid Plate for Patient RN compared with the 6 Month Experimental Standard

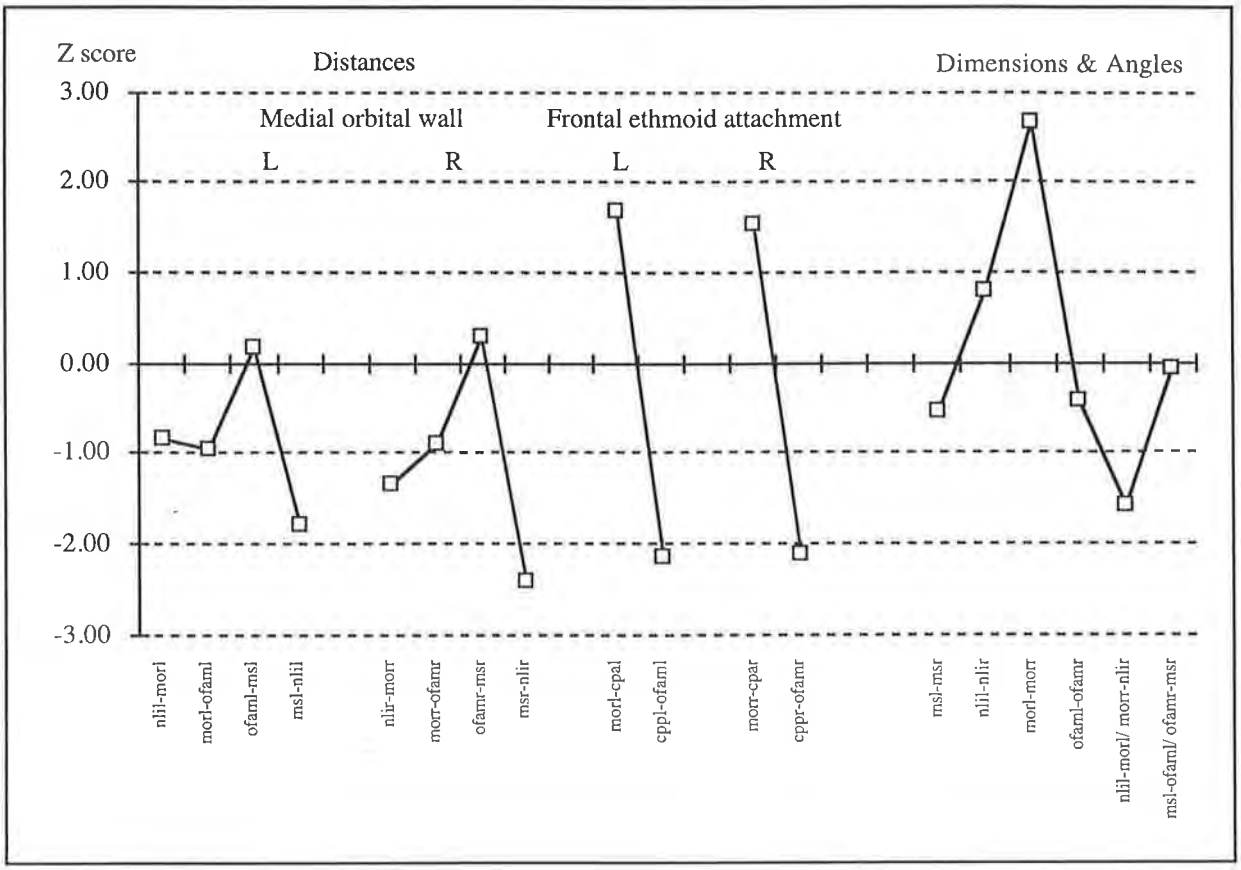

Figure 3.27(j) Z Scores of the Measurements of the Cribriform and Medial Ethmoid Plates for Patient RN compared with the 6 Month Experimental Standard

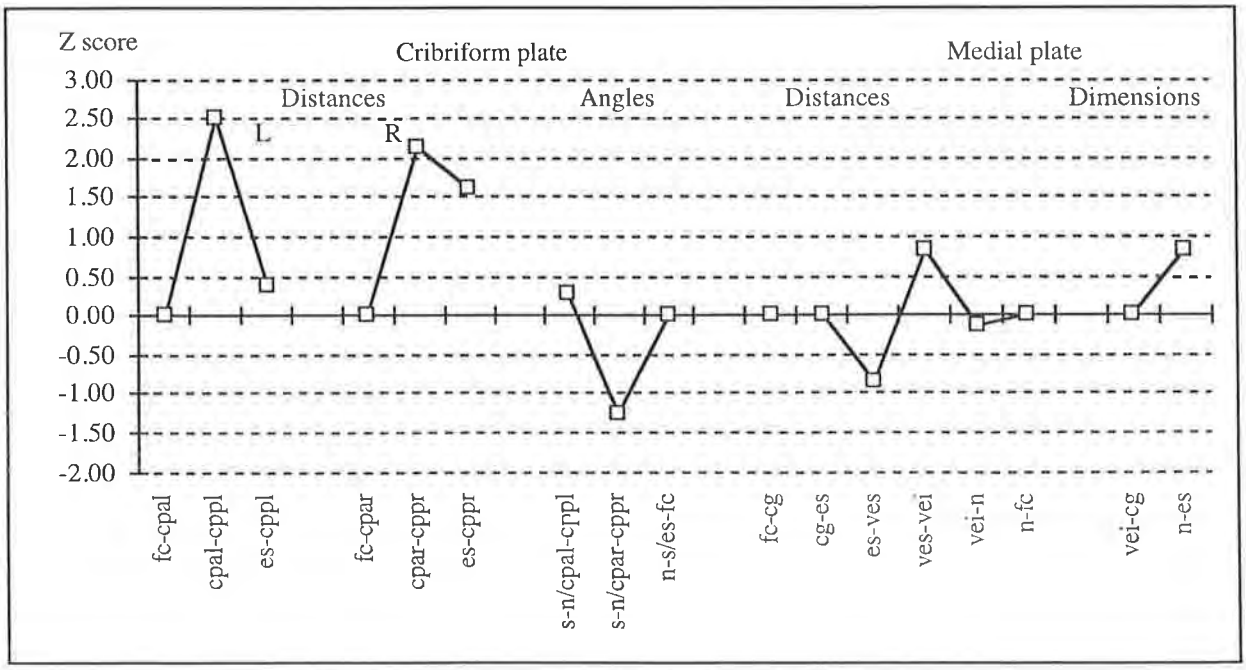

3.4.3.8 The Sphenoid Bone of Patient RN

Lesser Wing (Figure 3.27(k)):

Distances: The lesser wing measurements revealed reduced length of the wing (acl-spal, acr-spar, spal-es, spar-es).

Dimensions and Angles: The dimension between the tips of the wings (spal-spar) was reduced. The angle of the wings in the coronal plane was more acute (spal-es-spar) implying that the wings were swept up. In terms of projection from the midline (n-s/acl-spal, n-s/acr-spar), the angle of splay was more acute. This angle and the length of the sphenoid lesser wing, showed this region to be narrow and pushed forward, implying a significant growth restriction in this area.

Pterygoid Plate (Figure 3.27(k)):

Distances and Angles: The pterygoid plate in this patient was not significantly different from the experimental standard. Growth at this site follows the development of the maxilla and the arrival of the dentition. Any abnormality, therefore, would be expected to become more apparent at a later stage.

Greater Wing (Figure 3.27(l)):

Distances: The greater wing shows significant findings at the spheno-zygomatic suture (zfsl-gwll, (zfsr-gwlr) (see also zygomatic bone).

Dimensions and Angles: The greater wing dimensions and angles were within the limits of the experimental standard. The projection of the greater wing (zfsl-gwml/gwmr-zfsr) was normal. Landmarks on the squamous sphenoid bone (spt and spc) could not be identified bilaterally, due to fusion of the calvarial bone in this region and hence the distances of the lateral part of the bone could not be measured.

Figure 3.27(k) Z Scores of the Measurements of the Lesser Wing and Pterygoid Plate of the Sphenoid for Patient RN compared with the 6 Month Experimental Standard

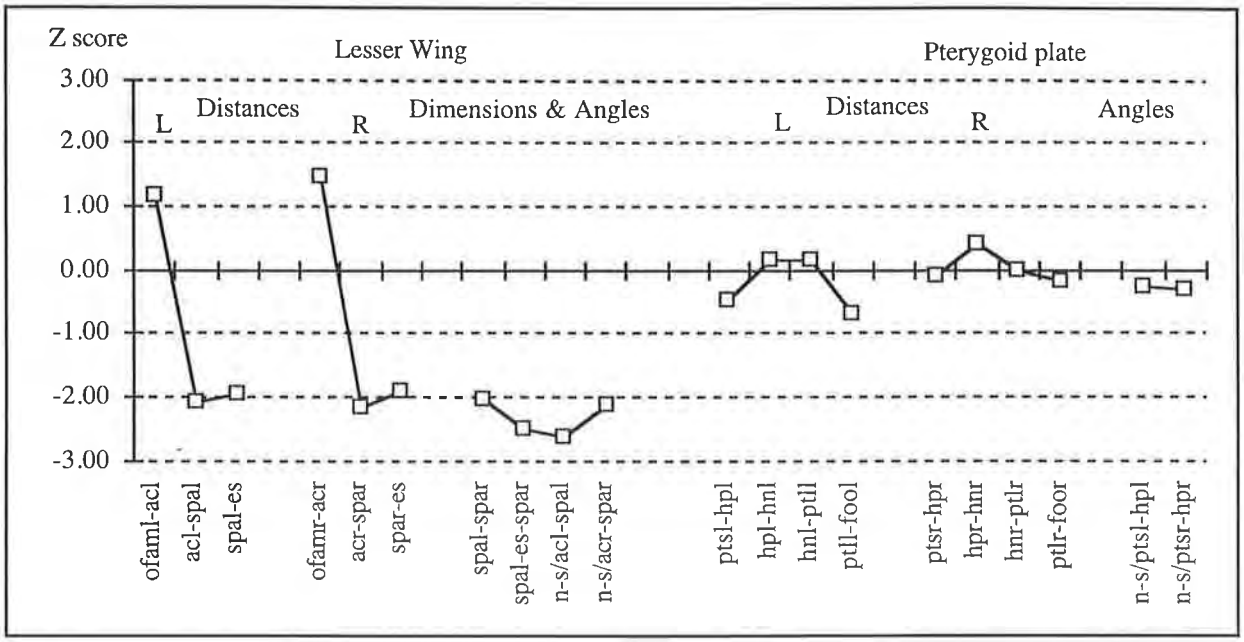

Figure 3.27(l) Z Scores of the Measurements of the Greater Wing of the Sphenoid for Patient RN compared with the 6 Month Experimental Standard

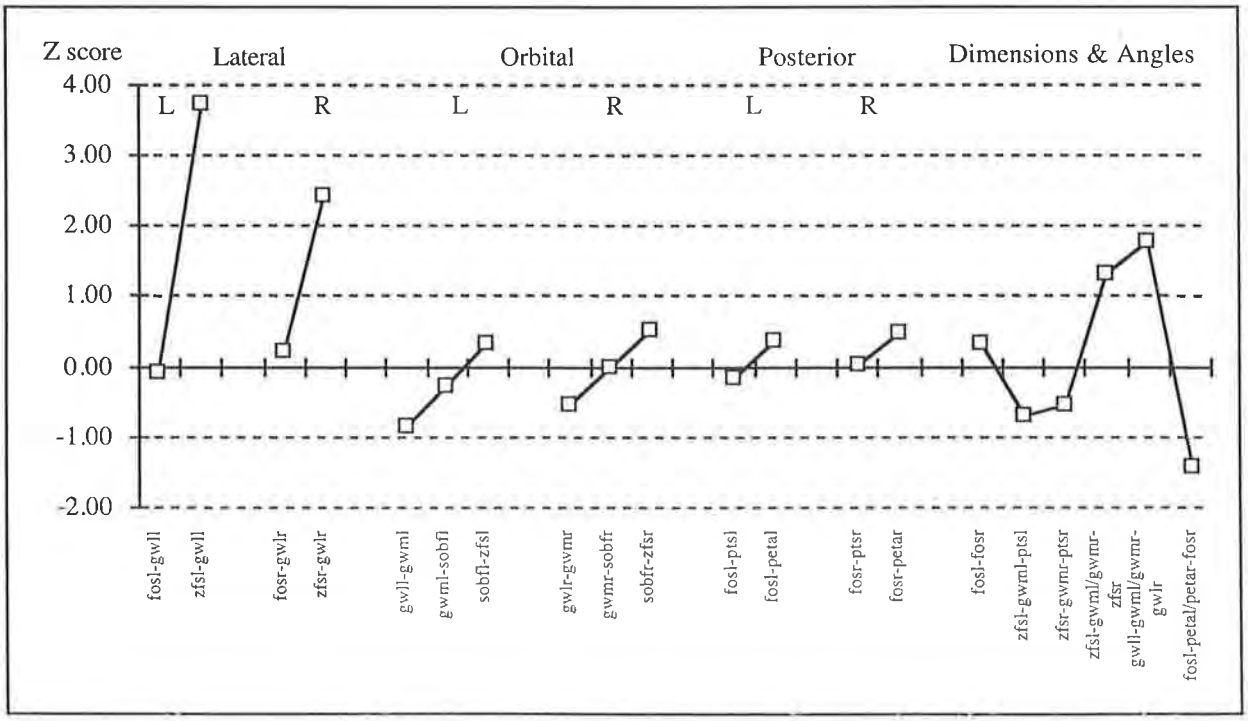

3.4.3.8 The Sphenoid Bone of Patient RN (continued):

Body of Sphenoid (Figure 3.27m):

Distances: The distances measured in the lateral/posterior sphenoid and in the sella were not significantly different from the experimental standard. Abnormalities were found anteriorly and in the base/floor of the sphenoid. Anteriorly, the greater wing mediale, optic foramen anterior mediale and the posterior cribriform plate landmarks were very close together, as seen by the reduced distances between them (cppl-ofaml, ofaml-gwml, cppr-ofamr, ofamr-gwmr). The base or floor of the body was increased in distance from the hormion to the superior part of the pterygoid plate (h-ptsl, h-ptsr) bilaterally.

Dimension and Angles: The dimension and angles of the body were not significantly different from the experimental standard.

Discussion: The sphenoid bone was different from the experimental standard in several regions. The lesser wings were greatly swept up and narrowed. The greater wing was not involved in a major way medially, but more so peripherally at the spheno-zygomatic suture. The anterior part of the body was abnormal at the region of the optic foramen where distances were reduced. This sphenoid bone in this patient appears to reflect an anterior growth restriction in the region of the fronto-sphenoid and fronto-ethmoid regions and laterally where there is fusion of the spheno-zygomatic and the squamous sphenoid bone sutures.

Figure 3.27(m) Z Scores of the Measurements of the Body of the Sphenoid for Patient RN compared with the 6 Month Experimental Standard

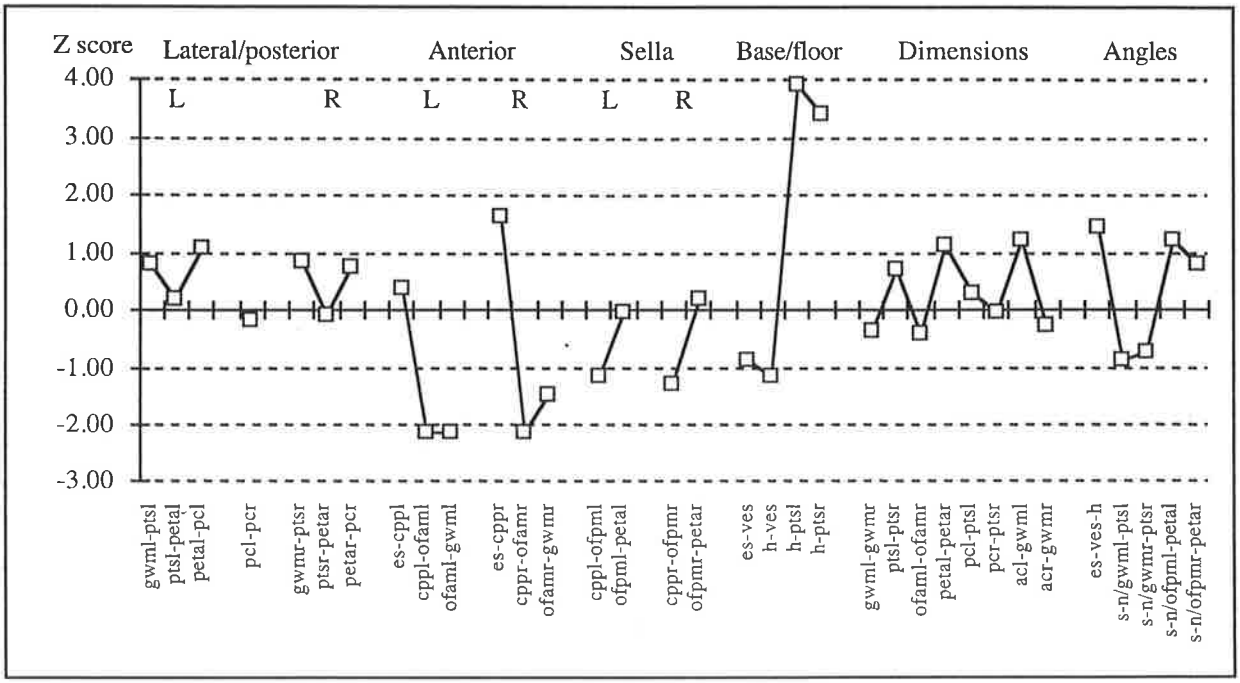

3.4.3.9 The Temporal Bone of Patient RN

Distances (Figure 3.27(n)):

Squamous Temporal Bone: The temporal squamous bone was measurable in this infant due to visibility of the asterion (as). The distances were not significantly different from the experimental standard with the exception of the distance from the asterion to the mastoidale (asr-mar) which was decreased on the right.

External Auditory Meatus: The configurations of the external auditory meati were similar bilaterally. The distance of the posterior-superior EAM rim (eampl-pol, eampr-por) was increased. The superior-anterior EAM rim was also increased on the right (por-eamar).

Zygomatic Process: The zygomatic process showed similar pattern profiles bilaterally. The length of the zygomatic arch (ztl-aul) was decreased on the left with a tendency to be decreased on the right (ztr-aur). The articular fossa to articular eminence distance (afr-aer) was increased on the right with a tendency to be increased on the left (afl-ael).

Petrous Temporal Bone (Figure 3.27(o)): The distances measured on the petrous temporal bone were not significantly different from the experimental standard.

Dimensions (Figure 3.27(o)): The dimensions of the temporal bone were also not significantly different. The angles of the zygoma projection (petal-aul-ztl, petar-aur-ztr) showed a tendency to be more obtuse than the experimental standard. The reason for this was not clear. The angle between the line of the auditory canals (pol-iaml/iamr-por) was reduced, while the angle between the petrous ridges (petpl-petal/petar-petpr) was not significantly different from the experimental standard.

Discussion: The temporal bone shows major discrepancies in the region of the external auditory meatus. The external auditory canal was distorted with the posterior point being situated laterally, producing an increased distance to this point. The angle of the auditory canal was reduced, implying that the external auditory canal may have been more posteriorly situated. This may have been related to calvarial suture involvement adjacent to this region.

Figure 3.27(n) Z Scores of the Distances of the Temporal Bone for Patient RN compared with the 6 Month Experimental Standard

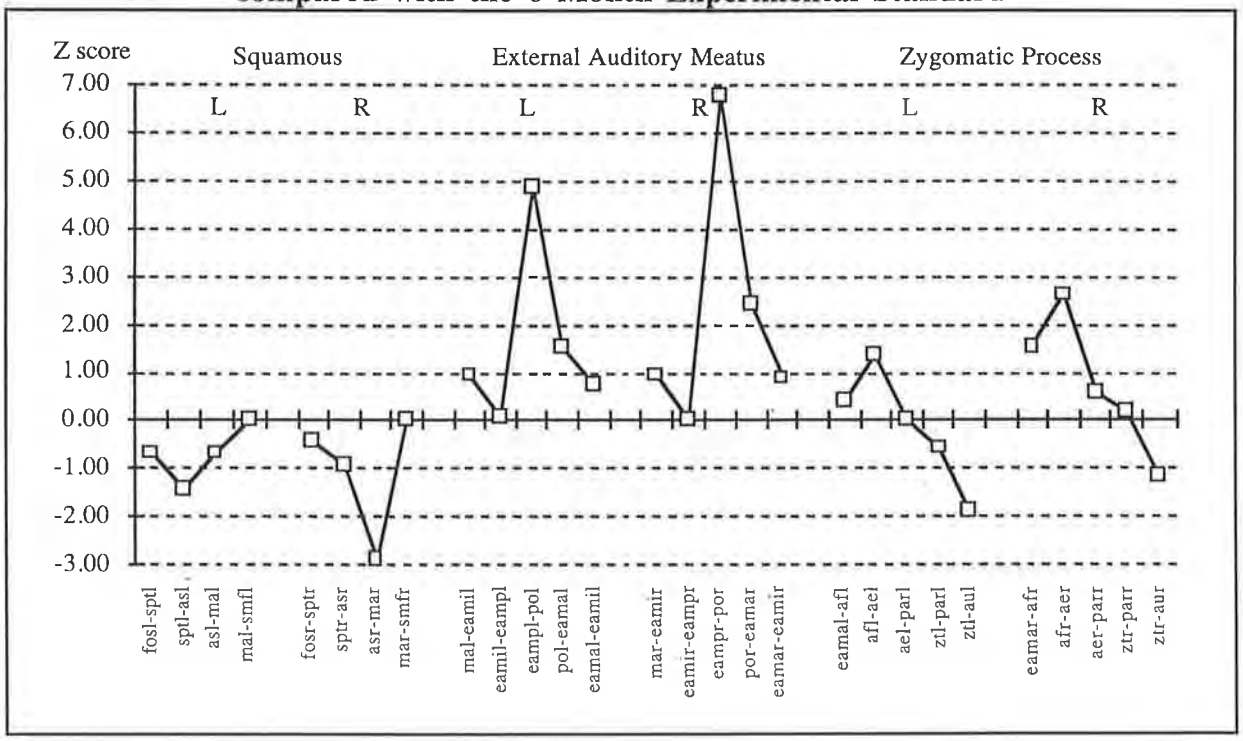

Figure 3.27(o) Z Scores of the Measurements of the Temporal Bone for Patient RN compared with the 6 Month Experimental Standard

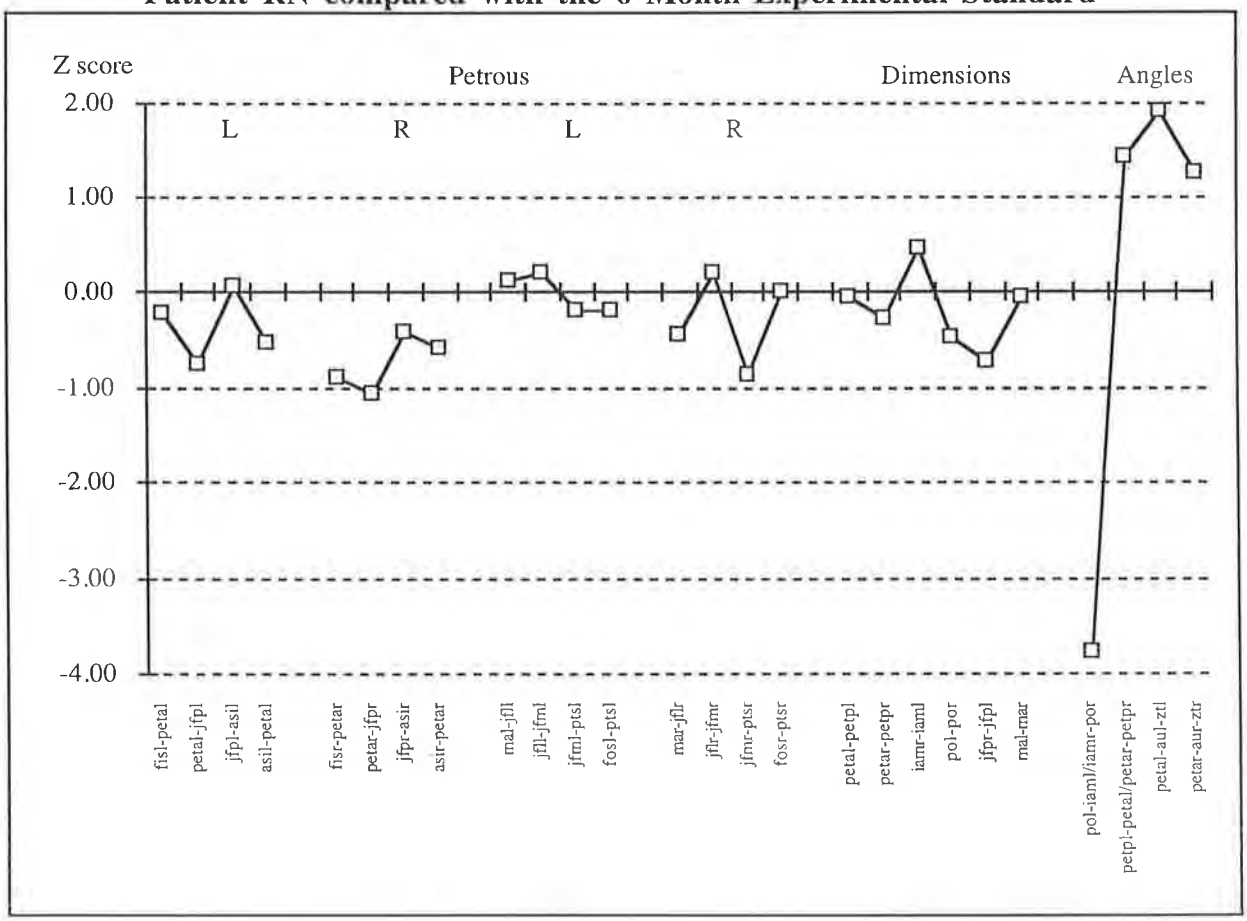

3.4.3.10 The Parietal Bone of Patient RN

Distances: A pattern profile for the parietal bone was not generated, as very few landmarks were able to be identified. The measurements recorded are reported in Appendix 2. The identification of the landmarks of the parietal bone revealed an increased distance of the spheno-parietal suture.

Discussion: The bregma could not be identified as a single landmark in this patient due to a widely patent anterior fontanelle and was not performed. Any values derived for the lengths of the coronal sutures was not considered accurate enough to report due to the curvature of the calvaria.

3.4.3.11 The Occipital Bone of Patient RN

Distances and Dimensions (Figure 3.27(p)): All distances around the occipital bone and involving the foramen magnum were not significantly different from the experimental standard. The opisthion was close to the internal occipital protuberance (o-iop) and represented a reduced posterior cranial fossa depth.

Discussion: The measurements of the occipital bone were similar to the experimental standard.

Figure 3.27(p) Z Scores of the Distances and Dimensions of the Occipital Bone for Patient RN compared with the 6 Month Experimental Standard

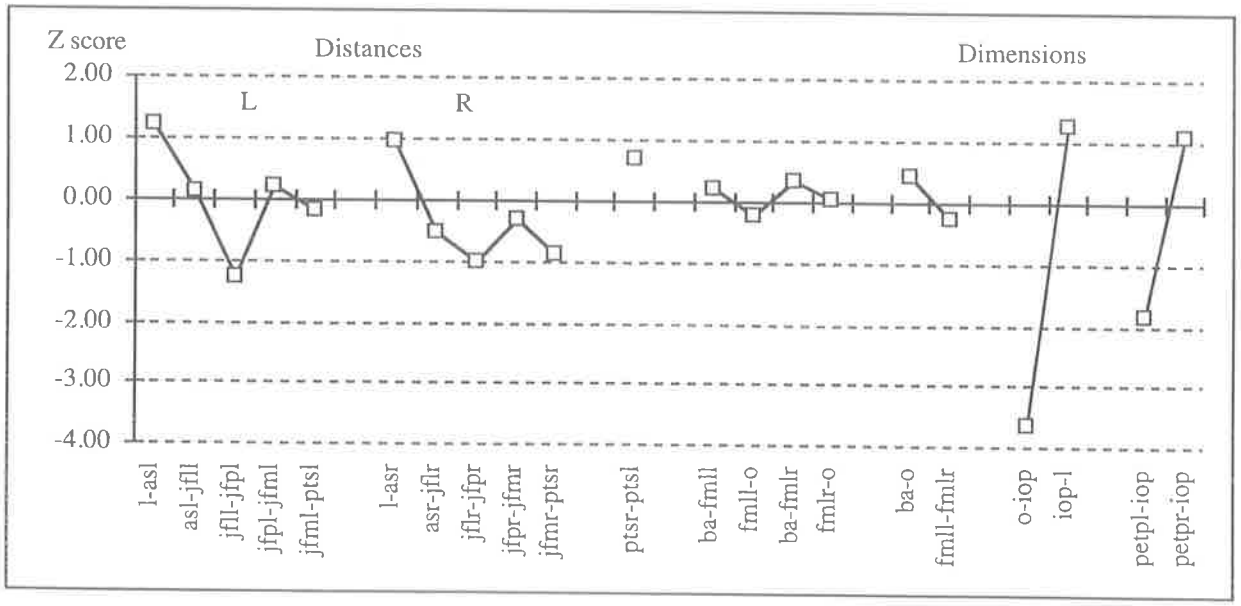

3.4.3.12 The Cranial Base Sutures of Patient RN

Anterior Cranial Fossa (Figure 3.27(q)): The sphenoid ethmoid synchondrosis (es-cppl, es-cppr) was normal. The attachment with the frontal bone (cppl-spal, cppr-spar) was shortened due to the short nature of the lesser wing. Laterally the spheno-zygomatic suture (zfsl-gwll, zfsr-gwlr) was increased in length.

Middle Cranial Fossa (Figure 3.27(q)): The distances in the middle cranial fossa were not significantly different from the experimental standard.

Posterior Cranial Fossa (Figure 3.27(q)): The posterior dimensions were not significantly different from the experimental standard.

Discussion: The majority of deformity was anteriorly and laterally. The frontal ethmoid attachment at the lateral side of the cribriform plate was presented with the lateral ethmoid plate data (Section 3.4.3.7) and is not shown here with the cranial base sutures. In this patient it showed a reduction in the distance posteriorly from the cribriform plate to the optic foramen (cpp-ofam) bilaterally. There appeared to be a relative reduction in size and presumably of growth in this anterior region in Patient RN. In contrast, lateral increased suture lengths were associated with calvarial suture fusion.

Figure 3.27(q) Z Scores of the Dimensions of the Cranial Base Sutures for Patient RN compared with the 6 Month Experimental Standard

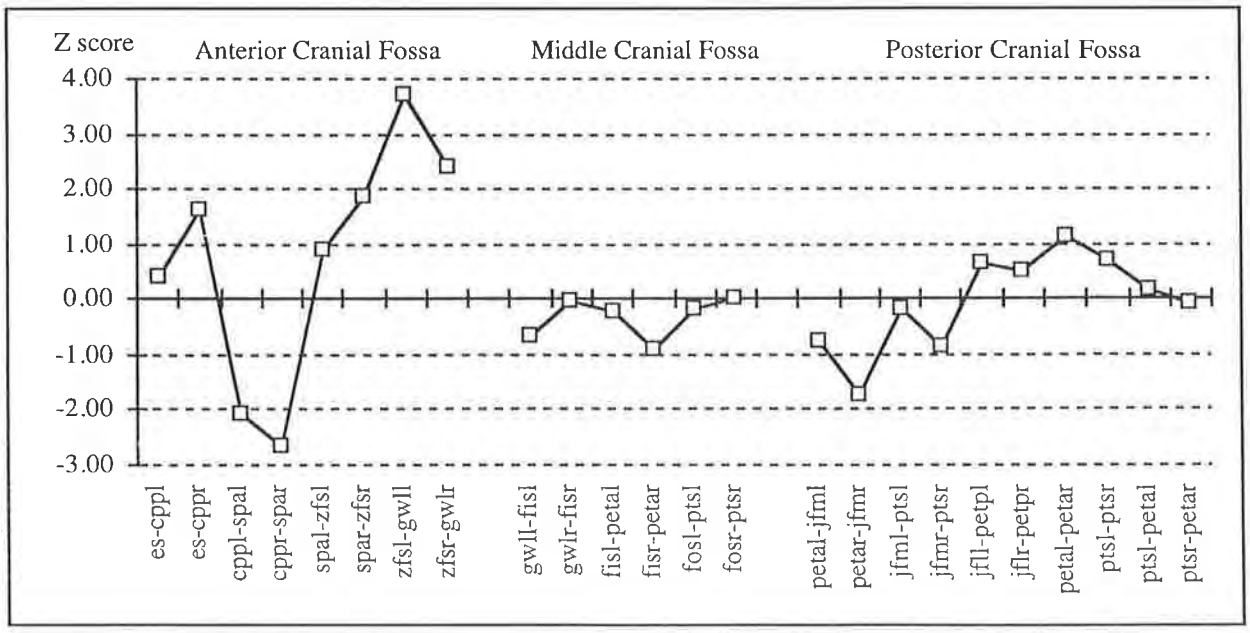

3.4.3.13 The Craniofacial Dimensions and Angles of Patient RN

Dimensions and Angles (Figure 3.27(r)): The patient's mouth was open during the CT scan making the measurements of the facial height and SNB angle (s-n-sm) invalid. The SNA angle was at the lower end of normal range. The cranial base angle (ba-s-n) was not significantly different from the experimental standard. The cranial base dimensions were also normal.

Discussion: The craniofacial dimensions for this infant were similar to the experimental standard and were related to the small size and young age of this child. The measurable pathology was located at the level of the ethmoid and greater wing of the sphenoid bone, rather than along the axis of the cranial base (ba-s-n) and did not impact on the facial heights or involve the occlusal levels.

Figure 3.27(r) Z Scores of the Craniofacial Dimensions and Angles for Patient RN compared with the 6 Month Experimental Standard

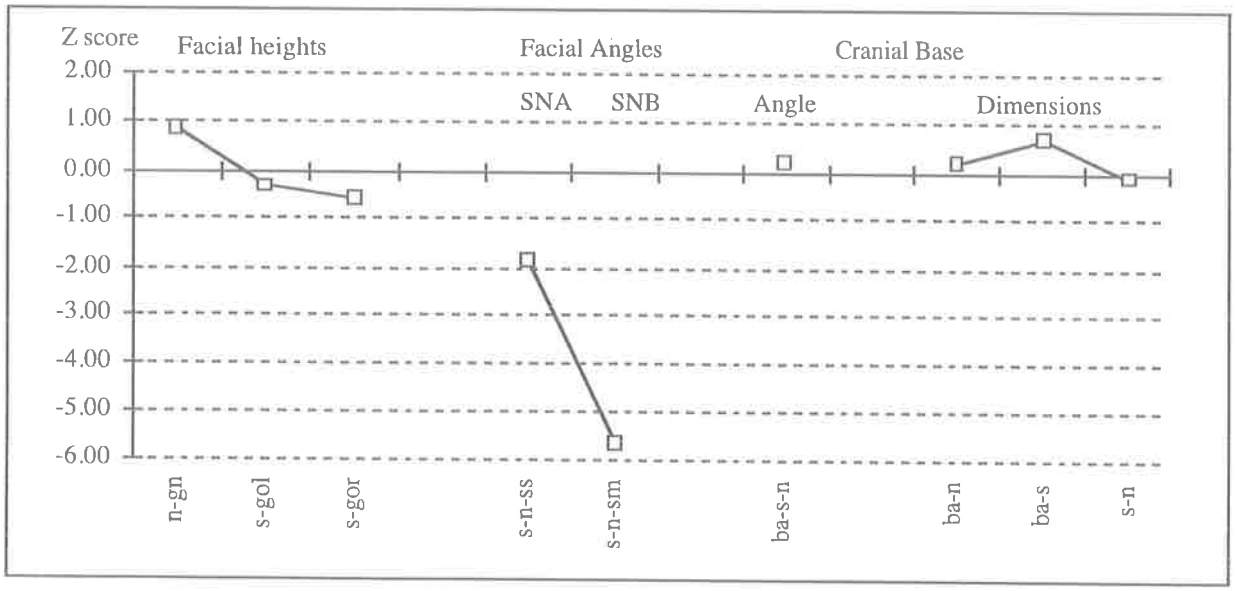

NB: Supramentale (sm) not accurate due to open mouth of patient.

3.4.4 Clinical and Radiographic Findings for Patient SH

Clinical Features

This child presented at the age of 5 months (Figure 3.2). There was no family history. The calvarial shape was brachycephalic with mild hypertelorism. The right eye was more proptosed than the left and a minor degree of orbital dystopia of the right orbit below the left was also found. The maxilla was small and the palate was high and arched. The upper airway was significantly narrowed producing arterial haemoglobin oxygen desaturation despite continuous positive airway pressure ventilation. The soft palate was split shortly after assessment with improvement in the upper airway function reported.

Lateral, Antero-Posterior and Basal Radiographs

Lateral, AP and basal views were available for review. The head shape was brachycephalic. Patency of all calvarial sutures was seen radiographically, although the coronal sutures were difficult to distinguish inferiorly. The spheno-occipital synchondrosis was patent on the lateral radiograph. The lateral view was slightly rotated and did not show the sella particularly well. There was no copper-beaten appearance of the calvaria. The AP view showed some sweeping up of the lesser wing of the sphenoid, although the orbits were not greatly involved in this process. The inter-orbital distance was not greatly increased. The development of the maxilla was consistent with the age of the patient, and the upper airway appeared obstructed with soft tissue, although this feature is difficult to reliably determine from radiographs.

3D CT Reconstruction

Calvarial bones: The calvarial bones of Patient SH showed a greater maturity of ossification than seen in Patient RN. The CT scan displayed the calvarial sutures in all areas. The metopic suture was visible as a faint line. The anterior fontanelle was widely patent, with the sutures becoming less distinct laterally and inferiorly. The skull shape was only slightly brachycephalic, The deformity appeared to be more severe at the level of the orbits, rather than at the level of the calvarial bones.

Cranial base: Ossification of the cribriform plate had occurred, and its borders were well demarcated. There was a small defect (error of exclusion) in the roof of the right orbit. The lesser wing was fused to the frontal bone. The greater wing of the sphenoid was protruding into the lateral part of the orbit. The superior orbital fissures were very short. The sella was unremarkable. The apex of the petrous temporal bones were lying in close proximity but not touching the sphenoid base. The spheno-occipital synchondrosis was not visible as being patent on the 3D CT reconstruction but was patent on plain radiograph and 2D axial CT slices. The clivus appeared steep with the suggestion of a more acute cranial base angle. The posterior part of the foramen magnum, between the condylar and squamous parts of the occipital bone, had not fused which was consistent with the age of the patient.

Orbital: The orbital aperture had a broad, squat appearance in contrast to the swept up harlequin mask appearance of the orbital aperture of Patient RN. The medial inter-orbital distance was slightly increased contributing to the mild orbital hypertelorism. Laterally the superior orbital fissure was short with anterior protrusion of the greater wing of the sphenoid into the orbit. The coronal suture extended down to the zygomatic bone giving the appearance of reduced anterior growth of the lateral orbital wall in this region. Additionally, the sutures between the temporal, squamous and zygomatic bones could not be identified. The arch of the zygoma was confluent with the squamous temporal and sphenoid bones for most of its distance.

Maxilla: The maxilla was not obviously hypoplastic. The nasal bones were relatively prominent.

3.4.5 Features of the CT Scan and 3D Reconstruction of Patient SH that made Landmark Identification difficult

Mandibular canal, mental foramen, supramentale, infra-orbital foramen, bregma and opisthocranion landmarks were not identified. No teeth were present at this age. The ectomolare points were selected at the most appropriate point on the lateral edge of the mandibular and maxillary arches. The ethmoid plate was easier to visualise on the 2D CT slices and 3D reconstructions than with the previous patient, Patient RN, due to the patient's greater maturity. The peri-orbital sutures and cranial base landmarks were identified from the regional bony contours and junctions defined in the landmarks (Figures 3.15-3.26).

3.4.6 Results and Discussion of the Quantitative Analysis of Patient SH compared with the 6 Month Experimental Standard

Figures 3.28(a)-(r)

3.4.6.1 The Mandible of Patient SH

Distances (Figure 3.28(a)): All distances were not significantly different from the experimental standard with the exception of the right anterior superior body length (id-em1ir) which was reduced.

Dimensions and Angles (Figure 3.28b): All the dimensions were not significantly different from the experimental standard. The majority of the mandibular angles were normal with the coronoid base-dental angles (ct-cb-em1i) being significantly more obtuse bilaterally.

Discussion: The mandible is essentially within normal limits with the exception of the coronoid base angles which were increased compared with the experimental. These findings confirm that mandibular deformity is not a feature of Crouzon syndrome at this early age.

Figure 3.28(a) Z Scores of the Distances of the Mandible for Patient SH compared with the 6 Month Experimental Standard

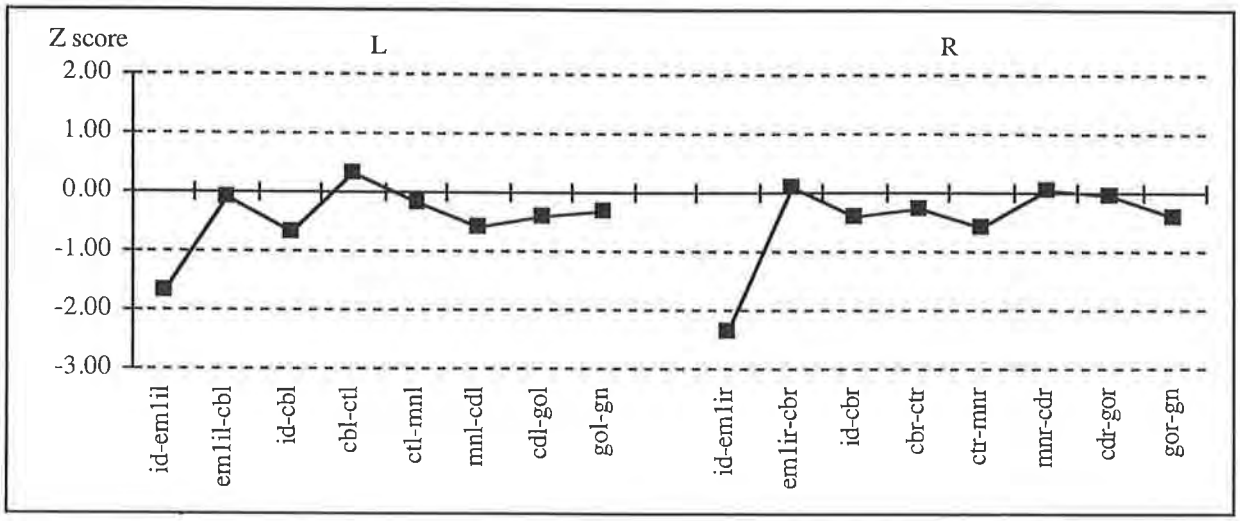

Figure 3.28(b) Z Scores of the Dimensions and Angles of the Mandible for Patient SH compared with the 6 Month Experimental Standard

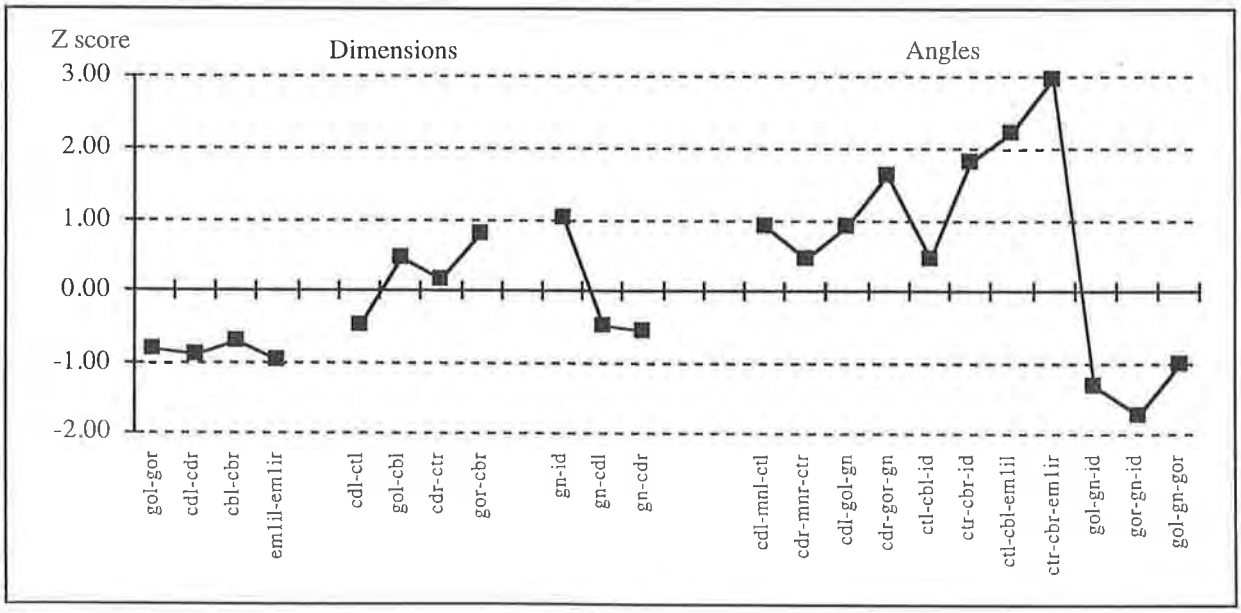

3.4.6.2 The Maxilla of Patient SH

Distances (Figure 3.28(c)): All distances of the maxilla were within the limits of the experimental standard.

Dimensions and Angles (Figure 3.28(d)): All dimensions were not significantly different from the experimental standard. Several angles, however, were increased compared with the experimental standard. The maxillary arch angle (gpfl-pr-gpfr) was increased. The superior maxillary splay (iobfl-msl/msr-iobfr), the left superior-occlusal angle (snml-msl/em1sl-pr) and the palatal-occlusal angles (ans-pns/em1s-pr) were significantly increased.

Discussion: The maxilla was quantitatively of normal size as shown by the distances and dimensions which were within the experimental standard range. Significant changes in the angles reflected an alteration in shape of the maxilla. The shape tended to be broad at the level of the maxillary occlusal arch and, superiorly, at the level of the orbital floor. The increased occlusal angles may have reflected an increase in height and width of the palatal arch in this patient at this age.

Figure 3.28(c) Z Scores of the Distances of the Maxilla for Patient SH compared with the 6 Month Experimental Standard

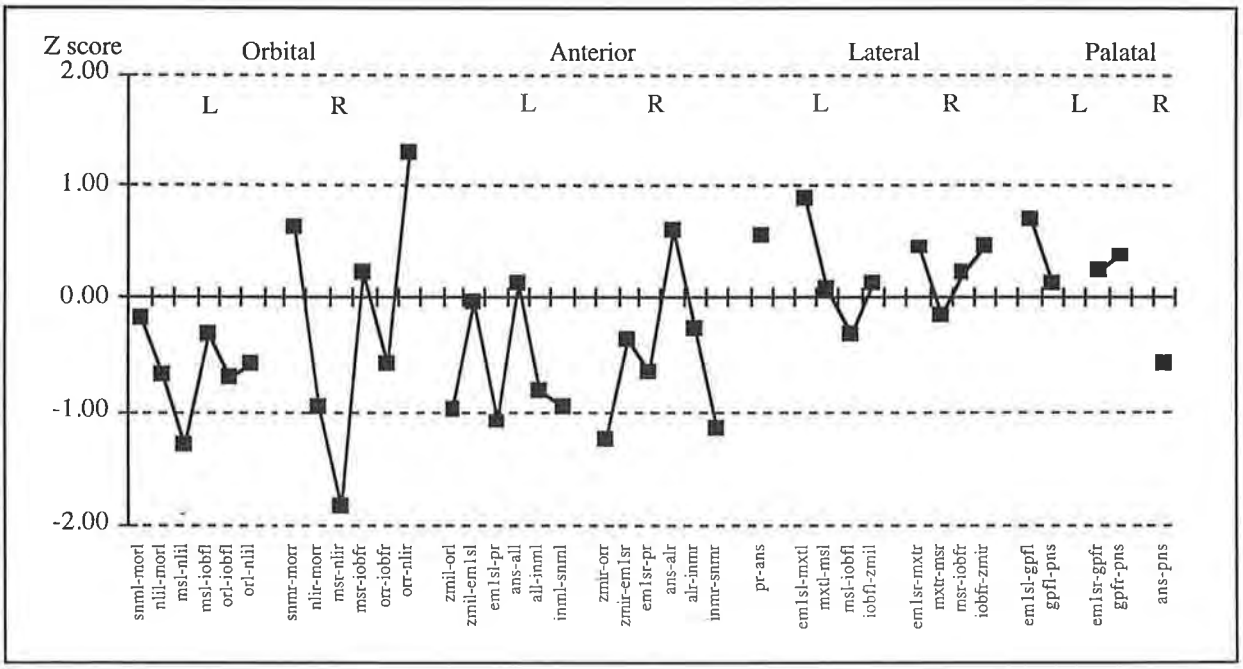

Figure 3.28(d) Z Scores of the Dimensions and Angles of the Maxilla for Patient SH compared with the 6 Month Experimental Standard

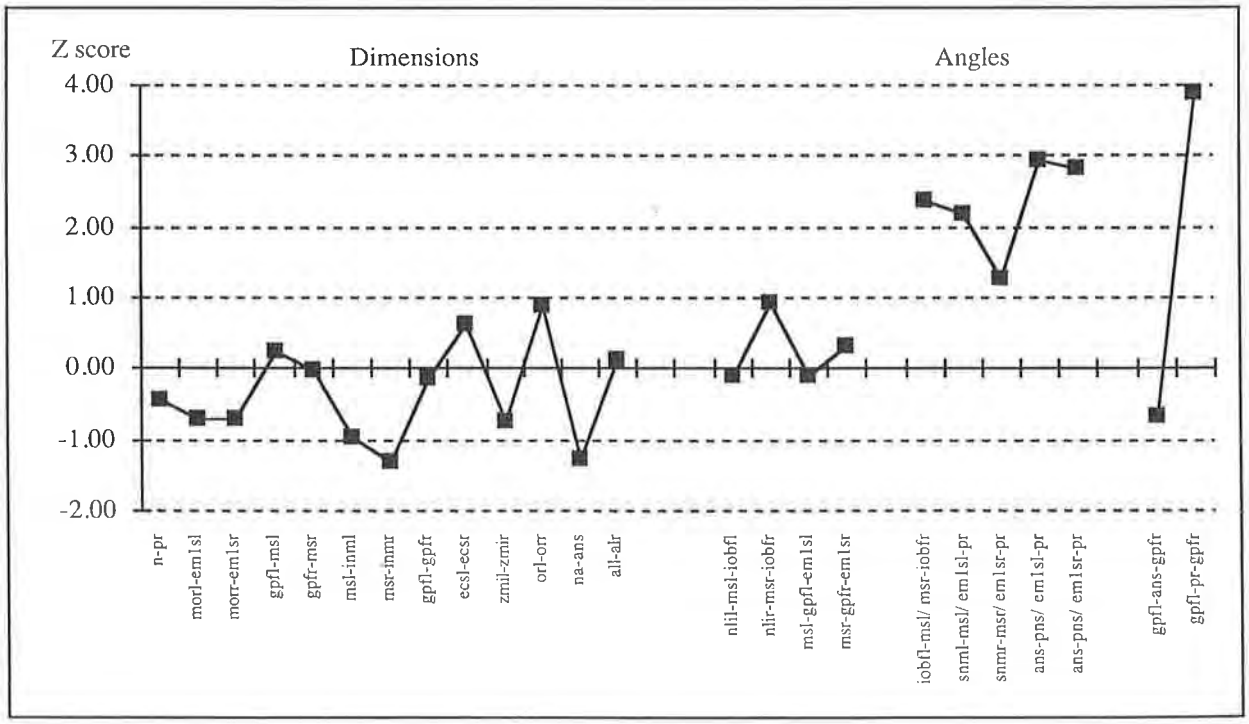

3.4.6.3 The Nasal Bones of Patient SH

Distances, Dimensions and Angles (Figure 3.28(e)): The width of the nasal bones inferiorly (na-inml, na-inmr) and superiorly at the naso-frontal suture (n-snml, n-snmr) were increased in length bilaterally while the lengths of the nasal bones were within normal limits. The total width of the nasal complex was increased inferiorly (inml-inmr) while the superior complex width was normal (snml-snmr). The nasal angles were within the experimental normal range.

Discussion: The nasal bones were mildly distorted tending to be broad, particularly at the inferior edge.

Figure 3.28(e) Z Scores of the Measurements of the Nasal Bones for Patient SH compared with the 6 Month Experimental Standard

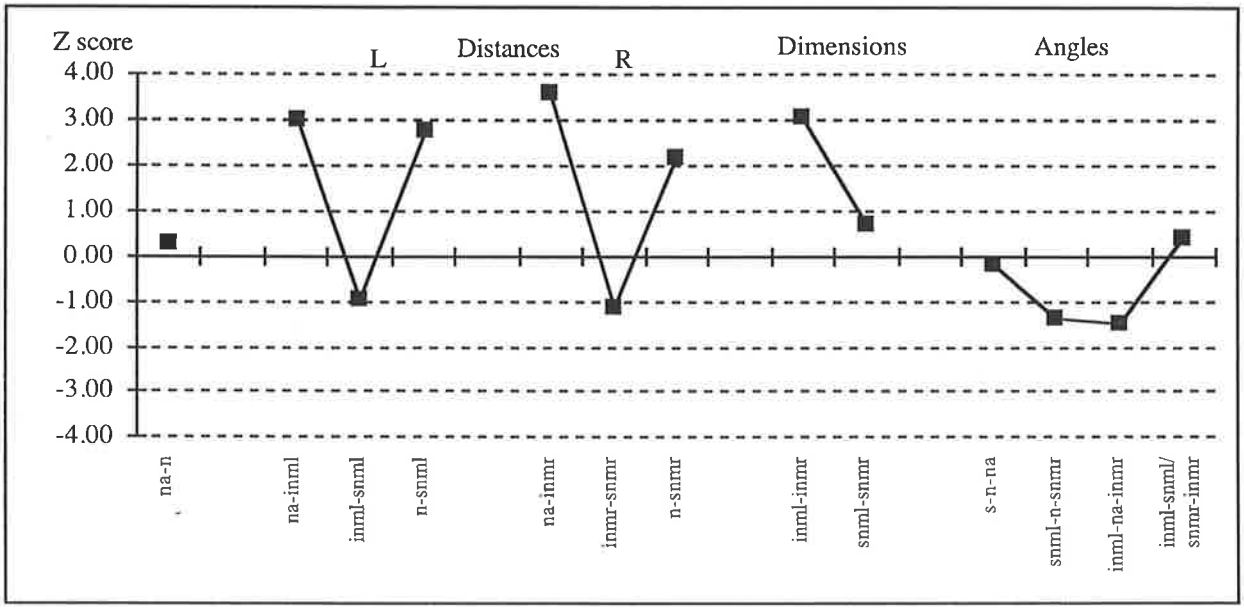

3.4.6.4 The Frontal Bone of Patient SH

Distances (Figure 3.28(f)):

Supra-orbital Region: The superior naso-frontal suture (n-snml, n-snmr) and the fronto-zygomatic suture (slorl-zfl, slorr-zfr) were increased in length bilaterally compared with the experimental standard (see also nasal and zygomatic bones). The right superior medial aspect of the orbital rim (morr-sorr) was decreased in distance and was asymmetrical from the left hand side.

Ethmoid Attachment: The fronto-ethmoid attachment was not significantly different from the experimental standard.

Sphenoid Attachment: The superior orbital fissure (ofaml-sobfl, ofamr-sobfr) was reduced in length compared with the experimental standard. A compensatory increase in length of the fronto-sphenoid suture (sobfl-zfsl, sobfr-zfsr) lateral to the superior orbital fissure was recorded. The lateral sphenoid distances were not significantly different from the experimental standard. The parietal attachment (spc-br) and sphenoid attachments (zfs-spc and spc-spa) were not recordable due to the fusion of sutures and hence poor visibility of landmarks in this region.

Dimensions (Figure 3.28(f)): The dimensions of the frontal bone were not significantly different from the experimental standard.

Discussion: This patient exhibited a less severe deformity of the frontal bone than the previous patient (Patient RN). The deformity was again found predominantly in the anterior and lateral regions of the bone. This was demonstrated by the lengthening of the fronto-zygomatic suture bilaterally and the lengthening of the orbital component of the spheno-frontal suture (sobfl-zfsl). The lateral lengthening was contrasted by the narrowing and decreased lateral extension of the superior orbital fissure. The junction of the frontal bone with the ethmoid bone was relatively spared in this individual. The pattern found in the frontal bone was consistent with involvement of cranial base sutures as a continuation of the calvarial suture fusion (or vice versa).

Figure 3.28(f) Z Scores of the Distances and Dimensions of the Frontal Bone for Patient SH compared with the 6 Month Experimental Standard

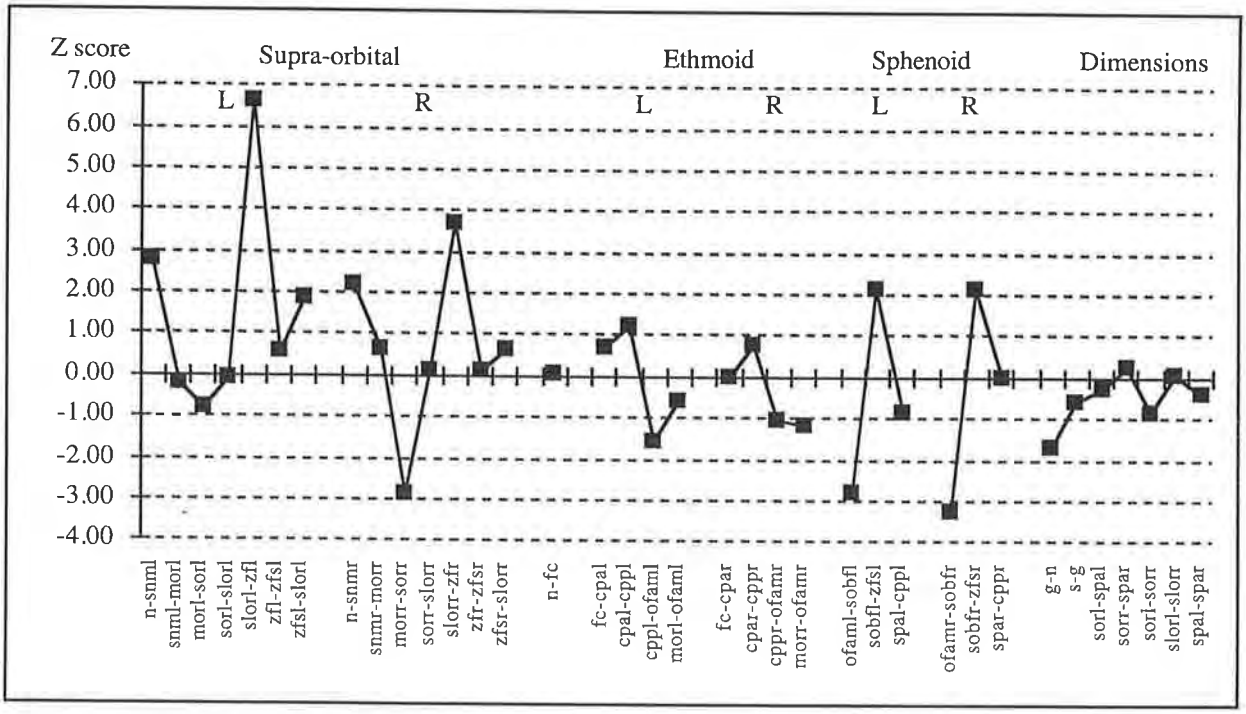

3.4.6.5 The Zygomatic Bone of Patient SH

Distances (Figure 3.28(g)): The majority of distances measured were within the limits of the experimental standard. The length of the fronto-zygomatic suture (slorl-zfl, slorr-zfr) was increased bilaterally (see also frontal bone). The spheno-zygomatic suture (zfsl-gwll, zfsr-gwlr) was not significantly different from the experimental standard. The distance from the inferior orbital fissure to the lateral tip of the greater wing (iobfl-gwll) was decreased on the left side. The inferior lateral margin of the orbit to the lateral orbital point (ilorl-lorl, ilorr-lorr) was reduced bilaterally.

Dimensions (Figure 3.28(g)): The dimensions were not significantly different from the experimental standard.

Discussion: The increased length of the fronto-zygomatic suture may be the result of sutural growth arrest, causing a compensatory increased growth in the direction perpendicular to the normal growth of the suture. The effect of the growth disturbance would be a decreased height of the zygomatic bone and in this patient a decreased height of the inferior anterior orbital rim was found bilaterally. The overall effect of suture involvement on the size of the orbital structure was not great as the majority of the dimensions of the zygomatic bone were not significantly different from the experimental standard.

3.4.6.6 The Vomerine Bone of Patient SH

Distances, Dimensions and Angles (Figure 3.28(h)): All distances, dimensions and angles were not significantly different from the experimental standard.

Discussion: The vomer was within the experimental standard range in this patient at this age.

Figure 3.28(g) Z Scores of the Distances and Dimensions of the Zygomatic Bone for Patient SH compared with the 6 Month Experimental Standard

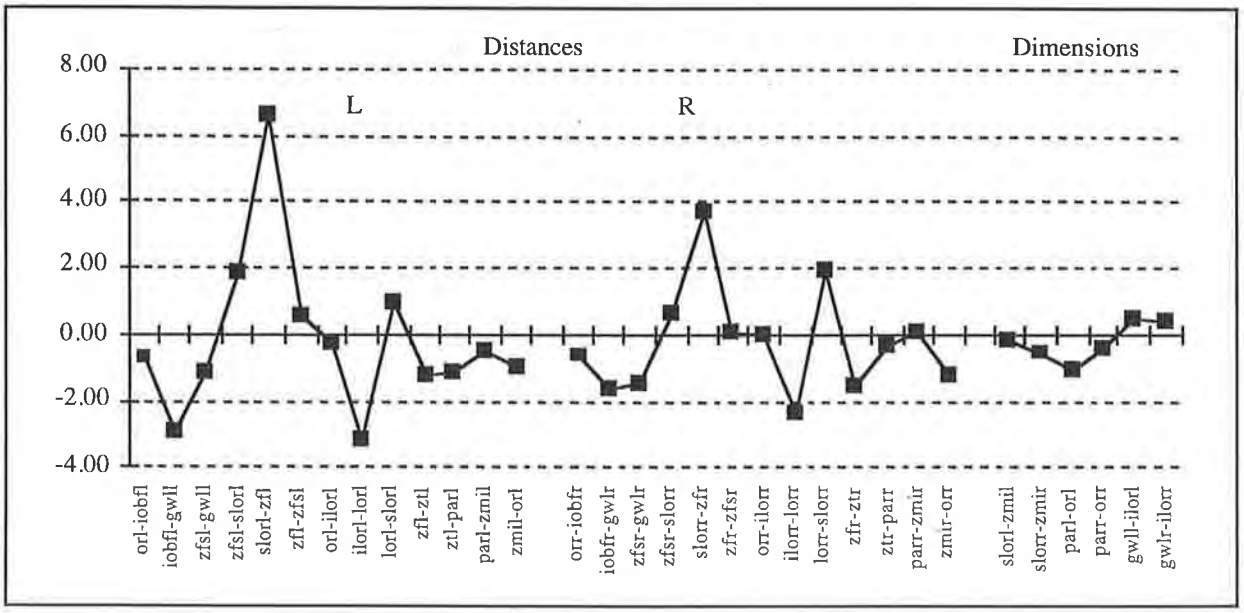

Figure 3.28(h) Z Scores of the Measurements of the Vomer for Patient SH compared with the 6 Month Experimental Standard

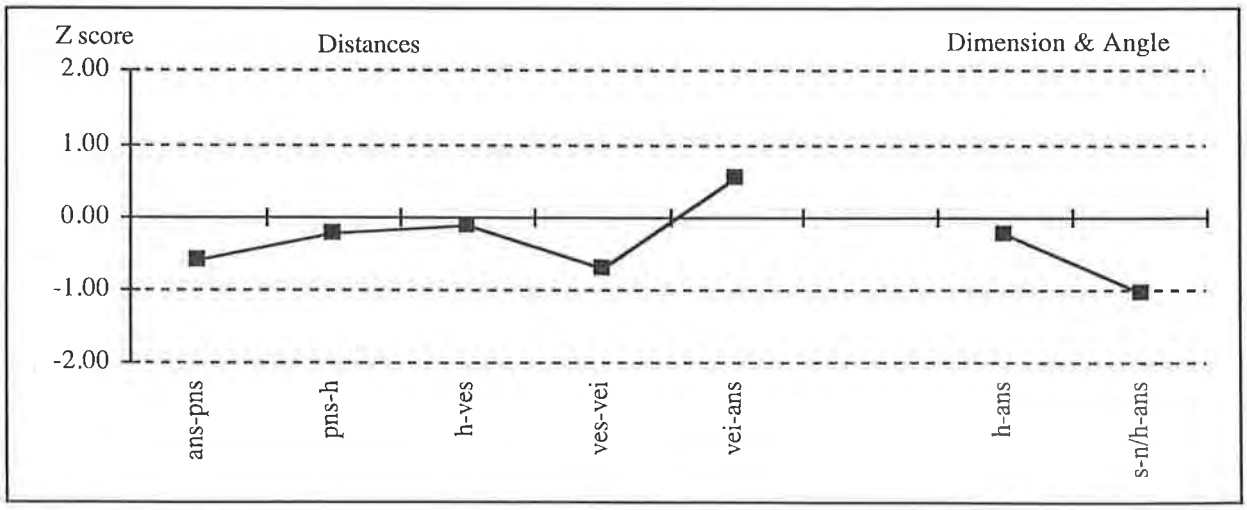

3.4.6.7 The Ethmoid Bone of Patient SH

Lateral Ethmoid Plate (Figure 3.28(i)):

Distances: The lateral ethmoid plate distances, forming the medial orbital wall, were not significantly different from the experimental standard. The junction of the lateral plate with the cribriform plate (that is, the fronto-ethmoid articulation), showed an increased width anteriorly (morl-cpal, morr-cpar) and normal distances posteriorly (cppl-ofaml, cppr-ofamr). The length of the medial part of the fronto-ethmoid articulation corresponds with the lateral length of the cribriform plate (cpal-cppl, cpar-cppr) and is recorded below.

Dimensions and Angles: The inter-orbital distances and the splay of the lateral plates was not significantly different from the experimental standard.

Cribriform Plate (Figure 3.28(j)):

Distances: The length and width of the cribriform plate were not significantly different from the experimental standard.

Angles: The cribriform plate angles were not significantly different from the experimental standard.

Medial Ethmoid Plate (Figure 3.28(j)):

Distances: The distances measured on the medial plate were not significantly different from the experimental standard.

Dimensions: All dimensions were not significantly different from the experimental standard.

Discussion: The lateral plate, the cribriform plate and the medial plate were normal. Anteriorly, the inter-orbital distance was normal. The anterior frontal ethmoid articulation (morl-cpal, morr-cpar) was increased in width. This appeared to be increased in a vertical direction, not greatly influencing the inter-orbital distance. Posteriorly this articulation was normal. The resultant shape of the ethmoid bone was wedge shaped, being broad and inferior anteriorly and narrower and slightly higher posteriorly. The appearance of the ethmoid bone was similar in nature to but less severe than that seen in Patient RN.

Figure 3.28(i) Z Scores of the Measurements of the Lateral Ethmoid Plate for Patient SH compared with the 6 Month Experimental Standard

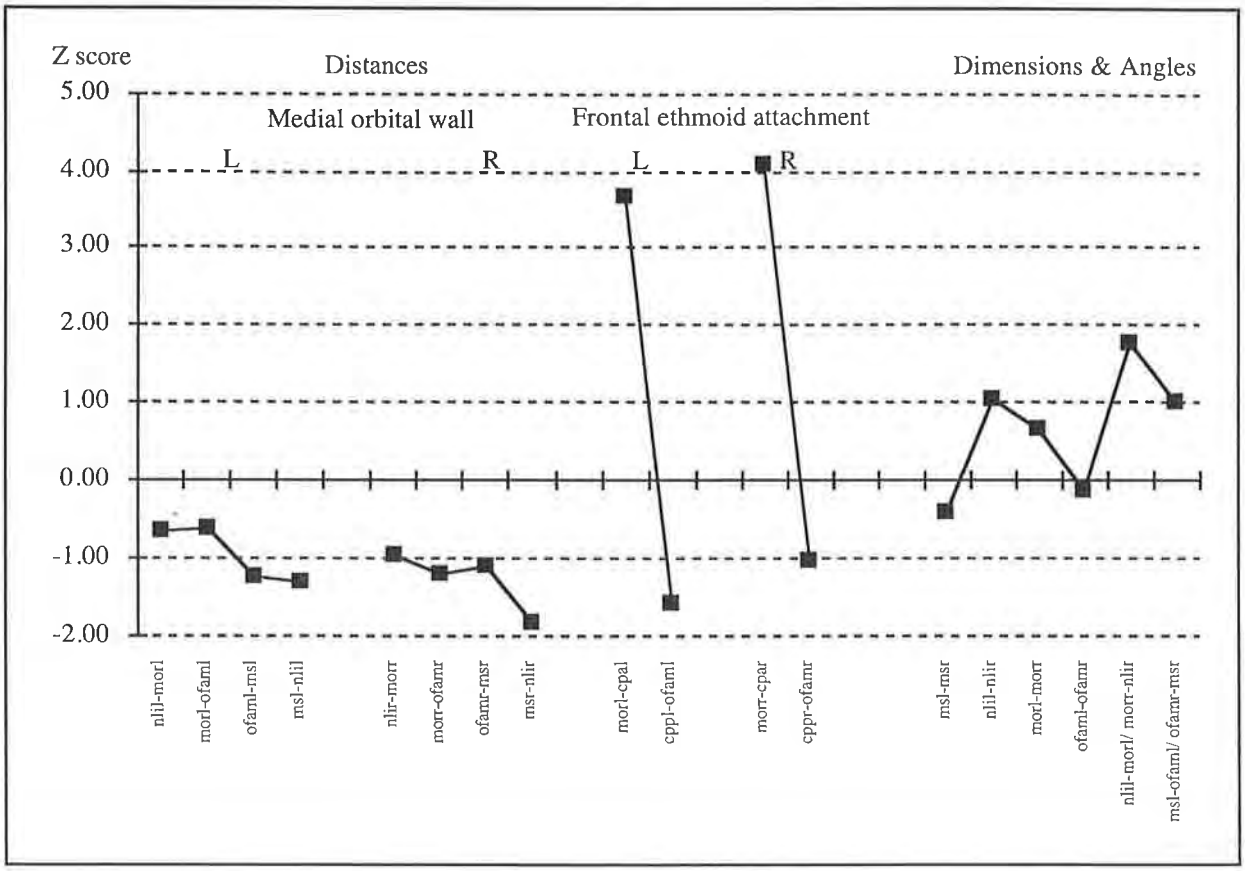

Figure 3.28(j) Z Scores of the Measurements of the Cribriform and Medial Ethmoid Plates for Patient SH compared with the 6 Month Experimental Standard

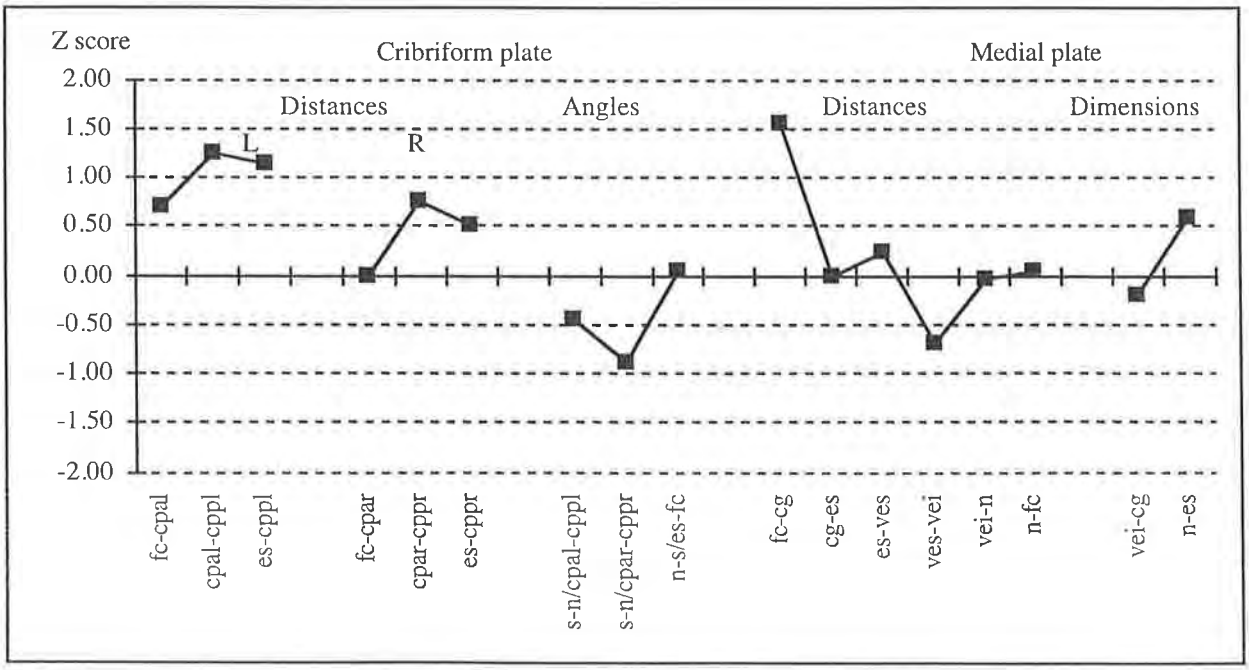

3.4.6.8 The Sphenoid Bone of Patient SH

Lesser Wing (Figure 3.28(k)):

Distances: The length of the lesser wings (acl-spal, acr-spar, spal-es, spar-es) were within the limits of the experimental standard. The distance from the optic foramen to the anterior clinoid (ofamr-acr) was increased on the right with a similar trend seen on the left side (ofaml-acl).

Dimensions and Angles: The dimension between the tips of the wings (spal-spar) were within the limits of the experimental standard. The angle of the wings in the coronal plane (spal-es-spar) and the angle of splay from the midline (n-s/acl-spal, n-s/acr-spar) were also not significantly different from the experimental standard.

Pterygoid Plate (Figure 3.28(k)):

Distances and Angles: The pterygoid plate in this patient was not significantly different from the experimental standard.

Greater Wing (Figure 3.28(l)):

Distances: Significantly increased measurements of the greater wing were identified at the spheno-frontal suture (sobfl-zfsl, sobfr-zfsr). This increase in length was found in conjunction with a decreased length of the superior orbital fissure (gwml-sobfl, gwmr-sobfr) (see frontal bone). The spheno-zygomatic suture was not significantly different from the experimental standard and has been reported previously (see zygomatic bone). Landmarks on the squamous sphenoid bone (spt and spc) could not be identified bilaterally, due to fusion of the calvarial bone in this region and hence the distances of the lateral part of the bone could not be measured.

Dimensions and Angles: The total angle of projection of the greater wing (zfsl-gwml/gwmr-zfsr) and the inferior greater wing protrusion (gwll-gwml/gwmr-gwlr) were increased. The more obtuse angles between the greater wings resulted from greater wings which were positioned more laterally than anteriorly.

Figure 3.28(k) Z Scores of the Measurements of the Lesser Wing and Pterygoid Plate of the Sphenoid for Patient SH compared with the 6 Month Experimental Standard

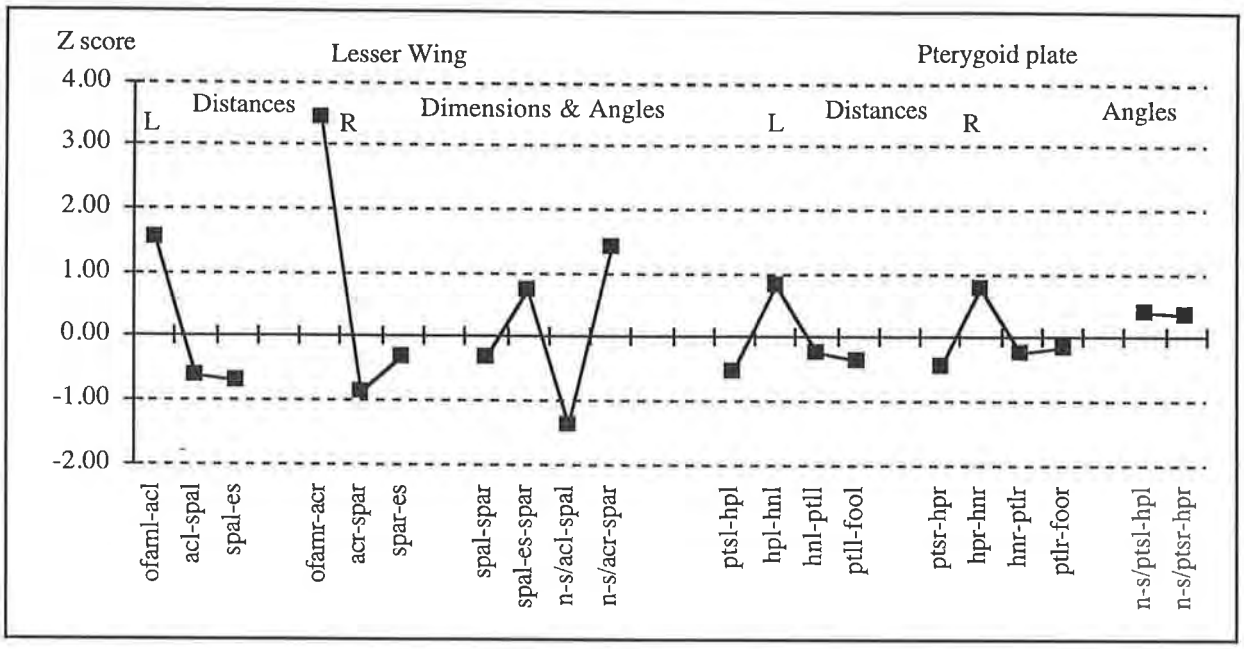

Figure 3.28(l) Z Scores of the Measurements of the Greater Wing of the Sphenoid for Patient SH compared with the 6 Month Experimental Standard

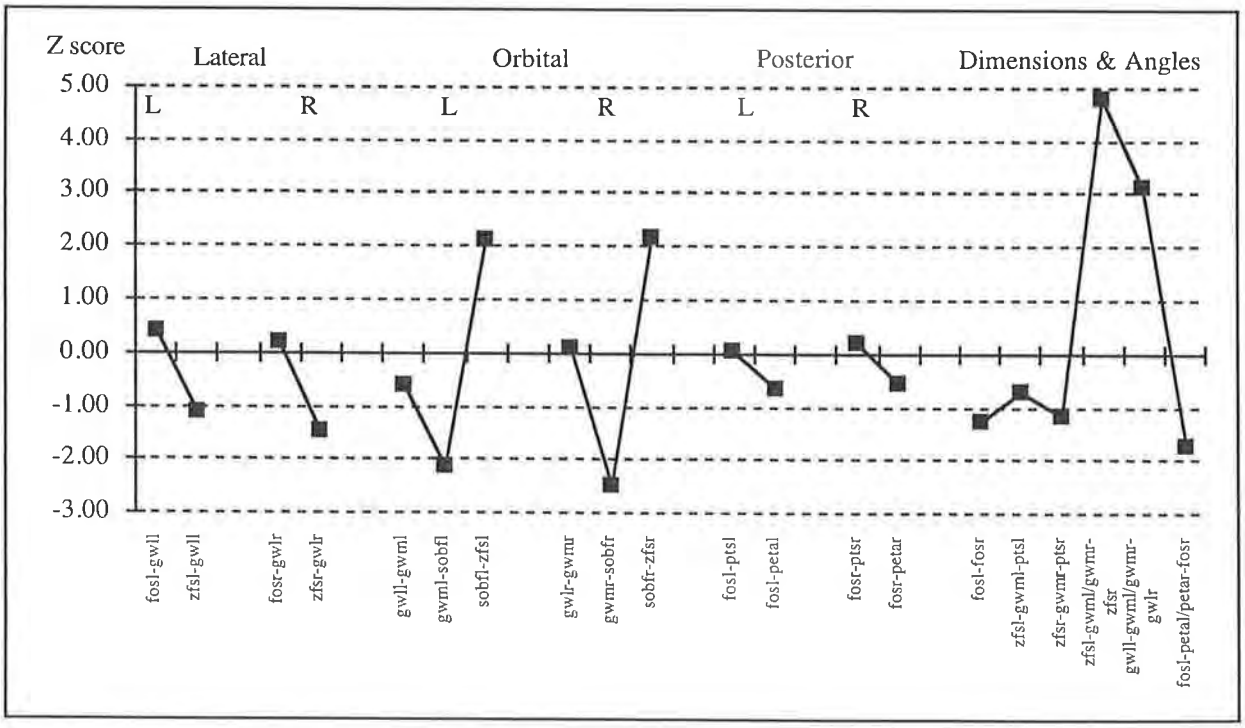

3.4.6.8 The Sphenoid Bone of Patient SH (continued)

Body of Sphenoid (Figure 3.28(m)):

Distances: The lateral body distances were not significantly different from the experimental standard however posteriorly the inter-posterior clinoid distance (pcl-pcr) was increased. Anteriorly, the measurements from the greater wing mediale, optic foramen anterior mediale and the posterior cribriform plate landmarks were not significantly different from the experimental standard. The sella was also normal. The base or floor of the body was decreased in distance from the hormion to the superior part of the pterygoid plate (h-ptsl, h-ptsr) bilaterally.

Dimensions and Angles: The dimensions of the body were not significantly different from the experimental standard with the inferior spheno-occipital synchondrosis (ptsl-ptsr) tending to be reduced. The anterior height of the body (acr-gwmr) was significantly increased. The angles were not significantly different from the experimental standard.

Discussion: This patient presented with a mild calvarial deformity but a more prominent orbital deformity. The predominant sphenoid abnormality was seen at the greater wings of the sphenoid, which were protruded laterally rather than anteriorly. The spheno-ethmoid synchondrosis was normal (see ethmoid bone), and many distances in the region of the cribriform plate and optic foramen were normal. The orbital proptosis appeared to have resulted from the sphenoid greater wing abnormality rather than from the ethmoid bone.

Figure 3.28(m) Z Scores of the Measurements of the Body of the Sphenoid for Patient SH compared with the 6 Month Experimental Standard

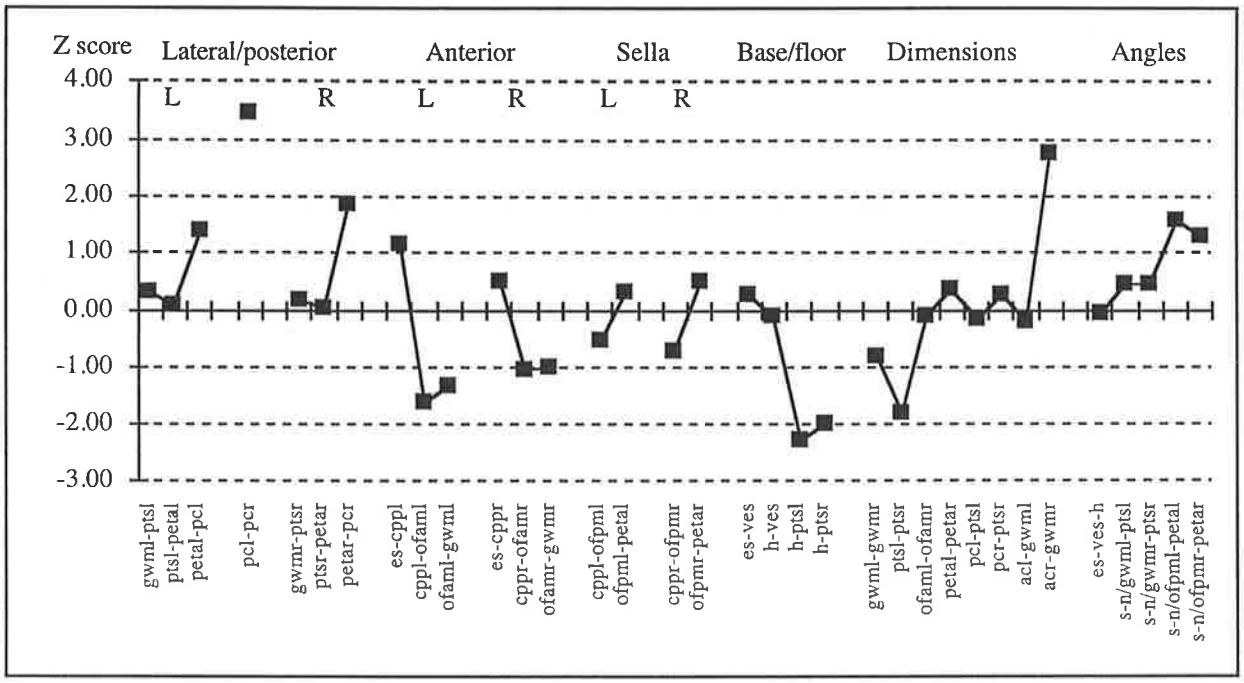

3.4.6.9 The Temporal Bone of Patient SH

Distances (Figure 3.28(n)):

Squamous Temporal Bone: The squamous temporal bone was measurable in this infant due to visibility of the asterion (as) and sphenion (spt). The distances were not significantly different from the experimental standard.

External Auditory Meatus: The configuration of the external auditory meatus was similar bilaterally, and similar to the previous patient (Patient RN). The superior-posterior EAM rim distance (porion to the posterior external auditory meatus) was increased.

Zygomatic Process: The zygoma showed similar pattern profiles, also with a tendency for the length of the zygomatic arch (ztl-aul, ztr-aur) to be decreased bilaterally. The articular fossa and articular eminence were not significantly different from the experimental standard.

Petrous Temporal Bone (Figure 3.28(o)): The petrous temporal bone was not significantly different from the experimental standard with the exception of the superior spheno-petrous temporal suture (fisl-petal, fisr-petar) which was decreased on the right with a tendency to be decreased on the left.

Dimensions and Angles (Figure 3.28(o)): The dimensions of the temporal bone were normal. The angles of the zygoma projection were more obtuse (petal-aul-ztl, petar-aur-ztr). This was consistent with the broadening of the middle cranial fossa and lateral protrusion of the greater wing of the sphenoid and the corresponding placement of the root of the zygomatic process (aul, aur). The angle of the auditory canal (pol-iaml/iamr-por) and the petrous temporal bone (petal-petpl/petar-petpr) were normal.

Discussion: The majority of the temporal bone was not significantly different from the experimental standard with distortion occurring at the external auditory meatus (similar to Patient RN). Greater abnormality occurred in the region of the zygomatic process which showed a tendency to be decreased in length with a more obtuse angle from the apex of the petrous bone. Fusion of the spheno-frontal sutures would inhibit the anterior growth of the zygomatic process and might have produced some distortion in the region of the external auditory canal. The angle of the auditory canal had not been altered, implying that the effect may have been more limited posteriorly than anteriorly.

Figure 3.28(n) Z Scores of the Distances of the Temporal Bone for Patient SH compared with the 6 Month Experimental Standard

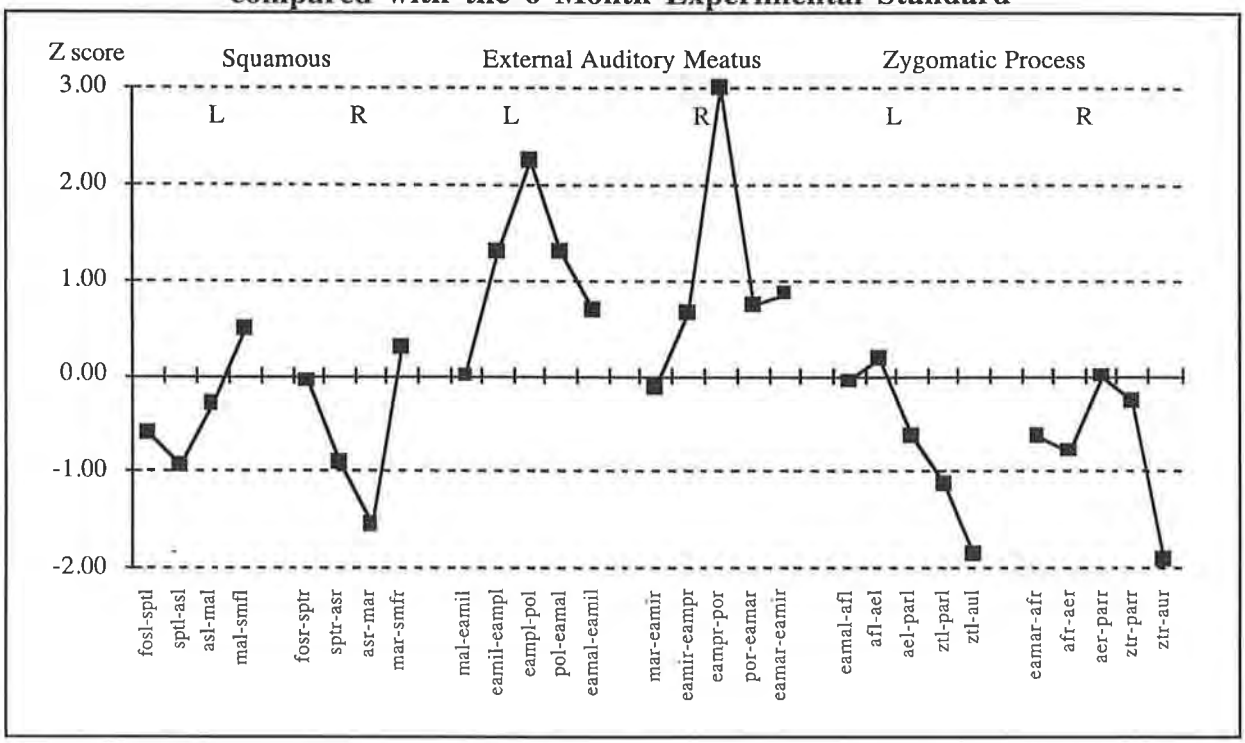

Figure 3.28(o) Z Scores of the Measurements of the Temporal Bone for Patient SH compared with the 6 Month Experimental Standard

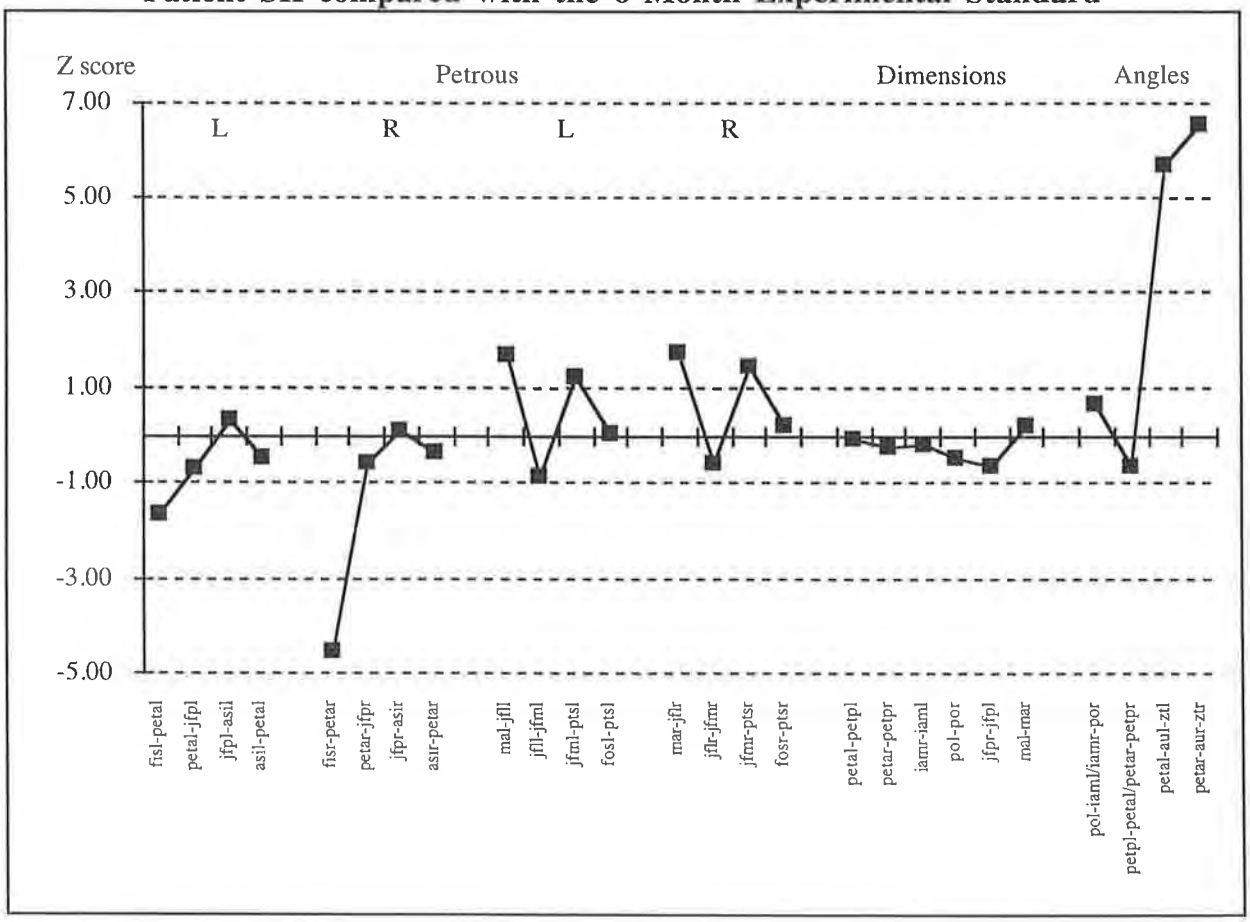

3.4.6.10 The Parietal Bone of Patient SH

Distances: The measurement of the parietal bone revealed an increased distance at the spheno-parietal suture. A pattern profile of Z scores was not generated for the parietal bone. The measurement data are reported in Appendix 2.

Discussion: The bregma was difficult to identify as a single landmark in this patient due to the widely patent anterior fontanelle and was not performed. Any subsequent value derived for the lengths of the coronal sutures was not considered accurate enough to report due to the inaccuracy of the bregma landmark and the curvature of the calvaria.

3.4.6.11 The Occipital Bone of Patient SH

Distances and Dimensions (Figure 3.28(p)): All distances around the occipital bone and involving the foramen magnum were not significantly different from the experimental standard. The spheno-occipital synchondrosis was presented elsewhere (see sphenoid bone and cranial base sutures). The dimensions were not significantly different from the experimental standard.

Discussion: The occipital bone was essentially normal in size and shape and not greatly distorted by the pathological process.

Figure 3.28(p) Z Scores of the Distances and Dimensions of the Occipital Bone for Patient SH compared with the 6 Month Experimental Standard

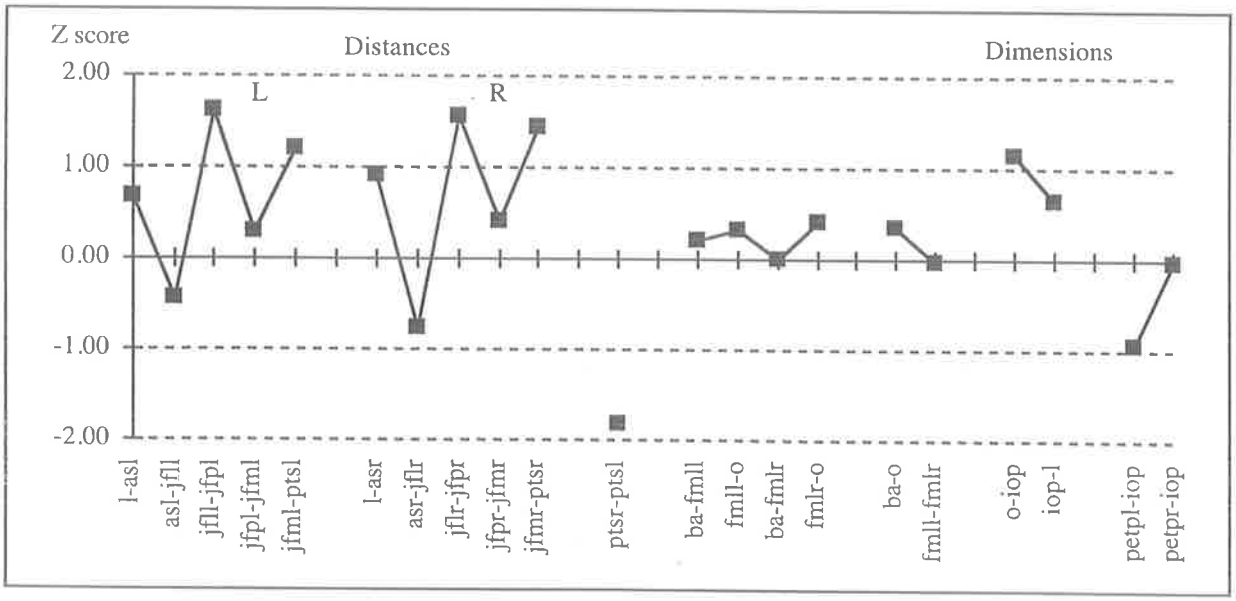

3.4.6.12 The Cranial Base Sutures of Patient SH

Anterior Cranial Fossa (Figure 3.28(q)): The anterior cranial fossa suture lengths were within the normal range.

Middle Cranial Fossa (Figure 3.28(q)): The superior spheno-petrous temporal suture (fisr-petar) was reduced in length on the right side, with a trend to be reduced on the left (fisl-petal).

Posterior Cranial Fossa (Figure 3.28(q)): The right medial temporo-occipital suture (superior) (petar-jfmr) length was increased on the right side. The other distances were normal except for the borderline reduced length of the inferior spheno-occipital synchondrosis (ptsl-ptsr).

Discussion: No strong patterns of suture deformity emerged in this infant.

Figure 3.28(q) Z Scores of the Dimensions of the Cranial Base Sutures for Patient SH compared with the 6 Month Experimental Standard

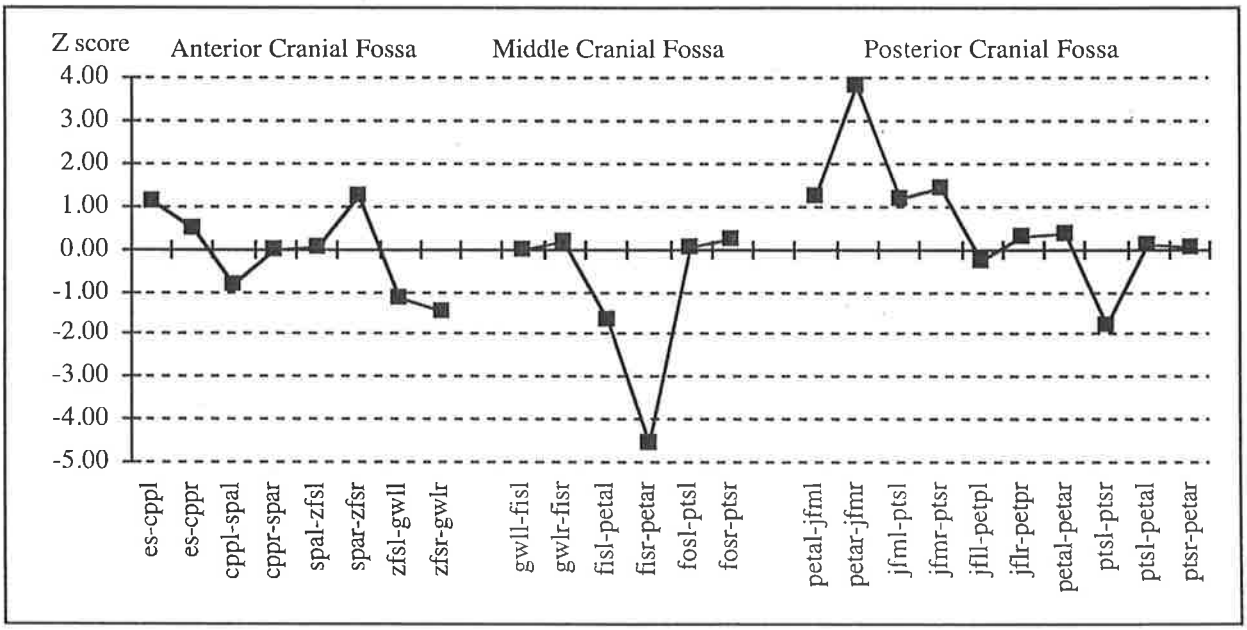

3.4.6.13 The Craniofacial Dimensions and Angles

Dimensions and Angles (Figure 3.28(r)): The patient's mouth was open during the CT scan making the measurements of the facial height and SNB angle (s-n-sm) invalid. The SNA was borderline low. The cranial base angle (ba-s-n) was significantly reduced, implying a significant kyphosis in this patient. The cranial base dimensions were not significantly different from the experimental standard.

Discussion: A deformity at the cranial base was demonstrated by the reduced cranial base angle. The other distances and dimensions of the bones and sutures measured in this patient do not adequately explain whether the deformity is a primary or secondary event. Most abnormalities were found peripherally at the maxilla, zygomatic bone, greater wing of sphenoid and lateral temporal bone. In conjunction with calvarial suture involvement (not measured) the deformity is more manifest externally on the craniofacial skeleton.

Figure 3.28(r) Z Scores of the Craniofacial Dimensions and Angles for Patient SH compared with the 6 Month Experimental Standard

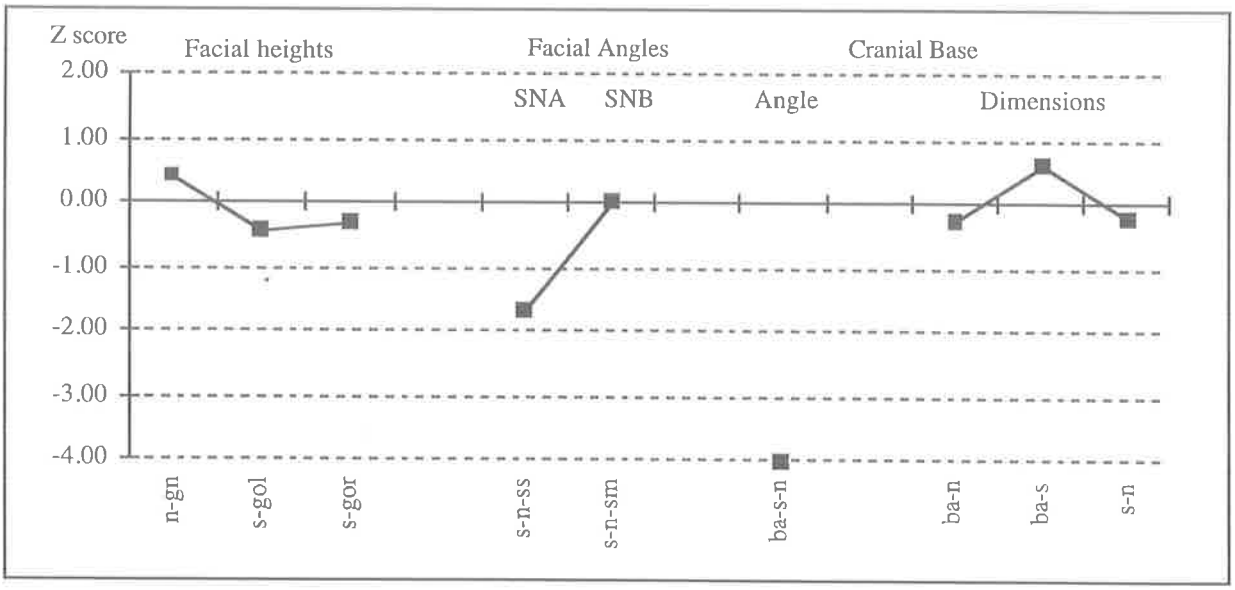

3.4.7 Clinical and Radiographic Findings for Patient JS

Clinical Features

Patient JS presented at the age of 21 months (Figure 3.3). There was no family history. The calvarial shape was turri-oxycephalic (cranial index = 81) Proptosis was evident with mild hypertelorism and the maxilla was hypoplastic. She had been slow to reach her milestones and there was evidence of papilloedema implying a degree of raised intracranial pressure. Ventilating tubes had been previously inserted for bilateral middle ear effusions. The upper airway was minimally restricted with snoring reported as being an intermittent problem. Formal airway assessment was not recorded. The posterior bodies of the cervical spine were fused from C5 - C6.

Lateral, Antero-Posterior and Basal Radiographs

Lateral and AP radiographs were available showing brachycephaly with a copper-beaten appearance of the calvaria. The calvarial sutures were all fused. The spheno-occipital synchondrosis was patent. The sella appeared small. Lesser wings of the sphenoid were swept up. The airway and maxilla appeared to be small but adequate.

3D CT Reconstruction

Calvarial bones: The skull shape was turricephalic with complete fusion of all bones except for a defect in the region of the sagittal suture. In general the CT reconstruction produced excellent visibility of the landmarks.

Cranial base: The cribriform plate was well displayed in the anterior cranial fossa. The plate appeared to be depressed compared with the bifrontal portions of the fossa which bulged up into the anterior fossa. Protrusion of the greater wing of the sphenoid into the orbit was noted. The lesser wing and petrous temporal bones swept steeply up laterally to join the calvarial bones. The jugum sphenoidale was slightly flat with prominent anterior clinoid processes. The middle cranial fossa including the sella was otherwise unremarkable. The spheno-occipital synchondrosis was identifiable as a faint line but not widely patent on the 3D CT reconstruction. The foramen magnum was shaped like a rhomboid.

Orbital: Mild lateral sweeping up of the aperture was seen. Slight bulging of the lateral orbital walls was present. The zygomatic bones were narrow and hypoplastic. The optic canal ran down then forward from the cranial base to the orbit with an elbow bend in its centre.

Maxilla: This bone was narrow and short in the vertical dimensions. The nasal bones had a prominent tip but were otherwise unremarkable.

3.4.8 Features of the CT Scan and 3D Reconstruction of Patient JS that made Landmark Identification difficult

The mental foramen, infra-orbital foramen could not be identified. The calvarial landmarks (l, as, br, spt, spc) could not be identified nor reliably estimated. The peri-orbital sutures and cranial base landmarks were identified from the regional bony contours and junctions defined in the landmarks (Figures 3.15-3.26). The inferior canine could not be seen. In general terms the 3D CT reconstruction enabled good visualisation of all key landmarks for the purpose of measurement.

3.4.9 Results and Discussion of the Quantitative Analysis of Patient JS compared with the 2 Year Old Experimental Standard

Figures 3.29(a)-(r)

3.4.9.1 The Mandible of Patient JS

Distances (Figure 3.29(a)): Most distances between the adjacent landmarks were not significantly different from the experimental standard. The coronoid base to coronoid tip distance (cbl-ctl, cbr-ctr) was marginally increased bilaterally and the coronoid tip to mandibular notch distance (ctl-mnl, ctr-mnr) was decreased bilaterally.

Dimensions and Angles (Figure 3.29(b)): The dimensions were not significantly different from the experimental standard except the distances between the coronoid bases (cbl-cbr) which was marginally decreased. The only angle which was significantly smaller was the anterior mandibular angle (gol-gn-gor).

Discussion: The mandible was essentially within the normal range, showing a minor tendency to being slightly narrow in the region of the coronoid base and anterior mandibular angle.

Figure 3.29(a) Z Scores of the Distances of the Mandible for Patient JS compared with the 2 Year Old Experimental Standard

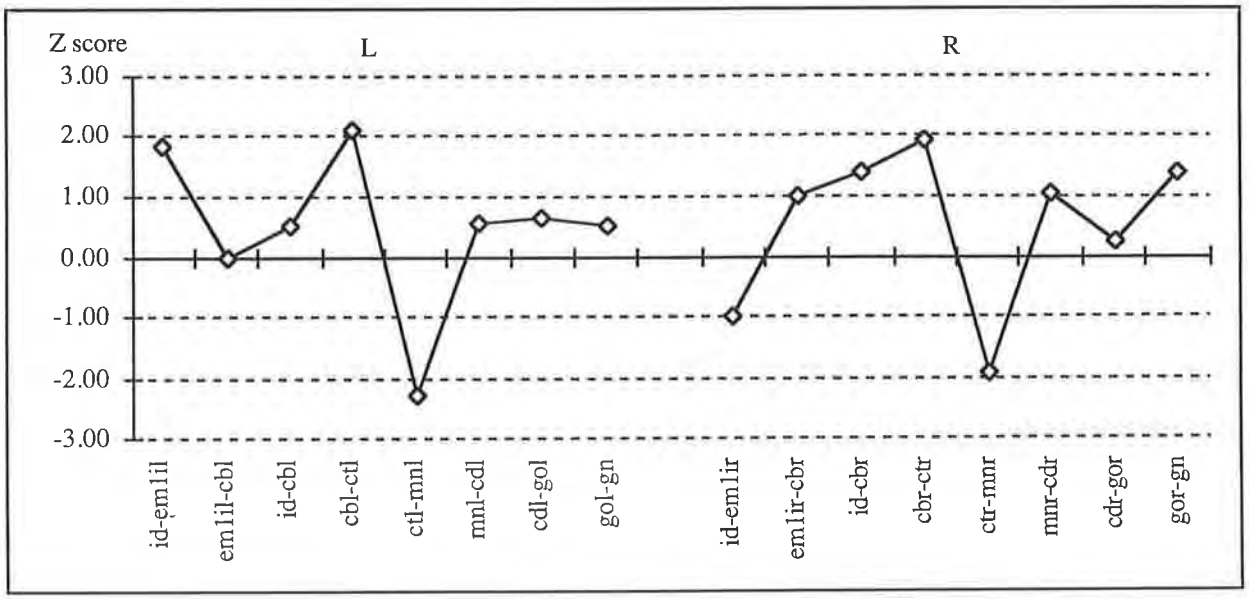

Figure 3.29(b) Z Scores of the Dimensions and Angles of the Mandible for Patient JS compared with the 2 Year Old Experimental Standard

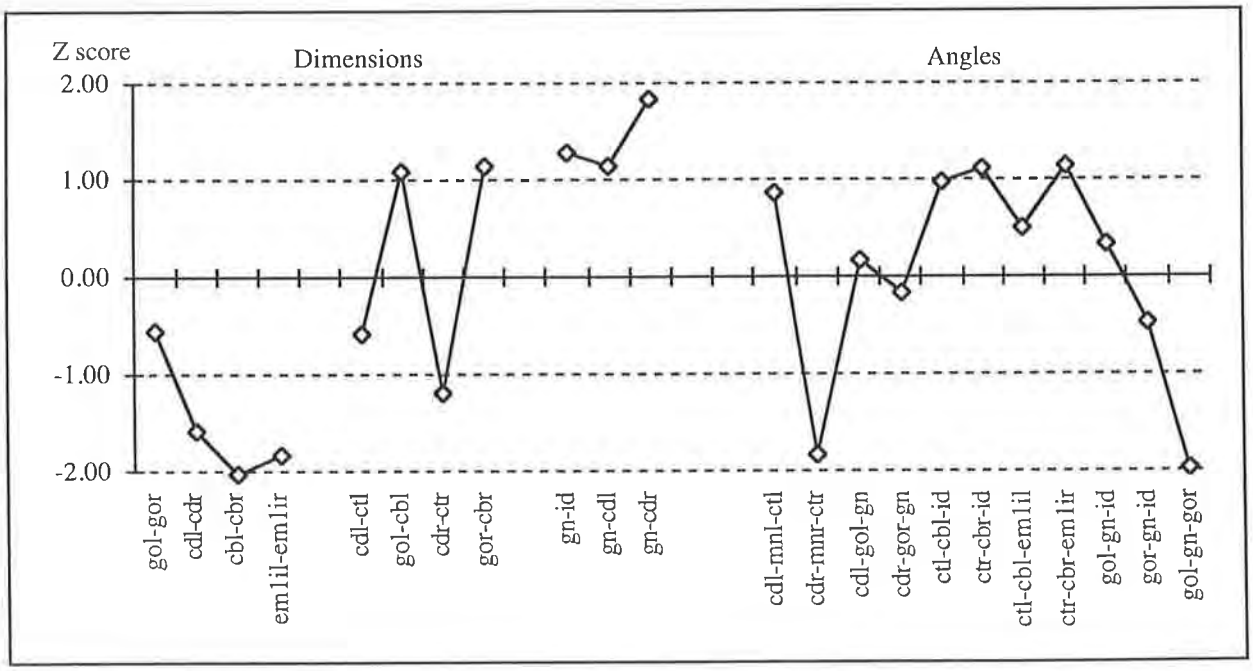

3.4.9.2 The Maxilla of Patient JS

Distances (Figure 3.29(c)): The length of the anterior zygo-maxillary suture (zmil-orl, zmir-orr) was increased on the left hand side, but not on the right side. The posterior maxillary wall height (mxtl-msl, mxtr-msr) was significantly reduced bilaterally compared with the experimental standard.

Dimensions and Angles (Figure 3.29(d)): The dimensions measured were not significantly different from the experimental standard. The maxillary arch angle (gpfl-pr-gpfr) and anterior palatal angle (gpfl-ans-gpfr) were reduced.

Discussion: The measurements of Patient JS suggest a minor degree of hypoplasia of the maxilla away from the experimental standard. The maxillary arch was narrow with reduced posterior height to the maxilla. An increase in length at the suture with the zygomatic bone particularly on the left side suggests abnormal growth at this site.

Figure 3.29(c) Z Scores of the Distances of the Maxilla for Patient JS compared with the 2 Year Old Experimental Standard

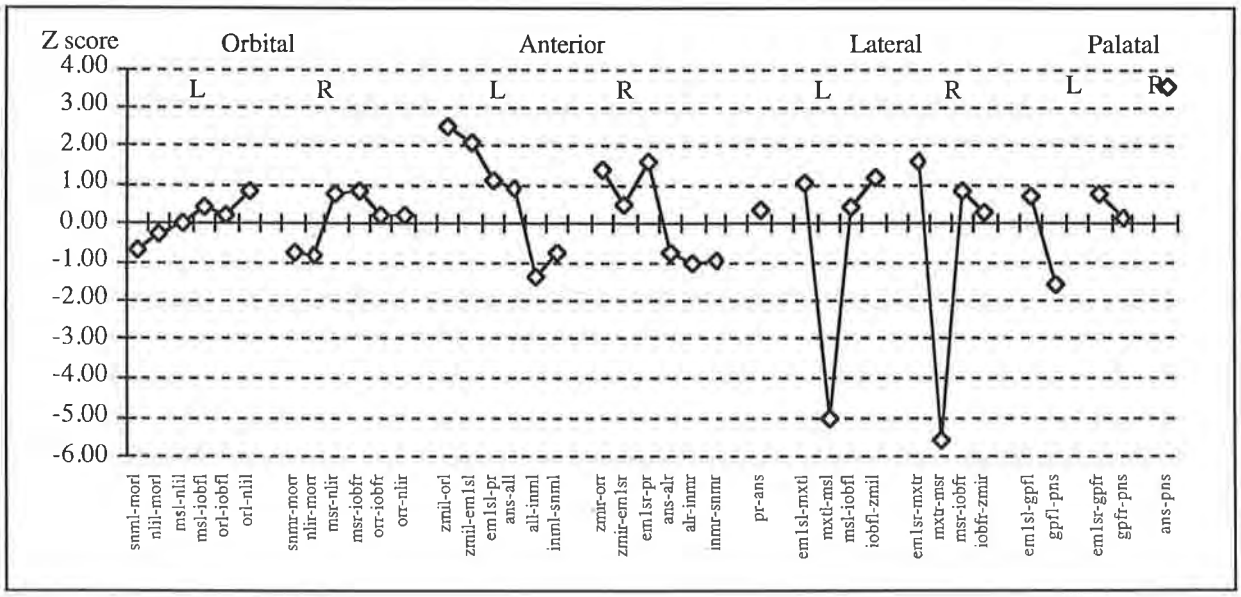

Figure 3.29(d) Z Scores of the Dimensions and Angles of the Maxilla for Patient JS compared with the 2 Year Old Experimental Standard

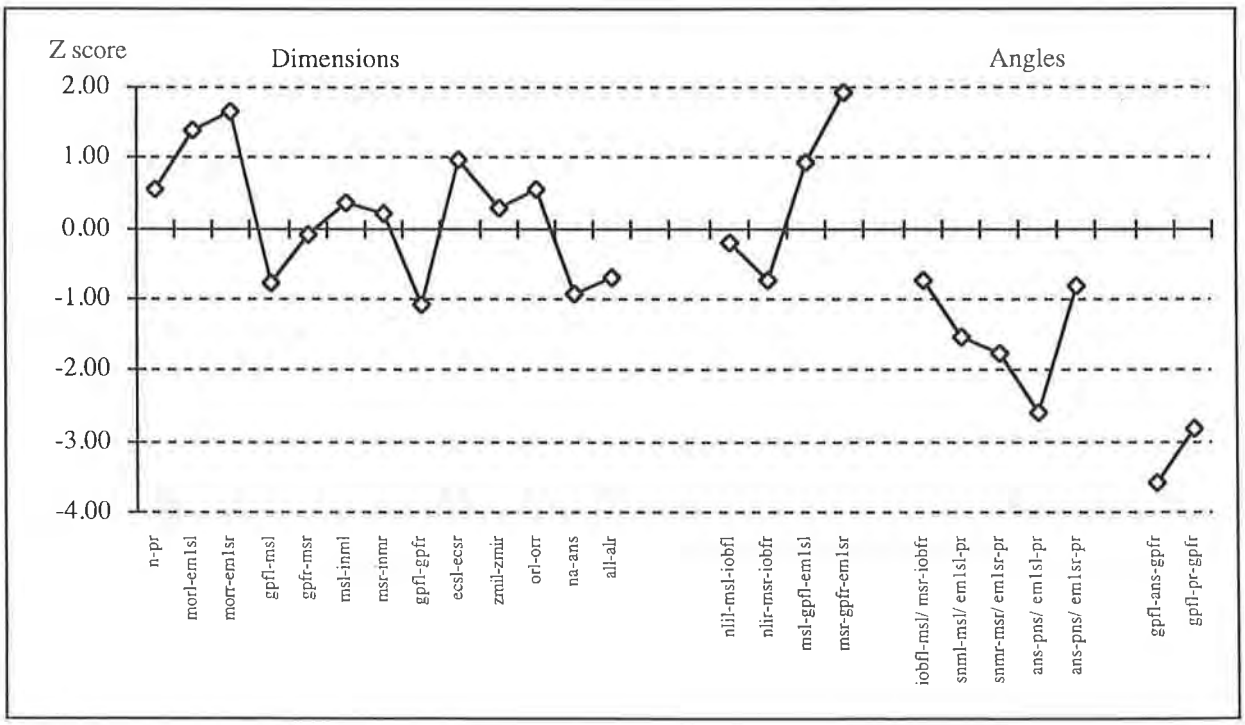

3.4.9.3 The Nasal Bones of Patient JS

Distances, Dimensions and Angles (Figure 3.29(e)): The width of the nasal bones were increased inferiorly (na-inml, na-inmr) bilaterally. Superiorly, the width of the nasal bones (n-snml, n-snmr) was increased on the left with a tendency to be increased on the right. The inferior width of the nasal complex was increased (inml-inmr). The inferior nasal angle (inml-na-inmr) was significantly reduced.

Discussion: The nasal bones had an increase in width at the junction with the frontal bone and inferiorly along the free lower border. The inferior angle of the free edge of the nasal bone was more acute suggesting a distortion in size and shape of the bones. A clear cause for the deformity cannot be identified from the measurements made, however it may be related to isolated sutural growth deformity or distortion from the maxilla and ethmoid bones.

Figure 3.29(e) Z Scores of the Measurements of the Nasal Bones for Patient JS compared with the 2 Year Old Experimental Standard

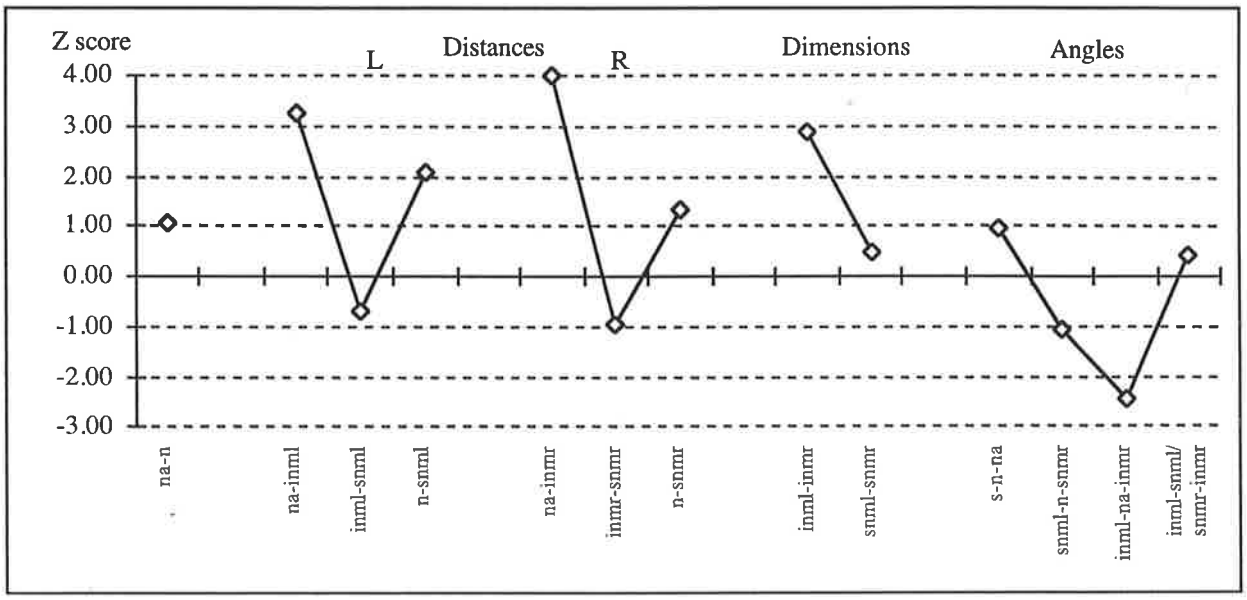

3.4.9.4 The Frontal Bone of Patient JS

Distances (Figure 3.29(f)):

Supra-orbital Region: The majority of distances of the supra-orbital region were within the limits of the experimental standard. The width of the superior nasal bone (n-snml) was increased on the left (frontonasal suture). The superior lateral distance of the orbit was increased bilaterally (sorl-slorl, sorr-slorr). The height of the orbit may be greater superiorly or the position of the superior lateral point of the orbit may be positioned more laterally to account for this.

Ethmoid Attachment: The greatest discrepancy in the frontal bone of this patient occurred at the attachment to the ethmoid. The frontal attachment was lengthened bilaterally at the level of the cribriform plate (cpal-cppl, cpar-cppr), while the anterior and posterior widths of the attachment were reduced (cppl-ofaml, cppr-ofamr and morl-ofaml, morr-ofamr).

Sphenoid Attachment: The distances around the superior orbital fissure were normal. The lateral distances to the squamous sphenoid bone could not be assessed. The parietal attachment (spcl-b, spcr-b) and sphenoid attachments (zfsl-spcl, zfsr-spcr and spcl-spal, spcr-spar) were not recordable due to the fusion of sutures and hence poor visibility of landmarks in this region.

Dimensions (Figure 3.29(f)): The main dimensions of the frontal bone were not significantly different from the experimental standard.

Discussion: The deformity in this patient was at the level of the cribriform plate. A lengthening of the cribriform plate was contrasted by a reduced width of the fronto-ethmoid attachment. This data contrasts with the data from the previous patients (Patients RN and SH) where the width of the attachment was increased. The fronto-zygomatic area was relatively uninvolved. The distances representing the cranial squamous sutures could not be measured.

Figure 3.29(f) Z Scores of the Distances and Dimensions of the Frontal Bone for Patient JS compared with the 2 Year Old Experimental Standard

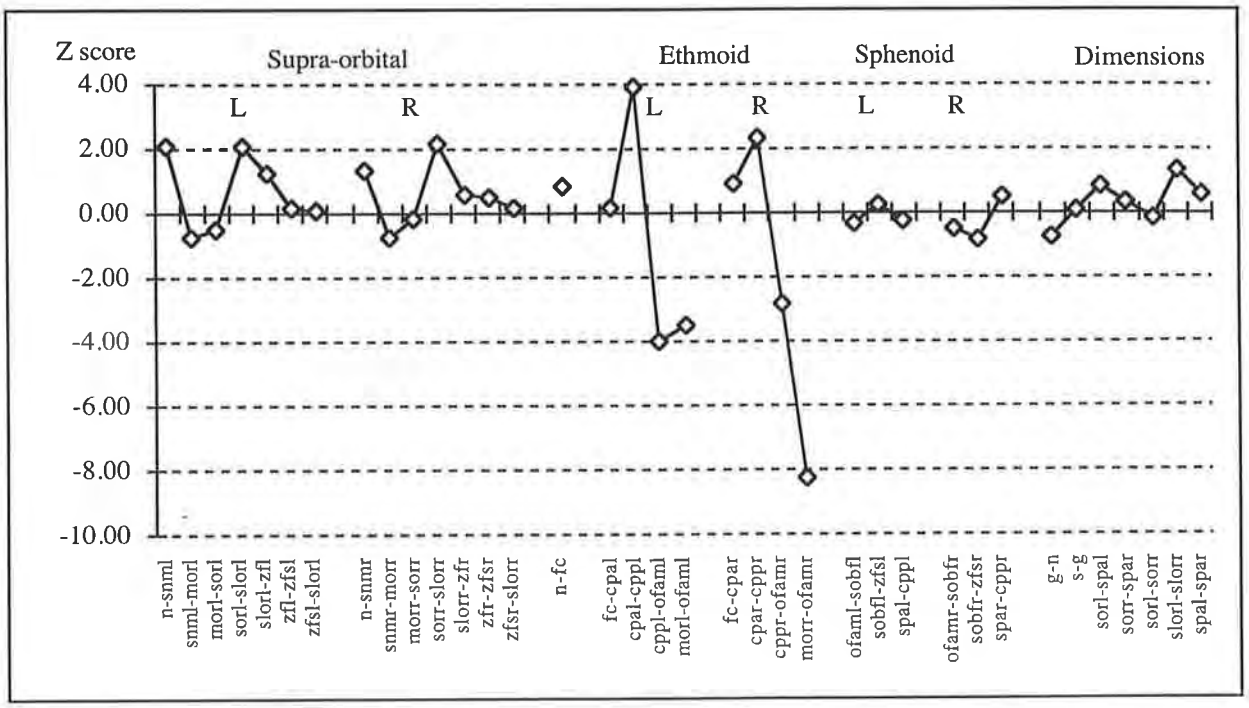

3.4.9.5 The Zygomatic Bone of Patient JS

Distances (Figure 3.29(g)): The majority of measurements were normal. The zygo-maxillary suture (zmil-orl) was increased on the left. On the left the distance from the inferior orbital rim to the inferior orbital fissure of the orbit was increased (orl-iobfl). The other sutures were of normal length.

Dimensions (Figure 3.29g): The dimensions were not significantly different from the experimental standard.

Discussion: The length of the zygo-maxillary suture was increased on one side. This does not appear to have had any major influence over the size of the zygomatic bone in this patient at this age.

Figure 3.29(g) Z Scores of the Distances and Dimensions of the Zygomatic Bone for Patient JS compared with the 2 Year Old Experimental Standard

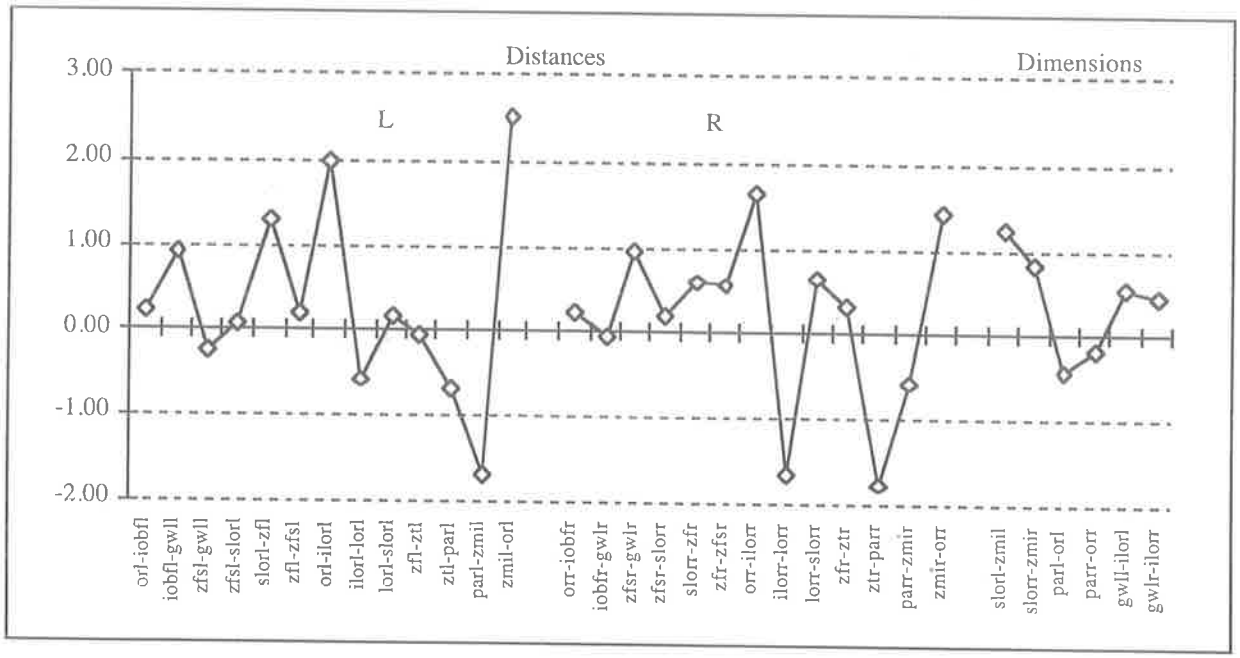

3.4.9.6 The Vomerine Bone of Patient JS

Distances, Dimensions and Angles (Figure 3.29(h)): All distances were not significantly different from the experimental standard, except the palatal length (ans-pns) which was increased. The dimensions and angles were not significantly different from the experimental standard.

Discussion: The vomer was not greatly different from the experimental standard in this patient at this age.

Figure 3.29(h) Z Scores of the Distances, Dimensions and Angles of the Vomer for Patient JS compared with the 2 Year Old Experimental Standard

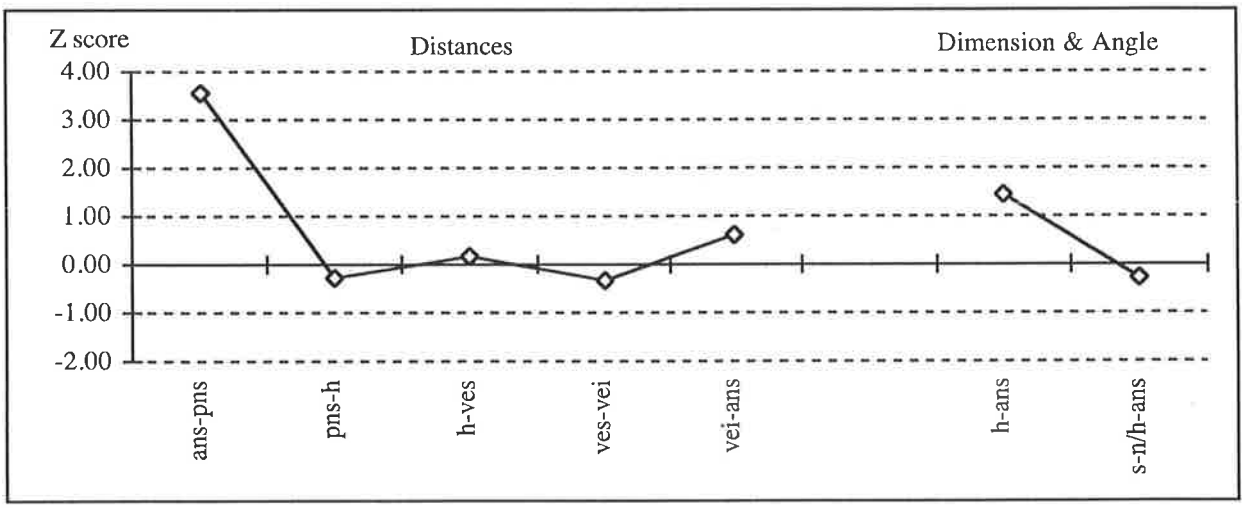

3.4.9.7 The Ethmoid Bone of Patient JS

Lateral Ethmoid Plate (Figure 3.29(i)):

Distances: In general, the lateral ethmoid plate distances (forming the medial orbital wall) were reduced. The distance from the optic canal to the medial orbital wall (morl-ofaml) was reduced bilaterally. The height of the medial orbital wall (ofamr-msr) was also reduced on the right. The junction of the lateral plate with the cribriform plate at its articulation with the frontal bone, showed reduced distances posteriorly (cppl-ofaml, cppr-ofamr) and a reduced distance anteriorly on the left (morl-cpal) (see frontal bone) (For cpal-cppl distance, see cribriform plate).

Dimensions and Angles: The other dimensions were normal, in particular the inter-orbital distance. The splay of the lateral plate was not significantly different from the experimental standard.

Cribriform Plate (Figure 3.29(j)):

Distances: The cribriform plate was of increased length bilaterally (cpal-cppl, cpar-cppr).

Angles: The cribriform plate was not angled down away from the sella-nasion line (s-n/cpar-cppr). In fact, the cribriform plate shows a tendency to be less depressed in this patient compared with the experimental standard.

Medial Ethmoid Plate (Figure 3.29(j)):

Distances: The distances measured on the medial plate were within the limits of the experimental standard.

Dimensions: The dimension from the nasion to the ethmoid spine (n-es) was increased.

Discussion: The lateral plate was reduced in length and, to some degree, in height. The cribriform plate showed an increase in length while the medial plate was normal. Anteriorly, the inter-orbital distance was normal. The width of the frontal ethmoid articulation (cppl-ofaml, cppr-ofamr) was reduced. The appearance of the ethmoid in this patient was of reduced orbital dimensions with normal or increased intracranial dimensions. The tendency for a wedge shaped ethmoid bone seen in the previous patients was not seen here.

Figure 3.29(i) Z Scores of the Measurements of the Lateral Ethmoid Plate for Patient JS compared with the 2 Year Old Experimental Standard

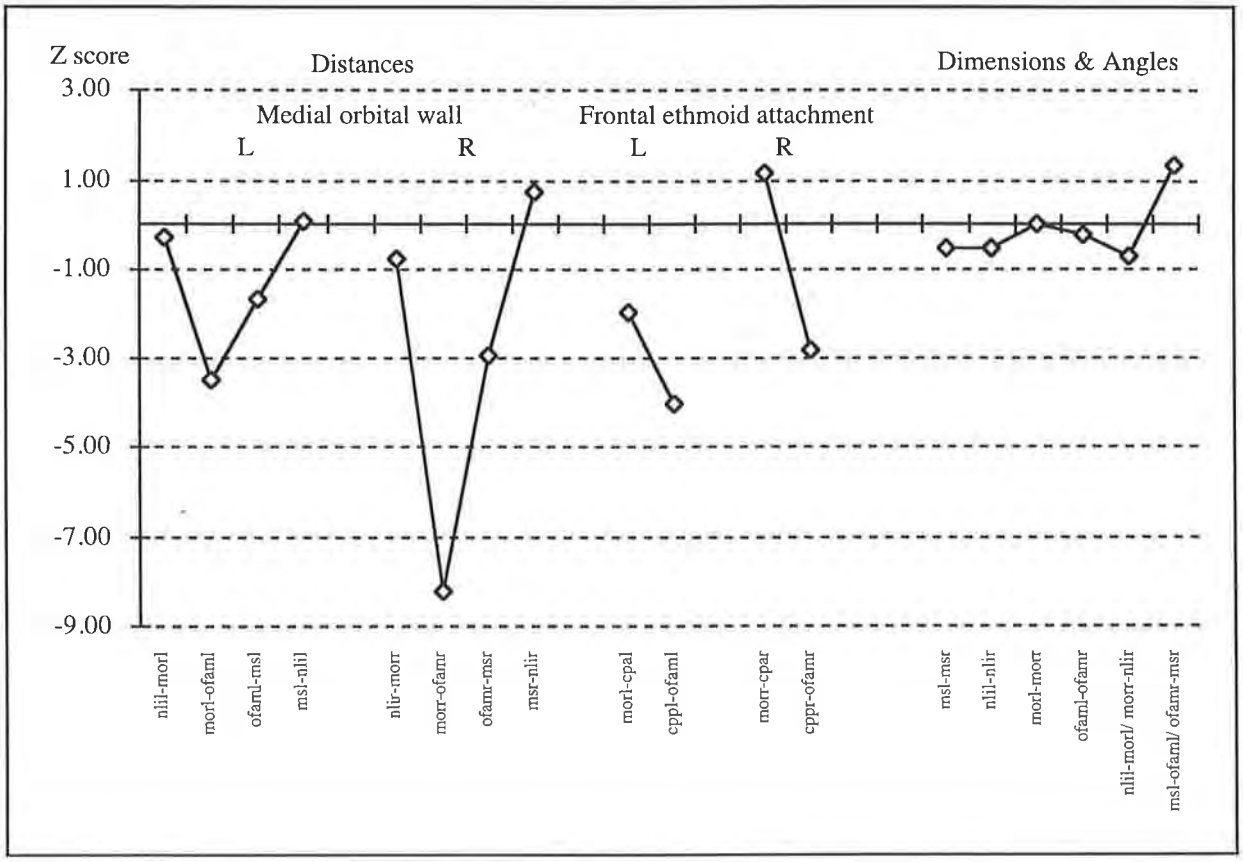

Figure 3.29(j) Z Scores of the Measurements of the Cribriform and Medial Ethmoid Plates for Patient JS compared with the 2 Year Old Experimental Standard

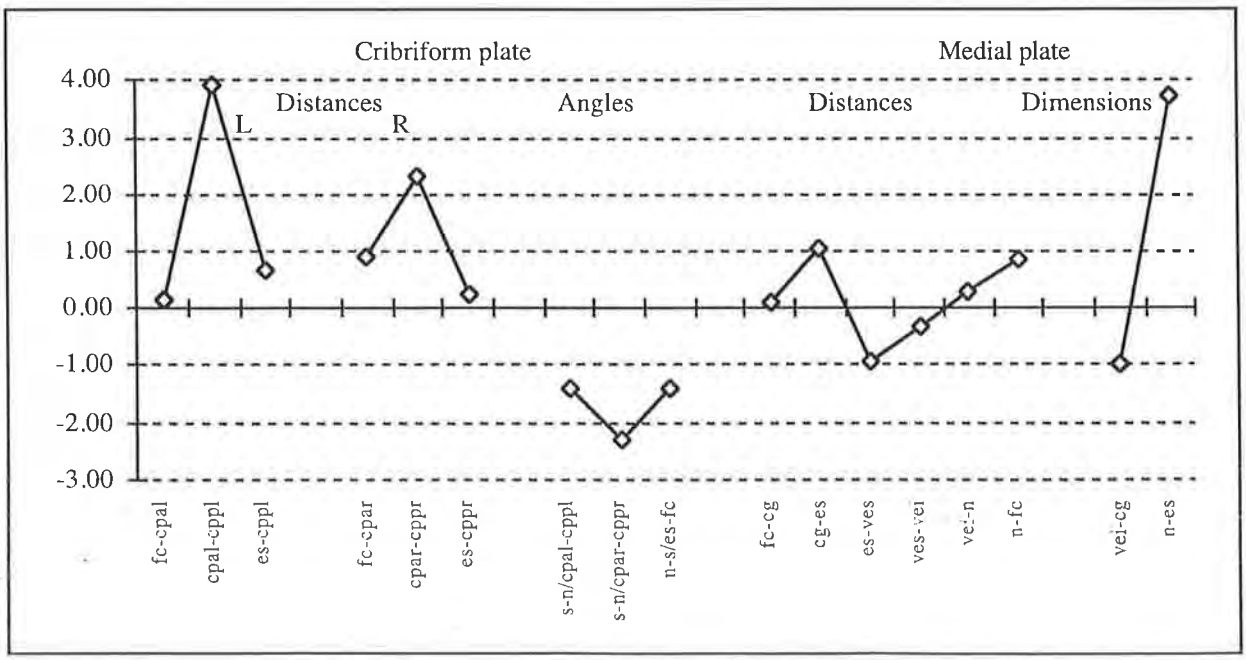

3.4.9.8 The Sphenoid Bone of Patient JS

Lesser Wing (Figure 3.29(k)):

Distances: The length of the medial part of the lesser wing (ofaml-acl) was increased on the left. Other distances were not significantly different from the experimental standard.

Dimensions and Angles: The angle of the lesser wings (spal-es-spar) was increased along with the splay of the lesser wings from the midline (n-s/acl-spal, n-s/acr-spar).

Pterygoid Plate (Figure 3.29(k)):

Distances and Angles: The pterygoid plate was not significantly different from the experimental standard.

Greater Wing (Figure 3.29(l)):

Distances: The majority of distances were not significantly different from the experimental standard. The inferior lateral length of the orbit (gwlr-gwmr) was significantly reduced on the right. The other distances were normal. Landmarks on the squamous sphenoid bone (spt and spc) could not be identified bilaterally, due to fusion of the calvarial bone in this region and hence the distances of the lateral part of the bone could not be measured.

Dimensions and Angles: The measured dimensions were within the limits of the experimental standard however. The anterior angles of the greater wing were all abnormal. The angle of splay of the greater wing (zfsl-gwml-ptsl, zfsr-gwmr-ptsr) was significantly reduced bilaterally. The protrusion of the greater wing was increased bilaterally (gwml-zfsl/gwmr-zfsr, gwml-gwll/gwmr-gwml).

Figure 3.29(k) Z Scores of the Measurements of the Lesser Wing and Pterygoid Plate of the Sphenoid for Patient JS compared with the 2 Year Old Experimental Standard

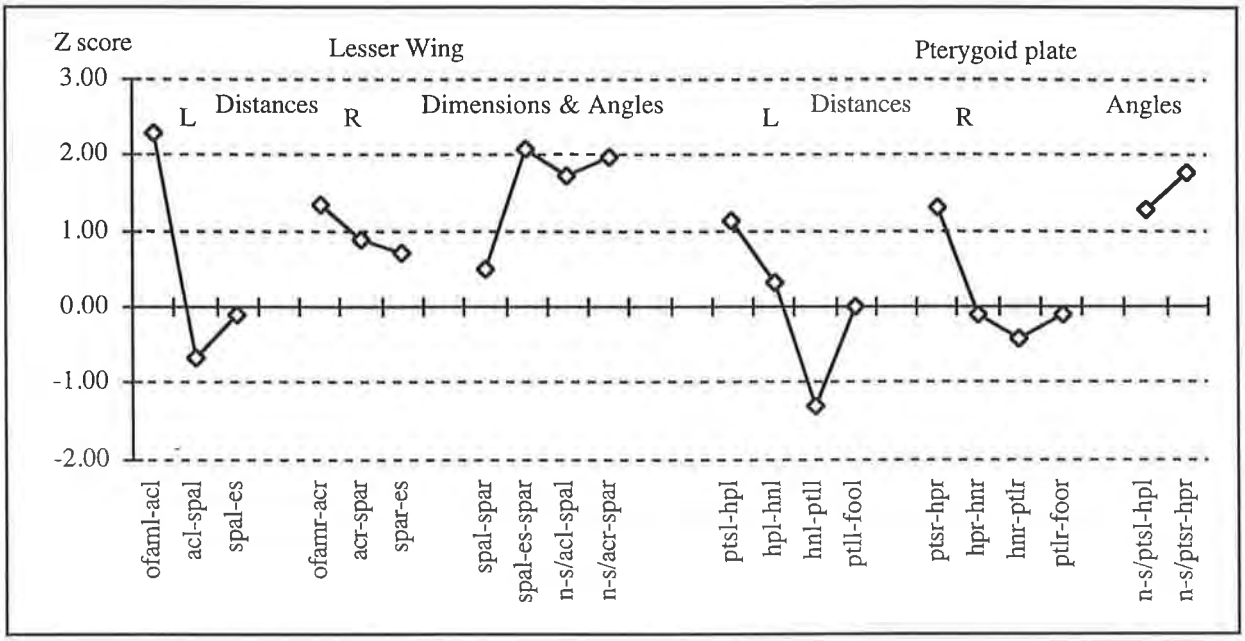

Figure 3.29(l) Z Scores of the Measurements of the Greater Wing of the Sphenoid for Patient JS compared with the 2 Year Old Experimental Standard

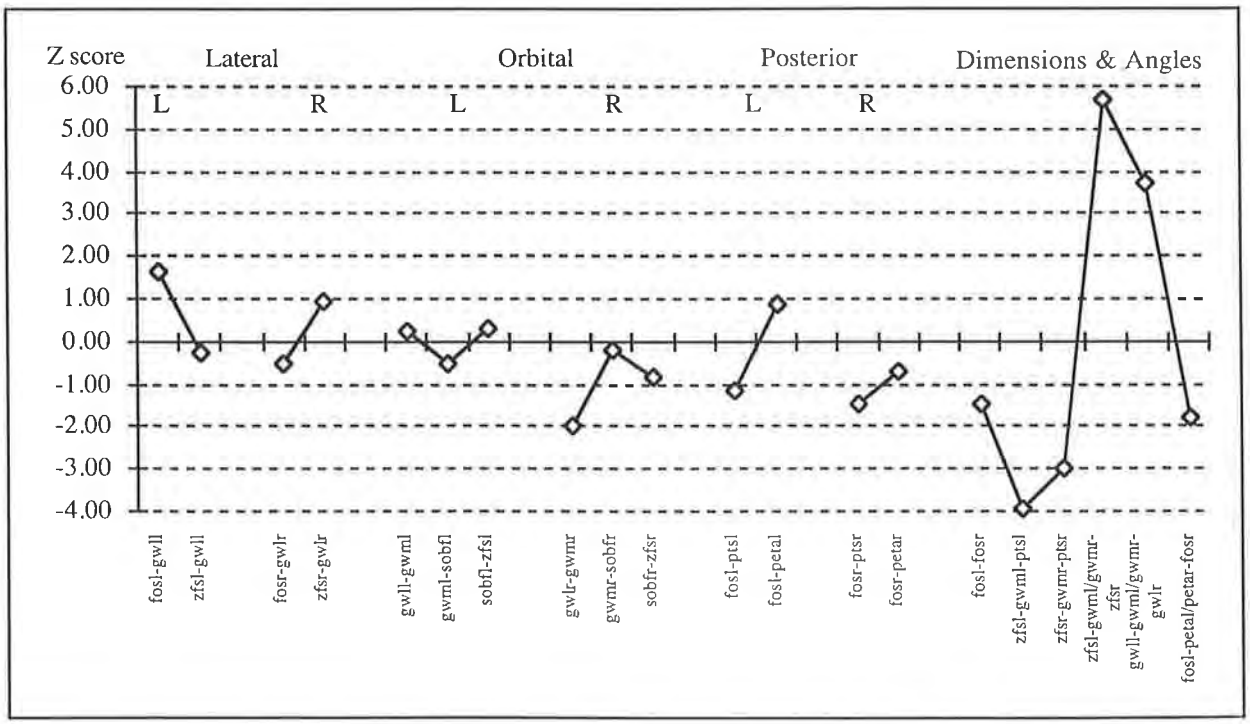

3.4.9.8 The Sphenoid Bone of Patient JS (continued)

Body of Sphenoid (Figure 3.29(m)):

Distances: The distances measured on the lateral /posterior and base/floor of the sphenoid body were not significantly different from the experimental standard. The anterior body showed a number of significantly reduced distances. The posterior frontal ethmoid attachment was reduced (cppl-ofaml, cppr-ofamr) (see frontal and ethmoid bones). Distances in the region of the jugum sphenoidale were also reduced anteriorly (cppl-ofpml, cppr-ofpmr).

Dimensions and Angles: The dimensions were significantly reduced between the medial points of the greater wings (gwml-gwmr) just above the left and right foramen rotundum. The superior spheno-occipital synchondrosis (petal-petar) was borderline reduced. The angles of the body from the midline (s-n/gwml-ptsl, s-n/ofpml-petal) were significantly decreased on the left side, implying this side was slightly narrower and/or less depressed than the other side.

Discussion: The most striking finding was the deformity of the sphenoid lesser and greater wings which were splayed laterally. The distances of the sphenoid bone were abnormal in the region of the posterior frontal ethmoid attachment where it contacts the sphenoid bone. The majority of growth disturbance appeared to occur peripherally with less severe involvement anteriorly.

Figure 3.29(m) Z Scores of the Measurements of the Body of the Sphenoid for Patient JS compared with the 2 Year Old Experimental Standard

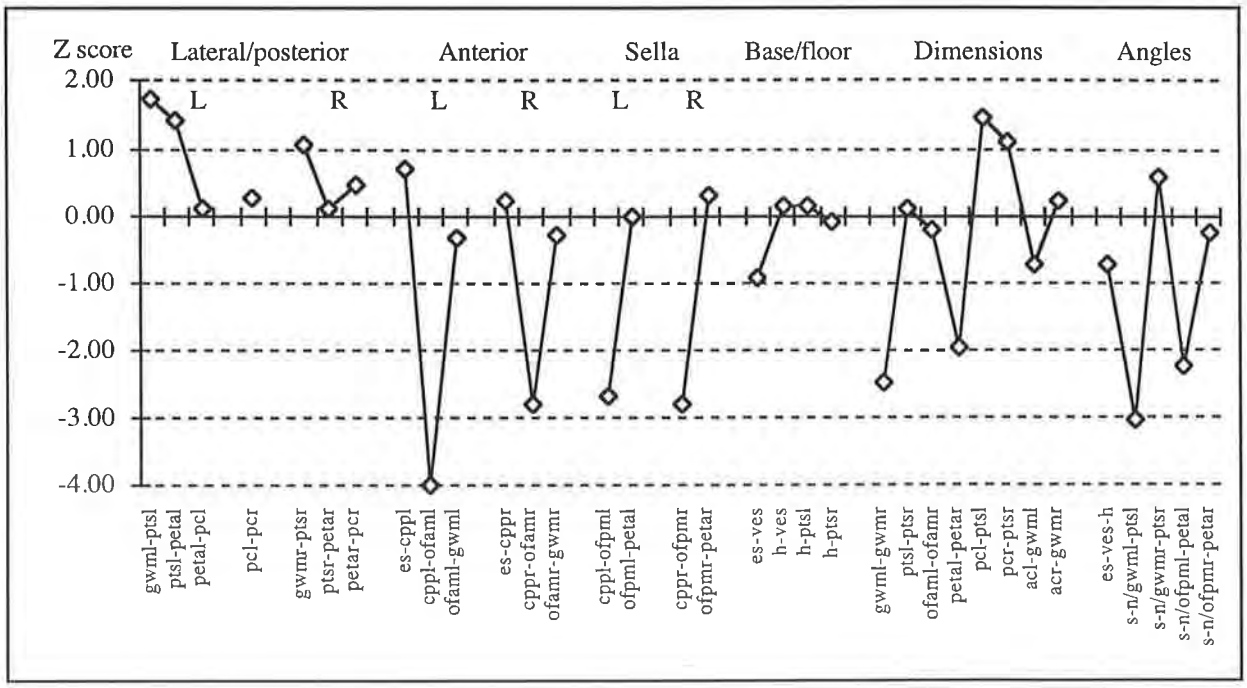

3.4.9.9 The Temporal Bone of Patient JS

Distances (Figure 3.29(n)):

Squamous Temporal Bone: The temporal squamous bone was not fully measurable in this child due to lack of visibility of the asterion (as) and sphenion (spt). The distances measured were not significantly different from the experimental standard.

External Auditory Meatus: The configuration of the external auditory meatus was similar bilaterally, and not significantly different from the experimental standard.

Zygomatic Process: The zygomatic process showed similar pattern profiles bilaterally, with a tendency for the height of the articular fossa (afl-ael, afr-aer) to be increased significantly bilaterally and the length of the zygomatic arch (ztl-aul) to be decreased bilaterally.

Petrous Temporal Bone (Figure 3.29(o)): The distances of the temporal bone showed the right jugular foramen to be narrowed (jflr-jfmr). The mastoid to jugular foramen distance (mar-jflr) was increased on the right.

Dimensions (Figure 3.29(o)): The petrous temporal ridge dimension (petal-petpl, petar-petpr) was significantly increased in length on the right with a tendency to be increased on the left. The dimension between the internal auditory meati (iaml-iamr) was reduced. The angle of the auditory canal (pol-iaml/iamr-por) tended to be increased. The petrous temporal bone angles (petpl-petal/petar-petpr) were significantly decreased compared with the experimental standard. The angle of the zygoma projection (petal-aul-ztl) was more obtuse on the left.

Discussion: Deformity was found in the zygomatic process of the temporal bone where the length of the zygomatic arch was reduced but the height, particularly of the articular fossa, was increased. The jugular foramen appeared to be narrowed while the mastoid process was prominent. The petrous temporal bone angles were reduced implying a more posterior angulation of the temporal bones. In summary the deformity was mainly at the region of the zygomatic process and the jugular foramen at the base of the petrous temporal bone.

Figure 3.29(n) Z Scores of the Distances of the Temporal Bone for Patient JS compared with the 2 Year Old Experimental Standard

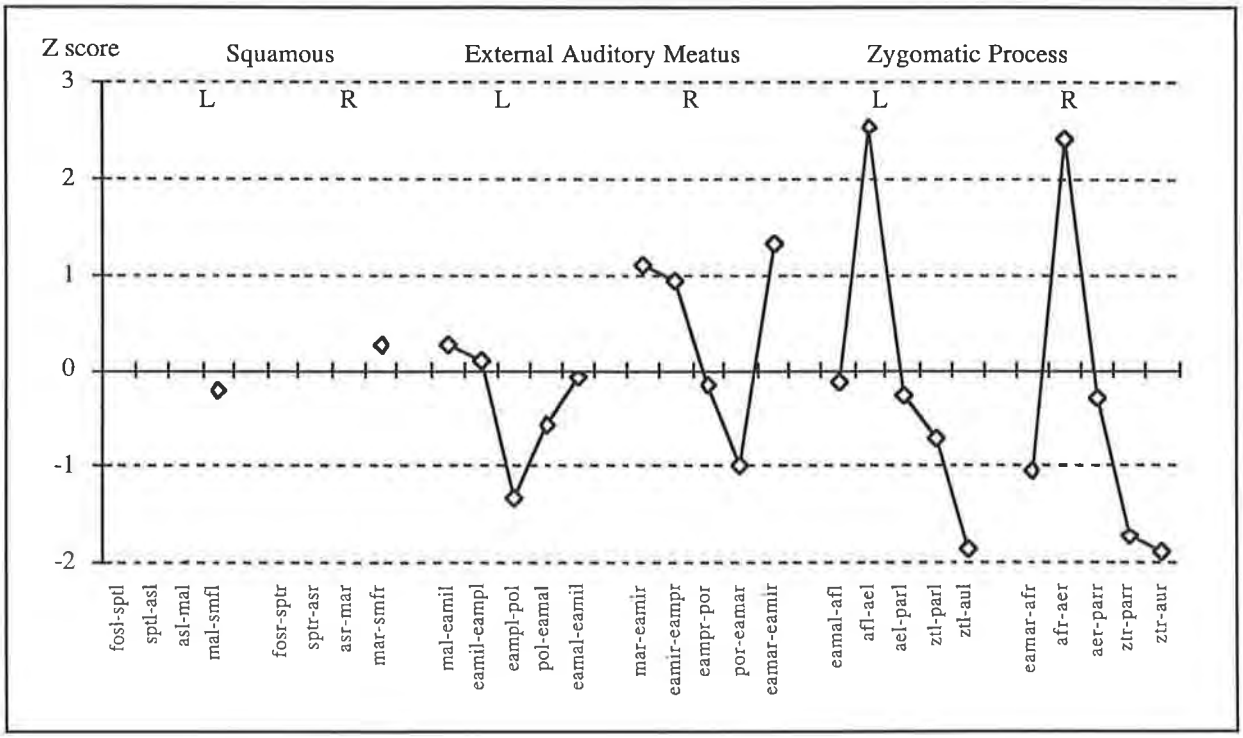

Figure 3.29(o) Z Scores of the Measurements of the Temporal Bone for Patient JS compared with the 2 Year Old Experimental Standard

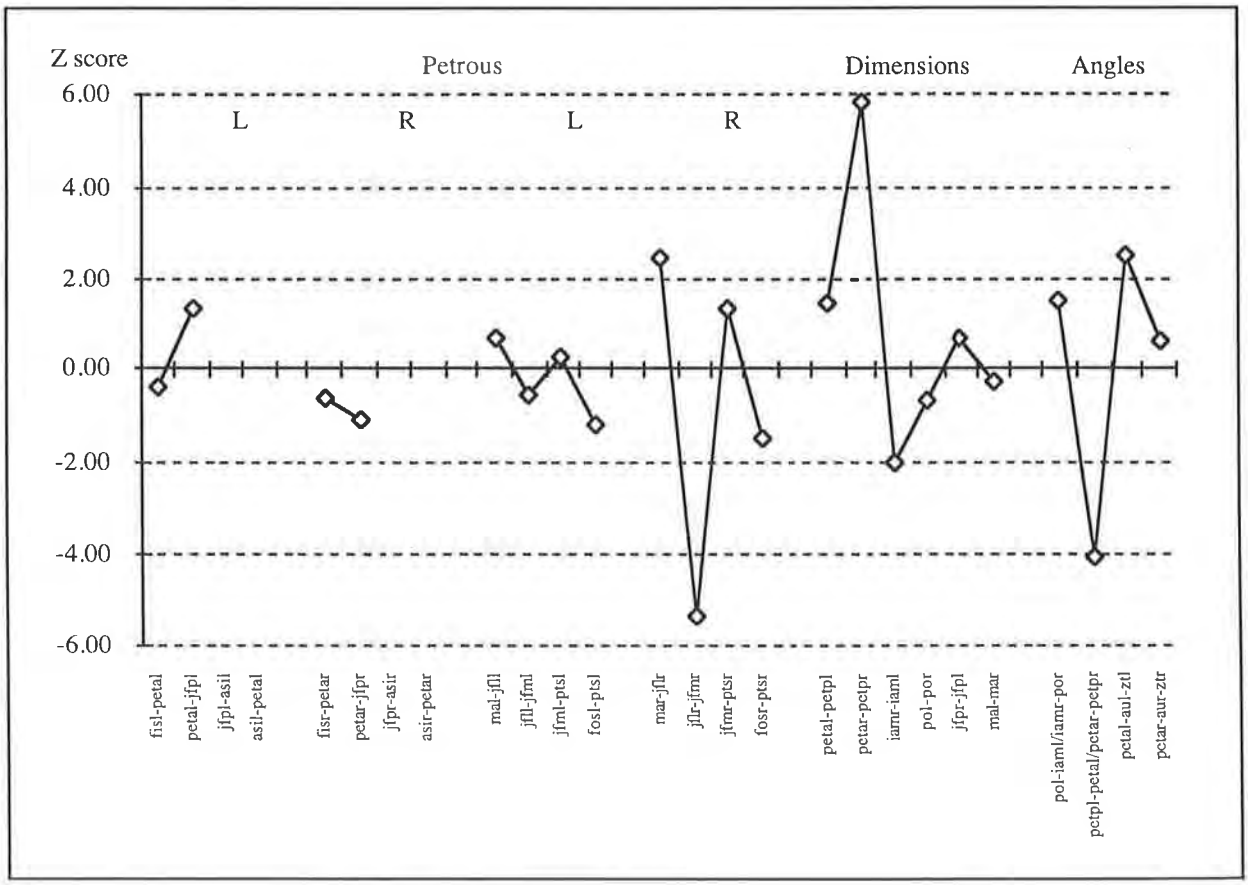

3.4.9.10 The Parietal Bone of Patient JS

Distances: The key landmarks for the parietal bone for Patient IP were not visible due to suture fusion and could not be reliably estimated. Therefore the parietal bone was not measured and a pattern profile of Z scores was not generated for the parietal bone. The measurement data for the experimental standard are reported in Appendix 2.

3.4.9.11 The Occipital Bone of Patient JS

Distances (Figure 3.29(p)): The majority of the distances around the occipital bone and involving the foramen magnum were not significantly different from the experimental standard. The exception was the right medial jugular foramen distance (jfpr-jfmr) which was significantly reduced. The spheno-occipital synchondrosis was discussed elsewhere (see sphenoid and cranial base sutures). The foramen magnum was slightly abnormal with reduced distance from the opisthion to the left foramen lateral point (fmll-o) and increased distances from basion to the right foramen magnum lateral point (ba-fmlr).

Dimensions (Figure 3.29(p)): The dimensions from the posterior petrous bone to the internal occipital protuberance (petpl-iop, petal-iop) were reduced bilaterally.

Discussion: The occipital bone confirmed a narrowing at the level of the right jugular foramen (see temporal bone). Several other measurements were slightly reduced and there was a mild shape distortion at the level of the foramen magnum.

Figure 3.29(p) Z Scores of the Measurements of the Occipital Bone for Patient JS compared with the 2 Year Old Experimental Standard

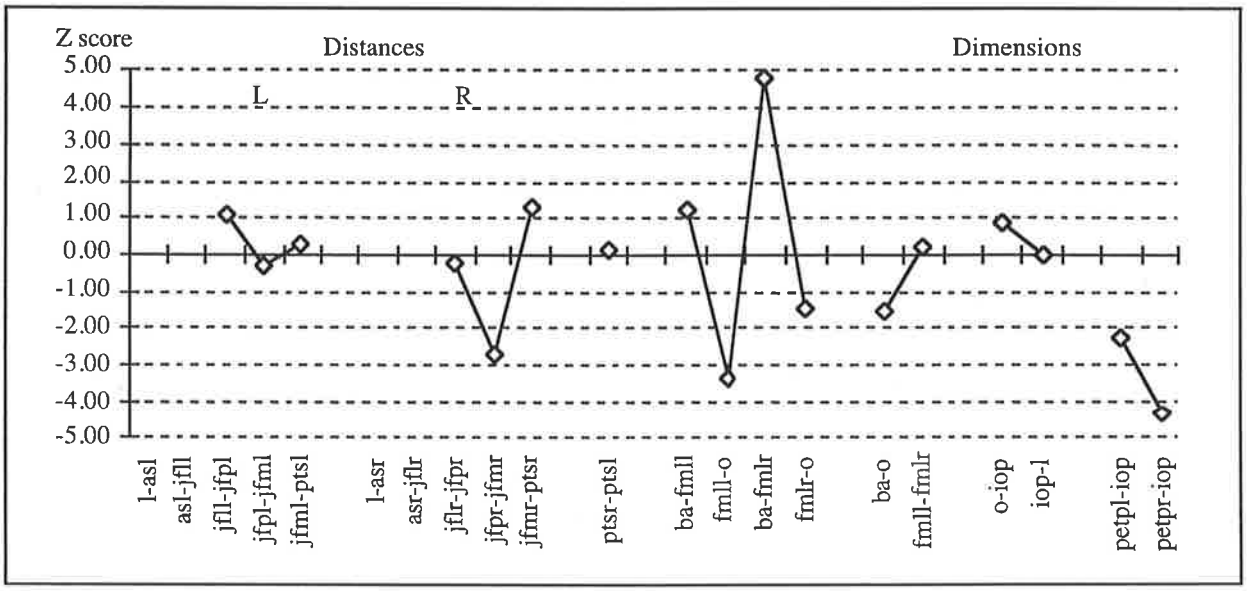

3.4.9.12 The Cranial Base Sutures of Patient JS

Anterior Cranial Fossa (Figure 3.29(q)): The sutures reported here were not significantly different from the experimental standard.

Middle Cranial Fossa (Figure 3.29(q)): The left spheno-squamous temporal suture (gwll-fisl) was increased in length. The right side was not involved.

Posterior Cranial Fossa (Figure 3.29(q)): The right occipital mastoid suture (superior) suture (jflr-petpr) was increased in length. The superior aspect of the spheno-occipital synchondrosis (petal-petar) was reduced in length.

Discussion: No distinct pattern of abnormality was identified from the suture distances presented here. Asymmetry of some measurements was present. The increased measurements were seen laterally while the reductions were more medial. Anteriorly, normal suture distances were found. From measurements of the individual bones, decreased dimensions were found anteriorly at the level of the frontal ethmoid attachment (see frontal, ethmoid and sphenoid bones). Laterally, the temporal-occipital suture complex was lengthened at various places. Medially the spheno-occipital synchondrosis was reduced in length. All calvarial sutures were fused and directly or indirectly complicate the expression of the sutures at the level of the cranial base.

Figure 3.29(q) Z Scores of the Dimensions of the Cranial Base Sutures for Patient JS compared with the 2 Year Old Experimental Standard

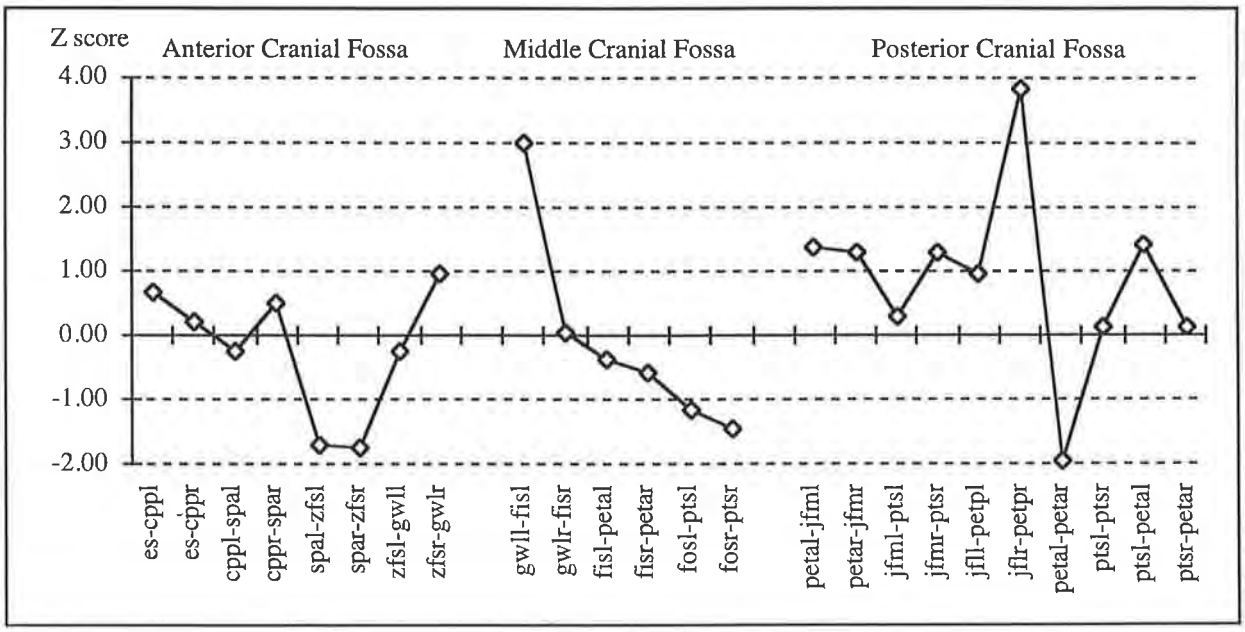

3.4.9.13 The Craniofacial Dimensions and Angles of Patient JS

Dimensions and Angles (Figure 3.29(r)): The anterior facial heights and SNB cannot be interpreted due to the open mouth of the patient when the CT scan was performed. The SNA and the cranial base angle was not significantly different from the experimental standard. The cranial base dimensions were not significantly different from the experimental standard.

Discussion: The midline cranial base was not greatly distorted based on the measurement data.

Figure 3.29(r) Z Scores of the Craniofacial Dimensions and Angles for Patient JS compared with the 2 Year Old Experimental Standard

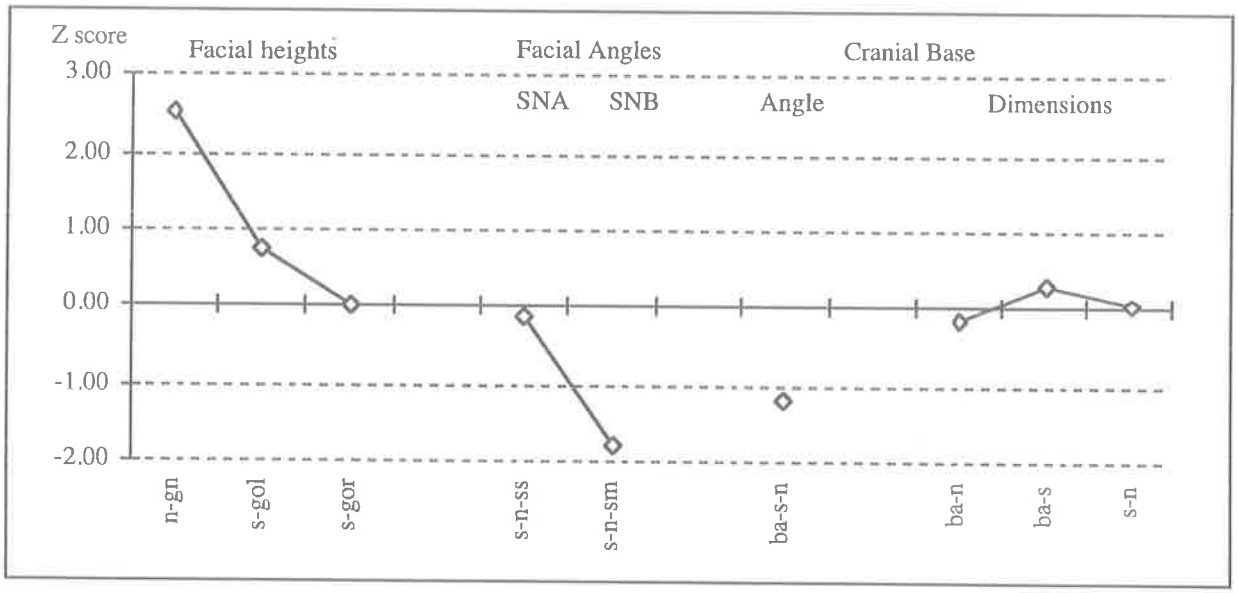

3.4.10 Clinical and Radiographic Findings for Patient IP

Clinical Features

This child with severe deformity presented from overseas at 21 months of age (Figure 3.4). The head shape was turricephalic with mild bi-temporal bulging. Severe proptosis with hypertelorism and strabismus were present. The maxilla was under-developed and the child was an obligate mouth breather. Evidence of raised intracranial pressure was found on clinical and radiological examination.

Lateral, Antero-Posterior and Basal Radiographs

Only lateral and antero-posterior skull radiographs were available for review. There was gross cranial deformity with turricephaly, and an extensive copper-beaten appearance with complete absence of all calvarial sutures. The spheno-occipital synchondrosis was seen to be patent in the lateral radiograph. The sella appeared to be elongated and attenuated and the cranial base angle more obtuse. The orbits were tall and swept up but difficult to see due to the copper-beaten appearance of the calvaria. Soft tissue proptosis was present in the lateral view. The maxilla was grossly deficient.

3D CT Reconstruction

Calvarial bones: The head shape was turricephalic with complete synostosis of the sutures. Small defects in the calvarial surface were present, where prolonged endocranial resorption had occurred. A degree of bi-temporal bulging of the calvarial bones could be seen however this did not represent an obvious cloverleaf deformity.

Cranial base: The anterior cranial fossa appeared very short, with broadening of the ethmoid cribriform plates. Bone resorption in this area made identification of the margins of the cribriform plate difficult. The cribriform plate did not appear as depressed as in other patients suggesting a more obtuse cranial base angle. The lesser wing of the sphenoid was swept up where it met the frontal bone. The sella was long and shallow with a steep jugum sphenoidale and clivus. The greater wing of the sphenoid was very prominent, bulging laterally into the orbit and the squamous temporal region. The middle cranial fossa was also fore-shortened. The

apex of the petrous temporal bones abutted the body of the sphenoid bone. The spheno-occipital synchondrosis was not identifiable on the 3D CT reconstructions. A grossly dysmorphic picture was seen generally.

Orbital: The orbits showed evidence of hypertelorism. The aperture of the orbits were increased in height. The most striking feature was the shallowness of the orbits with pronounced bulging forward of the lateral and medial orbital walls. The optic canals were found to be very low in the apex of the orbit, possibly as a result of the anterior and middle cranial fossa walls bulging downward and forward into the orbit. The zygomatic arch was pushed down and laterally by the temporal prominence.

Maxilla: The maxilla appeared to be narrow and short with the early development of a class III type relationship to the occlusion.

3.4.11 Features of the CT Scan and 3D Reconstruction of Patient IP that made Landmark Identification difficult

The mental, infra-orbital and stylomastoid foramina were not seen bilaterally. The calvarial landmarks (l, as, br, spt, spc) could not be identified nor reliably estimated. The peri-orbital sutures and cranial base landmarks were identified from the regional bony contours and junctions defined in the landmarks (Figures 3.15-3.26). The primary dentition was present at this age.

3.4.12 Results and Discussion of the Quantitative Analysis of Patient IP compared with the 2 Year Old Experimental Standard

Figures 3.30(a)-(r)

3.4.12.1 The Mandible of Patient IP

Distances (Figure 3.30(a)): The statistically significant increased distances compared with the experimental standard were the left anterior superior body length (id-em1il), the left anterior mandibular notch (ctl-mnl) and the right total superior body length (id-cbr).

Dimensions and Angles (Figure 3.30(b)): The intercondylar distance (cdl-cdr) was increased along with the left and right superior ramus widths (cdl-ctl, cdr-ctr). The right inferior ramus width (gor-cbr) was also increased. The angles measured on the mandible were not significantly different from the experimental standard.

Discussion: This patient was more dysmorphic than most. Many distances measured were larger than the experimental standard, in particular distances of the upper mandibular arch and ramus on the right side. The distinguishing feature in this patient was the laterally displaced positions of the mandibular condyle. This appeared to be a secondary effect resulting from the lateral growth of the temporal bone, caused by the severe craniostenosis.

Figure 3.30(a) Z Scores of the Distances of the Mandible for Patient IP compared with the 2 Year Old Experimental Standard

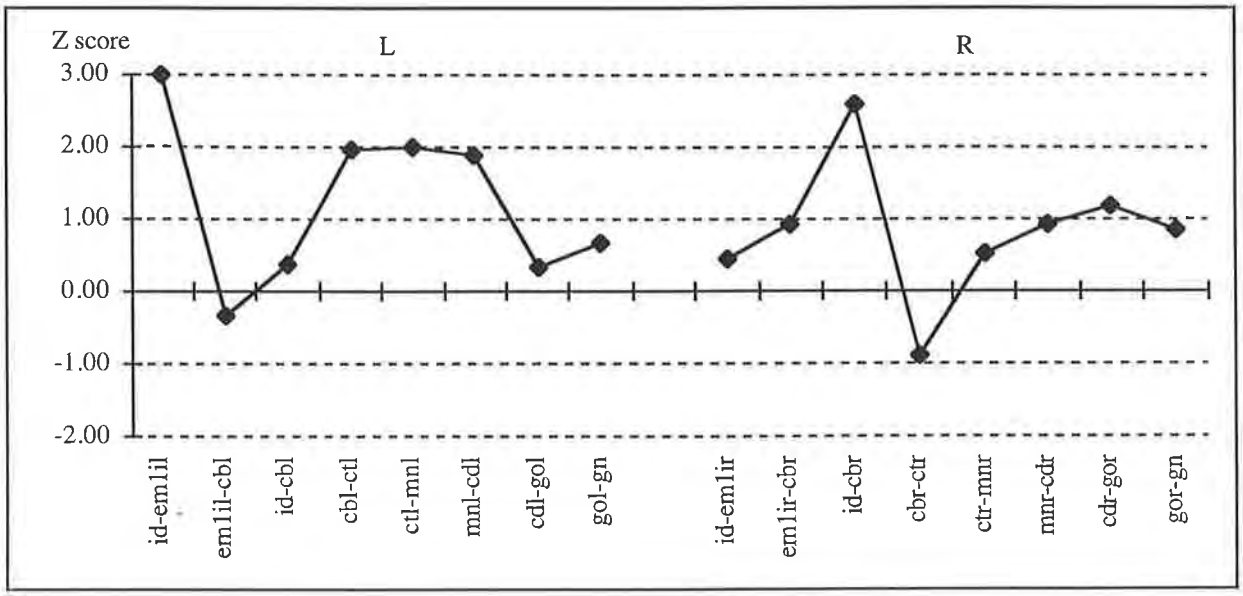

Figure 3.30(b) Z Scores of the Dimension and Angles of the Mandible for Patient IP compared with the 2 Year Old Experimental Standard

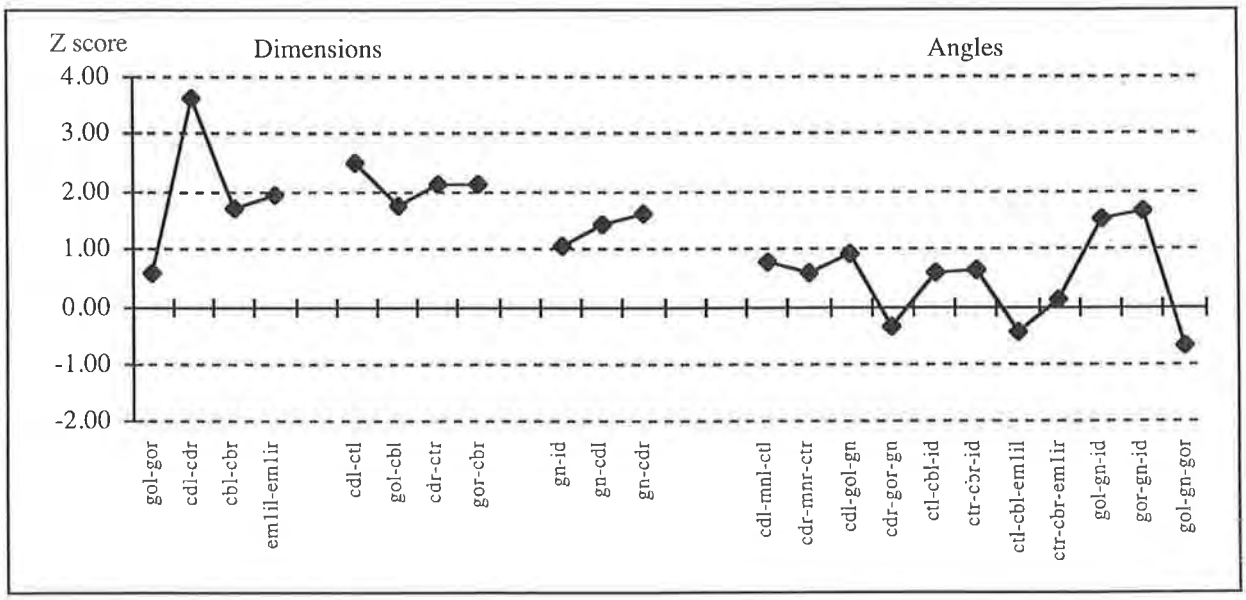

3.4.12 2 The Maxilla of Patient IP

Distances (Figure 3.30(c)): The majority of distances were abnormal in this patient compared with the experimental standard. The fronto-maxillary sutures (snml-morl, snmr-morr) and the medial infra-orbital rim (orr-nlir) on the left were increased in length. The orbital floor distances were reduced (msl-nlil, msr-nlir, msl-iobfl, orl-iobfl, orr-iobfr). The anterior distances were generally increased, including the zygo-maxillary sutures (zmil-orl, zmir-orr), the lateral maxillary wall (zmil-em1sl, zmir-em1sr), and the naso-maxillary sutures (inml-snml, inmr-snmr). The posterior maxillary distances (mxtl-msl, mxtr-msr) and the posterior zygo-maxillary suture (iobfl-zmil, iobfr-zmir) were increased. The palatal distances were within the normal limits of the experimental standard.

Dimensions and Angles (Figure 3.30(d)): The anterior midline height of the maxilla (n-pr) was increased implying an elongated face in this patient. The posterior heights (gpfl-msl, gpfr-msr) were increased with a reduced superior length (msl-inml, msr-inmr). The inferior maxillary width (zmil-zmir) and the superior inter-orbital width (orl-orr) were increased while the nasal aperture (na-ans) was increased in height. The angles were not significantly different from the experimental standard except for the left orbital floor angle (nlil-msl-iobfl) which was reduced.

Discussion: The majority of significant measurements for Patient IP were larger than the experimental standard. This is in contrast to the concept that patients with Crouzon syndrome have hypoplasia of the maxilla. The configuration of the maxilla in Patient IP was of increased height and width (especially superiorly) but with a reduced anterior projection. The position of the maxilla is determined by the actual size of the bone and the distortion from surrounding bones. The height and anterior protrusion of the maxilla are determined by the position of the maxilla in relation to the cranial base structures, evidence of suture abnormality with adjacent bones and the deforming forces of distant calvarial synostosis.

Figure 3.30(c) Z Scores of the Distances of the Maxilla for Patient IP compared with the 2 Year Old Experimental Standard

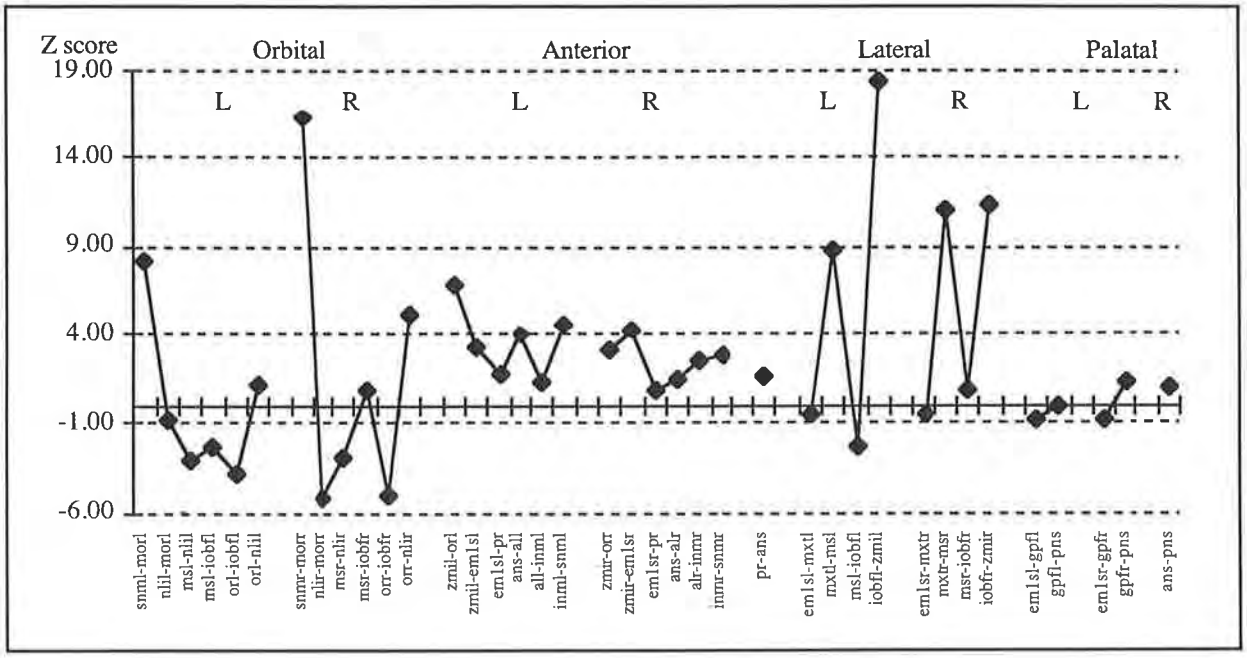

Figure 3.30(d) Z Scores of the Dimensions and Angles of the Maxilla for Patient IP compared with the 2 Year Old Experimental Standard

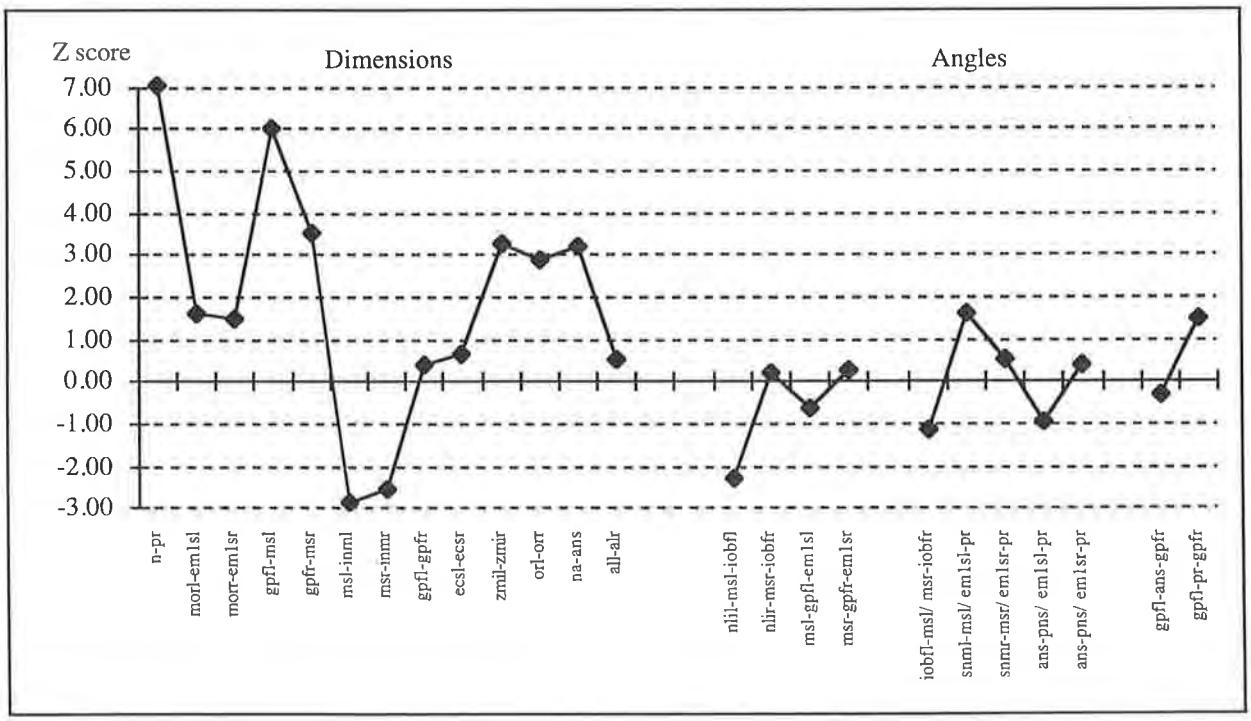

3.4.12.3 The Nasal Bones of Patient IP

Distances, Dimensions and Angles (Figure 3.30(e)): The lengths and widths of the nasal bone were increased bilaterally (na-n, na-inml, na-inmr, inml-snml, inmr-snmr, n-snml, n-snmr) relative to the experimental standard. The width of the inferior nasal complex (inml-inmr) was also significantly increased. The angle of the nasal bones compared with the cranial base (s-n-na) was reduced, as was the angle of the nasal bones (snml-n-snmr, inml-na-inmr).

Discussion: The nasal complex was increased in length both laterally and medially and may be related to the fronto-nasal and naso-maxillary sutures (see frontal bone and maxilla). The increased lengths and reduced nasal angles are consistent with the elongated and flattened features of the maxilla.

Figure 3.30(e) Z Scores of the Measurements of the Nasal Bones for Patient IP compared with the 2 Year Old Experimental Standard

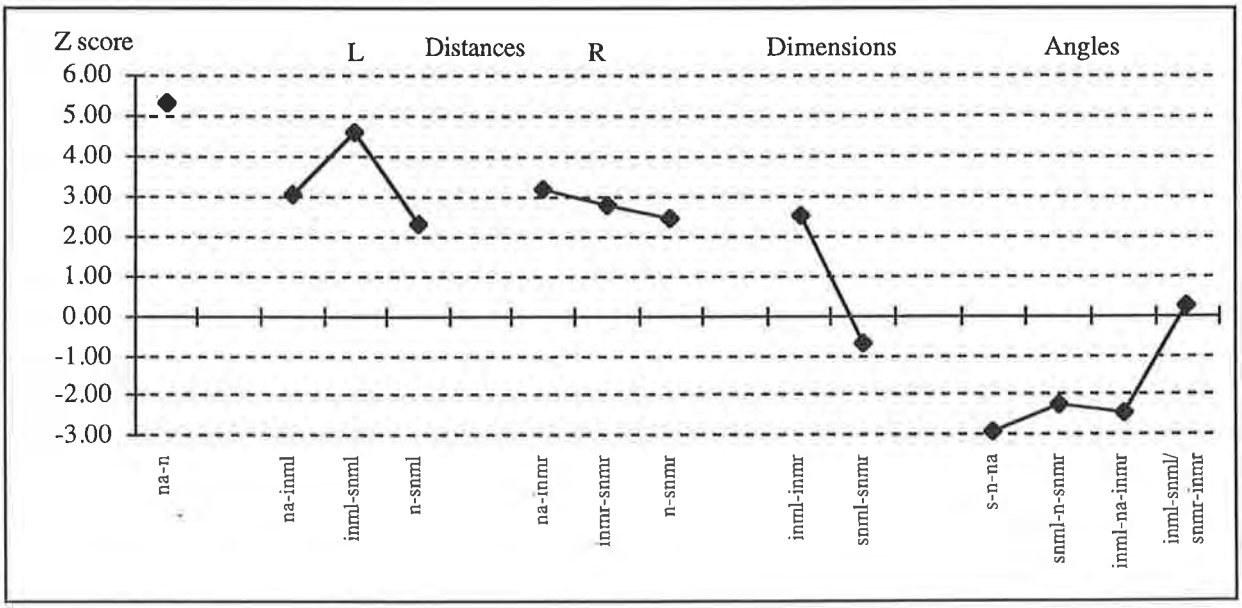

3.4.12.4 The Frontal Bone of Patient IP

Distances (Figure 3.30(f)):

Supra-orbital Region: The distances of the supra-orbital region were generally significantly increased compared with the experimental standard with some very large Z scores recorded. Increases were found at the fronto-nasal suture (n-snml, n-snmr), the fronto-maxillary suture (snml-morl, snmr-morr), the superior orbital rim (morl-sorl, morr-sorr, sorl-slorl, sorr-slorr) and the fronto- zygomatic suture (slorr-zfr, zfl-zfsl, zfr-zfsr, zfsl-slorl, zfsr-slorr).

Ethmoid Attachment: The frontal ethmoid attachment distances were found to be mainly reduced. The exception was the increased distance at the anterior frontal ethmoid attachment (fc-cpal, fc-cpar). The frontal attachment was within normal limits at the level of the cribriform plate (cpal-cppl, cpar-cppr) but the medial orbital wall (morl-ofaml, morr-ofamr) was reduced.

Sphenoid Attachment: The length of the superior orbital fissure (ofaml-sobfl, ofamr-sobfr) was significantly increased. The parietal attachment (spc-br) and sphenoid attachments (zfs-spc and spc-spa) were not recordable due to the fusion of sutures and hence poor visibility of landmarks in this region.

Dimensions (Figure 3.30(f)):The dimensions measured on the frontal bone were increased significantly from the experimental standard at the anterior superior orbital width (sorl-sorr, slorl-slorr) and decreased in the anterior cranial fossa depth (sorl-spal, sorr-spar).

Discussion: The deformity in this patient was found at the level of the cribriform plate medially, in the orbit and frontal bone and at the fronto-zygomatic suture laterally. The ethmoid bone was reduced in size in many regions, while the sphenoid and lateral zygomatic junctions were increased in size. The distances representing the cranial squamous sutures could not be measured, but were clearly fused and were related to the surrounding bony deformity.

Figure 3.30(f) Z Scores of the Distances and Dimensions of the Frontal Bone for Patient IP compared with the 2 Year Old Experimental Standard

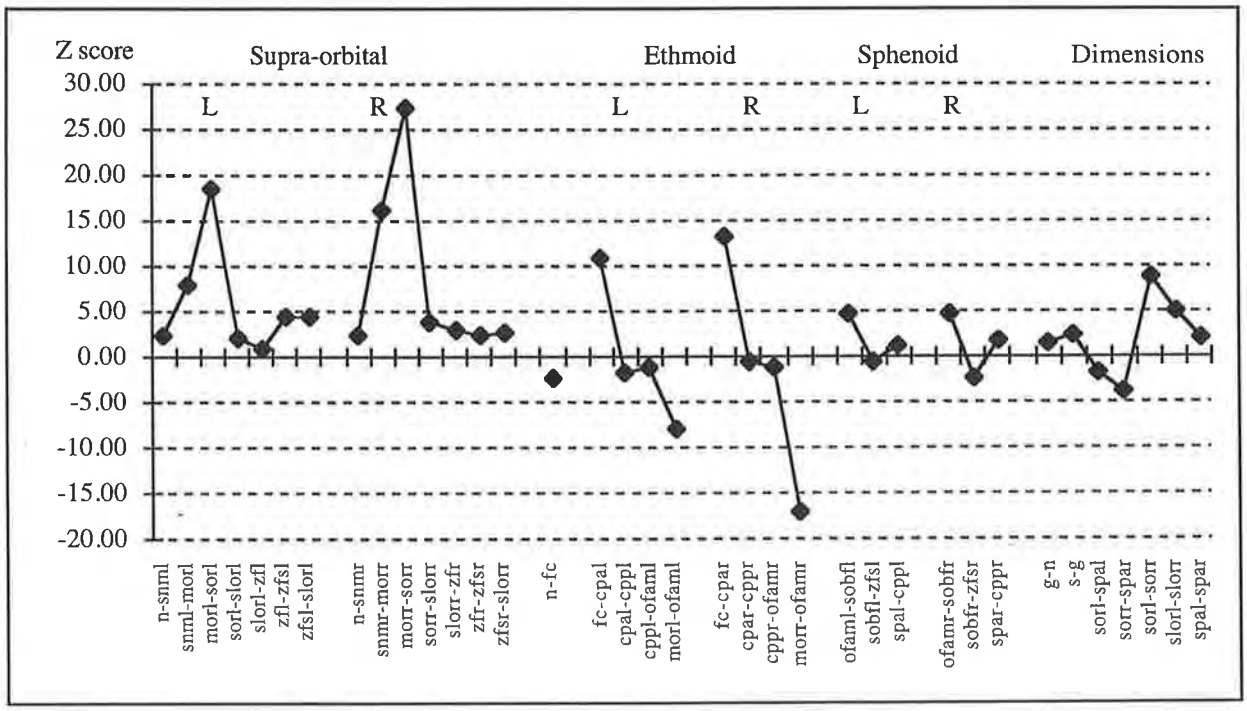

3.4.12.5 The Zygomatic Bone of Patient IP

Distances (Figure 3.30(g)): The majority of measurements were significantly different from the experimental standard. The inferior orbital fissure was significantly closer to the orbital rim (orl-iobfl, orr-iobfr) bilaterally. The inferior orbital fissure was an increased distance from the greater wing of the sphenoid (iobfl-gwll, iobfr-gwlr) bilaterally. The spheno-zygomatic suture (zfsl-gwll, zfsr-gwlr) and fronto-zygomatic sutures (zfsl-slorl, zfsr-slorr, slorr-zfr, zfl-zfsl, zfr-zfsr) were increased in length. The distances representing the inferior and lateral orbital rim (orl-ilorl, orr-ilorr, ilorl-lorl, ilorr-lorr) were also increased bilaterally. The lateral orbital rim (lorl-slorl, lorr-slorr) was reduced in height bilaterally. The height of the frontal process (zfl-ztl, zfr-ztr) however, was increased bilaterally. The anterior length of the zygomatic arch (parl-zmil, parr-zmir) was reduced bilaterally. The zygo-maxillary suture (zmil-orl, zmir-orr) was increased bilaterally.

Dimensions (Figure 3.30(g)): The dimensions showed an increased height (slorl-zmil, slorr-zmir) bilaterally with a tendency for reduced depth of the zygomatic bone (gwlr-ilorr).

Discussion: In this patient a large number of measurements representing the articulation with the sphenoid, frontal and maxillary bones were abnormal. This was reflected in the altered dimensions of the zygomatic bone. The bone was increased in its vertical height and contributed to the swept up appearance of the orbit. The increased number of significant measurements reflect the severity of the qualitative findings, with the sphenozygomatic sutures most severely involved.

3.4.12 6 The Vomerine Bone of Patient IP

Distances, Dimensions and Angles (Figure 3.30(h)): The distances measured were not significantly different from the experimental standard. The longitudinal dimension was not significantly different from the experimental standard. The angle of the vomer relative to the cranial base (s-n/h-ans), however, was significantly increased. This may be related to the cranial base deformity and the maxillary deformity in this severely affected child.

Discussion: The vomer was of normal size but its axis was directed downwards in this patient.

Figure 3.30(g) Z Scores of the Distances and Dimensions of the Zygomatic Bone for Patient IP compared with the 2 Year Old Experimental Standard

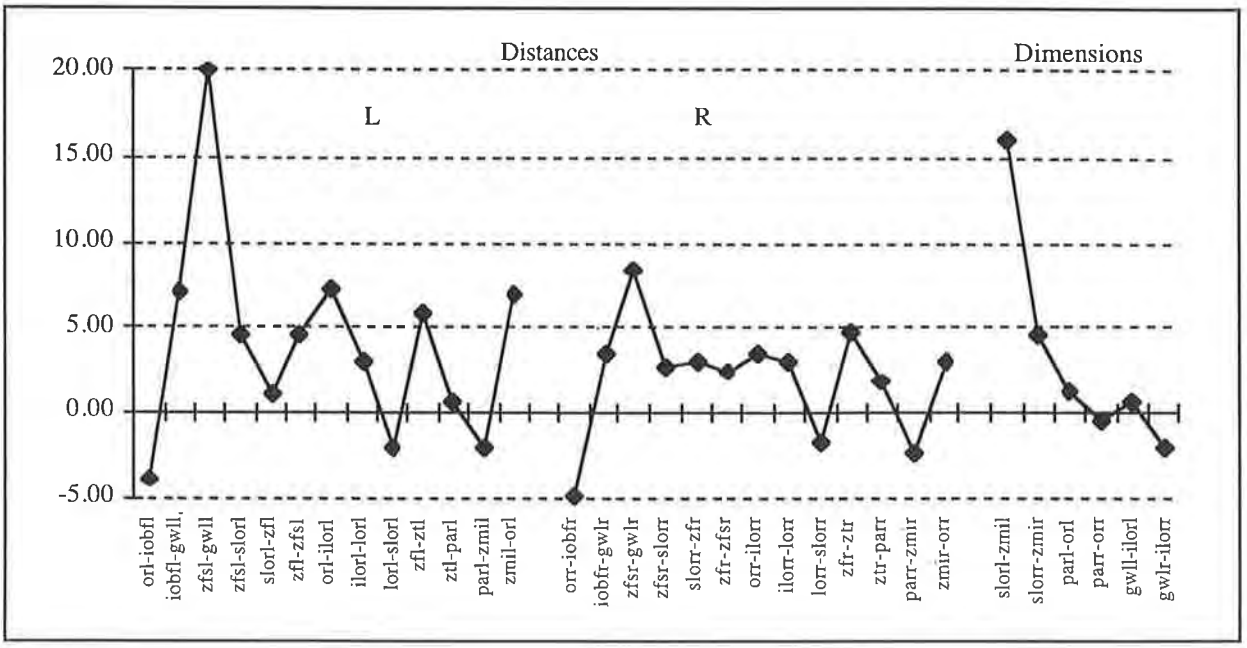

Figure 3.30(h) Z Scores of the Measurements of the Vomer for Patient IP compared with the 2 Year Old Experimental Standard

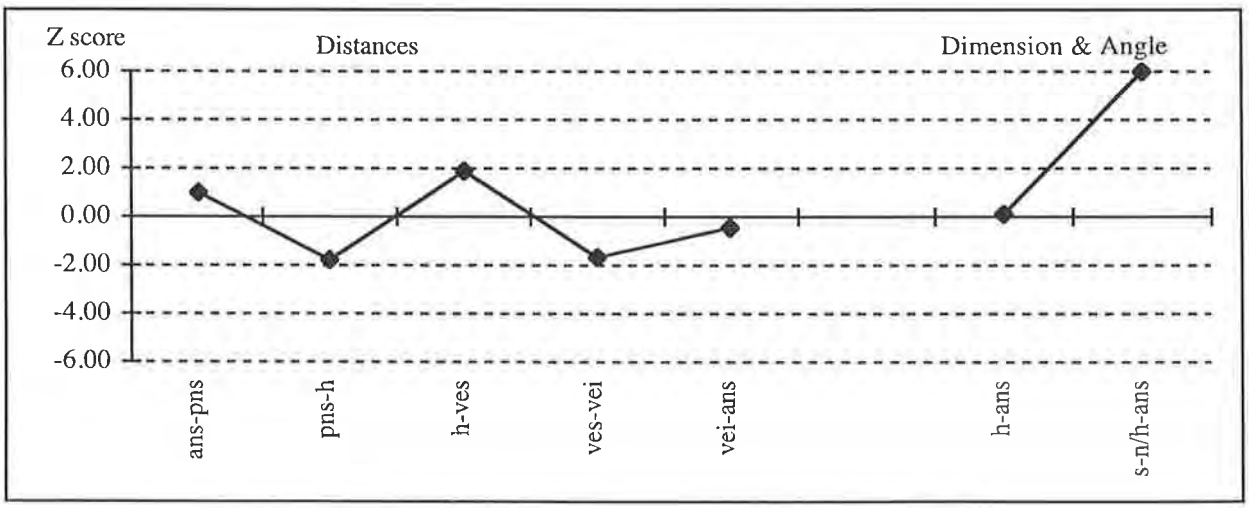

3.4.12.7 The Ethmoid Bone of Patient IP

Lateral Ethmoid Plate (Figure 3.30(i)):

Distances: The lateral ethmoid plate distances, forming the medial orbital wall, were generally reduced. The orbital component of the frontal ethmoid attachment (morl-ofaml, morr-ofamr) was reduced in length bilaterally. The height of the medial orbital wall (ofaml-msl, ofamr-msr) and the junction of the lateral plate at its inferior border with the maxilla (msl-nlil, msr-nlir) are also reduced. The junction of the lateral plate with the cribriform plate, in other words its articulation with the frontal bone, showed a reduced distance anteriorly on the left (morl-cpal) (for cpal-cppl distance, see cribriform plate).

Dimensions and Angles: The anterior dimensions between medial orbital walls (inter-orbital distance) (morl-morr) and the anterior inferior width between the nasolacrimal inferius points (nlil-nlir) were increased. The splay of the lateral plate (nlil-morl/morr-nlir) was decreased anteriorly with a tendency for an increased angle of splay (msl-ofaml/ofamr-msr) posteriorly.

Cribriform Plate (Figure 3.30(j)):

Distances: The cribriform plate had a greatly increased width (fc-cpal, fc-cpar, es-cppl, es-cppr) bilaterally with lengths in the normal range.

Angles: The cribriform plate was significantly depressed or laterally splayed (s-n/cpal-cppl, s-n/cpar-cppr) in this patient.

Medial Ethmoid Plate (Figure 3.30(j)):

Distances: The medial plate had several significantly different distances compared with the experimental standard. These included an increased posterior height of the crista galli (cg-es), an increased distance of the septal attachment (n-vei) and a decreased distance from the nasion to foramen caecum (n-fc).

Dimensions: The height of the medial plate was increased (vei -cg).

Discussion: The ethmoid bone in this patient was considerably distorted. The lateral plate was reduced in length and in height. The cribriform plate was increased in width while the medial plate had a shape which was increased in height and tended to be reduced in length. Anteriorly, the inter-orbital distance was increased. The ethmoid had the typical distortion of the broad cribriform plate, which was depressed and with a reduced orbital component.

Figure 3.30(i) Z Scores of the Measurements of the Lateral Ethmoid Plate for Patient IP compared with the 2 Year Old Experimental Standard

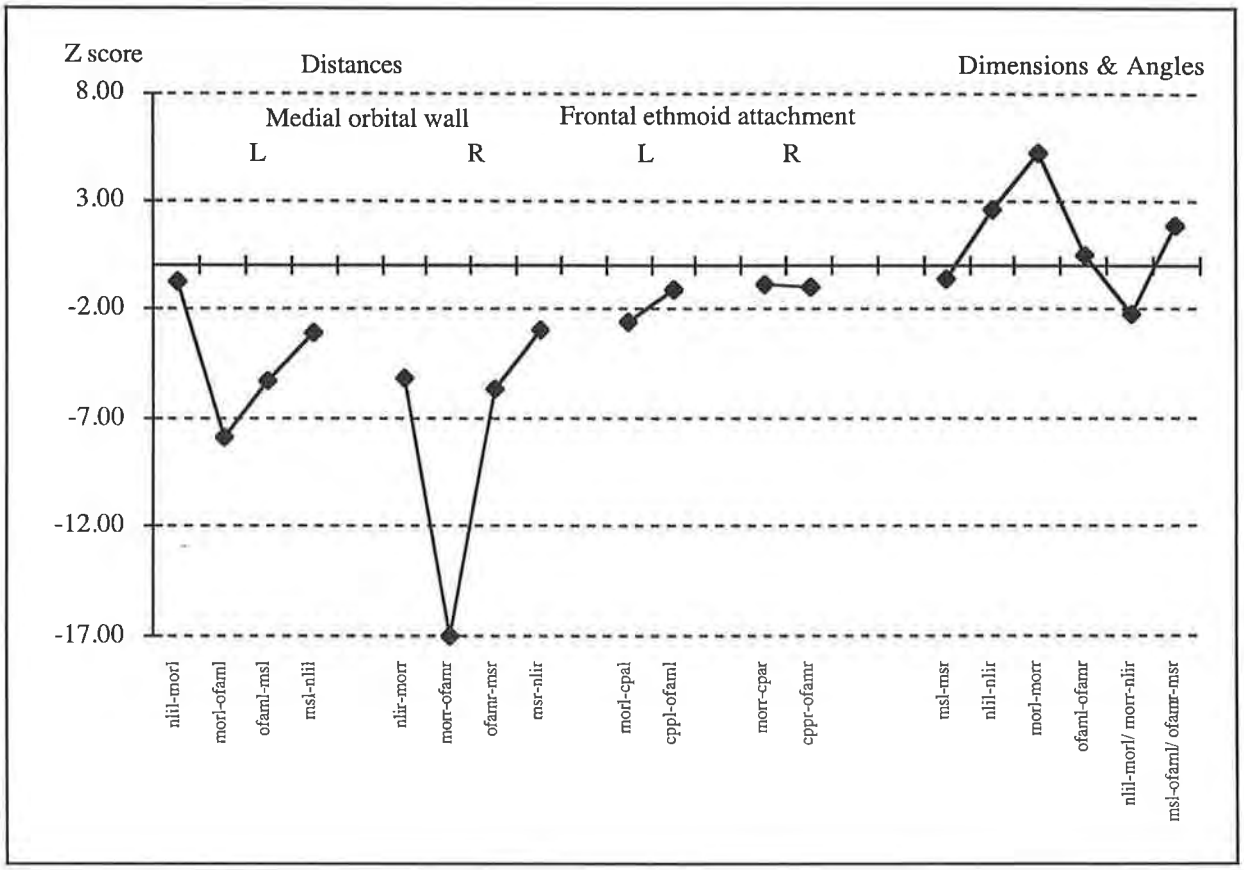

Figure 3.30(j) Z Scores of the Measurements of the Cribriform and Medial Ethmoid Plates for Patient IP compared with the 2 Year Old Experimental Standard

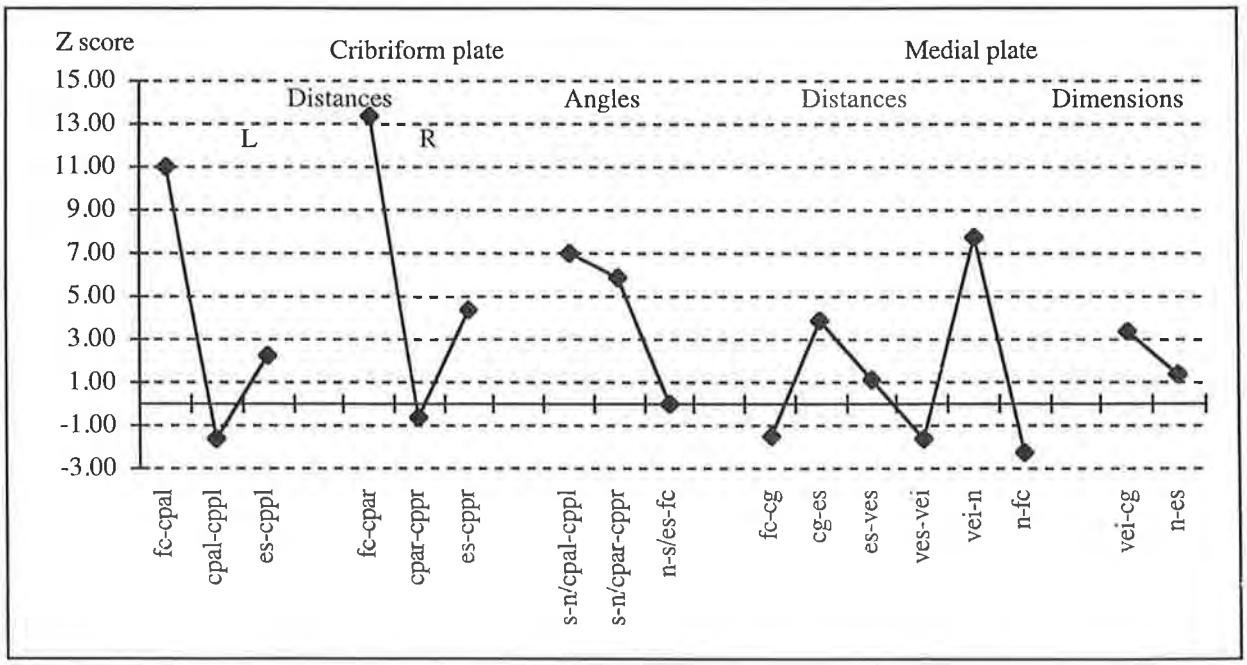

3.4.12.8 The Sphenoid Bone of Patient IP

Lesser Wing (Figure 3.30(k)):

Distances: The length of the lesser wing (acl-spal, acr-spar, spal-es, spar-es) was increased relative to the experimental standard bilaterally.

Dimensions: The dimension between the tips of the wings was also increased (spal-spar). The angle of the lesser wings (spal-es-spar) was reduced, implying they were more swept up, while the splay of the lesser wings from the midline (n-s/ac-spa) was normal.

Pterygoid Plate (Figure 3.30(k)):

Distances: The pterygoid plate was reduced in height on the left side (ptsl-hpl, ptll-fool).

Angles: The axis of the pterygoid plates was significantly increased bilaterally, implying the plates were angled laterally and/or more posteriorly from the midline than the experimental standard.

Greater Wing (Figure 3.30(l)):

Distances: Many significant findings were found in this patient. Laterally the distances of the greater wing were increased particularly at the spheno-zygomatic suture (zfsl-gwll, zfsr-gwlr) and along the floor of the middle cranial fossa (fosl-gwll) on the left side. Additionally, the orbital measurements were increased at the level of the inferior lateral orbital length (gwll-gwml, gwlr-gwmr) and the superior orbital fissure (gwml-sobfl, gwmr-sobfr) bilaterally. The distance of the orbital spheno-frontal suture (sobfr-zfsr) on the right was reduced, however. The posterior part of the left greater wing was increased in length at the posterior middle cranial fossa (fosl-petal). Landmarks on the squamous sphenoid bone (spt and spc) could not be identified bilaterally, due to fusion of the calvarial bone in this region and hence the distances of the lateral part of the bone could not be measured.

Dimensions and Angles: The dimensions and the angles of protrusion were not significantly different from the experimental standard with the exception of the inferior splay of the greater wing (gwll-gwml/gwmr-gwlr) which was increased. The angle between the posterior sutures was reduced (fosl-petal/petar-fosr).

Figure 3.30(k) Z Scores of the Measurements of the Lesser Wing and Pterygoid Plate of the Sphenoid for Patient IP compared with the 2 Year Old Experimental Standard

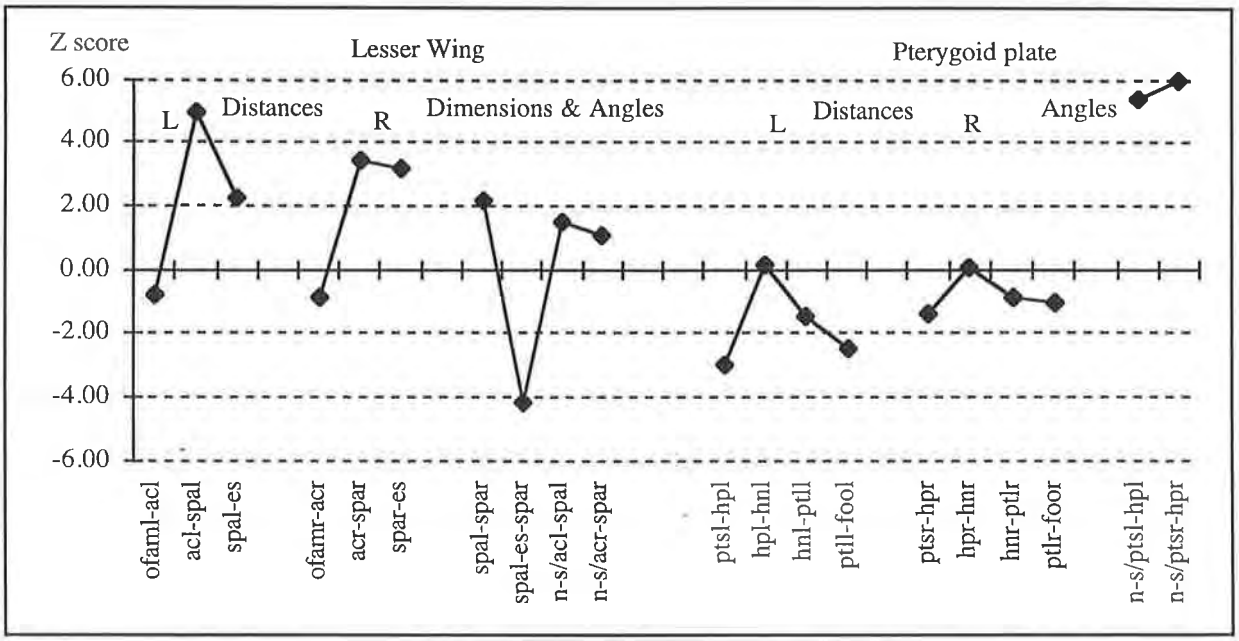

Figure 3.30(l) Z Scores of the Measurements of the Greater Wing of the Sphenoid for Patient IP compared with the 2 Year Old Experimental Standard

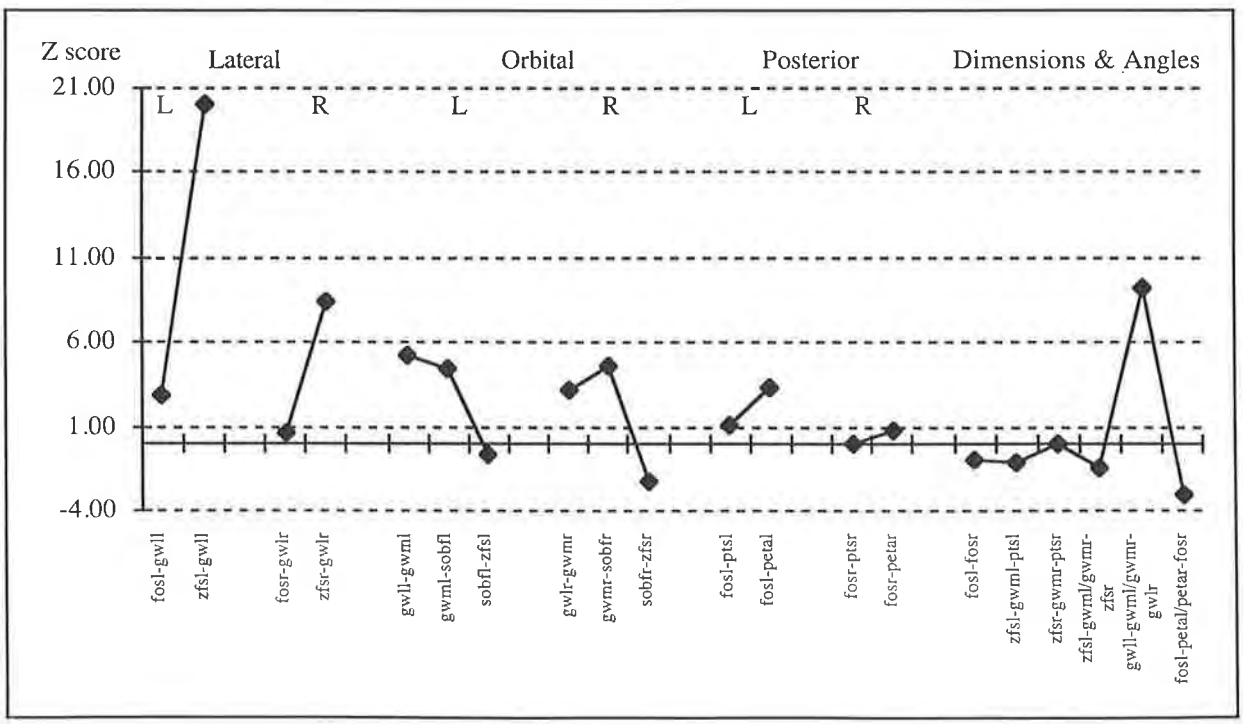

3.4.12.8 The Sphenoid Bone of Patient IP (continued)

Body of Sphenoid (Figure 3.30(m)):

Distances: The lateral and posterior sphenoid body were abnormal. The length of the body (gwml-ptsl, gwmr-ptsr) was increased bilaterally. The lateral height of the spheno-occipital synchondrosis (ptsl-petal, ptsr-petar) was increased bilaterally. Anteriorly, an increased width of the spheno-ethmoid synchondrosis (es-cppl, es-cppr) was recorded. In the sella, the optic foramen was in close proximity to the posterior cribriform plate (cppl-ofpml, cppr-ofpmr) with a corresponding increase in length of the sella (ofpml-petal, ofpmr-petar). The distances of the floor of the body were not significantly different from the experimental standard.

Dimensions and Angles: The dimensions revealed a reduced distance between the greater wing medial points (gwml-gwmr). The superior spheno-occipital synchondrosis (petal-petar) was normal. The posterior height in the region of the posterior clinoid processes (pcl-ptsl, pcr-ptsr) was increased. The lower body angle (s-n/gwml-ptsl) was significantly reduced on the left side but increased on the right side (s-n/gwmr-ptsr). The upper body angle (s-n/ofpml-petal, s-n/ofpmr-petar) was significantly reduced on bilaterally.

Discussion: Patient IP had the most severe deformity of all the patients examined. The measurements of the sphenoid bone reflected this with many significant findings. Anteriorly the lesser wings were long and swept up, with involvement of the spheno-ethmoid synchondrosis. The greater wing was increased in height and some of the lengths. The body revealed an increase in the size of the sella, particularly in the length and height, with some evidence of narrowing. The cause of the deformity in Patient IP appeared to be twofold, with the primary suture pathology distorting the growth of the anterior and lateral elements and the secondary effects of the craniosynostosis causing endocranial bone absorption in the region of the sella. The effect of the distortion of the spheno-occipital synchondrosis and the spheno-temporal sutures is discussed later (see temporal and cranial base sutures).

Figure 3.30(m) Z Scores of the Measurements of the Body of the Sphenoid for Patient IP compared with the 2 Year Old Experimental Standard